Nitrosyl Halides and bis-Acetylacetonates of Ruthenium and Osmium: Synthetic and Spectro-electrochemical Investigation of Ligand Additivity in Redox-active Transition Metal Complexes

A thesis submitted for the degree of Doctor of Philosophy of

The Australian National University

Research School of Chemistry

by

Dmitri Menglet

February 1996

Посвящается памяти моей бабушки
Валентины Григорьевны Королёвой

To the memory of my grandmother,
Mrs Valentina Grigor'evna Korolyova

Grau, teurer Freund, ist alle Theorie,

Und grün des Lebens goldner Baum.

Johann Wolfgang von Goethe

Declaration

Except where specific reference is made to other sources, the work presented in this thesis is the work of the author. It has not been submitted, in whole or in part, for any other degree.

Dmitri Menglet

Acknowledgments

I would like to express my profound gratitude to my supervisor, Dr Graham Heath, for his scientific leadership and kindly advice during my course of research. I would like to thank Professor Martin Bennett and Dr Lucjan Dubicki for extremely helpful and inspiring discussions. Thanks also to Mr Horst Neumann for the syntheses of many *bis*-acetylacetonato complexes of ruthenium, Dr Anthony Willis and Dr David Hockless for solving the X-ray structures, Dr Richard Bramley, Dr Paul Prenzler and Dr Sue Boyd for recording EPR spectra, Dr John MacLeod and Mrs Jenny Rothschild for the FAB Mass Spectra.

I am very grateful to Miss Sandra Nissen, Dr Klaus Moock and Dr Stuart Macgregor for proof-reading this thesis and making careful corrections.

Many thanks to the people who cut through the "red tape" and helped me to become a Ph.D. student at the R.S.C. in 1991: Professor Alan Sargeson, Professor Athel Beckwith (School Dean at the time), Dr Graham Heath, Miss Penny Richardson and Mrs Maureen Slocum.

I would like to thank my tutors, demonstrators and supervisors at M.V. Lomonosov Moscow State University, particularly Professor Anatoli Konstantinovich Yatsimirskiy and Professor Alexandre Dmitrievich Ryabov, for sharing with me their knowledge of Chemistry during my time at M.S.U. (in 1985-90).

Special thanks to my school teacher of English, Mrs Sofia Yakovlevna Rudaya, for giving me command of the language sufficient for communicating with my colleagues and for writing this thesis.

Finally, I would like to thank my parents, my brother and friends for their help, care and support.

Abstract

The present thesis is devoted to the study of the ligand additivity effects in the six-coordinate complexes of ruthenium and osmium. The systems under study include complexes of the following types: $[MX_5L]^{z-}$, $[MX_4LL']^{z-}$ (M = Ru and Os; X = Cl and Br; L and L′ = NO^+, CO, *etc.*) and $[M(acac)_2LL']$ (M = Ru and Os; acac = 2,4-pentanedionate; L and L′ = Cl, CH_3CN, PR_3, *etc.*). Special emphasis is put on the electrochemical and optical spectro-electrochemical characterisation of these complexes and on the relationships between the redox potentials and the energies of charge-transfer transitions.

Chapter 1 briefly outlines the historical perspective of additivity in chemistry, introduces the topic of the present work, and delineates the scope of this thesis.

Chapter 2 reviews literature methods of preparation of the mixed halide nitrosyl complexes of ruthenium and osmium, and describes the synthesis and characterisation of the compounds prepared in this work. The structure and metal-binding modes of the nitrosyl moiety are discussed, and the crystallographic and spectroscopic (IR and EPR) evidence is presented for linear mode of coordination of the nitrosyl (NO^+) ligand in the complexes considered here.

Chapter 3 describes the electrochemical and spectro-electrochemical (UV-VIS-NIR) characterisation of the mixed halide nitrosyl complexes of ruthenium and osmium, and comparison with their analogues of stoichiometry $[MX_5L]$ and $[MX_4LL']$. Non-linear ligand effects on E^o in species such as $[OsBr_4(CH_3CN)(NO)]^{1-}$ are discussed. Linear relationships between the ligand-to-metal charge-transfer band energies and E^o in a wide range from -1.5 to +1.5 V (*versus* Ag/AgCl) are established for the arrays of the chloride and bromide complexes. The frontier electron orbitals are mapped *versus* $Os^{III/II}$ couple for a progression of mixed osmium bromide complexes. The apparent

instability of hypothetical $[Ru^{III}Br_5(NO)]^{1-}$ is considered within the framework of the collected spectro-electrochemical data.

Chapter 4 is devoted to the investigation of the electrochemical and spectral properties of the *bis*-acetylacetonato complexes of ruthenium and osmium ($[M(acac)_2L_2]$]) in the light of ligand additivity concepts. The dependence of E^o ($M^{III/II}$ and $M^{IV/III}$) on the ligand (L, L′) donor / acceptor properties and the ligand arrangement (*cis* or *trans*) is contemplated. Plotting of the E^o values *versus* the sums of Lever's electrochemical parameters (ΣE_L) reveals different polarisabilities of the *cis* and *trans* $\{Ru(acac)_2\}$ binding sites. Linear relationships between the optical charge-transfer band energies and E^o, similar to those found for the halide complexes in Chapter 3, are confirmed for series of *cis* and *trans* complexes. A linear additive relationship between stoichiometry and electronic properties is established for the set of *trans*-$[Ru(acac)_2(CH_3CN)_n(Cl)_{2-n}]^z$ (n = 0, 1, 2) complexes. In conclusion the properties of the analogous $[M^{III/II}(acac)_3]^{0/1-}$ and $[M^{III/II}(acac)_2Cl_2]^{1-/2-}$ (M = Ru or Os) are juxtaposed.

Appendix 1 explores the electrochemistry of *cis*- and *trans*- $[OsBr_4(L)_2]^{z-}$ (L = CH_3CN and CO) complexes.

Appendix 2 presents the X-ray crystal structures determined in the course of this work.

Table of Contents

Introduction

For centuries humankind has sought to gain understanding and thus control of the physical and chemical phenomena in the surrounding world. However, the accumulated lore of nature matures into a rigorous scientific discipline only when the strict language of mathematics becomes applicable. A quantitative approach enables a scientist to specify the properties of a given system under study. The behaviour of these systems may then be encompassed by scientific laws. One of the early chemical laws was the law of conservation of weight, first formulated in 1748 by Mikhail Vasil'evich Lomonosov and later (in 1789) generalised by Antoine Laurent Lavoisier.[1a] With the discovery of the periodic law by Dimitri Ivanovich Mendeleev in 1869, it became possible to predict various properties of the chemical elements. Mendeleev wrote: *"If in a given group there are elements R_1, R_2, R_3, and in the row containing one of them, say R_2, the element Q precedes it and the element T follows it; then the properties of R_2 are derived from the properties of R_1, R_3, Q and T. Thus, for example, the atomic weight of R_2 = 1/4 (R_1+R_3+Q+T). For example, selenium is situated in group VI between sulfur (S = 32) and tellurium (Te = 127), and in the 5th row arsenic (As = 75) precedes it and bromine (Br = 80) follows it. From the aforesaid, the atomic weight of selenium = 1/4 (32+127+75+80) = 78.5 - a number close to reality."** By exploiting this cross-additivity Mendeleev predicted the properties of a number of previously unknown elements. This provides a pioneering example of an application of the additivity principle in chemistry.

---

* Quoted from ref. 1b. Translated from Russian by D. Menglet

The additivity principle has a long history in coordination chemistry. In 1894 Werner and Miolati described a linear correlation between the composition of certain platinum and cobalt inorganic compounds and their molar electroconductivity (Figure 1.1).[2] The classical Werner - Miolati electroconductivity progressions not only supported the coordination theory devised by Werner, but gave one of the first examples of a simple link existing between ligand composition of the coordination sphere and the macroscopic properties of metal complexes.

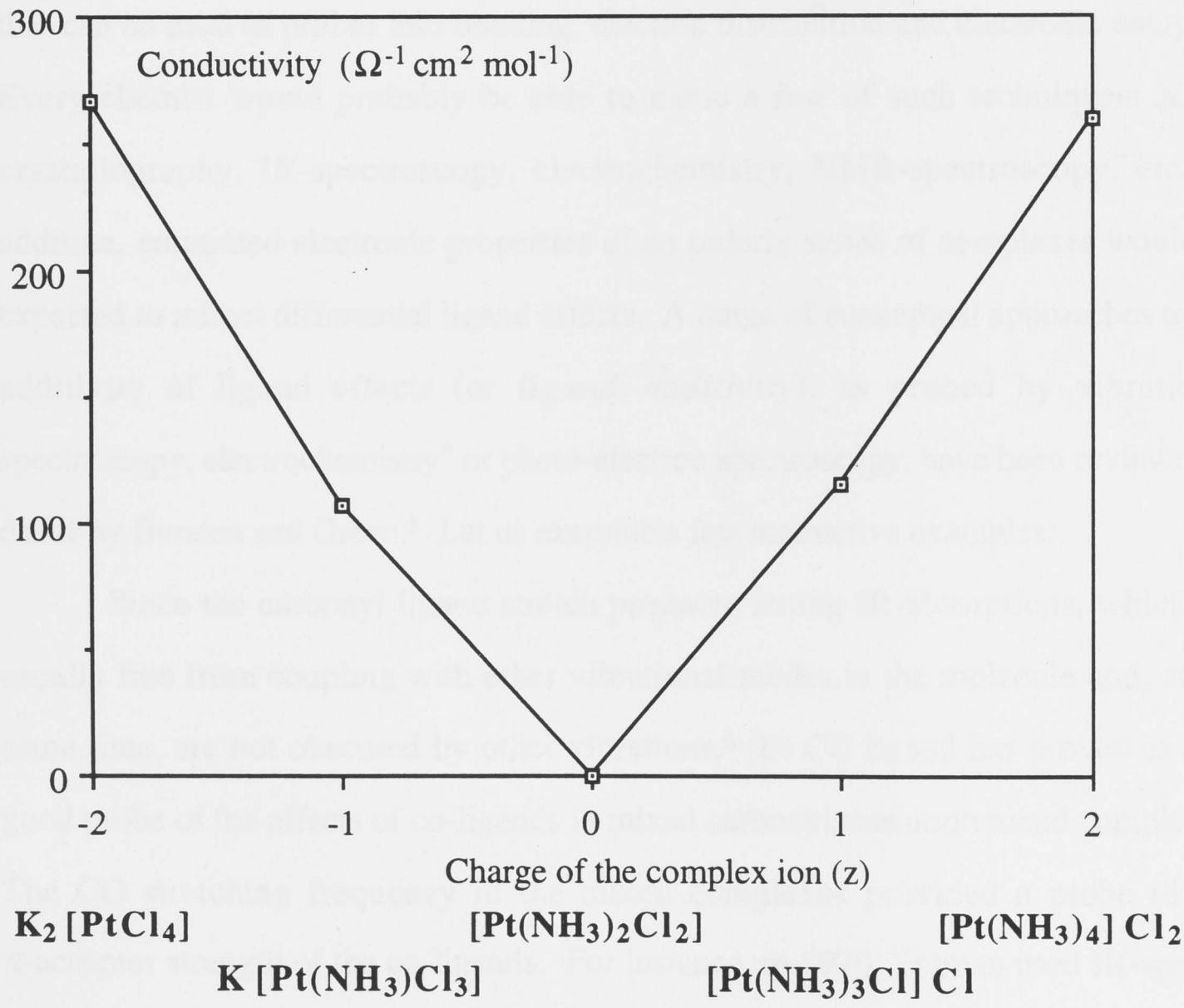

Figure 1.1 *Diagram showing orderly change of molar electroconductivity in a series of* $[Pt(NH_3)_{4-n}Cl_n]^z$ *(n = 0 - 4) complexes.*[2]

The spectrochemical series also represents an array of ligands ranked according to their cumulative (addditive) effect on the frequency of the *'d-d'* spectral bands of a specified central metal ion.[3]

One of the major objectives of contemporary coordination chemistry is to understand and systematise the changes that occur in various properties of coordinated transition metal ions when one ligand is substituted by another. A ligand effect has been conventionally defined as *"...the changes that occur in the kinetics and thermodynamics of reactions when the electronic and steric properties of ligands or incipient ligands are altered."*[4] In 1988, Bursten and Green rephrased the above definition: *"...ligand effects are the changes that occur in bonding, electron distribution, and electronic energies in transition metal complexes when the electronic properties of ligands are altered."*[5] A variety of different experimental methods exist that can be used as probes into bonding, electron distribution and electronic energies. Every chemist would probably be able to name a few of such techniques: X-ray crystallography, IR-spectroscopy, electrochemistry, NMR-spectroscopy, *etc.* In addition, computed electronic properties of an orderly series of complexes would be expected to reflect differential ligand effects. A range of conceptual approaches to the additivity of ligand effects (or *ligand additivity*), as probed by vibrational spectroscopy, electrochemistry* or photo-electron spectroscopy, have been reviewed in detail by Bursten and Green.[5] Let us examine a few instructive examples.

Since the carbonyl ligand stretch produces strong IR-absorptions, which are usually free from coupling with other vibrational modes in the molecule and, at the same time, are not obscured by other vibrations,[6] the CO ligand has proved to be a good probe of the effects of co-ligands in mixed carbonyl transition metal complexes. The CO stretching frequency in the mixed complexes provided a probe of the π-acceptor strength of the co-ligands. For instance, in 1970, Tolman used IR-spectra of the $Ni(CO)_3(PR_3)$ complexes to scale and classify the donor / acceptor properties of a large number of phosphine ligands.[7] It is known that the CO stretching frequencies are higher in homoleptic $M(CO)_6$ complexes than in mixed-ligand complexes of the

---

* The models of electrochemical ligand additivity relevant to this work will be re-examined in greater detail in Chapters 3 and 4.

form $[M(CO)_{6-n}L_n]$ where L is a *weaker* π-acceptor than CO, and that ν(CO) falls steadily with the increasing degree of CO-substitution, n.[8] This fall in ν(CO) is said to reflect the strengthening of π-backbonding between the metal and CO ligand, as the competition for the metal $d\pi$ electrons eases. In the particular case where the incoming ligand L is an isocyanide (RNC), then a complementary trend is found in ν(NC): in the homoleptic isocyanide complexes ν(NC) takes its lowest value, and it increases in a regular way with the number of co-existing CO ligands. Sarapu and Fenske discussed this effect for a series of manganese complexes $[Mn(CO)_{6-n}(CH_3NC)_n]^{1+}$ (n = 0 to 6).[9] Even without a rigorous analysis of the force constants, it is possible to

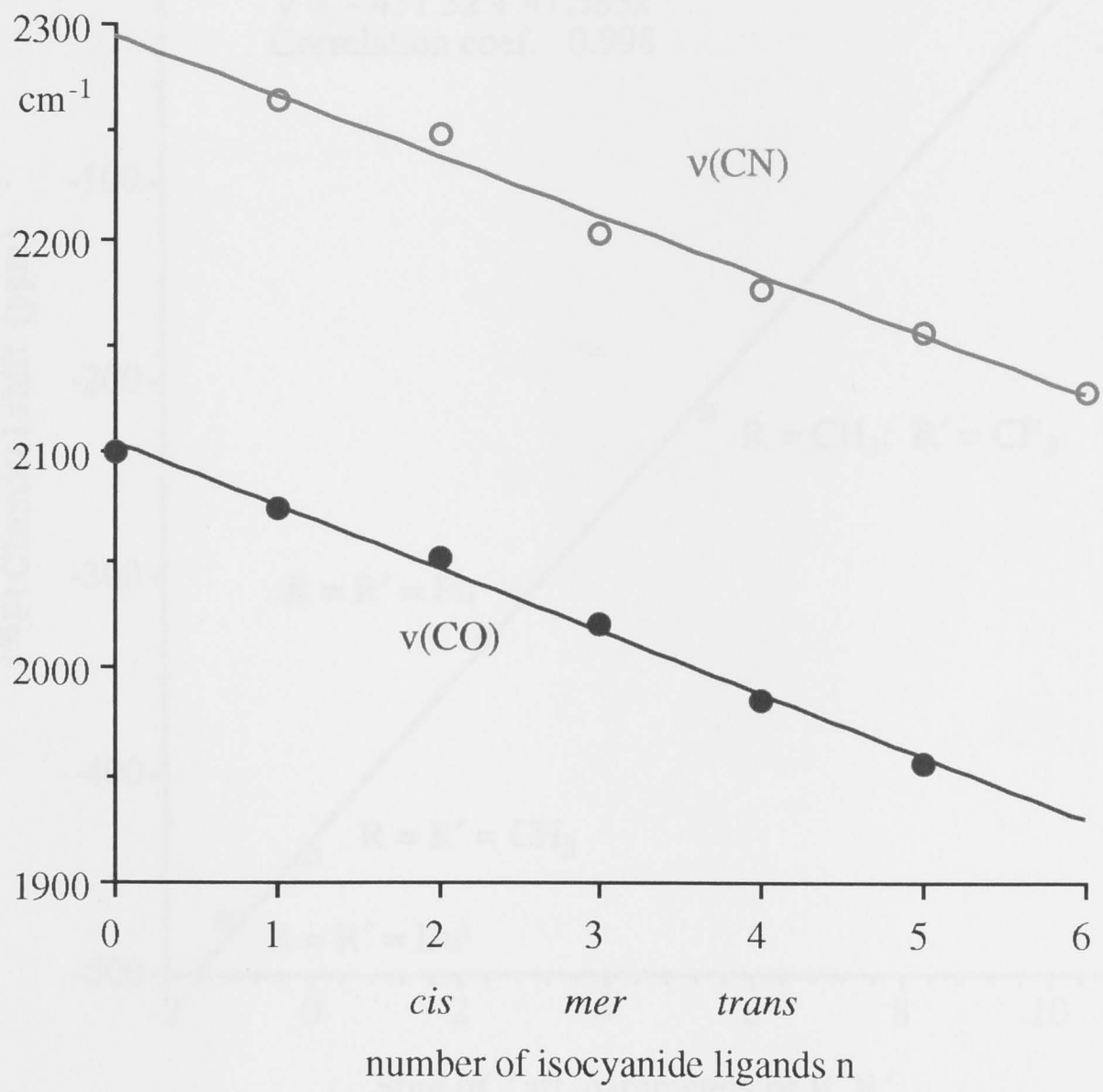

Figure 1.2 *A plot of ν(CO) and ν(CN) versus n for the series of manganese complexes $[Mn(CO)_{6-n}(CH_3NC)_n]^{1+}$ (n = 0 to 6). Data from ref. 9.*

see that both ν(CO) and ν(CN) stretching frequencies are linearly dependent on the degree of substitution, n (Figure 1.2). This is a representative example of a *linear* accumulation of ligand effects (*i.e. linear ligand additivity*).

Around the same time, Bonder showed that ^{13}C carbonyl chemical shifts are proportional to CO infrared stretching force constants for a series of $[M(CO)_5L]$ complexes (M = Mo, Cr; L is an amine, phosphine, arsine or stibine ligand).[10]

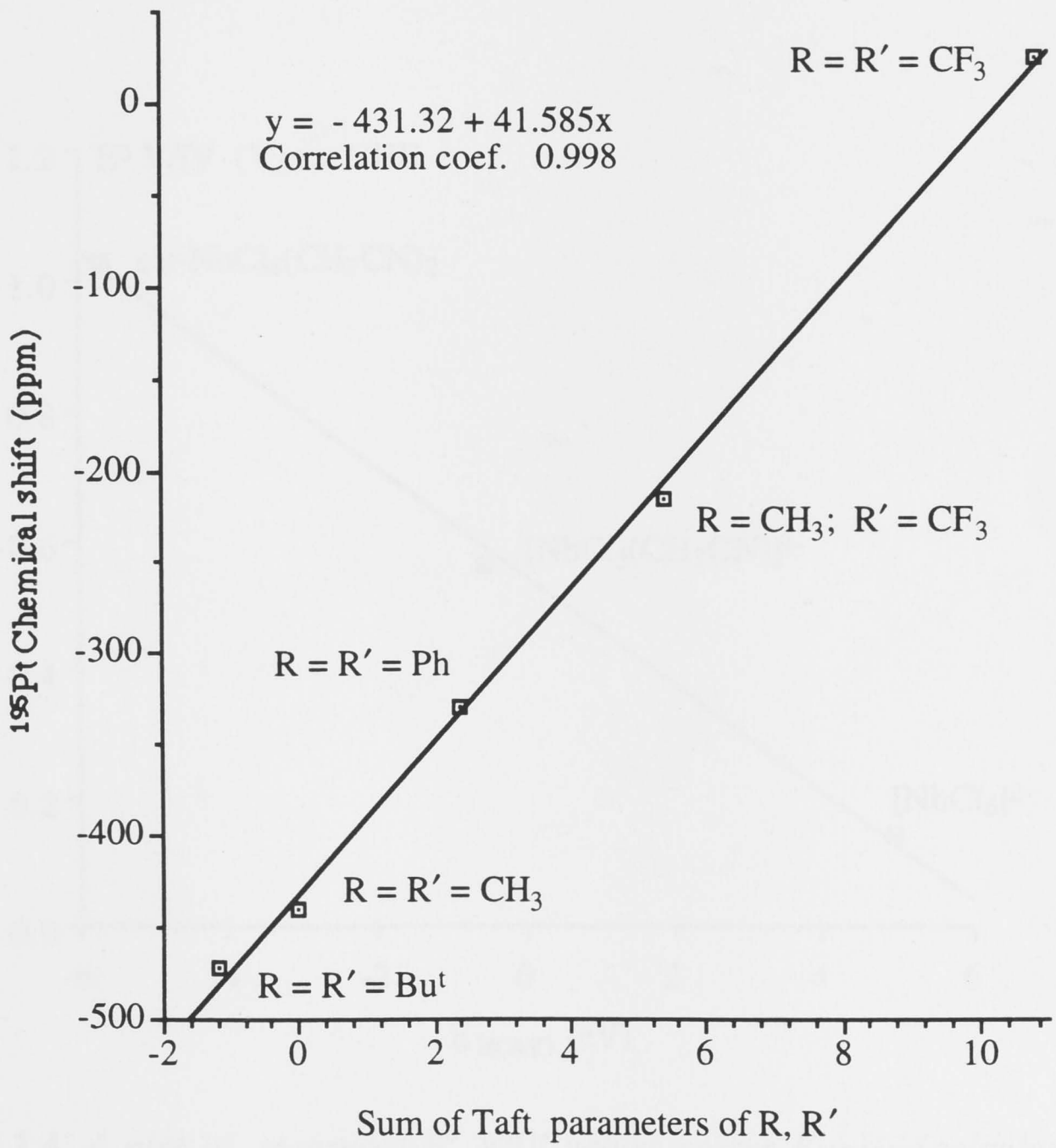

Figure 1.3 *A linear relationship between ^{195}Pt chemical shift and the sum of Taft parameters of R and R′ in the $[Pt^{II}(R(CO)CH(CO)R')_2]$ complexes. Data from ref. 11.*

A recent example of the use of NMR as a direct probe for the influence that the ligands exert on the central metal ion itself comes from our laboratory. For a series of substituted *bis*-acetylacetonato platinum(II) complexes of the form $[Pt(R(CO)CH(CO)R')_2]$ (where R, R' = ^tBu, Me, Ph, CF_3, etc), a faithful linear relationship has been found between the ^{195}Pt chemical shift (over a wide range of *ca.* 500 ppm) and the sum of Taft parameters for R and R' (Figure 1.3).[11]

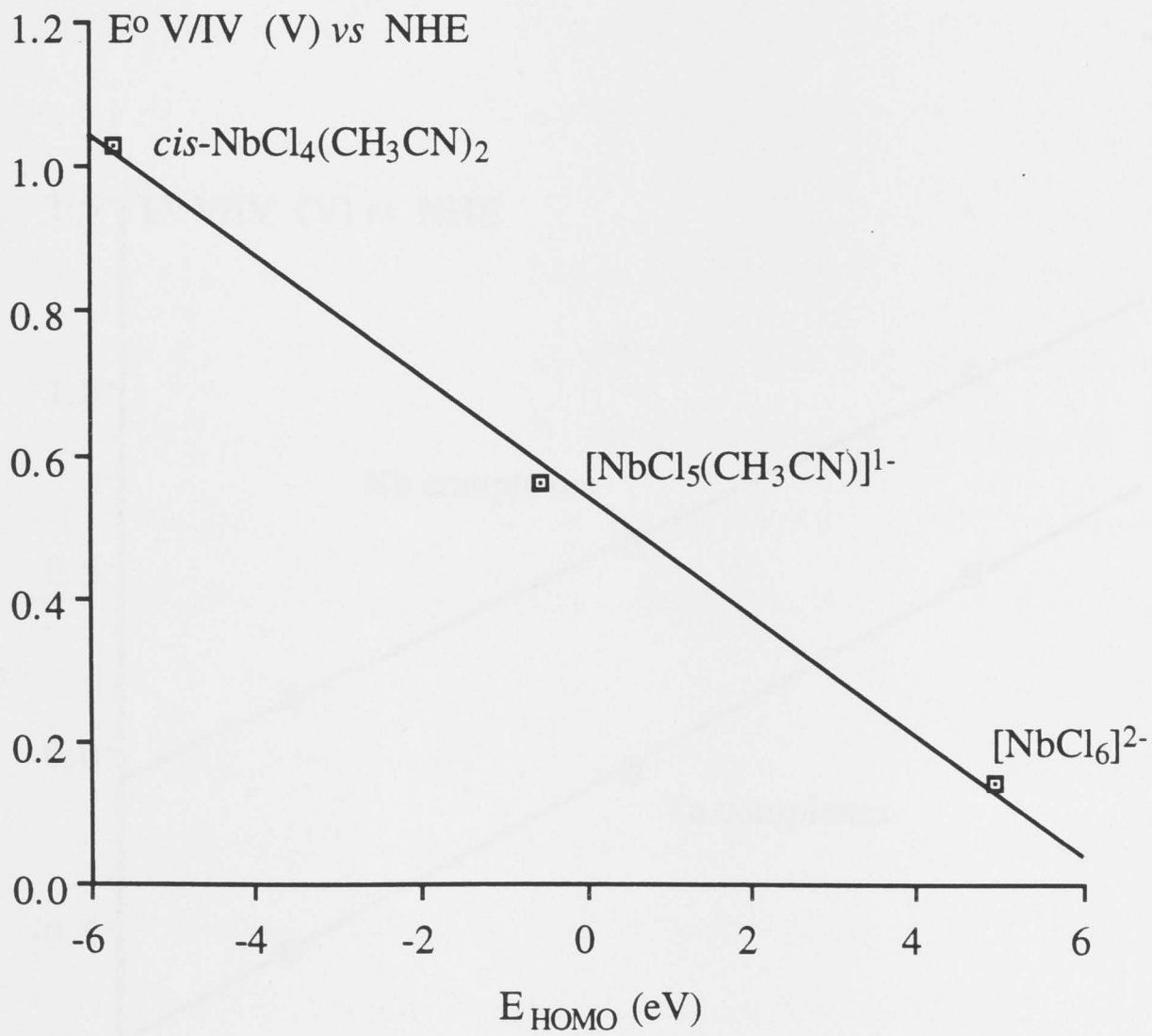

Figure 1.4 *A plot of measured E^o V/IV values versus E_{HOMO} (calculated by Fenske - Hall method[15]) for a series of niobium (IV) complexes. Data from ref. 14.*

In connection with probing ligand influence on electronic properties, the particular significance of the E^o values quantified by electrochemical experiments depends on an extension of Koopmans' theorem.[5,12] This theorem relates the molecular Ionisation Energy and Electron Affinity (the work involved in removal or addition of an electron) to the underlying molecular HOMO and LUMO energy levels respectively. By extension to solution-phase redox processes this theorem can be applied to metal complexes, so that comparative E^o measurements may be provisionally associated with trends in the frontier orbital energies. A vivid illustration of this, and one of the earliest demonstrations of an orderly correlation between first ionisation energies and solution-phase reversible redox potentials, was provided by the 1986 study of the photo-electron spectroscopy and voltammetric data for a family of $[Ru(R(CO)CH(CO)R')_3]$ complexes.[13]

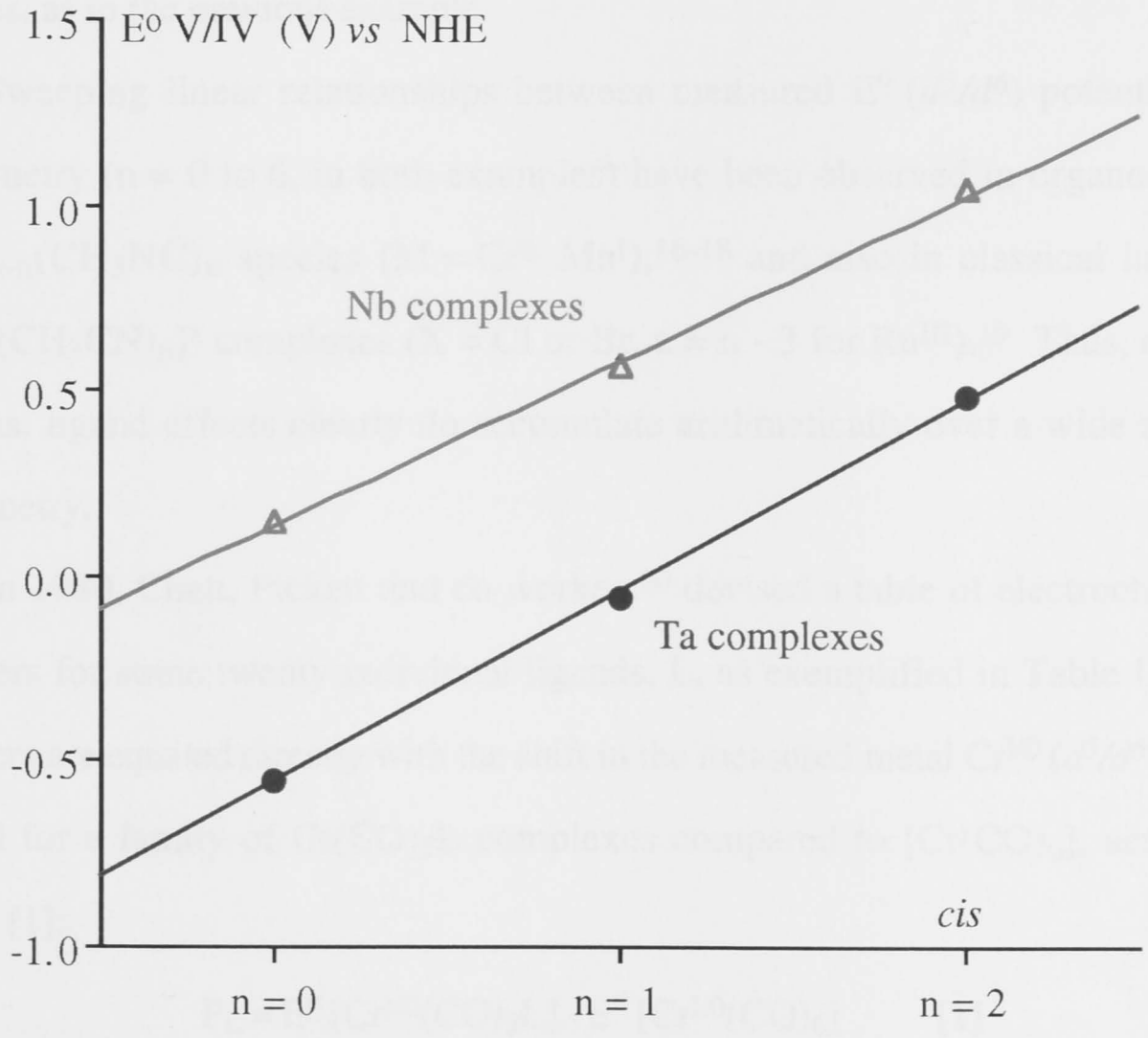

Figure 1.5 *A plot of measured E^o V/IV values versus n for the series of $[MCl_{6-n}(CH_3CN)_n]^{z-}$ complexes (M = Nb and Ta). Data from ref. 14.*

A number of investigations attempting to correlate theoretically computed HOMO energies with E^o measurements have been undertaken.[5] For instance, Bursten *et al.*[14] observed a linear relationship between E^o for the metal-based d^0/d^1 couple and the HOMO energies calculated by Fenske-Hall method[15] for a series of niobium (IV) complexes (Figure 1.4). The latter correlation was supported by the obvious connection between E^o and composition for these particular complexes (Figure 1.5). Bursten concluded that :*"The ligand additivity model would predict that each successive replacement has the same effect, regardless of how many ligands have already been substituted. This non-intuitive result is well supported by Fenske-Hall MO calculations on the substitution series."*[5]

Below we shall provide an unsettling case where present computational methods fail to predict the strongly non-linear ligand electronic effects encountered in some mixed halide carbonyl complexes. So, from the viewpoint of a so-called "bench chemist", correlations of experimental data with calculated parameters may seem less convincing unless backed by a correlation of two or more *experimentally* determined properties, as in the previous example.

Sweeping linear relationships between measured E^o (d^5/d^6) potentials and stoichiometry (n = 0 to 6, in both examples) have been observed in organometallic $M(CO)_{6-n}(CH_3NC)_n$ species ($M = Cr^0, Mn^I$),[16-18] and also in classical inorganic $[RuX_{6-n}(CH_3CN)_n]^z$ complexes (X = Cl or Br, z = n - 3 for Ru^{III}).[19] Thus, on some occasions, ligand effects clearly do accumulate arithmetically over a wide range of stoichiometry.

In 1980, Chatt, Pickett and co-workers[20] devised a table of electrochemical P_L parameters for some twenty individual ligands, L, as exemplified in Table 1.1. These parameters are equated directly with the shift in the measured metal $Cr^{I/0}$ (d^5/d^6) electrode potential for a family of $Cr(CO)_5L$ complexes compared to $[Cr(CO)_6]$, according to equation [1]:

$$P_L = E^o[Cr^{I/0}(CO)_5L] - E^o[Cr^{I/0}(CO)_6] \qquad [1]$$

The real significance of the exercise is *this ranking of ligands turn out to be transferable* in an internally consistent way to the electrode potential shifts encountered for the same

series of ligands replacing one another on a different metal binding site. Thus one finds that, for a new family of complexes $[M_SL]$ (where M_S is an alternative conserved binding site), the electrode potentials are still linearly related to P_L:

$$E^o([M_SL]) = E_S + \beta P_L \qquad [2]$$

Here E_S and β are regarded as measures of the the *electron-richness* and *polarisability* respectively of a particular binding site M_S. It is an important attribute of this model that each different metal binding site is accorded a distinctive polarisability, and that this parameter acts in concert with the ligand P_L value to determine the resultant shift in E^o for the complex $[M_SL]$ as one ligand replaces another. More generally, it can be seen that a well-founded scheme which allows central ion redox potentials to be realistically estimated (especially where the complexes are unknown or the measurements impractical) will have wide use in areas such as new synthesis and may provide better understanding of the behaviour of active sites in bio-inorganic chemistry. In addition, a knowledge of the ligand effects on E^o makes possible rational "tuning" of the central metal-based redox potential, to improve the catalytic properties of transition metal complexes. For example, the Rh^{III}/Rh^{I} couple can be adjusted by modifying the ligand environment in order to improve the electro-catalytic efficiency of rhodium complexes in the hydride transfer process utilised for electrochemical regeneration of the reduced form of NAD cofactor (NADH).[21,22]

In 1990 Lever proposed a table of more than two hundred individual electrochemical ligand parameters, E_L, which could be used to systematise the redox couples for an almost limitless range of compounds.[23] According to this scheme, the E^o value for a given transition metal redox couple (*e.g.* Ru^{III}/Ru^{II}) should be linearly proportional to the sum of the E_L values of the coordinated ligands *for any permutation* of the 200 tabulated ligands:

$$E_{obs}(vs.\ \text{NHE}) = S_M[\Sigma E_L] + I_M \qquad [3]$$

Table 1.1 *Selected ligand P_L parameters.*[20] *The ligands, L, are arranged in order of the displacement of the $[Cr(CO)_5L]^{1+/0}$ couple from that of $[Cr(CO)_6]^{1+/0}$; see text.*

Ligand, L	Ligand P_L parameters, (V)
NO^+	+1.40
CO	0.00
$P(OPh)_3$	-0.18
PPh_3	-0.35
CH_3NC	-0.43
CH_3CN	-0.58
C_5H_5N (Py)	-0.59
NH_3	-0.77
Br^-	-1.17
Cl^-	-1.19
OH^-	-1.55

where S_M and I_M are constants for a given redox couple. Actually, S_M necessarily converges on unity for the $Ru^{III/II}$ couple because the original ligand E_L values were quantified largely by analysis of electrochemical data for numerous $[Ru(bipy)_2L_2]$ complexes. For the characteristic couples of other transition metal ions, we emphasise that S_M is expected to take a characteristic *constant* value, and, in particular, 1.01 is recommended as the universal value for $Os^{III/II}$ in non-aqueous media.[23]

Lever's equation [3] has the same algebraic form as the one proposed by Chatt, Pickett and co-workers (equation [2]). However, in a certain sense, Lever's additivity model may seem to be a step backwards from the earlier one. By asserting that shift in observed electrode potentials can be predicted from the appropriate tabulated E_L values *via* equation [3] for any combination or arrangement of ligands, one explicitly ignores the possibility of a different polarisability for the same metal ion in different binding sites. Thus, in its basic form, this model does not encompass differences in E^o between geometric isomers, or the possible non-linear accumulation of the ligand effects in some series of the type $[ML_{6-n}L'_n]$.

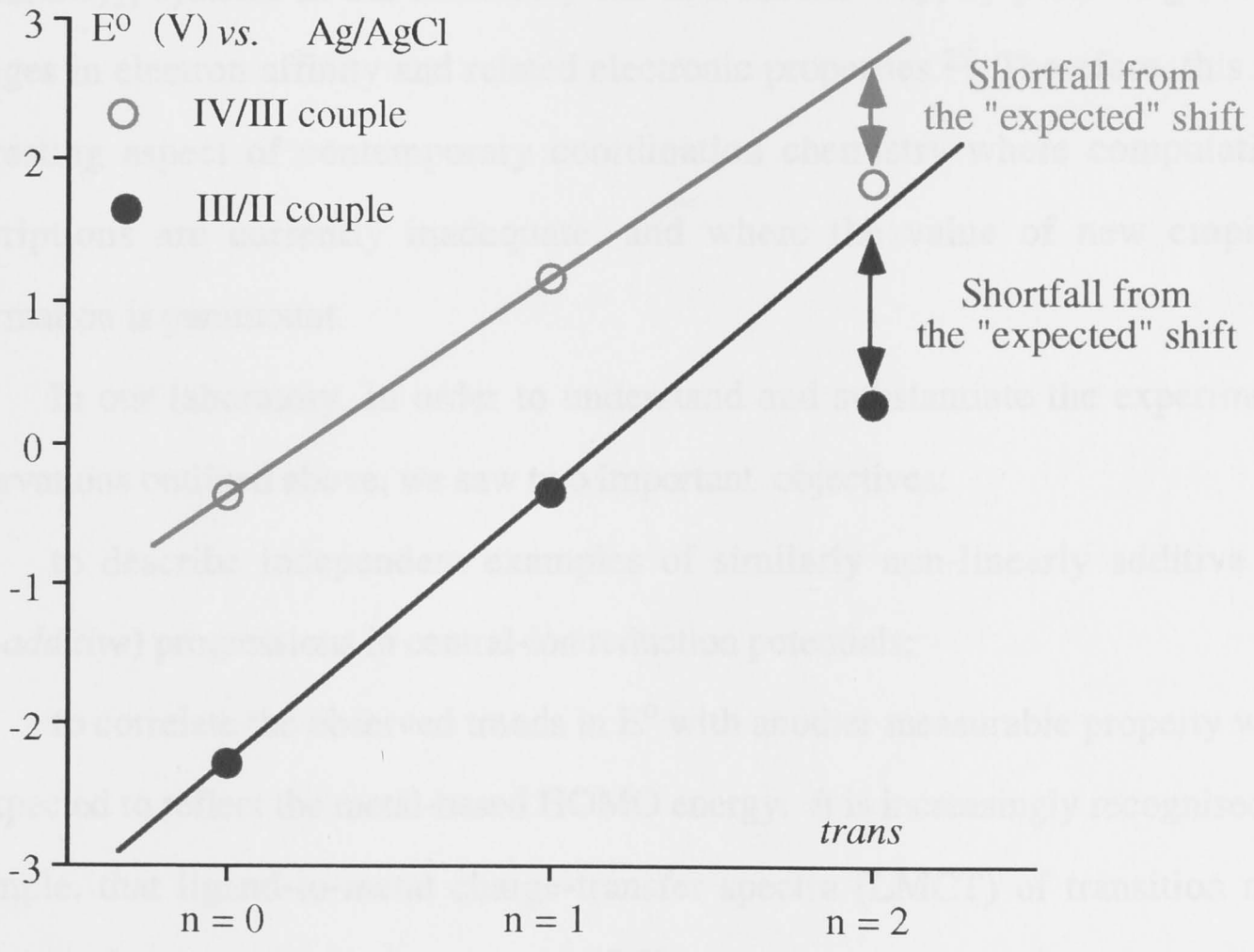

Figure 1.6 *A plot of the IV/III and III/II couples versus n for the series of* $[OsBr_{6-n}(CO)_n]^{z-}$ *complexes. Data from ref. 24.*

However, soon after these developments,[19, 23] Heath and Humphrey reported a strongly non-linear progression in the IV/III and III/II redox couples for a short series of mixed halide / carbonyl complexes of the form $[OsBr_{6-n}(CO)_n]^{z-}$ (n = 0, 1, *trans*-2), with the effect of the first halide replacement by CO being roughly *three times* greater than the second (Figure 1.6).[24] Irregular progressions in both couples also were found for the related three-membered *trans*-$[OsBr_4(CO)_{2-n}(RCN)_n]^{z-}$ family .

These experimental results are obviously inconsistent with Bursten's earlier prediction regarding the linear accumulation of the ligand effects, and with Lever's linear ligand additivity model as well(*vide supra*). It seemed that the non-additive effects are readily evident in substitutional series of complexes containing co-ligands with strongly contrasting electronic properties (*e.g.* π-donor halides in company with pronounced π-acceptor carbonyl ligands), but not when "like replaces like" as with the CO / RNC and halide / RCN series. It should be mentioned that high-quality density functional MO calculations performed comparatively on $[MX_6]$, $[MX_5(CO)]$ and *trans*-$[MX_4(CO)_2]$ systems in our laboratory fail in a similar way, by predicting uniform changes in electron affinity and related electronic properties.[25] Therefore, this is an interesting aspect of contemporary coordination chemistry where computational descriptions are currently inadequate, and where the value of new empirical information is paramount.

In our laboratory, in order to understand and substantiate the experimental observations outlined above, we saw two important objectives:

1) to describe independent examples of similarly non-linearly additive (*i.e. non-additive*) progressions in central-ion reduction potentials;

2) to correlate the observed trends in E^o with another measurable property which is expected to reflect the metal-based HOMO energy. It is increasingly recognised, for example, that ligand-to-metal charge-transfer spectra (LMCT) of transition metal complexes* can provide such a measure.[19, 26]

One of the main aims of the present work is to make a systematic study of the electronic properties of the mixed halide/nitrosyl complexes of ruthenium and osmium.

---

* The relation between the energies of charge-transfer transitions and the electrochemical parameters will be discussed at length in Chapters 3 and 4.

The nitrosyl ligand (NO^+) is a substantially stronger π-acceptor than CO. For example, its P_L factor is +1.40 V, which means that E^o for $[Cr^{I/0}(CO)_5(NO^+)]^{2+/+}$ is more positive by 1.40 V (!) than E^o for $[Cr^{I/0}(CO)_6)]^{+/0}$ (Table 1.1).[20] Hence, there is a real possibility of finding exaggerated non-linear ligand additivity effects in the halide nitrosyl complexes, which would be of considerable interest in themselves and perhaps shed further light on the previously uncovered carbonyl systems. The optical properties should also be strongly responsive to such effects, as noted above. In the case of the ruthenium nitrosyl complexes (at least), spectro-electrochemical stategies come into their own because of the spectroscopically informative oxidation state (Ru^{III}, d^5) is otherwise inaccessible.

Chapter 2 describes the necessary synthetic and structural studies of the ruthenium and osmium halide nitrosyl compounds. For example, it was important to demonstrate that the nitrosyl complexes under study contain a linear M-NO^+ moiety, rather than bent M-NO^-, as their electronic properties differ significantly. As might be expected, some effort was required to develop reliable routes even to certain long-known compounds, and other compounds of strategic importance were previously unknown. For voltammetric and spectro-electrochemical studies in non-aqueous solvents on anionic complexes, there is the additional need to isolate the material with a suitable counter-cation, such as $[Bu^n_4N]^+$ or $[BzPh_3P]^+$, to ensure organosolubility. In the case of the nitrosyl complexes, we found this requires some finesse, perhaps because the increased lability of any ligand coordinated *trans* to NO^+. In any event, some progress has been made in extending and systematising this area of synthesis.

Chapter 3 describes the electrochemical and spectro-electrochemical characterisation of these ruthenium and osmium nitrosyl complexes, and compares the collected electrochemical and spectral data with those of analogous $[MX_5L]^{z-}$ and *trans*-$[MX_4LL']^{z-}$ complexes measured in our laboratory (where L = CO, PR_3, CH_3CN, *etc.*). The relationship between E^o values varying across a very wide range (*ca.* 3 V) and the ligand-to-metal charge-transfer band energies for arrays of both chloride and bromide complexes are established. The additivity of ligand effects in

particular species such as *trans*-$[Os^{III}Br_4(CH_3CN)(CO)]^{1-}$ and newly prepared *trans*-$[Os^{II}Br_4(CH_3CN)(NO^+)]^{1-}$ provide further insight.

The second broad aspect of the present work, described in Chapter 4, is the study of an orderly family of *bis*-acetylacetonato complexes of the form $[M(acac)_2LL']$ (where M = Ru, Os; L = Cl, $N(CH_3)_3$, CH_3CN, PPh_3, *etc.*), including a significant number of *cis/trans* isomeric pairs. This was prompted by some earlier observations within the group (in collaboration with Professor M.A. Bennett),[27] which revealed there could be a significant difference in E^o values for the *cis* and *trans* isomeric forms for relatively moderate π-acid ligands such as L = PPh_3 or Bu^tNC. Since Lever's linear ligand addivity model does not distinguish between the different geometric isomers (*vide supra*), it is important to determine the extent to which the experimentally observed ligand effects depend on the ligand arrangement. For this purpose, we analyse in some detail the electronic properties of the *cis* and *trans bis*-acetylacetonato complexes of ruthenium and osmium. The relationship between measured E^o values and Lever's E_L electrochemical parameters has been tested, and the behaviour of the observed charge-transfer bands (both acac to metal, and metal to acac) is also examined.

The classical β-diketonate ligand system is of considerable importance in many areas of coordination chemistry, yet in electronic terms it is by no means "innocent". It has been very interesting in the course of this work to see whether the strategies developed to measure and interpret ligand additivity effects on simpler systems (as in Chapter 3) were equally productive for $\{M(acac)_2\}$ binding sites.

In 1991, lack of the appropriate test compounds prevented Heath and Duff from analysing *cis*-analogues of their instructive *trans*-$[RuX_4(RCN)_2]^{1-}$ complexes for isomer-sensitive effects on the redox couples.[19] However, the osmium bromide analogue was isolated in the course of the present work. Appendix 1 investigates the comparative electrochemistry of the *cis* and *trans*-$[OsBr_4(L)_2]^{z-}$ complexes, with L = CH_3CN and CO, in the light of the information gained for the *cis* and *trans* $\{M(acac)_2\}$ systems described in Chapter 4.

Finally, although beyond the scope of this thesis, the recent, extraordinary developments regarding the critical physiological and biochemical roles played by NO as a ubiquitous neuro-transmitter and electron-transfer agent must be mentioned. Many of these findings immediately pre-date or coincide with the present study. They have been have been reviewed from a biochemical viewpoint.[28] At present, venerable sodium nitroprusside, $Na_2[Fe(CN)_5(NO)]$, is widely used clinically as a blood-pressure lowering agent. There must be the prospect of informed development of new metallo-nitrosyl agents for *in-vivo* NO delivery, both to aid physiological research and for therapeutic use.[28] One promising line of current research involves photochemically induced dissociation of NO, and might be used specifically to target hard tumours. In these circumstances, the efforts made in Chapter 3 to accurately rank the influence of coordinated NO^+ on the optical and redox properties of its transition metal complexes seem very timely.

References

1. Nekrasov, B.V. *Osnovy obshchei khimii (The Fundamentals of General Chemistry),* 2nd ed., Khimiya, Moscow **1969**; *vol. 1*, a) 16; b) 216
2. Werner, A., Miolati, A. *Z. phys. Chem.* **1894**, *14*, 506
3. Jørgensen, C.K. *Absoption Spectra and Chemical Bonding in Complexes, 2nd ed.*, Pergamon Press, Oxford, **1964**, Ch. 7
4. Golovin, M.N., Rahman, M.M., Belmonte, J.E., Giering, W.P. *Organometallics* **1985**, *4*, 1981
5. Bursten, B.E., Green, M.R. *Prog. Inorg. Chem.* **1988**, *36*, 393 and references therein
6. Nakamoto, K. *Infrared and Raman Spectra of Inorganic and Coordination Compounds, 4th ed.*, Wiley-Intersience, New York, **1986**, 291
7. Tolman, C.A. *J. Am. Chem. Soc.* **1970**, *92*, 2953
8. Cotton, F.A., Kraihanzel, C.S., *J. Am. Chem. Soc.* **1962**, *84*, 4432
9. Sarapu, A.C., Fenske, R.F. *Inorg. Chem.* **1975**, *14*, 247
10. Bonder, G.M. *Inorg. Chem.* **1975**, *14*, 2694
11. Prenzler, P.D., Heath, G.A, Lee, S.B., Raptis, R.G. *J. Chem. Soc., Chem. Commun.* **1996**, submitted for publication
12. Flurry, R.L.Jr. *Quantum Chemistry: An Introduction*, Prentice-Hall, Englewood Cliffs, New Jersey, **1983**, Section 7.10
13. Aynetchi, S., Hitchcock, P.B., Seddon, E.A., Seddon, K.R., Yousif, Y.Z., Zora, J.A., Stuckey, K. *Inorg. Chim. Acta* **1986**, *113*, L7
14. Bursten, B.E., Green, M.R., Katovic, V., Kirk, J.R., Lightner, D.Jr. *Inorg. Chem.* **1986**, *25*, 831
15. Hall, M.B., Fenske, R.F. *Inorg. Chem.* **1972**, *11*, 768
16. Treichel, P.M., Dirreen, G.E., Mueh, H.J. *J. Organomet. Chem.* **1972**, *44*, 339
17. Conner, J.A., Jones, E.M., McEwen, G.K., Lloyd, M.K., McCleverty, J.A. *J. Chem. Soc., Dalton Trans.* **1972**, 1246

18. Pickett, C.J., Pletcher, D. *J. Organomet. Chem.* **1975**, *102*, 327

19. Duff, C.M., Heath, G.A. *Inorg. Chem.* **1991**, *30*, 2528

20. Chatt, J., Kan, C.T., Leigh, G.J., Pickett, C.J., Stanley, D.R. *J. Chem. Soc., Dalton Trans.* **1980**, 2032

21. Ruppert, R., Herrmann, S., Steckhan, E. *J. Chem. Soc., Chem. Commun.* **1988**, 1150

22. Ryabov, A.D., Menglet, D., Levi, M.D. *J. Organomet. Chem.* **1991**, *421*, C16

23. Lever, A.B.P. *Inorg. Chem.* **1990**, *29*, 1271

24. Heath, G.A., Humphrey, D.G. *J. Chem. Soc., Chem. Commun.* **1991**, 1668

25. Macgregor, S.A. *Personal communication*

26. Lever, A.B.P. *Inorganic Electronic Spectroscopy, 2nd edn.*, Elsevier, Amsterdam, **1984**

27. Wallace, L. *Ph.D. Thesis* A.N.U.,Canberra, **1991**, Ch. 5

28. Clarke, M.J., Gaul, J.B., *Structure and Bonding* **1993**, *81*, 147

Chapter 2

Synthesis and Structure of Ruthenium and Osmium Mixed Halide Nitrosyl Complexes

As outlined in the introductory chapter, non-linear ligand additivity effects have been previously observed in coordination compounds containing carbonyl ligands, which are strong π-acceptors. The nitrosyl ligand has even stronger π-acceptor properties, which is why we are interested in NO-containing complexes. In this chapter we first survey aspects of the synthesis and reactions of ruthenium and osmium mixed halide nitrosyls, including recent developments in our laboratory. Finally, we discuss their structures and the nature of bonding of the nitrosyl moiety in these complexes.

2.1 Halo-nitrosyl Complexes - A Review

Various methods of preparation of transition metal nitrosyl complexes are extensively reviewed in the chemical textbooks,[1] as well as in the original literature.[2,3] We shall restrict ourselves to a brief survey of the synthesis mainly of "binary" nitrosyl-halide complexes of ruthenium and osmium, which are limited in number.

The formation of nitric oxide complexes is a well known feature of the coordination chemistry of ruthenium. Ruthenium compounds that have been in contact with NO, NO_2 or nitric acid should be suspected of incorporating a nitrosyl moiety. In fact, one might inadvertently prepare a nitrosyl complex from often impure commercial ruthenium trichloride. Thus a nitrosyl derivative of bis-dithio-acetylacetonato ruthenium was synthesised from a "$Ru(NO)Cl_3$" contaminated starting material.[4]

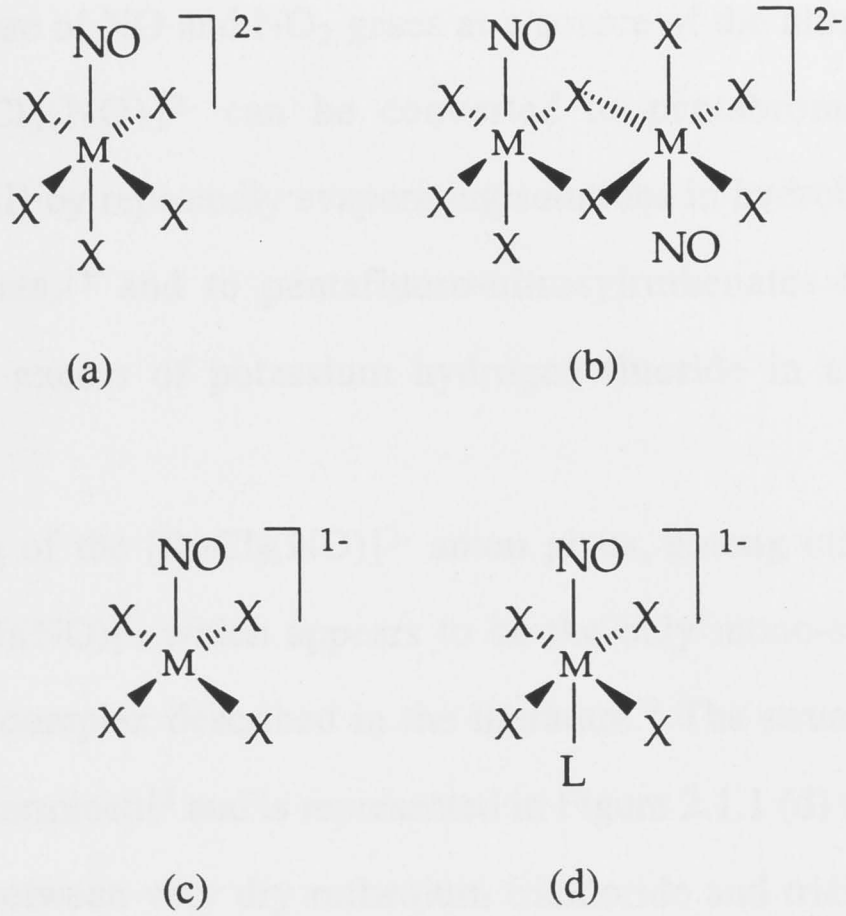

Figure 2.1.1 *The structural formulae of various divalent nitrosyl-halide complexes (M = Ru or Os; X = halide): (a) $[MX_5(NO)]^{2-}$; (b) dimeric edge-sharing $[M(NO)X_4]_2^{2-}$; (c) square pyramidal complex $[MX_4(NO)]^-$; (d) tetragonal tetrahalo-nitrosyl complex $[MX_4(NO)(L)]^-$, L is a neutral ligand. Trivalent forms, where known, are described in the text.*

Purple crystalline potassium pentachloro-nitrosylruthenate(II) was prepared for the first time in the middle of the last century by C.C. Claus, the discoverer of ruthenium, by fusing ruthenium metal with a mixture of KOH and KNO_3 followed by dissolution in hydrochloric acid, evaporation to minimal volume and subsequent precipitation of the crystals by adding a concentrated KCl solution.[5,6] Claus, however, thought these crystals to be "$RuCl_4$•2KCl." A compound of this formulation would have a very similar metal content to $K_2[RuCl_5(NO)]$. It was not until 1888 that A. Joly[7,8] proved the compound to be "$RuCl_3$(AzO), 2KCl".* Joly also prepared the compound by adding HCl to a solution containing ruthenium trichloride and potassium nitrite.[7] A number of routes to $[RuCl_5(NO)]^{2-}$ salts have since become known and the structure established as 2.1.1 (a).[9] A convenient method described by J.M. Fletcher *et*

* "Az" stands for nitrogen (*azote*) making the formulation equivalent to $K_2[RuCl_5(NO)]$

al. utilises a mixture of NO and NO_2 gases as a source of the nitrosyl moiety.[10] Once synthesised, $[RuCl_5(NO)]^{2-}$ can be converted to pentabromo- and penta-iodo-nitrosylruthenate(II) by repeatedly evaporating solutions in hydrobromic or hydroiodic acid, as appropriate,[11] and to pentafluoro-nitrosylruthenates by fusing it with a three-to-five fold excess of potassium hydrogen fluoride in a nickel or platinum crucible.[12,13]

Hydrolysis of the $[RuCl_5(NO)]^{2-}$ anion gives, among other aqua complexes, *trans*-$[RuCl_4(H_2O)(NO)]^-$, which appears to be the only mono-substituted tetragonal tetrahalo-nitrosyl complex described in the literature.[9] The structure of this complex anion has been determined[14] and is represented in Figure 2.1.1 (d) (L = H_2O).

Reaction between very dry ruthenium trichloride and trichloronitromethane is reported to yield polymeric $[Ru(NO)Cl_3]_x$.[15] A dimeric ruthenium nitrosyl-halide complex, featuring an edge-sharing molecule $[Ru(NO)Cl_4]_2^{2-}$ (Figure 2.1.1, (b)), is also described in the literature. The complex was prepared from $[Ru(NO)Cl_3]_x$ by addition of triphenylmethyl phosphonium chloride in dichloromethane and isolated as a triphenylmethyl phosphonium salt.[15] The dimer was characterised by elemental analysis, IR-spectroscopy, and its crystal structure was determined from X-ray diffraction data. Another poorly characterised and possibly impure compound, proposed to have a binuclear formulation $K_3[Ru_2(NO)_2Cl_9]$,* was reported as a product of $[Ru(NO)Cl_3(H_2O)_2]$ in HBr in the presence of $SnCl_2$.[16]

Though osmium nitrosyl chemistry is not as extensive as that of ruthenium, a number of osmium halo-nitrosyl complexes have been isolated and characterised.[17] The first complexes of the type $[OsX_5(NO)]^{2-}$ (X = Cl, Br, I) can be found in the literature as early as 1903,[18] when they were prepared by the action of the appropriate hydrohalic acid on salts of $[Os(NO)(OH)(NO_2)_4]^{2-}$. Alternative routes to such complexes have been discovered,[17,18] even for X = F.[19] In 1991, Bhattacharyya *et al.* reported another preparation of pentahalo-nitrosylosmate(II) salts by treating bisoxalato-nitrosylosmate(II) with hot concentrated hydrohalic acid.[20] Recently, in our laboratory, a $[Os^{III}Cl_5(NO)]^-$ salt was synthesised by using Ag^+ to abstract chloride from a

---

* This product might well be $K_2[Ru(NO)Cl_4]_2 \cdot KCl$.

1,2-dichloromethane solution of hexachloro-osmate(IV) in the presence of nitrosonium hexachlorophosphate.[21] Reduction of the metal from the oxidation state IV to III is apparently spontaneous. The relevant complex however was not isolated at that stage, but further reduced *in situ* by tetrabutylammonium borohydride to $[OsCl_5(NO)]^{2-}$. The monomeric square pyramidal $[OsCl_4(NO)]^{1-}$ complex has been also reported (Figure 2.1.1, (c)).[22] It makes an interesting contrast to the dimeric ruthenium complex of the same empirical formula (*vide supra*).

It is possible, using oxidation by lead dioxide of the $[OsX_5(NO)]^{2-}$ salts, to prepare and isolate pentahalide complexes containing the $Os(NO)^{4+}$ moiety.[23] On the contrary, the corresponding $[RuCl_5(NO)]^{1-}$ is unstable at ambient temperature and can be only prepared by electrochemical oxidation of the familiar $[RuCl_5(NO)]^{2-}$ complex in a chilled solution.[24]

2.2 Synthesis and Characterisation of Halo-nitrosyl Complexes - Present Work

Our objective was to study metal halide nitrosyl tetragonal complexes, so a family of such complexes was prepared from the appropriate starting materials. As further electrochemical and spectroscopic studies were to be carried out in non-aqueous media (*e.g.* dichloromethane, acetonitrile), the complexes, which are all anionic, had to be isolated as organosoluble salts. These derivatives incorporate such counter-cations

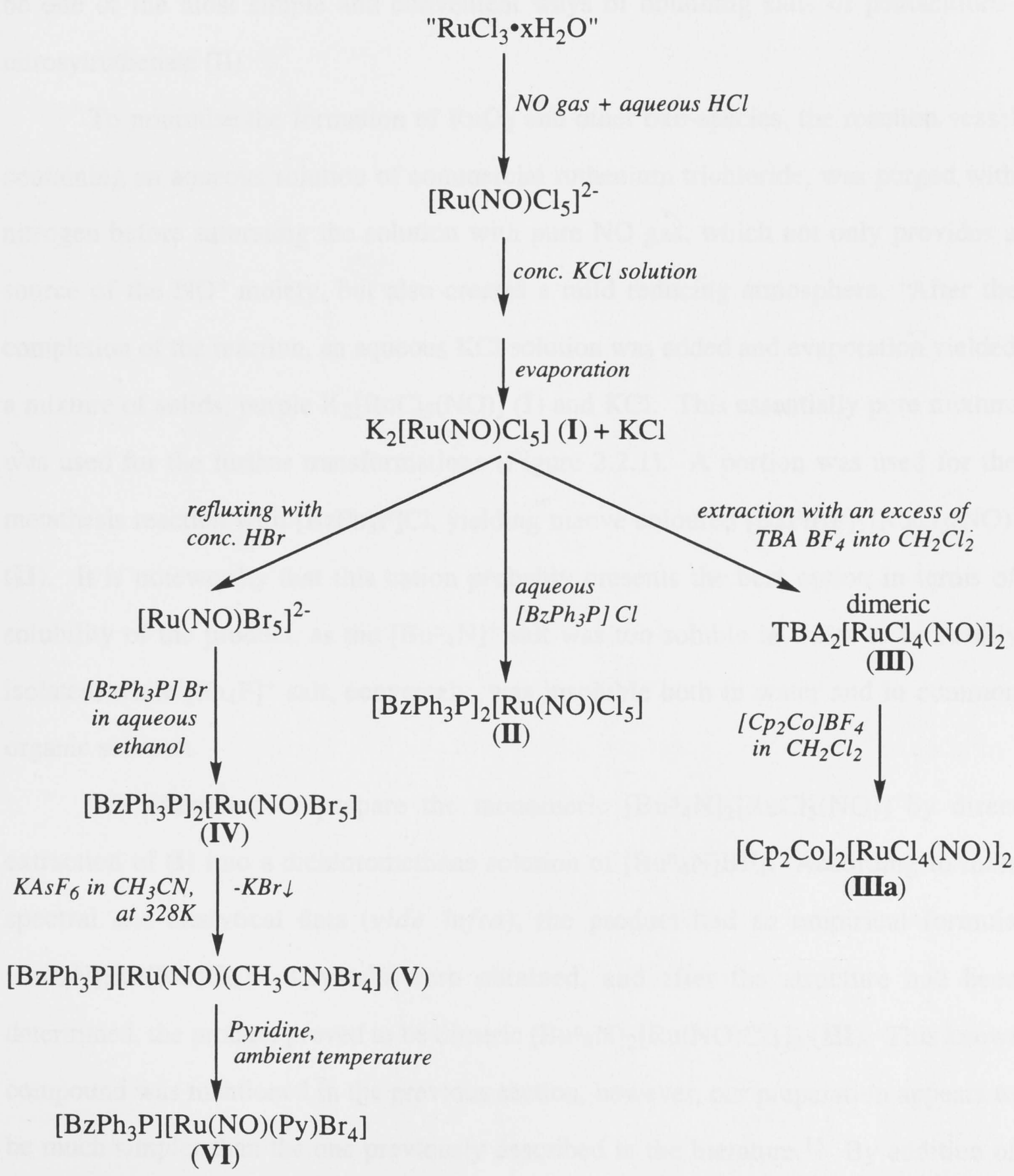

Figure 2.2.1 *Preparative routes to various ruthenium halo-nitrosyl complexes*

as tetra-n-butylammonium ($[Bu^n_4N]^+$), tetraphenylphosphonium ($[Ph_4P]^+$) or benzyltriphenylphosphonium ($[BzPh_3P]^+$).

As outlined in the previous section, there are a number of preparatory routes to ruthenium and osmium halo-nitrosyl complexes. Thus we were able to use literature methods as a basis for the synthesis of some of the compounds discussed here, although in many cases, these methods were modified in the light of our experience. The synthetic routes to ruthenium complexes adopted in our laboratory are schematically shown in Figure 2.2.1. The method described by Fletcher *et al.*[10] (*vide supra*) seems to be one of the most simple and convenient ways of obtaining salts of pentachloro-nitrosylruthenate (II).

To minimise the formation of RuO_2 and other oxo-species, the reaction vessel containing an aqueous solution of commercial ruthenium trichloride, was purged with nitrogen before saturating the solution with pure NO gas, which not only provides a source of the NO^+ moiety, but also creates a mild reducing atmosphere. After the completion of the reaction, an aqueous KCl solution was added and evaporation yielded a mixture of solids, purple $K_2[RuCl_5(NO)]$ (**I**) and KCl. This essentially pure mixture was used for the further transformations (Figure 2.2.1). A portion was used for the metathesis reaction with $[BzPh_3P]Cl$, yielding mauve coloured $[BzPh_3P]_2[RuCl_5(NO)]$ (**II**). It is noteworthy that this cation probably presents the best option in terms of solubility of the product, as the $[Bu^n_4N]^+$ salt was too soluble in water to be readily isolated, while $[Ph_4P]^+$ salt, conversely, was insoluble both in water and in common organic solvents.

We attempted to prepare the monomeric $[Bu^n_4N]_2[RuCl_5(NO)]$ by direct extraction of (**I**) into a dichloromethane solution of $[Bu^n_4N]BF_4$. According to mass spectral and analytical data (*vide infra*), the product had an empirical formula $[Bu^n_4N][Ru(NO)Cl_4]$. Crystals were obtained, and after the structure had been determined, the product proved to be dimeric $[Bu^n_4N]_2[Ru(NO)Cl_4]_2$ (**III**). This known compound was mentioned in the previous section, however, our preparation appears to be much simpler than the one previously described in the literature.[15] By addition of

$[CoCp_2]BF_4$ to dichloromethane solution of (**III**), the cobaltocenium salt (**IIIa**) was obtained.

Another portion of the mixture of (**I**) and KCl was repeatedly recrystallised with hot concentrated HBr to give, on addition of $[BzPh_3P]Br$ or $[Bu^n{}_4N]Br$, the corresponding salts of $[RuBr_5(NO)]^{2-}$ (compounds (**IV**) and (**IVa**)* respectively). The new *trans*-substituted bromo complexes (**V**) and (**VI**) were prepared, as shown in Figure 2.2.1. We discovered that the chloro complexes do not undergo *trans*-substitution reactions as easily as their bromo analogues, and complexes of the formula $[RuCl_4(L)(NO)]^{1-}$ could not be prepared.

We have already mentioned that in 1990 in this laboratory D.G. Humphrey prepared $[Os^{II}Cl_5(NO)]^{2-}$ complex in two steps from hexachloroosmate(IV) according to the scheme:

$$[Os^{IV}Cl_6]^{2-} \xrightarrow[CH_2Cl_2]{NOPF_6,\ Ag^+} [Os^{III}Cl_5(NO)]^{1-} + AgCl\downarrow$$

$$[Os^{III}Cl_5(NO)]^{1-} \xrightarrow[CH_2Cl_2]{BH_4^-} [Os^{II}Cl_5(NO)]^{2-}$$

This method was conceptually a new one, as the halide array is already assembled around the metal centre in this case, before the nitrosyl moiety is introduced. A certain disadvantage of this route is the metal's spontaneous lowering of oxidation state from IV to III during the first step with no apparent reducing agent present. On the contrary, NO^+ (derived from $NOPF_6$) creates quite an oxidising environment. Therefore it would be beneficial to use NO gas instead (*vide supra*). Another useful modification of the method would be the use of $[Os^{IV}X_5(thf)]^-$ precursor (X = Cl or Br), since such complexes are known to have an extremely labile tetrahydrofuran ligand,[21] which could be readily substituted *in situ* by other ligands. These strategies both proved worthwhile. The osmium(III) nitrosyl complexes were further reduced to their divalent forms *in situ* by an appropriate tetrahydroborate salt. This is advisable because the very

* This compound is not shown in figure 2.2.1

Table 2.2.1 *The results of the elemental analysis*

Compounds	Empirical formulae	Mass %, Found (Calculated)			
		C	H	N	halogen
$[BzPh_3P]_2$ $[RuCl_5(NO)]$ (**II**)	$C_{50}H_{44}P_2RuCl_5NO$	60.02 (59.16)	4.59 (4.37)	1.35 (1.38)	17.86 (17.64)
$[BzPh_3P]_2$ $[RuBr_5(NO)]$ (**IV**)	$C_{50}H_{44}P_2RuBr_5NO$	47.89 (48.53)	3.32 (3.58)	1.15 (1.13)	32.04 (32.29)
$[Bu^n{}_4N]_2$ $[RuBr_5(NO)]$ (**IVa**)	$C_{32}H_{72}N_3RuBr_5O$	37.46 (37.85)	7.45 (7.15)	4.08 (4.14)	39.59 (39.34)
$[BzPh_3P]$ $[RuBr_4(CH_3CN)(NO)]$ (**V**)	$C_{27}H_{25}PRuBr_4N_2O$	38.68 (38.37)	2.96 (2.98)	3.09 (3.31)	38.18 (37.82)
$[BzPh_3P]$ $[RuBr_4(Py)(NO)]$ (**VI**)	$C_{30}H_{27}PRuBr_4N_2O$	40.55 (40.80)	2.90 (3.08)	3.10 (3.17)	36.38 (36.19)
$[Bu^n{}_4N]_2$ $[Ru(NO)Cl_4]_2$ (**III**)	$C_{32}H_{72}N_4Ru_2Cl_8O_2$	36.72 (37.35)	6.98 (7.06)	5.79 (5.45)	27.43 (27.21)
$[CoCp_2]_2$ $[Ru(NO)Cl_4]_2$ (**IIIa**)	$C_{20}H_{20}Co_2N_2Ru_2Cl_8O_2$	26.69 (26.00)	2.27 (2.18)	2.72 (3.03)	30.39 (30.69)
$[BzPh_3P]_2$ $[OsCl_5(NO)]$ (**VII**)	$C_{50}H_{44}P_2OsCl_5NO$	54.82 (54.38)	3.61 (4.02)	1.21 (1.27)	–
$[BzPh_3P]_2$ $[OsBr_5(NO)]$ (**VIII**)	$C_{50}H_{44}P_2OsBr_5NO$	44.60 (45.27)	3.33 (3.34)	0.94 (1.06)	–
$[BzPh_3P]$ $[OsBr_4(CH_3CN)(NO)]$ $\bullet 0.5\ (C_6H_6)$ (**IX**)	$C_{30}H_{27}POsBr_4N_2O$	37.17 (37.06)	2.70 (2.80)	2.73 (2.88)	–

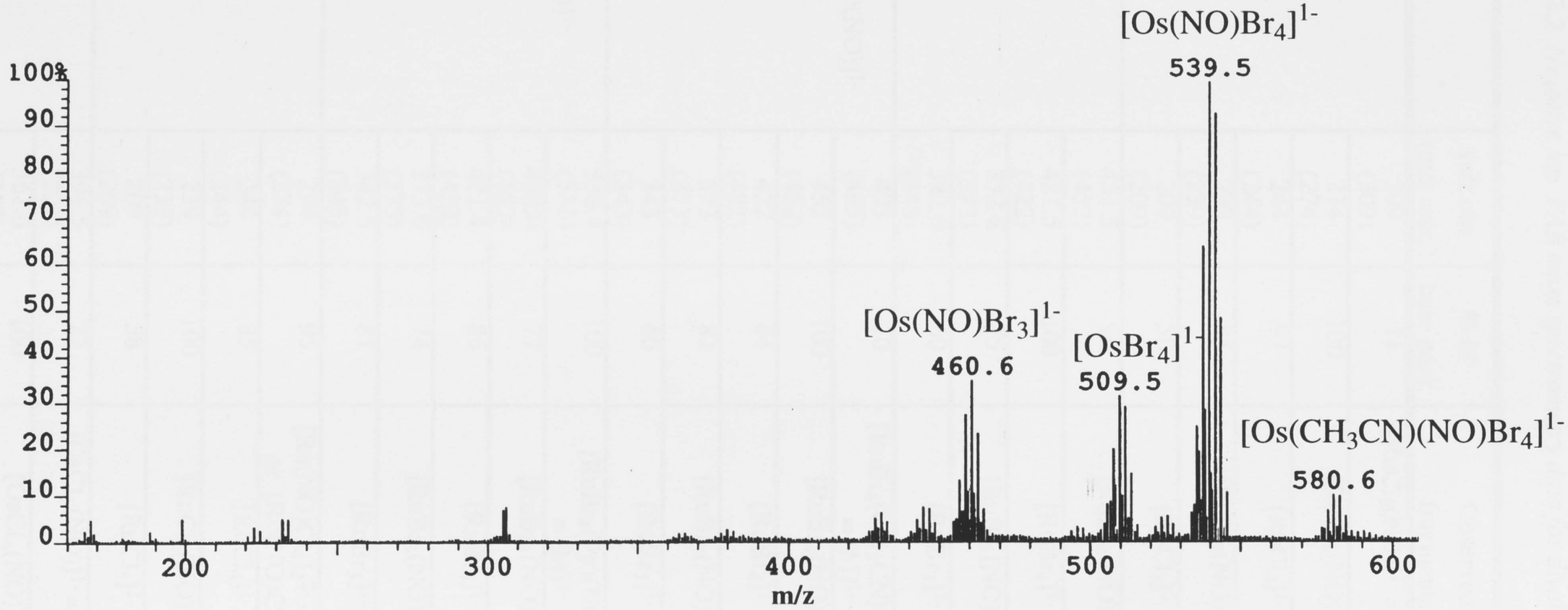

Figure 2.2.2 *Negative ion Fast Atom Bombardment (FAB) mass-spectrum of $[OsBr_4(CH_3CN)(NO)]^{1-}$ complex anion.*

Table 2.2.2 *Negative ion FAB mass spectrometry data for divalent complexes.*

Complex anion	m/z obs. (m/z calc.)	% of base peak	Observed fragments
$[RuCl_5(NO)]^{2-}$	309 (309)	11	$[RuCl_5(NO)]^{1-} = [M]^{1-}$
	274 (274)	100	$[RuCl_4(NO)]^{1-}$
	244 (244)	97	$[RuCl_4]^{1-}$
	239 (239)	85	$[RuCl_3(NO)]^{1-}$
	209 (209)	50	$[RuCl_3]^{1-}$
$[RuBr_5(NO)]^{2-}$	451.5 (452)	90	$[RuBr_4(NO)]^{1-}$
	421.5 (422)	100	$[RuBr_4]^{1-}$
	372.6 (373)	75	$[RuBr_3(NO)]^{1-}$
	342.6 (343)	60	$[RuBr_3]^{1-}$
$[RuBr_4(CH_3CN)(NO)]^{1-}$	493 (493)	10	$[RuBr_4(CH_3CN)(NO)]^{1-} = [M]^{1-}$
	452 (452)	100	$[RuBr_4(NO)]^{1-}$
	422 (422)	64	$[RuBr_4]^{1-}$
	373 (373)	83	$[RuBr_3(NO)]^{1-}$
	343 (343)	60	$[RuBr_3]^{1-}$
$[RuBr_4(Py)(NO)]^{1-}$	530.4 (531)	100	$[RuBr_4(Py)(NO)]^{1-} = [M]^{1-}$
	452.0 (452)	77	$[RuBr_4(NO)]^{1-}$
	421.4 (422)	86	$[RuBr_4]^{1-}$
	373.0 (373)	74	$[RuBr_3(NO)]^{1-}$
	342.5 (343)	81	$[RuBr_3]^{1-}$
$[Ru(NO)Cl_4]_2^{2-}$	274 (274)	95	$[Ru(NO)Cl_4]_2^{2-} = [M]^{2-}$ or $[Ru(NO)Cl_4]^{1-}$
	244 (244)	85	$[RuCl_4]^{1-}$
	239 (239)	100	$[RuCl_3(NO)]^{1-}$
	209 (209)	58	$[RuCl_3]^{1-}$
$[OsCl_5(NO)]^{2-}$	396.5 (397)	27	$[OsCl_5(NO)]^{1-} = [M]^{1-}$
	361.6 (362)	100	$[OsCl_4(NO)]^{1-}$

Table 2.2.2 (cont.)

Complex anion	m/z obs. (m/z calc.)	% of base peak	Observed fragments
$[OsBr_5(NO)]^{2-}$	620 (621)	31	$[OsBr_5(NO)]^{1-} = [M]^{1-}$
	590 (591)	34	$[OsBr_5]^{1-}$
	539 (540)	100	$[OsBr_4(NO)]^{1-}$
	509 (510)	62	$[OsBr_4]^{1-}$
	458 (461)	47	$[OsBr_3(NO)]^{1-}$
$[OsBr_4(CH_3CN)(NO)]^{1-}$	580.6 (581)	11	$[OsBr_4(CH_3CN)(NO)]^{1-} = [M]^{1-}$
	539.5 (540)	100	$[OsBr_4(NO)]^{1-}$
	509.5 (510)	31	$[OsBr_4]^{1-}$
	460.6 (461)	33	$[OsBr_3(NO)]^{1-}$

positive III/II couples make work-up of osmium (II) far more convenient. The synthetic procedure used is summarised below (for X = Cl or Br):

$$\text{The 1}^{st}\text{ step} \quad [Os^{IV}X_6]^{2-} \xrightarrow[\substack{50\%\ thf,\\ 50\%\ CH_2(Cl)CH_2Cl}]{Ag[CF_3SO_3]} [Os^{IV}X_5(thf)]^{1-} + AgCl_{\downarrow}$$

$$\text{The 2}^{nd}\text{ step} \quad [Os^{IV}X_5(thf)]^{1-} \xrightarrow[CH_2Cl_2]{NO\ gas} [Os^{III}X_5(NO)]^{1-}$$

$$\text{The 3}^{rd}\text{ step} \quad [Os^{III}X_5(NO)]^{1-} \xrightarrow[CH_2Cl_2]{BH_4^-} [Os^{II}X_5(NO)]^{2-}$$

Both chloro (**VII**) and bromo (**VIII**) complexes were isolated as $[BzPh_3P]^+$ salts. While the first step is an overnight reaction, the second and third are complete within a few

minutes. It has to be emphasised that the above reactions must be carried out under dry nitrogen gas.

Previously unreported $[OsBr_4(CH_3CN)(NO)]^{1-}$ (**IX**) was prepared by solvolysis of the corresponding pentahalo-nitrosyl complex (**VIII**) in acetonitrile in the presence of $Ag[CF_3SO_3]$:

$$[Os^{II}Br_5(NO)]^{2-} \xrightarrow[CH_3CN]{Ag[CF_3SO_3]} [Os^{II}Br_4(CH_3CN)(NO)]^{1-} + AgBr_{\downarrow}$$

Neither for ruthenium nor for osmium did we succeed in synthesising a chloro analogue. This result is supported by a report of the five-coordinate $[OsCl_4(NO)]^-$ complex, which *does not react with acetonitrile*.[22] The difference between the bromo and chloro complexes is a subject of ongoing chemical investigation and theoretical calculations.[25]

All the complexes prepared were characterised by elemental analysis. These results are presented in Table 2.2.1. Negative ion fast atom bombardment (FAB) mass spectrometry results for the divalent complexes are presented in the Table 2.2.2. Previous mass spectral studies[21] indicated that mono-substituted halide complexes of osmium(III) $[OsX_5(L)]^{1-}$ often do not produce molecular ion peaks. It is worth noting that every complex studied here, with the exception of $[RuBr_5(NO)]^{2-}$, revealed the molecular ion peak. Most of them are relatively low in intensity, however, the spectrum of $[RuBr_4(Py)(NO)]^{1-}$ shows a strong molecular ion peak, perhaps indicating the exceptional stability of this species.

Available crystal structures and the IR and EPR-spectra are examined in the following section, while the electrochemistry and UV/VIS spectra will be discussed in the next chapter.

2.3 The Metal Nitrosyl Moiety - Aspects of Structure and Bonding

Before one can contemplate the influence of a nitrosyl ligand on a given metal centre, it is necessary to determine the NO coordination mode, as it is well known that this can vary from a linear positively charged NO^+ group,* with a triple N-O bond, to a bent negatively charged NO^- group, with an effective double N-O bond (Figure 2.3.1).[1,28] The binding mode of a nitrosyl ligand is of critical importance to its additive contribution to the observed E^o values and other properties of a given nitrosyl complex. Knowledge of geometry (*cis* or *trans*) of the hitherto unreported complexes $[MBr_4(NO)(L)]^{1-}$ is also necessary for further analysis of their electronic properties.

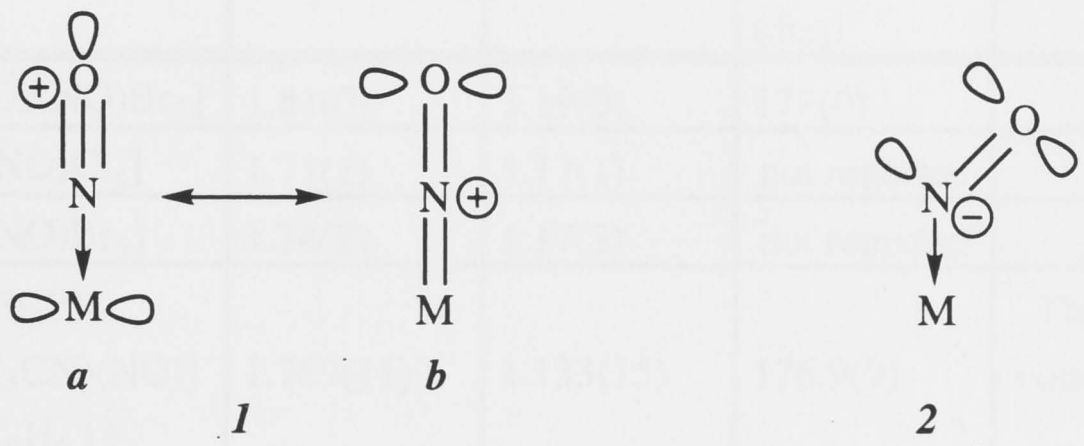

Figure 2.3.1 *Lewis structures of linear (**1**) and bent (**2**) nitrosyl moiety. Linear nitrosyl (**I**) is represented by two resonance structures (**1a** and **1b**): the greater the contribution of the structure **1b**, the greater the extent of π-backbonding. The formal charge on the linear NO is +1. Bending of NO (**2**) completely withdraws an electron pair from the metal, making a formal charge of -1 on the nitrosyl .*

Halo-nitrosyl complexes of ruthenium and osmium are known to contain a linear NO^+ moiety with a formal triple bond.[20,29,30,31] The crystal structures of the triphenylbenzylphosphonium salts of $[OsBr_4(CH_3CN)(NO)]^{1-}$, $[RuBr_4(CH_3CN)(NO)]^{1-}$

---

* As a ligand, NO^+ is isoelectronic to CO and formally acts as a "2-electron σ-donor, 2-electron π-acceptor." It is important to understand, however, that the local charge on a nitrosyl group (as determined by X-ray photoelectron spectroscopy) could be close to zero or even negative due to extremely strong π-backbonding (ref. 26, 27). Therefore in calling the ligand NO^+ we merely attribute a formal charge of +1, in order to emphasise electronic similarities with the carbonyl ligand.

and $[RuBr_4(Py)(NO)]^{1-}$ (compounds (**V**), (**VI**) and (**IX**)) were determined by X-ray diffraction.* Determining precise geometric data for nitrosyl complexes is usually not an easy task. Both the relatively large thermal wagging motion of the oxygen atom of the NO group and crystallographic disorder may contribute to the shortening of the apparent bond length.[28,32] The geometry of the complexes however was determined

Table 2.3.1 *Structural characteristics of NO moiety in the studied and related halo-nitrosyl complexes.**

Compound	M-N , Å	N-O , Å	M-N-O (deg)	Source
$[HPhen]_2\,[Os(NO)Br_5]$	1.81(0)	1.19(0)	172(0)	20
$K_2\,[Os(NO)Cl_5]$	1.71(1)	1.17(1)	not reported	34
$K_2\,[Os(NO)Br_5]$	1.74(2)	1.17(3)	not reported	34
$[BzPh_3P]$ $[OsBr_4(CH_3CN)(NO)]$ $\bullet 0.5\,(C_6H_6)$ [a]	1.769(11)	1.133(15)	176.9(9)	This work complex **IX**
$(NH_4)_2\,[Ru(NO)Cl_5]$	1.738(2)	1.131(3)	176.7(5)	30
$K_2\,[Ru(NO)Br_5]$	1.724(17)	1.175(24)	174.4(1.3)	31
$[BzPh_3P]$ $[RuBr_4(CH_3CN))(NO)]$ $\bullet 0.5\,(C_6H_6)$	1.722(7)	1.094(11)	176.2(7)	This work complex **V**
$[BzPh_3P]$ $[RuBr_4(Py)(NO)]$ $\bullet 0.5\,(C_6H_6)$	1.785(7)	1.001(10)	177.7(7)	This work complex **VI**
(NEt_4) $[Re(NO)(EtOH)Br_4]$	1.723(15)	1.19(2)	169(3)	32
(NEt_4) $[Re(NO)(CH_3CN)Br_4]$	1.771(11)	0.99(2)	178(6)	32

* See Appendix 2.

[a] For this compound it was noticed that the thermal ellipsoid for the nitrogen of the NO moiety was elongated in the direction of the N–O vector and that the N-O bond was unreasonably short (0.95(1)Å). A similar phenomenon had previously been observed for the structure of $[Os(NO)Br_5]^{2-}$ where there was disordering of the NO and Br groups (ref. 20). A model was set up with a Br atom of occupancy 0.05 at 2.51Å from the Os on the Os–O vector and with N and O having occupancy 0.95. Agreement factors were slightly improved, the N-O distance was now sensible and the thermal ellipsoids on N and O were more as expected, so this model has been retained and is presented here.

conclusively: all three compounds have a *trans*-configuration and contain a linear NO^+ group. The bond lengths can be related to the published data for other nitrosyl complexes: selected bond lengths and angles are shown in Table 2.3.1. The observed N-O distances should be compared with 1.06 Å, which is the length of a purely triple bond in the nitrosonium cation[33] and also with similar to N-O bond lengths determined for a number of ruthenium and osmium halo-nitrosyl complexes (usually around 1.1 Å).[28,29,30,31,34] One would expect a certain degree of N-O bond elongation, compared to the uncoordinated nitrosonium cation, as a consequence of π-interaction with the π-backbonding central ion. Osmium (II) is generally deemed to be a better π-backbonding central ion than ruthenium (II). Indeed, $[RuBr_4(CH_3CN)(NO)]^{1-}$ (**V**) appears to have a nitrosyl ligand *less* perturbed (in other words, less elongated) by π-backbonding (1.094 Å) than its osmium analogue (**IX**) (1.133 Å).*

The frequencies of the N-O stretches observed are shown in the Table 2.3.2. Their values are much higher than 1620 cm^{-1}, and this is a clear indication of the linear NO^+ coordination mode.[35] The values are lower for osmium complexes than for their ruthenium analogues, consistent with osmium (II) being a better π-backbonder than ruthenium (II). Moreover, N-O stretch energies are higher in acetonitrile-tetrahalo complexes than in pentahalo complexes, by about 40 cm^{-1}. This suggests that the π-interaction between the metal centre and NO group in such complexes is weakened by the introduction of a moderate π-acceptor acetonitrile ligand in place of a π-donating halide. Thus the IR data are consistent with the presence of a linear NO group and with the anticipated variations in the extent of π-backbonding. However it is necessary to exercise caution when interpreting these subtle changes, as the observed NO stretching frequency may vary depending on the counter-cation[36]: for example, for the $[RuCl_5(NO)]^{2-}$ complex NO stretching frequency is 1900 cm^{-1} in the potassium salt and only 1840 cm^{-1} in the $[BzPh_3P]^+$ salt.

EPR spectroscopy provides another powerful tool for determination of the symmetry of paramagnetic metal complexes.[37] A number of ruthenium (III) complexes of C_{4v} symmetry, including $[Ru^{III}Cl_5(CO)]^{2-}$ species, have been studied previously by

---

* The difference between N-O bondlengths in complexes **V** and **IX** is 0.039 Å. The X-ray diffraction data is of limited accuracy, and the relatively large standard deviation makes the two N-O bondlengths not statistically different. However the IR data (*vide infra*) confirms that π-backbonding is stronger in the osmium (**IX**) rather that in ruthenium (**V**) complex.

Table 2.3.2 *Selected IR peaks of the present complexes.*

Compound	NO vibrations, cm^{-1}	Other characteristic vibrations, cm^{-1}
$K_2[RuCl_5(NO)]$ (**I**)	1900 s (KCl pellet)	
$[BzPh_3P]_2[RuCl_5(NO)]$ (**II**)	1840 s (KCl pellet), 1850 s (CH_2Cl_2 solution)	
$[Bu^n{}_4N]_2[Ru(NO)Cl_4]_2$ (**III**)	1870 s (KCl pellet), 1880 s (CH_2Cl_2 solution)	
$[BzPh_3P]_2[RuBr_5(NO)]$ (**IV**)	1825 s (KBr pellet)	
$[BzPh_3P]$ $[RuBr_4(CH_3CN)(NO)]$ (**V**)	1865 s (KBr pellet), 1875 s (CH_3CN solution)	2300,2320 w (KBr pellet) - CN vibration
$[BzPh_3P]_2[OsCl_5(NO)]$ (**VII**)	1795 s (KCl pellet)	
$[BzPh_3P]_2[OsBr_5(NO)]$ (**VIII**)	1800 s (KBr pellet)	
$[BzPh_3P]$ $[OsBr_4(CH_3CN)(NO)]$ $\bullet 0.5\,(C_6H_6)$ (**IX**)	1850 s (KBr pellet), 1830 s (CH_3CN solution)	2305,2330 w (KBr pellet) - CN vibration

means of EPR spectroscopy: the spectrum of the carbonyl complex reveals two g-values ($g_\perp = 2.25$ and $g_\parallel = 1.95$).[38] However, an EPR study of the electro-generated $[Ru^{III}Cl_5(NO)]^{1-}$ species produced a spectrum with a broad resonance signal.[24] The spectrum was originally interpreted as having three g-values. Thus the uniaxial structure of the trivalent nitrosyl species (*i.e.* linear rather than bent) remained open to doubt. The EPR spectra of the analogous $[Ru^{III}Cl_5(CO)]^{2-}$ and $[Ru^{III}Cl_5(NO)]^{1-}$ species were recorded again in the present work, in order to confirm the retention of uniaxial symmetry in the trivalent state. The trivalent nitrosyl complex is very unstable at ambient temperature and had to be bulk electro-generated at 223 K (-50 °C) from the familiar $[Ru^{II}Cl_5(NO)]^{2-}$ complex immediately prior to the EPR experiment. Both the carbonyl and the nitrosyl species produced typical uniaxial EPR spectra (Figures 2.3.2

and 2.3.4). Hyperfine coupling with the ^{101}Ru and ^{99}Ru nuclei was resolved in both spectra (Figures 2.3.3 and 2.3.4). These EPR data allow us to infer that the $[Ru^{III}Cl_5(CO)]^{2-}$ and $[Ru^{III}Cl_5(NO)]^{1-}$ species have similar uniaxial geometry. Therefore bending of the M-N-O moiety following the $Ru^{II} \rightarrow Ru^{III}$ oxidation of the central ion may be ruled out.

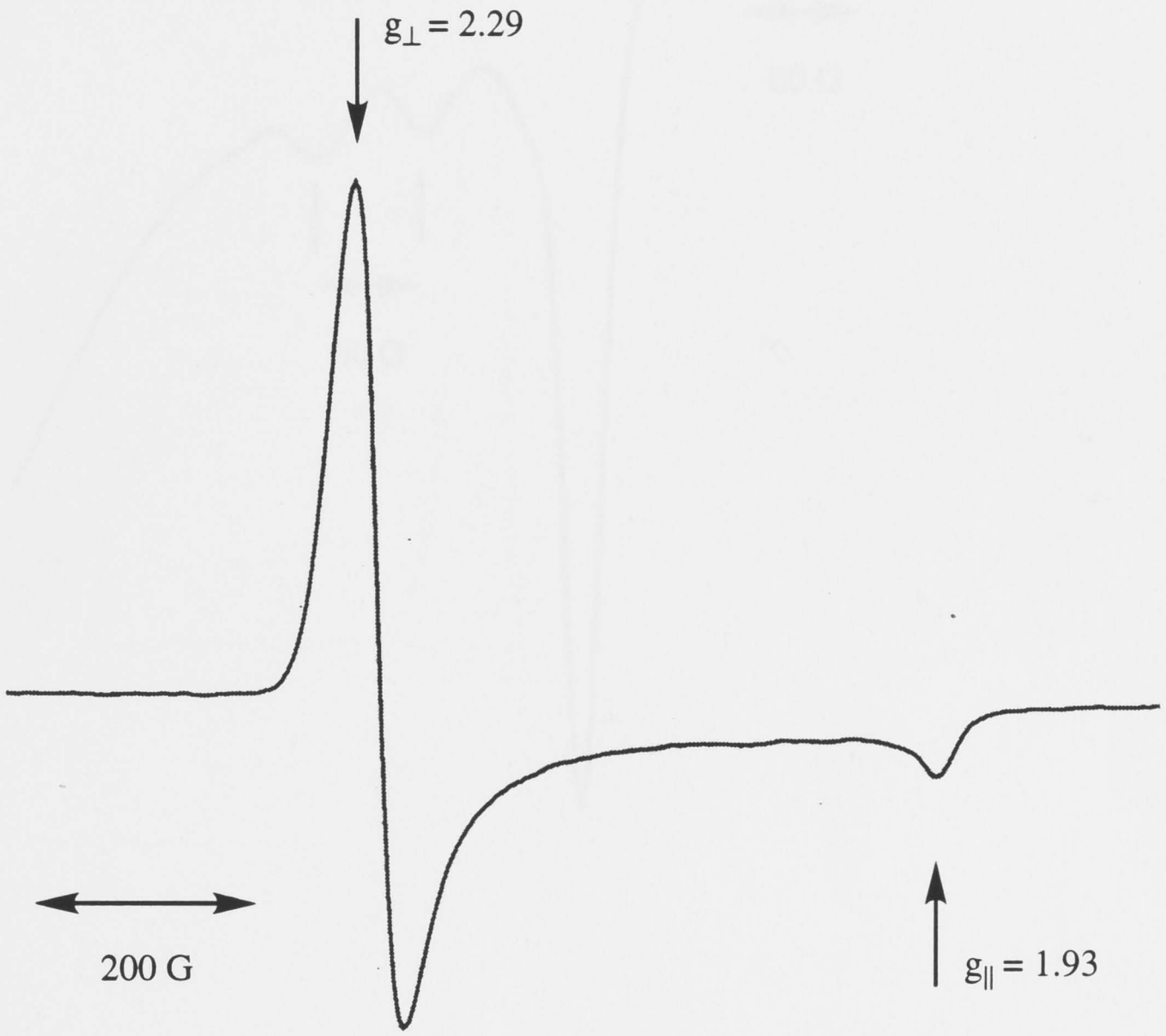

Figure 2.3.2 *EPR spectrum of the* $[Ru^{III}Cl_5(CO)]^{2-}$ *complex (microwave frequency 8.98 GHz (the X-band); modulation amplitude 6 G; microwave power 22 mW; temperature 40 K).*

Figure 2.3.3 *Hyperfine coupling to ^{101}Ru and ^{99}Ru in the EPR spectrum of $[Ru^{III}Cl_5(CO)]^{2-}$ (expansion of the $g_{||}$ component, Figure 2.3.2). The isotopes have natural abundances of 17.0 and 12.7 % respectively. Both isotopes have spin 5/2, and their magnetic moments are similar. The observed hyperfine coupling constant $A_{||} \cong 60$ G. The same applies to the spectrum of the nitrosyl species (Figure 2.3.4).*

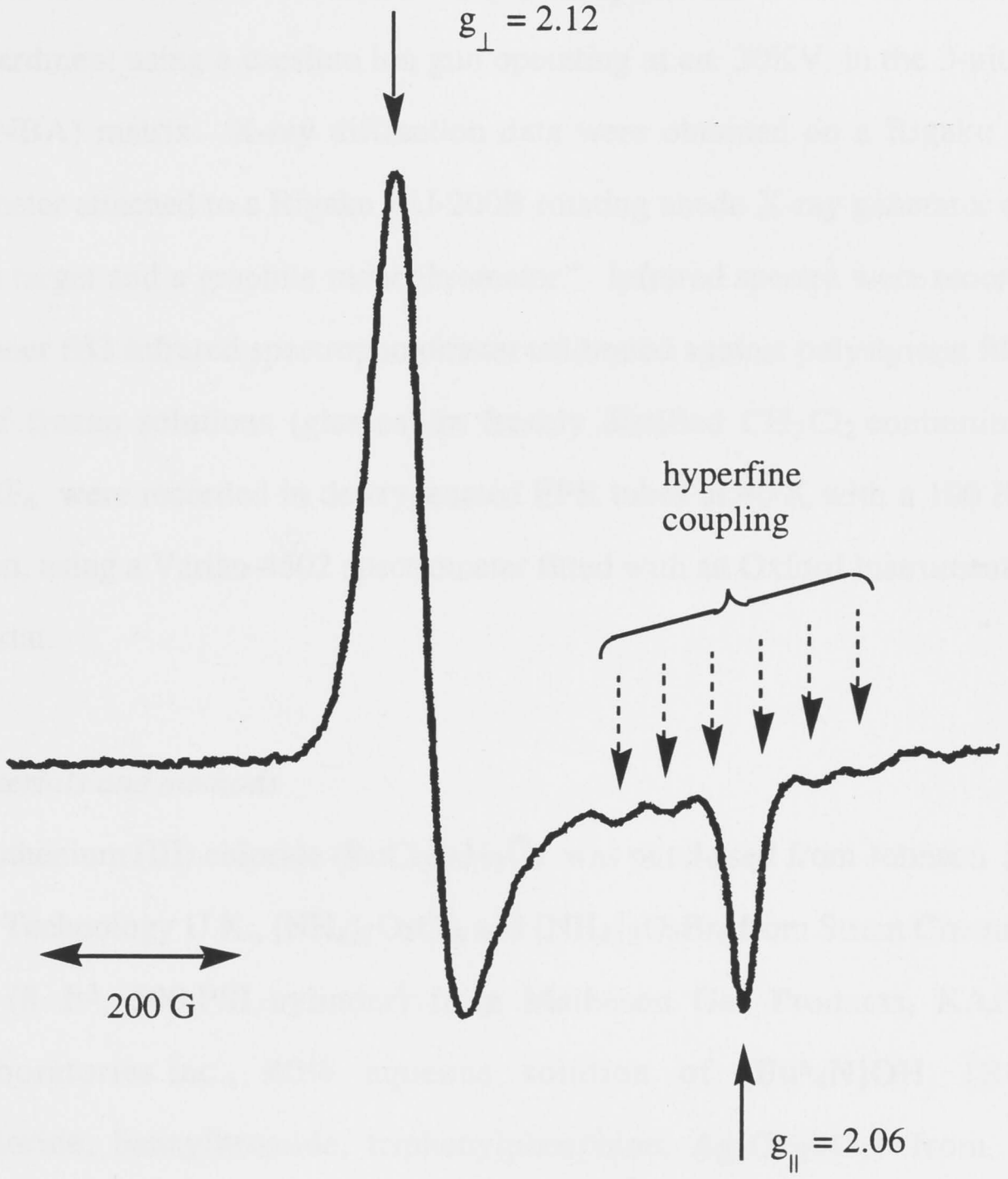

Figure 2.3.4 *EPR spectrum of the $[Ru^{III}Cl_5(NO)]^{1-}$ species (microwave frequency 34.72 GHz (the Q-band); modulation amplitude 4 G; microwave power 5 mW; temperature 40 K). $A_{\parallel} \cong 50$ G. The Q-band was used to achieve better resolution between closely positioned parallel and perpendicular components. The singly occupied d_{xy} orbital lies in the $[MCl_4]$ plane, thus there is no overlap between the SOMO and nitrogen orbitals. Therefore no hyperfine coupling with the nitrogen nucleus is observed.*

2.4 Experimental

2.4.1 General remarks

Elemental analyses were performed by the Microanalytical Services Unit at the Research School of Chemistry, A.N.U. Negative ion fast atom bombardment mass spectra were obtained on a VG ZAB2-SEQ mass spectrometer with ionisation by Cs^+ ion bombardment using a caesium ion gun operating at *ca.* 30KV, in the 3-nitrobenzyl alcohol (NBA) matrix. X-ray diffraction data were obtained on a Rigaku AFC-6R diffractometer attached to a Rigaku RU-200B rotating anode X-ray generator equipped with a Cu target and a graphite monochromator.* Infrared spectra were recorded on a Perkin Elmer 683 infrared spectrophotometer calibrated against polystyrene film. EPR spectra of frozen solutions (glasses) in freshly distilled CH_2Cl_2 containing 0.5 M $[Bu^n_4N]BF_4$ were recorded in deoxygenated EPR tubes at 40 K with a 100 KHz field modulation, using a Varian-4502 spectrometer fitted with an Oxford Instruments helium flow cryostat.

2.4.2 Materials and methods

Ruthenium (III) chloride ($RuCl_3 \bullet xH_2O$) was purchased from Johnson Matthey, Materials Technology U.K., $[NH_4]_2OsCl_6$ and $[NH_4]_2OsBr_6$ from Strem Chemicals Inc., NO gas (8 ft^3, 500 PSI cylinder) from Matheson Gas Products, $KAsF_6$ from K&K Laboratories Inc., 40% aqueous solution of $[Bu^n_4N]OH$, $[Bu^n_4N]Br$, benzylchloride, benzylbromide, triphenylphosphine, $Ag[CF_3SO_3]$ from Aldrich Chemical Co., hydrohalic acids, organic solvents, KCl and HBF_4 from Ajax Chemicals and $NaBH_4$ from Fluka AG. $[Bu^n_4N]BF_4$ was obtained by neutralising commercial aqueous $[Bu^n_4N]OH$ with HBF_4. The product was recrystallised three times from methanol/water (4:1) and dried *in vacuo* for 8 hours. $[BzPh_3P]Cl$ and $[BzPh_3P]Br$ were prepared from triphenylphosphine and benzylchloride or benzylbromide respectively according to literature methods.[39] $[BzPh_3P]BH_4$ was prepared by mixing aqueous

---

* Please see Appendix 2.

solutions of $[BzPh_3P]Cl$ and $NaBH_4$,* and was subsequently dried *in vacuo* for 5 hours. $[BzPh_3P]_2OsCl_6$ and $[BzPh_3P]_2OsBr_6$ were prepared from the ammonium salts by dissolving the latter in the appropriate dilute aqueous hydrohalic acid and adding solutions of $[BzPh_3P]Cl$ or $[BzPh_3P]Br$** respectively. The product precipitates immediately and, after having been collected by filtration, washed with distilled water and dried, is recrystallised from CH_2Cl_2/diethyl ether and dried *in vacuo.* Ruthenium (III) pentachloro- and pentabromocarbonyl complexes were prepared as described in the literature.[40] $[Ph_4P]_2[RuCl_5(CO)]$ and $[Ph_4P]_2[RuBr_5(CO)]$ were precipitated from aqueous solution (pH *ca.* 5) by addition of $[Ph_4P]Cl$ or $[Ph_4P]Br$ respectively. The carbonyl complexes were recrystallised from CH_2Cl_2/diethyl ether and dried *in vacuo*. The individuality of $[Ph_4P]_2[RuCl_5(CO)]$ and $[Ph_4P]_2[RuBr_5(CO)]$ was confirmed by TLC on SiO_2 plates with CH_2Cl_2/CH_3CN (2:1, v:v) mixture as the eluent and by cyclic voltammetry (see Chapter 3). The $[Ru^{III}Cl_5(NO)]^{1-}$ complex generated from the divalent species by electrochemical oxidation in bulk for the EPR experiments was checked by comparison of its UV/VIS spectrum with the one obtained in the OTTLE cell (see section 3.3). The $[Ru^{III}Cl_5(NO)]^{1-}$ complex is a very strong oxidant, therefore it is important to avoid any contact of its solution with potentially reducing materials (*e.g.* steel needles or cannulas).

2.4.3 Synthesis of ruthenium and osmium halide nitrosyl complexes

Potassium pentachloro (nitrosyl) ruthenate (II) and potassium chloride mixture

Ruthenium (III) chloride (2 g) was dissolved in distilled water (50 mL) in the reaction flask and purged with nitrogen gas for an hour. Then NO gas was bubbled through the reaction mixture for a further hour. The solution was then left under NO gas for 10 hours. After purging the reaction vessel with N_2, 12M HCl (2 mL) and KCl (2 g) were added. The solution was passed through a paper filter and evaporated to dryness to give *ca.* 4 g of very dark purple material. The IR spectrum (KCl pellet)

---

* $NaBH_4$ must be dissolved in 2M NaOH solution

** $[BzPh_3P]Br$ is insufficiently soluble in water and has to be dissolved in aqueous ethanol (1:1, v:v).

showed an extremely intense band, $\nu(NO) = 1920\ cm^{-1}$. The complex salt $K_2[RuCl_5(NO)]$ was not separated from KCl as the mixture could be conveniently used for the further reactions.

Benzyltriphenylphosphonium pentachloro (nitrosyl) ruthenate (II)

$K_2[RuCl_5(NO)]$/KCl mixture (0.10 g) was dissolved in 1M HCl (20 mL) and an aqueous solution of $[BzPh_3P]Cl$ (0.5 g) was added. The mauve-coloured precipitate was washed by water, a small volume of cold ethanol and diethyl ether. After recrystallisation from CH_2Cl_2/diethyl ether and drying *in vacuo* 0.21 g (0.2 mmol) the solid $[BzPh_3P]_2[RuCl_5(NO)]$ was obtained.

Tetra-n-butylammonium di-μ-chloro-bis(trichloro (nitrosyl) ruthenate (II))

$K_2[RuCl_5(NO)]$/KCl mixture (0.10 g) was stirred with a solution of $[Bu^n_4N]BF_4$ (0.25 g) in CH_2Cl_2 (20 mL) for 16 hours. The red solution was evaporated to 5 mL and ethanol (15 mL) was added. When the solution was cooled, orange crystals precipitated. They were washed with a small volume of cold ethanol and diethyl ether and dried *in vacuo*.

Yield: 0.10 g (0.1 mmol) $[Bu^n_4N]_2[RuCl_4(NO)]_2$.

Cobaltocenium di-μ-chloro-bis(trichloro (nitrosyl)ruthenate (II))

$[Bu^n_4N]_2[RuCl_4(NO)]_2$ (0.05 g, 0.05 mmol) was dissolved in warm (*ca.* 310 K) CH_2Cl_2 (ca. 10 mL) and $[(C_5H_5)_2Co]\ BF_4$ (0.015 g, 0.05 mmol) was added. After stirring the mixture for 30 min the resulting red crystals were separated from the mother liquor by centrifugation. The product was repeatedly washed by CH_2Cl_2 and diethyl ether and dried in vacuo at 360 K.

Yield: 0.03 g (0.03 mmol; 60 %) $[(C_5H_5)_2Co]_2[RuCl_4(NO)]_2$.

Benzyltriphenylphosphonium pentabromo (nitrosyl) ruthenate (II)

$K_2[RuCl_5(NO)]$/KCl mixture (0.20 g) was dissolved in 12M HBr (50 mL) and warmed to 350 K for 24 hours. The solution was evaporated to dryness. The IR

spectrum of the solid (KBr pellet) shows only one intense peak ν(NO) = 1880 cm^{-1}. $K_2[RuBr_5(NO)]$ was not isolated, but redissolved in 1M HBr (20 mL). $[BzPh_3P]Br$ (1.00 g), dissolved in aqueous ethanol (1:1, v:v), was added to immediately precipitate the light green solid. The product was washed with water, ethanol and diethyl ether, recrystallised from CH_2Cl_2/diethyl ether and dried *in vacuo*.

Yield: 0.37 g (0.3 mmol) $[BzPh_3P]_2[RuBr_5(NO)]$.

Tetra-n-butylammonium pentabromo (nitrosyl) ruthenate (II)

This compound was prepared using the procedure analogous to the previous one, the only difference being that an aqueous solution of $[Bu^n{}_4N]Br$ (1.00 g) was used instead of the $[BzPh_3P]Br$ solution.

Yield: 0.27 g (0.27 mmol) $[Bu^n{}_4N]_2[RuBr_5(NO)]$.

Benzyltriphenylphosphonium trans tetrabromo (acetonitrile)(nitrosyl) ruthenate (II)

$[BzPh_3P]_2[RuBr_5(NO)]$ (0.31 g, 0.25 mmol) was dissolved in acetonitrile (20 mL) under nitrogen gas. 0.05 M $KAsF_6$ solution in acetonitrile (5 mL) was added. The reaction mixture was stirred at 320 K for 12 hours, yielding a red-purple solution and a fine white precipitate (KBr). The solution was cooled to the ambient temperature and filtered under nitrogen gas through a bed of celite, in order to remove the precipitate. The filtrate was evaporated to a small volume (*ca.* 3 mL) and benzene (*ca.* 10 mL) was added to induce the slow formation of dark red crystals of the hemi-benzene solvate. Benzene of crystallisation was removed by drying the product *in vacuo* at 350 K for 6 hours.*

Yield: 0.14 g (0.17 mmol; 68 %) $[BzPh_3P][OsBr_4(CH_3CN)(NO)]\bullet 0.5\ (C_6H_6)$.

Benzyltriphenylphosphonium trans tetrabromo (nitrosyl)(pyridine) ruthenate (II)

$[BzPh_3P][RuBr_4(CH_3CN)(NO)]$ (0.05 g, 0.06 mmol) was dissolved in pyridine (*ca.* 3 mL). The solution was allowed to stand for 2 hours. Diethyl ether was added to

---

* A few crystals were not dried i*n vacuo*, but were retained for X-ray crystal structure analysis.

induce precipitation of the dark mauve crystals of the product. The crystals were dried *in vacuo* at 340 K for 4 hours.

Yield: 0.45 g (0.05 mmol; 83 %) $[BzPh_3P][RuBr_4(Py)(NO)]$.

Benzyltriphenylphosphonium pentachloro (nitrosyl) osmate (II)

$[BzPh_3P]_2OsCl_6$ (0.33 g, 0.3 mmol) was dissolved in a mixture of tetrahydrofurane and 1,2-dichloroethane (40 mL, 1:3, v:v) under nitrogen gas. $Ag[CF_3SO_3]$ (0.08 g, 0.3 mmol) was added, and the formation of a dark clumpy precipitate was initially observed. The reaction mixture was stirred with the exclusion of light for 14 hours at 335 K. During that time the dark precipitate dissolved and a fine white precipitate (AgCl) formed. The solution was cooled to ambient temperature and filtered under nitrogen gas through a bed of celite. The filtrate, containing $[Os^{IV}X_5(thf)]^-$, was evaporated to dryness and redissolved in dry CH_2Cl_2 (30 mL). Dry NO gas was passed through the solution for 20 min. In that time a vivid colour change from yellow to intense purple took place, indicating the formation of $[Os^{III}Cl_5(NO)]^{1-}$. When a two-fold excess of $[BzPh_3P]BH_4$ (0.11 g, 0.3 mmol) was added, the solution became almost colourless, and was evaporated to a small volume (*ca.* 5 mL). Upon addition of diethyl ether, an off-white solid was obtained. It was recrystallised from CH_2Cl_2/diethyl ether and dried *in vacuo*.

Yield: 0.22 g (0.2 mmol; 67 %) $[BzPh_3P]_2[OsCl_5(NO)]$.

Benzyltriphenylphosphonium pentabromo (nitrosyl) osmate (II)

This compound was prepared by a method analogous to the previous one, but using $[BzPh_3P]_2OsBr_6$ as a starting material (0.70 g, 0.5 mmol). A brown microcrystalline product was obtained.

Yield: 0.46 g (0.35 mmol; 70 %) $[BzPh_3P]_2[OsBr_5(NO)]$.

Trans benzyltriphenylphosphonium tetrabromo (acetonitrile)(nitrosyl) osmate(II)

$[BzPh_3P]_2[OsBr_5(NO)]$ (0.25 g, 0.2 mmol) was dissolved in acetonitrile (20 mL) under nitrogen gas. $Ag[CF_3SO_3]$ (0.05 g, 0.2 mmol) was added, and the

reaction mixture was stirred with the exclusion of light for 16 hours. A fine white precipitate (AgBr) was formed. After filtration through a bed of celite the filtrate volume was reduced to *ca.* 5 mL and diethyl ether/benzene mixture (15 mL, 1:1, v:v) was slowly added. The product precipitated as dark red crystals containing benzene of crystallisation.

Yield: 0.15 g (0.15 mmol; 75 %) $[BzPh_3P][OsBr_4(CH_3CN)(NO)]\bullet 0.5\ (C_6H_6)$.

2.5 References

1. Greenwood, N.N., Earnshaw, A. *Chemistry of the Elements*, Pergamon Press, Oxford, **1985**, 515-520
2. Caulton, K.G. *Coord. Chem. Rev.* **1975**, *14*, 317, and references therein
3. Mingos, D.M.P., Sherman, D.L. *Adv. Inorg. Chem.* **1989**, *34*, 293, and references therein
4. Heath, G.A., Martin, R.L. *Australian J. Chem.* **1970**, *23*, 2297
5. *Gmelins Handbuch Der Anorganische Chemie*, Verlag Chemie, GMBH., Weinheim/Bergstr. und Berlin, **1938** (Nachdruck **1955**), 93
6. Fedorenko, N.V. *Razvitie Issledovanii Platinovykh Metallov v Rossii (Development of Platinum Metals Research in Russia)*, Nauka, Moscow, **1985**, 77-78
7. Joly, A. *C. r. Acad. sci.* **1888**, *107*, 994
8. Joly, A. *C. r. Acad. sci.* **1889**, *108*, 1300
9. Seddon, E.A., Seddon, K.R. *The Chemistry of Ruthenium*, Elsevier, Amsterdam, **1984**, 1106-1115, and references therein
10. Fletcher , J.M., Jenkins, I.L., Lever, F.M., Martin, F.S., Powell, A.R., Todd, R. *J. Inorg. Nucl. Chem.* **1955**, *1*, 378
11. Durig, J.R., McAlister, W.A., Willis, J.N.Jr., Mercer, E.E. *Spectrochim. Acta* **1966**, *22*, 1091
12. Sinitsin, N.M., Svetlov, A.A. *Koord. Khim.* **1980**, *6*, 281
13. Tarasov, V.P., Kirakosyan, G.A., Buslaev, Y.A., Svetlov, A.A., Sinitsin, N.M. *Inorg. Chim. Acta* **1983**, *69*, 239
14. Khodashova, T.S., Porai-Koshits, M.A., Sergienko, V.S., Parpiev, N.A., Bokii,G.B. *J. Struct. Chem. (U.S.S.R.),* **1972**, *13*, 1024
15. Fenske, D., Denant, U., Dehnicke, K. *Z. Naturforsch.* **1985**, *40b*, 1672
16. Mukaida, M. *Bull. Chem. Soc. Japan* **1970**, *43*, 3805
17. Lay, P.A., Harman, W.D. *Adv. Inorg. Chem.* **1991**, *37*, 219

18. Griffith, W.P. in *Comprehensive Coordination Chemistry*, Pergamon Press, Oxford, **1987**, *4*, 519, and references therein

19. Sinitsin, N.M., Septsova, N.M., Svetlov, A.A. *Russian J. Inorg. Chem.* **1983**, *28*, 1464

20. Bhattacharyya, R., Saha, A.M., Ghosh, P.N., Mukherjee, M., Mukherjee, A.K. *J. Chem. Soc., Dalton Trans.* **1991**, 501

21. Humphrey, D.G. *Ph.D. Thesis* A.N.U.,Canberra, **1992,** 212

22. Czeska, B., Dehnicke, K., Fenske, D. *Z. Naturforsch.* **1983**, *38b*, 1031

23. Svetlov, A.A., Sinitsin, N.M., Fal'kengof, A.T., Kokunov, Yu.V. *Russian J. Inorg. Chem.* **1990**, *35*, 1007

24. Coombe, V.T., Heath, G.A., Stephenson, T.A., Tocher,D.A. *J. Chem. Soc., Chem. Commun.* **1983**, 303

25. Heath, G.A., Macgregor, S.A. *Personal communication*

26. Chen, H.W., Jolly, W.L. *Inorg. Chem.* **1979**, *18*, 2548

27. Nefedov, V.I., Sinitsin, N,M., Salyn', Ya.,V., Baier, L. *Soviet J. Coord. Chem.* **1975**, *1*, 1332

28. Feltham, R.D., Enemark, J.H. *Topics in Stereochemistry* **1981**, *12*, 155

29. Zarhoul, R., Faure, R., Deloume, J.-P. *J. Crystalogr. Spectrosc. Res.* **1992**, *22*, 601

30. Veal, J.T., Hodgson, D.J. *Inorg. Chem.* **1972**, *11*, 1420

31. Mikhailov, Yu.N., Kanishcheva, A.S., Svetlov, A.A. *Russian J. Inorg. Chem.* **1989**, *34*, 1603

32. Caini, G., Giusto, D., Manassero, M., Sansoni, M. *J. Chem. Soc., Dalton Trans.* **1975**, 2156

33. Cotton, F.A., Wilkinson, G. *Advanced Inorganic Chemistry,* 5th ed., Wiley-Intersience, New York, **1988,** 322

34. Salomov, A.S., Mikhailov, Yu.N., Kanishcheva, A.S., Svetlov, A.A., Sinitsin, N.M., Porai-Koshits, M.A., Papriev, N.A. *Russian J. Inorg. Chem.* **1988**, *33*, 1496

35. Nakamoto, K. *Infrared and Raman Spectra of Inorganic and Coordination Compounds,* 4th ed., Wiley-Intersience, New York, **1986**, 309

36. Bobkova, E.Yu., Borkovskii, N.B., Svetlov, A.A., Novitskii, G.G. *Russian J. Inorg. Chem.* **1994**, *39*, 796

37. Mabbs, F.E., Collison, D. *Electron Paramagnetic Resonance of d Transition Metal Compounds,* Elsevier, Amsterdam, **1992**

38. Sakaki, S., Yanase, Y., Hagiwara, N., Takeshita, T., Naganuma, H., Ohyoshi, A., Ohkubo, K. *J. Phys. Chem.* **1982,** *86,* 1038

39. Michaelis, A., von Soden, H. *Justus Liebigs Ann. Chem.* **1885**, *229*, 295

40. Colton, R., Farthing, R.H. *Australian J. Chem.* **1971**, *24*, 903

Chapter 3

Electrochemistry and Spectroscopy of Ruthenium and Osmium Nitrosyls and Related Complexes: Implications for the Ligand Additivity Concept

Having discussed the synthetic procedures and structural features of an orderly family of ruthenium and osmium nitrosyl halide complexes in the previous chapter, we now proceed to the electrochemical and spectro-electrochemical characterisation. We shall compare their electronic properties with those of the related carbonyl- and acetonitrile-substituted complexes of ruthenium and osmium, studied previously, and discuss the relationship between the charge-transfer spectra and the redox parameters. Finally, we shall examine causes of the irreversible electrochemical behaviour of the ruthenium bromo nitrosyl species.

3.1 Voltammetric Study

3.1.1. General

The voltammetry reported in this work was obtained in a jacketted but otherwise conventional three-electrode[1a] (working, reference and auxiliary) cell. Platinum disk or bead electrodes were utilised. Voltammograms were recorded for dichloromethane or acetonitrile solutions containing tetra-n-butylammonium tetrafluoroborate as supporting electrolyte, in 0.5 M and 0.2 M concentrations respectively. The solutions were routinely deoxygenated by purging with N_2 or Ar, and blanketted during the measurements. The electrode potentials are quoted *versus* the Ag/AgCl reference electrode, against which ferrocene ([$FeCp_2$]) is oxidised at +0.55 V.

In what follows the abbreviations CV and acV stand for cyclic voltammetry and alternating current voltammetry respectively. As we did not intend to analyse the electrochemical (thermodynamic) reversibility of these systems in great detail, the descriptions of *reversibility* or *irreversibility* refer, unless otherwise specified, to chemical reversibility,[1b] our main criterion being the equal magnitude of anodic and cathodic peak currents in the CV response. The separation of the anodic and cathodic peak potentials, ΔE_p,* for all present reversible cyclic voltammograms lies between 45 mV and 80 mV, therefore they are close to reversible *Nernstian waves.*[1c]

Low temperatures, typically between 223 K (-50^0 C) and 243 K (-30^0 C), have been used routinely to improve chemical reversibility by restricting decomposition of electrode products.

3.1.2 Preliminary Remarks

Before we report the new results for the present family of halo-nitrosyl complexes, it is instructive to review briefly the redox behaviour of the parent hexahalides as well as the related acetonitrile- and carbonyl-substituted complexes** . For $[MX_6]^{z-}$ species (M = Ru, Os; X =Cl, Br), the electrode potentials E^o (IV/V (d^3/d^4), IV/III (d^4/d^5) and III/II (d^5/d^6)) have been previously reported by Graham Heath and his colleagues.[2-6] The difference in redox couples between corresponding chloride and bromide complexes is small (and it can be indeed of positive or negative voltage), as the overall donor properties (σ and π) of these halide ligands are presumably similar. Replacement of a single halide ion by a neutral, less π–basic ligand causes a considerable anodic (positive) shift in metal-based redox couples. The effect of multiple stepwise substitution of halide ligands by acetonitrile on the electrode potentials have been described in our laboratory for both ruthenium and osmium complexes.[4-8] In the series $[MX_{6-n}(RCN)_n]^{z-}$ (M = Ru, Os; X =Cl, Br; RCN = CH_3CN or PhCN ; n = 0 to 6 for Ru and 0 to 2 for Os) both the IV/III (d^4/d^5) and the

---

* The value of ΔE_p must be close to 2.3RT/nF (n is the number of electrons transferred) for a reversible Nernstian electrode reaction

** The electrochemical data for some carbonyl and acetonitrile-substituted complexes and the parent hexahalides are presented in the table 3.1.1.

III/II (d^5/d^6) couples display stepwise shifts close to + 0.6 V per halide displaced (Fig. 3.1.1). These electrochemical observations at once confirmed the applicability of additive ligand electrochemical parameters[4,5,6] and then, upon translation from $[MX_{6-n}(RCN)_n]^{z-}$ to $[OsX_{6-n}(CO)_n]^{z-}$ systems, demonstrated their limitations.[7] The carbonyl halide complexes of osmium reveal an undeniably irregular stepwise shift in E^o in the series $[OsX_{6-n}(CO)_n]^{z-}$ (X =Cl, Br; n = 0-2, *trans* when n = 2): since the effect of introducing the second carbonyl is much less than the first. Such observations are in clear disagreement with the linear ligand additivity model, which expressly assumes that each successive replacement has the same effect on the properties of a complex. The presence of carbonyl halves the conventional + 0.6 V CH_3CN / X shift in observed E^o, which becomes only + 0.3 V when the complexes $[OsX_5(CO)]^{2-}$ and $[OsX_4(CO)(CH_3CN)]^{1-}$ (X = Cl or Br) are juxtaposed. This is equally incompatible with the tenets of Lever's ligand additivity model,[9,10] and was one of the reasons for the detailed study described in the next subsection. The electrochemical data for the corresponding ruthenium halo-carbonyl complexes have not been published hitherto.

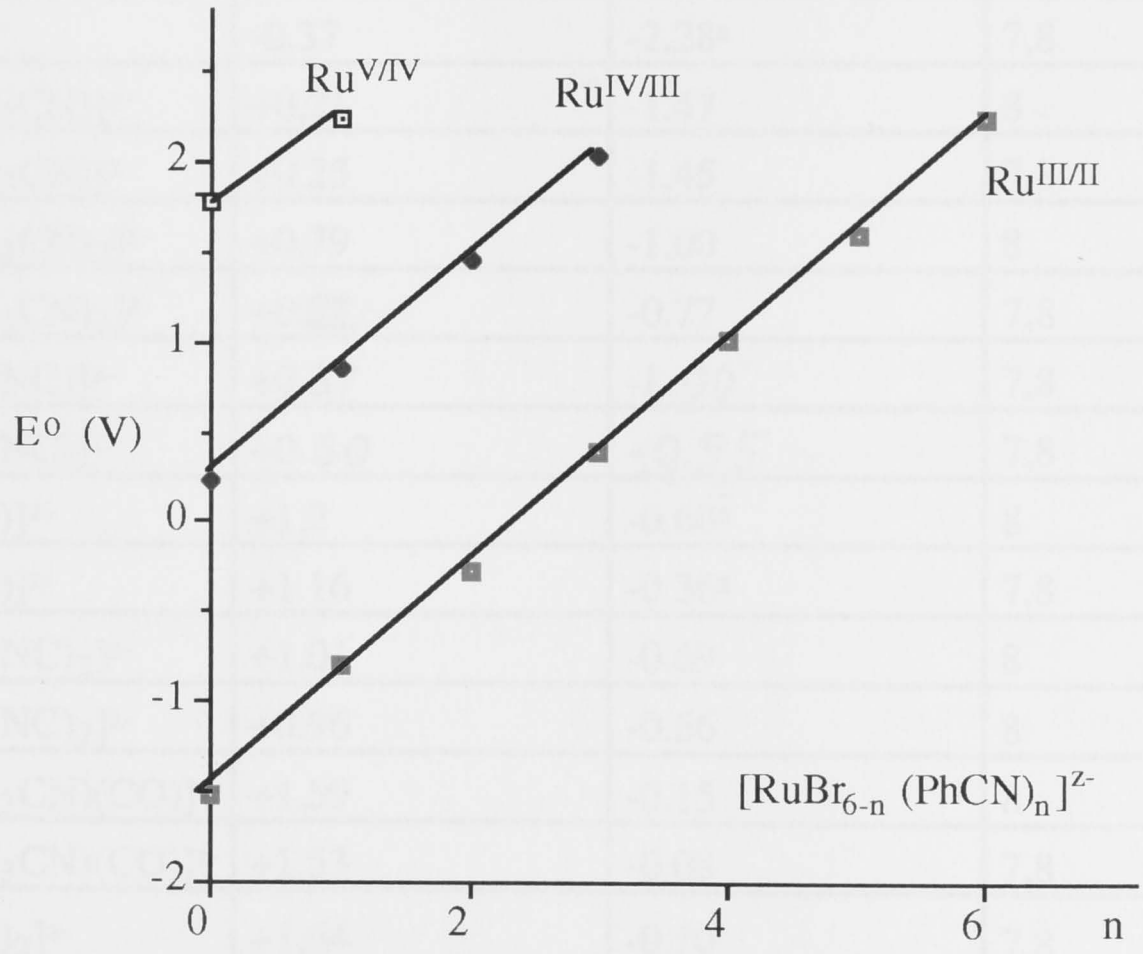

Figure 3.1.1 *Variation in redox potentials of the series* $[RuBr_{6-n}(PhCN)_n]^{z-}$ *(n = 0-6) as a function of stoichiometry of the complex. Data from ref. 4.*

Table 3.1.1 *Electrode potentials for the IV/III and III/II metal-based redox couples of some $[MX_6]^{z-}$, $[MX_5(L)]^{z-}$ and trans $[MX_4(L)_2]^{z-}$ complexes of ruthenium (shaded cells) and osmium.*

Stoichiometry of the complexes	E^o IV/III (V)	E^o III/II (V)	Source
$[RuCl_6]^{z-}$	+0.02	-1.5[a]	3
$[RuBr_6]^{z-}$	+0.22	-1.51[a]	4,5
$[RuCl_5(CH_3CN)]^{z-}$	+0.82	not observed	4,5
$[RuCl_5(PhCN)]^{z-}$	+0.86	-0.80[a]	4,5
$[RuBr_5(PhCN)]^{z-}$	+0.78	not observed	4,5
$[RuCl_4(As(CH_3)_3)_2]^{z-}$	+0.99	-0.65	23
$[RuCl_4(CH_3CN)_2]^{z-}$	+1.45	-0.38	4,5
$[RuCl_4(PhCN)_2]^{z-}$	+1.45	-0.27	4,5
$[RuBr_4(PhCN)_2]^{z-}$	+1.41	-0.15	4,5
$[RuCl_4(Bu^tNC)_2]^{z-}$	+1.52	-0.31	6
$[RuBr_4(Bu^tNC)_2]^{z-}$	+1.40	-0.22	6
$[RuCl_5(CO)]^{z-}$	not observed	+0.40	this work
$[RuBr_5(CO)]^{z-}$	not observed	+0.44	this work
$[OsCl_6]^{z-}$	-0.57	-1.93[a]	3
$[OsBr_6]^{z-}$	-0.37	-2.28[a]	7,8
$[OsCl_5(CH_3CN)]^{z-}$	+0.21	-1.47	8
$[OsBr_5(CH_3CN)]^{z-}$	+0.25	-1.45	7,8
$[OsCl_4(CH_3CN)_2]^{z-}$	+0.79	-1.00	8
$[OsBr_4(CH_3CN)_2]^{z-}$	+0.82	-0.77	7,8
$[OsCl_5(Bu^tNC)]^{z-}$	+0.37	-1.00	7,8
$[OsBr_5(Bu^tNC)]^{z-}$	+0.50	-0.95	7,8
$[OsCl_5(CO)]^{z-}$	+1.2	-0.60[a]	8
$[OsBr_5(CO)]^{z-}$	+1.16	-0.36[a]	7,8
$[OsCl_4(Bu^tNC)_2]^{z-}$	+1.01	-0.69	8
$[OsBr_4(Bu^tNC)_2]^{z-}$	+0.96	-0.66	8
$[OsCl_4(CH_3CN)(CO)]^{z-}$	+1.59	-0.15	8
$[OsBr_4(CH_3CN)(CO)]^{z-}$	+1.53	-0.08	7,8
$[OsCl_4(CO)_2]^{z-}$	+1.64	-0.10	7,8
$[OsBr_4(CO)_2]^{z-}$	+1.84	+0.27	7,8

[a] Irreversible

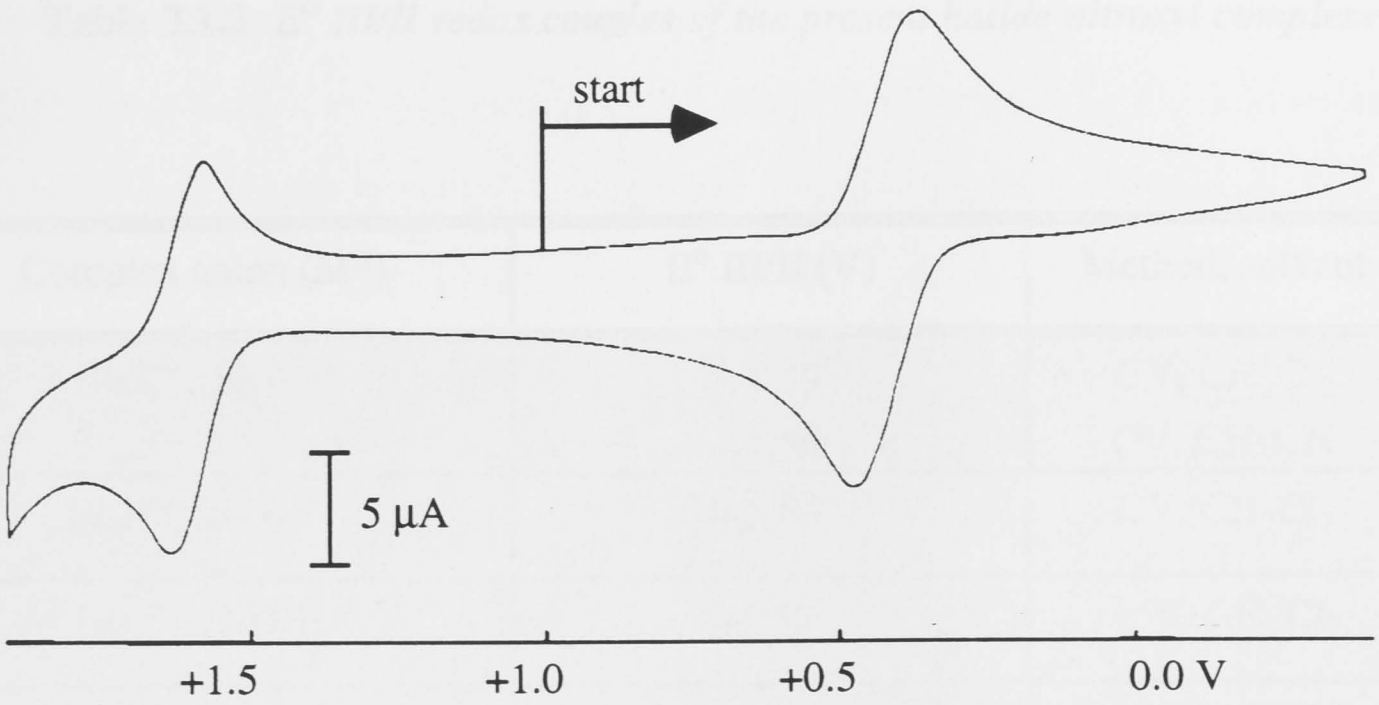

Figure 3.1.2 *Cyclic voltammogram (III/II redox couples) of the* $[Ru^{III/II}Cl_5(NO^+)]^{1-/2-}$ *(on the left) and* $[Ru^{III/II}Cl_5(CO)]^{2-/3-}$ *(on the right) anions present at similar concentrations in dichloromethane at 223 K.*

3.1.3 Voltammetry of the Halide Nitrosyl Complexes

The NO^+ ligand is an *extremely* strong π-acceptor; as such it withdraws the electron density from the central ion via π-interaction with the metal *d*-orbitals. Therefore one can expect a *very* large anodic shift in the redox potentials of the present halide nitrosyl complexes relative to the parent hexahalides or even the corresponding carbonyls (Figure 3.1.2). Indeed the initial electrochemical study[11] of the $[RuCl_5(NO)]^{2-}$ complex demonstrated that it has a very positive oxidation potential (E^o III/II = +1.53 V). The oxidation generates a turquoise coloured Ru(III) (d^5) complex. In addition, as was mentioned in section 2.1, this redox couple behaves reversibly only at temperatures below 233 K. However, the potential is still within the usual electrode potential window in dichloromethane (from +2.0 V to -2.0 V) available in organic solvents such as dichloromethane and acetonitrile.

As expected, the III/II redox couples for the halide nitrosyl complexes proved to be quite positive (Table 3.1.2). The subsequent IV/III couple for all complexes would certainly lie far beyond +2.0 V, as the IV/III - III/II gap normally has a value between

Table 3.1.2 *E^o III/II redox couples of the present halide nitrosyl complexes at 235K.*

Complex anion (M^{II})	E^o III/II (V)	Method, solvent
$[RuCl_5(NO)]^{2-}$	+1.59 +1.56	CV, CH_2Cl_2 CV, CH_3CN
$[RuCl_4(NO)]_2^{2-}$	+2.18[a]	CV, CH_2Cl_2
$[RuBr_5(NO)]^{2-}$	+1.52[b]	acV, CH_2Cl_2
$[RuBr_4(CH_3CN)(NO)]^{1-}$	+1.86[b]	acV, CH_3CN
$[RuBr_4(Py)(NO)]^{1-}$	+1.80[b]	acV, CH_2Cl_2
$[OsCl_5(NO)]^{2-}$	+1.20	CV, CH_2Cl_2
$[OsBr_5(NO)]^{2-}$	+1.20	CV, CH_2Cl_2
$[OsBr_4(CH_3CN)(NO)]^{1-}$	+1.51	CV, CH_3CN

1.5 and 2.0 volts,* and therefore was not observed. Notably, the *ruthenium bromide* nitrosyl complexes show irreversible electrode processes, as opposed to Ru / Cl and Os / (Cl or Br) nitrosyl complexes. The cause of this will be discussed in the next section, in the context of the electronic structure of these complexes. The reversible electrochemical behaviour of the majority of the complexes enables us to electro-generate the corresponding metal (III) derivatives and characterise them by spectroscopic methods (*vide infra*). As will be seen, access to the M(III) (d^5) state is most important for better understanding of their molecular and electronic structure.

An instructive comparison can be drawn between monomeric $[RuCl_5(NO)]^{2-}$ and edge-sharing dimeric $[RuCl_4(NO)]_2^{2-}$. The latter has its first oxidation, corresponding to the III/II couple of one of the ruthenium atoms in the dimer, at +2.18 V, some 0.6 V more positive than the E^o III/II of $[RuCl_5(NO)]^{2-}$. A comparison

---

[a] Reversible only when very dry conditions are observed.
[b] Irreversible, *i.e.* CV lacks a return wave even at 235 K. This potential corresponds to the observed anodic peak potential.
* See in table 3.1.1

of the electrochemistry of $[OsCl_6]^{z-}$ and $[OsCl_5]_2^{z-}$ tells a similar story,[7,12] the corresponding oxidations are always more difficult to achieve in the edge-sharing dimer. This reflects the fact that, in sum, there are only four anionic halide ligands per ruthenium (as the bridging halides are shared) in the dimer compared to five in the monomer. This increases the local positive charge on the metal-centre and hence makes it harder to remove an electron. In the light of these observations, one might ask, whether nitriles as π-acids contribute significantly to the observed stepwise + 0.6 V electrode potential shift[4] in the series $[MX_{6-n}(RCN)_n]^{z-}$ (see Figure 3.1.1), or are merely accompanying the decrease in the number of halides attached to the metal.

An important result of the voltammetric experiments comes from a comparison of the nitrosyl complexes with their direct carbonyl and acetonitrile analogues (Figure 3.1.3). Firstly, if one compares the redox properties of the parent hexahalide with those of the monosubstituted $[MX_5(L)]^{z-}$ species (L = CH_3CN, CO or NO^+), one can see that the anodic shift of the III/II couple between $[MX_6]^{z-}$ and $[MX_5(L)]^{z-}$ increases significantly from L = CH_3CN to L = NO^+. This corresponds to the dramatic strengthening of π-acidity in the progression CH_3CN, CO and NO^+. Secondly, in both carbonyl and nitrosyl complexes, exchange of the *trans* halide ligand by CH_3CN results in a positive shift of the III/II couple by *ca.* 0.3 V, which is only half the "expected shift" (*vide supra*) of *ca.* 0.6 V for such a substitution. This phenomenon is apparently caused by the greater ability of the carbonyl or nitrosyl ligands to withdraw electron density from the central ion so reducing its *polarisability*.[13] In the carbonyl or nitrosyl complexes this effect is so marked that the influence of the further substitution of the halides by the nitrile ligands is limited. This observation confirms and extends the previous conclusion[7] that the effect of a halide / CH_3CN substitution on the metal's redox properties depends on the other ligands present. The effect of an incoming ligand (replacing halide) is thus shown to be dependent on whether the site is *trans* to a π-donor (halide) or a mild π-acid (nitrile), on the one hand, or a strong π-acid (CO or NO^+), on the other. In Chapter 4 and Appendix 1 we shall demonstrate that the *trans* arrangement of ligands L/L′ is particularly prone to the attenuation of their joint influence exerted on the central metal ion. This geometric aspect shows an important

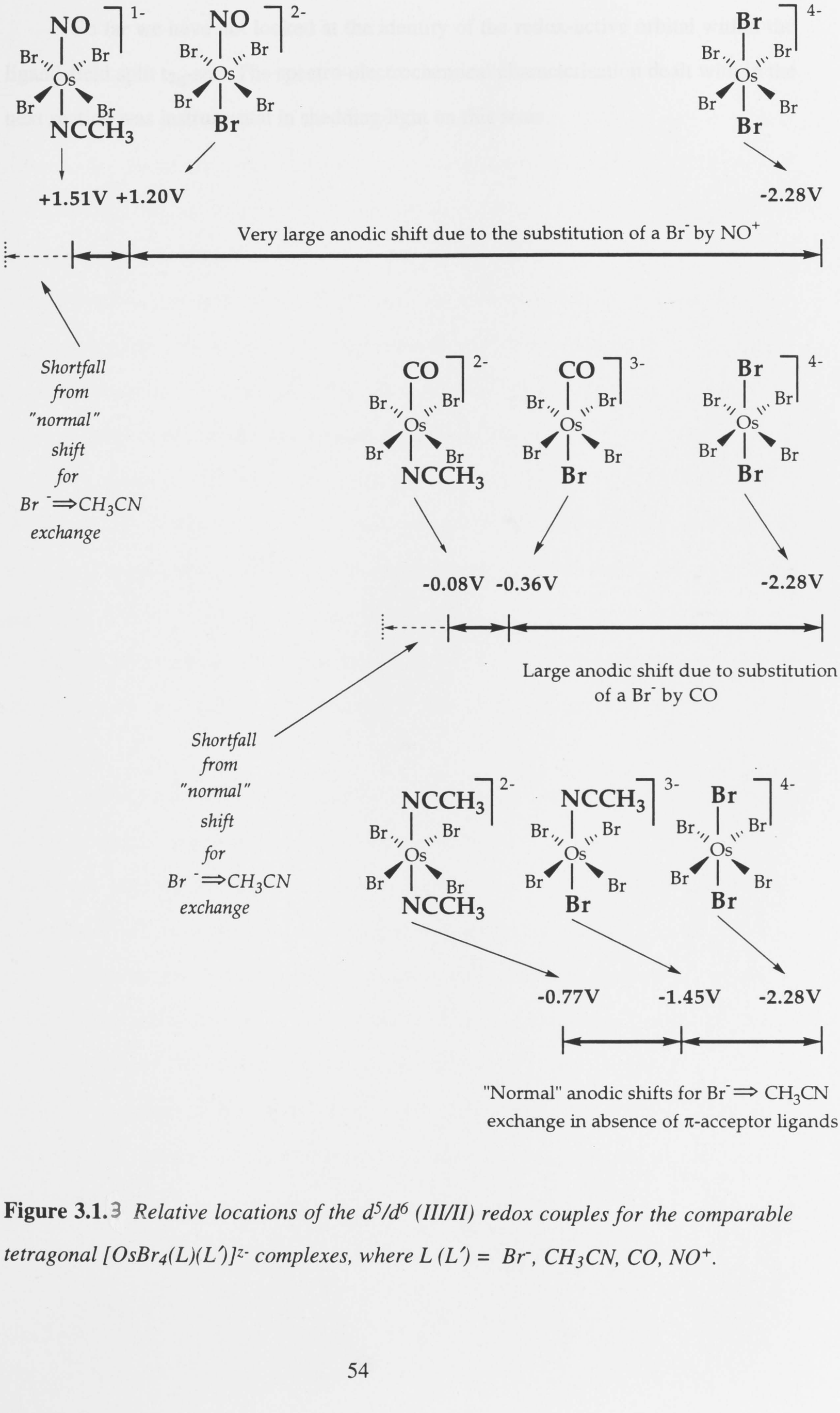

Figure 3.1.3 *Relative locations of the d^5/d^6 (III/II) redox couples for the comparable tetragonal $[OsBr_4(L)(L')]^{z-}$ complexes, where L (L') = Br^-, CH_3CN, CO, NO^+.*

limitation ignored in simplistic versions of the linear ligand additivity principle.

So far we have not looked at the identity of the redox-active orbital within the ligand-field split t_{2g}-set. The spectro-electrochemical characterisation dealt with in the next section was instrumental in shedding light on this issue.

3.2 Spectro-electrochemical Study

3.2.1 Preliminary remarks

The tetragonal complexes described earlier are isolated as metal (II) compounds. These tetragonal complexes of divalent ruthenium and osmium have a d^6 configuration, where the orbital subset of the metal *d*-shell related to the t_{2g} set of a regular octahedron is filled. The NO^+ ligand, in particular, stabilises the low oxidation state through its partial positive charge and strong π-acceptor ability. Consequently the metal centre has only higher e_g-derived orbitals available for ligand-to-metal charge-transfer transitions. Indeed, the UV-VIS spectra of the present complexes in their divalent state do not exhibit any intense absorptions below 40000 cm^{-1}. On the other hand d^5 ruthenium (III) and osmium (III) halide complexes $[MX_6]^{3-}$, $[MX_5(L)]^{2-}$ and $[MX_4(L)(L')]^{1-}$, where the ligands L and L′ are acetonitrile, carbonyl and other ligands, are known to have rich UV-VIS spectra dominated by *halide-to-metal* charge-transfer transitions.[5,6,7,8,14,15] Therefore in the present study spectro-electrochemical methods are applied for *in situ* electro-generation and UV-VIS spectroscopic investigation of the otherwise unavailable d^5 ruthenium (III) and osmium (III) nitrosyl halide complexes.

The explicit study of the ligand-to-metal charge-transfer spectra of the heavy metal complexes began with the hexahalides in the 1950's, when Christian Klixbüll Jørgensen published a paper entitled "Electron Transfer Spectra of Hexahalide Complexes".[16] In that work, the strong absorption bands observed in the UV-VIS spectra of many metal hexahalides complexes ($[MX_6]^{z-}$) were discussed. Jørgensen wrote: *"The wave-numbers of these bands behave qualitatively as expected for an electron transfer from the halide to the central ion: they decrease with increasing oxidizing character of the central ion and with reducing character of the halide ion."* He suggested that such bands arise as an intramolecular redox process, or one-electron promotion:

$$\underset{d^n}{[M^n(X_6^{6-})]^{z-}} \xrightarrow{h\nu} \underset{d^{n+1}}{{}^*[M^{n-1}(X_6^{5-})]^{z-}}$$

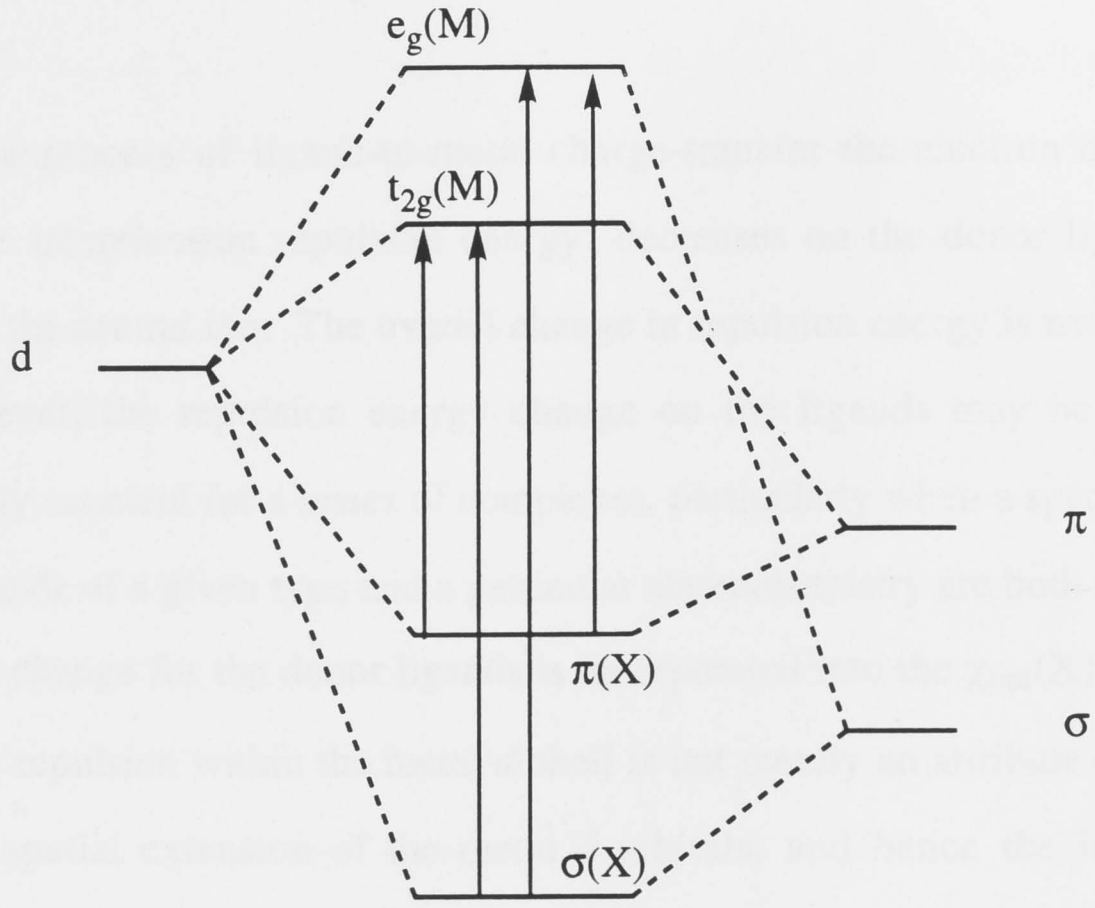

Figure 3.2.1 *Simplified MO diagram (the splitting and mixing of the halide σ and π-orbitals are neglected), illustrating possible ligand-to-metal charge-transfer transitions in octahedral hexahalide complexes.*

Even today this concept is of great importance for spectro-electrochemical studies, as it inspires us to correlate optical and redox data. From a large body of data Jørgensen devised an *optical electronegativity* (χ_{opt}) scale.[17,18] It was proposed that the energy (ν_{LMCT}) of the first symmetry-allowed* band in the charge-transfer spectrum was proportional to the difference in optical electronegativity of the halide and the central ion according to the following expression:

$$\nu_{LMCT}\,(cm^{-1}) = 30000\,(cm^{-1})\,[\chi_{opt}(X) - \chi_{opt}(M)] + E_{sp},$$

where $\chi_{opt}(X)$ and $\chi_{opt}(M)$ are optical electronegativities of the ligand and the metal respectively, and the constant 30000 cm^{-1} was required to correlate χ_{opt} with the Pauling electronegativity scale; E_{sp} is the spin pairing energy, which is a measure of

* The charge-transfer transitions between any two gerade (or two ungerade) orbitals are symmetry-forbidden.

the change in the interelectron repulsion within the metal *d*-shell for the charge-transfer transition.

In the process of ligand-to-metal charge-transfer the electron density (and therefore the interelectron repulsion energy) decreases on the donor ligand(s) and increases on the central ion. The overall change in repulsion energy is not necessarily zero. However, the repulsion energy change on the ligands may be considered approximately constant for a series of complexes, particularly when a specific number of donor ligands of a given type and a particular stereochemistry are both retained. In this case the change for the donor ligands is incorporated into the $\chi_{opt}(X)$ value. The interelectron repulsion within the metal *d*-shell is not merely an attribute of the metal itself. The spatial extension of the metal *d*-orbitals, and hence the interelectron repulsion energy, is quite dependent on its ligand environment (ligands' σ- and π-donor / acceptor properties) in a given complex. More covalently bound ligands (*e.g.* Br^-, I^-) tend to delocalise the metal's *d-electron cloud* and thereby reduce the metal *d* interelectron repulsion energy. This phenomenon (*the nephelauxetic effect*) was first described by Jørgensen and Schäffer.[19] The precise evaluation of the effects of the interelectronic repulsion is, regrettably, not trivial.[20]

It should be emphasised that Jørgensen's equation is designed for the homoleptic $[ML_6]^z$-type complexes. The optical electronegativities cannot be expected to remain unchanged for the heteroleptic species, as different ligands may affect the energies of the metal, as well as, other ligands π-orbitals involved in the LMCT. Thus Jørgensen's optical electronegativity scale can be successfully used for prediction of approximate energies of the charge-transfer bands in homoleptic metal complexes, however, it cannot be generally applied to complexes containing two or more kinds of ligands with diverse donor / acceptor properties.

It is worthwhile taking a closer look at the nature of the LMCT transitions occurring in d^5 metal hexahalide complexes before examining the substituted systems. A simplified MO diagram for metal - halide interactions is presented in Figure 3.2.1. The σ and π-orbitals of the coordinated halides are the donor levels, while the partially occupied t_{2g} and unoccupied e_g orbitals of the central metal ion are the acceptor levels.

They give rise to four possible types of LMCT transitions (in order of increasing energy): π to t_{2g} , π to e_g , σ to t_{2g} , σ to e_g. Even for $[MX_6]^{z-}$ systems, with fully equivalent ligands, the situation becomes more complicated as ligand σ and π molecular orbitals are now split primarily due to interactions between the six halides within the coordination sphere to provide the so-called "molecular symmetry orbitals." The six σ-orbitals transform as $a_{1g} + e_g + t_{1u}$, while π-orbitals transform as $t_{1u} + t_{2u} + t_{1g} + t_{2g}$.[20] This increases the number of possible transitions from 4 to 14. For the low-spin d^5 $[IrCl_6]^{2-}$ complex (with only one hole in low-lying t_{2g} set), the four lowest energy LMCT bands are assigned as π(Cl) to t_{2g}(M) transitions (Figure 3.2.2). Transitions from t_{1g}(Cl) and t_{2g}(Cl) to t_{2g}(M) are very weak, as transitions between gerade orbitals are symmetry-forbidden. Transitions from the t_{1u}(Cl) orbital into vacant e_g(M) orbitals are more intense, but lie to higher energy. The halide-to-metal charge-transfer spectra for many other transition metal hexahalides have been recorded and assigned.[20]

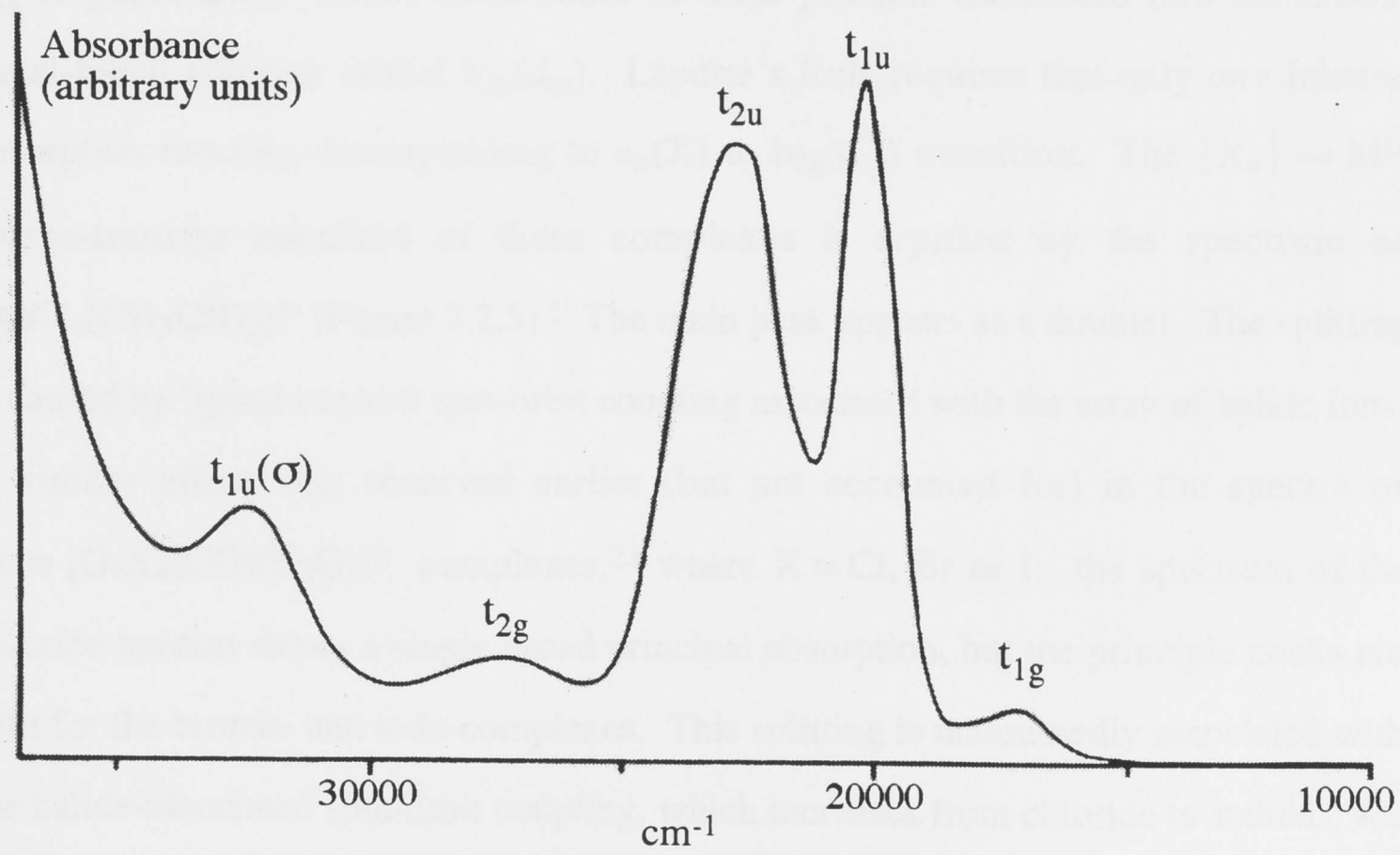

Figure 3.2.2 *UV-Visible spectrum of d^5 $[IrCl_6]^{2-}$. The spectrum is comprised of the four π(Cl) to t_{2g}(d) and one σ(Cl) to t_{2g}(d) transitions. The absorptions are labelled according to the symmetry of the halide-based donor levels.*

Our next step is to examine d^5 complexes of D_{4h} symmetry (*trans*-$[MX_4L_2]^{z-}$), where L is generally a neutral ligand and potentially a π-acceptor (*e.g.* Bu^{t}NC, CO, *etc.*) rather than a π-donor like halide X^-. The main difference between these tetragonal complexes and those of octahedral symmetry comes as a result of the positive tetragonal field imposed on the central ion. Due to tetragonal distortion, the metal t_{2g} subshell is further split into $e_g(d_{xz}$ and $d_{yz})$ and $b_{2g}(d_{xy})$, while the e_g subshell is split into a_{1g} and b_{1g} orbitals, as shown in Figure 3.2.3. Thus the relatively destabilised, singly occupied $b_{2g}(d_{xy})$ orbital becomes the lowest available metal acceptor orbital. It is important to note that this acceptor orbital lies in the plane defined by the central ion and the four π-donor halide ligands ($\{MX_4\}$ fragment), so the electron hole is now restricted to the XY plane. Thus the intense optical charge-transfer spectra of these complexes are dominated by the planar $\{MX_4\}$ chromophore.

Let us now turn to the halide-based donor orbitals. Due to the decrease in the number of halide ligands (compared to the hexahalide complexes), the number of potential donor π-levels is now only three, rather than four: a_{2g}, e_u (doubly degenerate), b_{2g} (Figure 3.2.4). Hence there could be three possible transitions into the lowest metal-based acceptor orbital $b_{2g}(d_{xy})$. Laporte's Rule requires that only *one* intense absorption remains, corresponding to $e_u(X)$ to $b_{2g}(d_{xy})$ transition. The $\{X_4\} \rightarrow M^{III}$ charge-transfer manifold of these complexes is typified by the spectrum of $[RuCl_4(CH_3CN)_2]^{1-}$ (Figure 3.2.5).[5] The main peak appears as a doublet. The splitting is caused by ligand-centred spin-orbit coupling associated with the array of halide ions. A similar effect was observed earlier (but not accounted for) in the spectra of *trans* $[OsX_4(CO)(H_2O)]^{1-}$ complexes,[21] where X = Cl, Br or I: the spectrum of the chloride species shows a single broad principal absorption, but the principle peaks are split for the bromo- and iodo-complexes. This splitting is undoubtedly associated with the halide-associated spin-orbit coupling, which increases from chloride to iodide. We shall see, that in most halide nitrosyl complexes examined in this work, the principal $e_u(X)$ to $b_{2g}(d_{xy})$ charge-transfer band is either broadened (chlorides) or even split into two bands (bromides) because of the spin-orbit coupling.

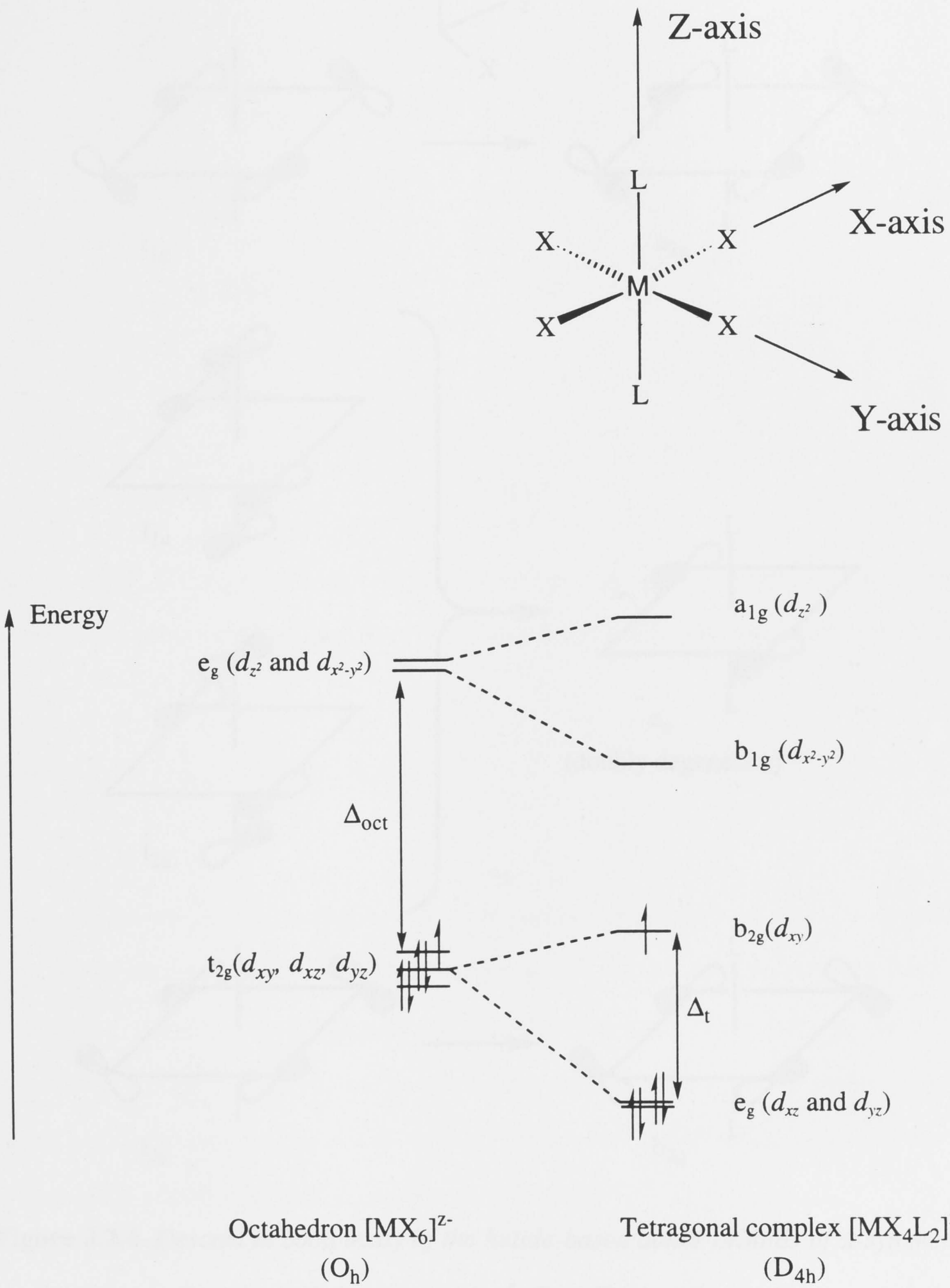

Figure 3.2.3 *Schematic representation of the splitting of the d-shell of a regular d^5 octahedral complex in a tetragonally distorted D_{4h} system, where the axial ligands L are more π-acidic than X (e.g. trans $[Os^{III}Cl_4(CO)_2]^{1-}$). For the tetragonal complexes of C_{4v} symmetry (e.g. $[OsCl_5(NO)]^{1-}$) the schematic orbital diagram is analogous, but the "g" descriptions are lost.*

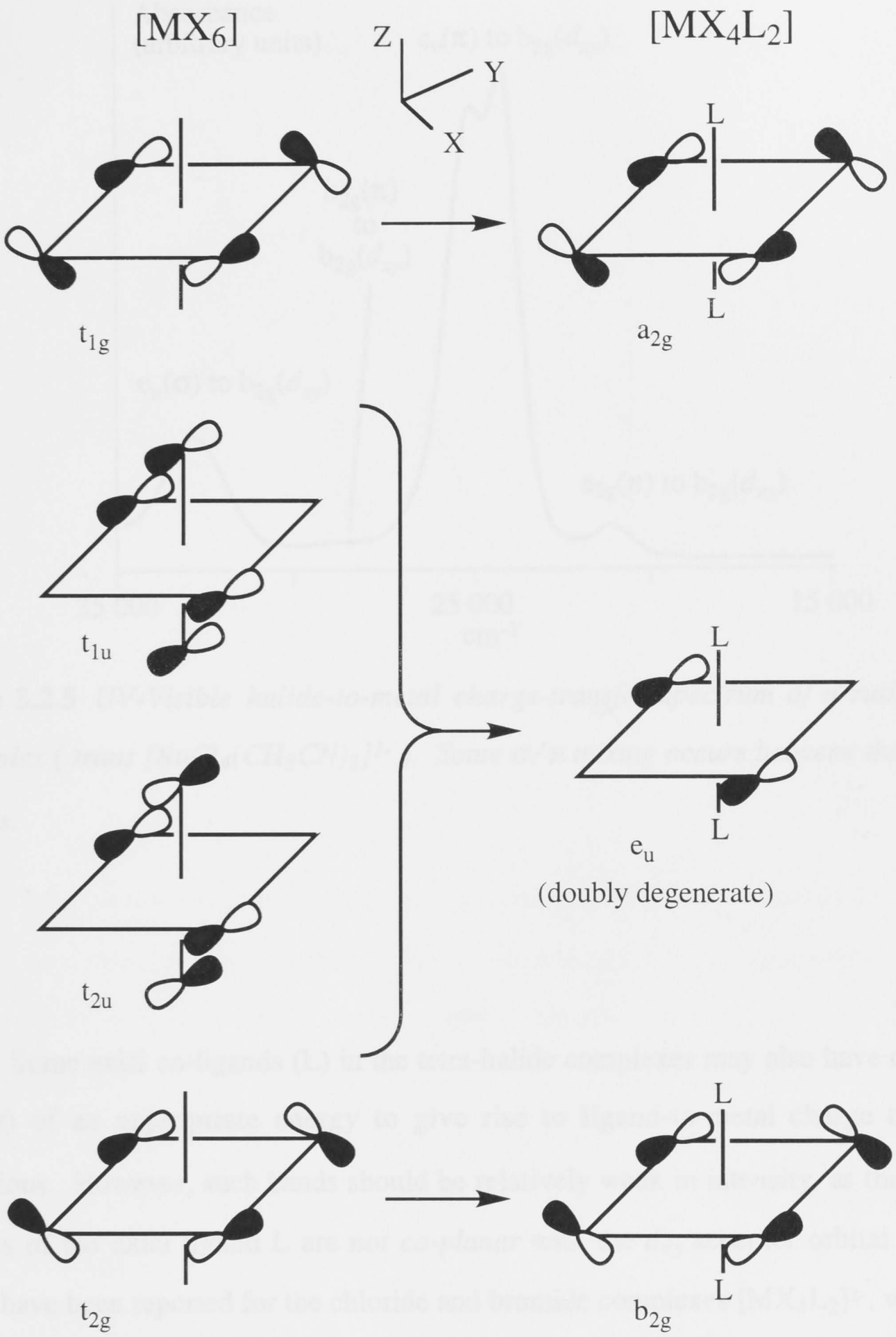

Figure 3.2.4 *Descent in complexity of the halide-based donor orbitals of π-symmetry participating in the principal charge-transfer.*[5] *For effective electronic promotion such orbitals are required to be co-planar with the metal-based dπ acceptor orbital (the one lying in the XY-plane selected for this Figure): in the case of* $[MX_6]^{z-}$ *the acceptor is one of the* t_{2g} (d_{xy}, d_{xz} *or* d_{yz}) *orbitals, while in the case of* $[MX_4L_2]^{z-}$ *it is the* b_{2g} (d_{xy}) *orbital, as shown in the Figure 3.2.3.*

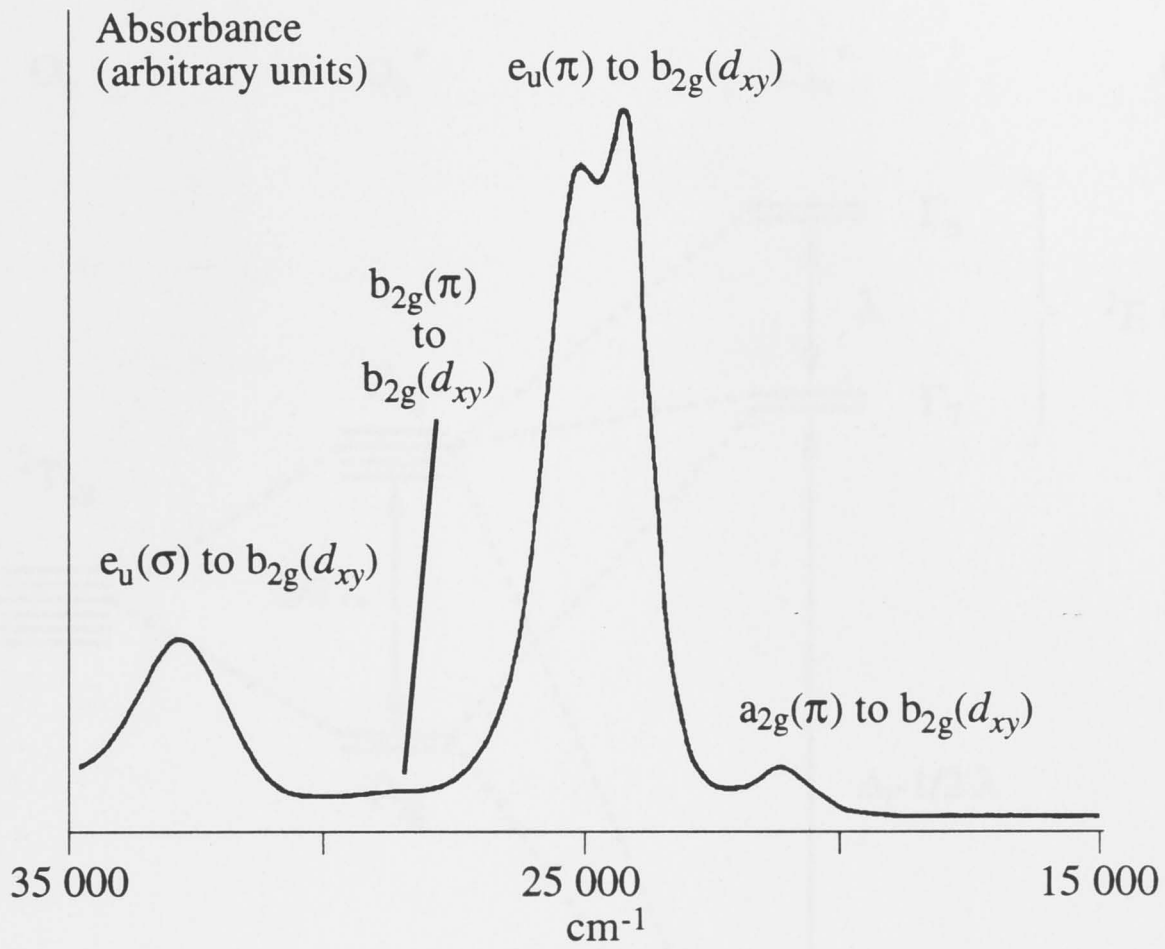

Figure 3.2.5 *UV-Visible halide-to-metal charge-transfer spectrum of a ruthenium d^5 complex (trans $[RuCl_4(CH_3CN)_2]^{1-}$). Some σ/π mixing occurs between the halide orbitals.*

Some axial co-ligands (L) in the tetra-halide complexes may also have orbitals (σ or π) of an appropriate energy to give rise to ligand-to-metal charge transfer transitions. However, such bands should be relatively weak in intensity, as the donor orbitals of the axial ligand L are *not co-planar* with the d_{xy} acceptor orbital. Such bands have been reported for the chloride and bromide complexes $[MX_4L_2]^{z-}$, where L is phosphine or arsine, and M is osmium or ruthenium.[22,23]

The $[MX_4LL']^{z-}$ or $[MX_5L]^{z-}$ complexes have C_{4v} symmetry, and the Laporte Rule cannot be applied rigorously as these complexes lack a centre of inversion. However their electronic spectra display very similar characteristic absorptions and are interpreted in the same way as the D_{4h} systems.

Transitions within the $t_{2g}(M)$ related subshell of a tetragonally substituted system are expected to give rise to yet another type of very weak low-frequency absorptions, which have been recognised in the spectra of tetragonal osmium halide

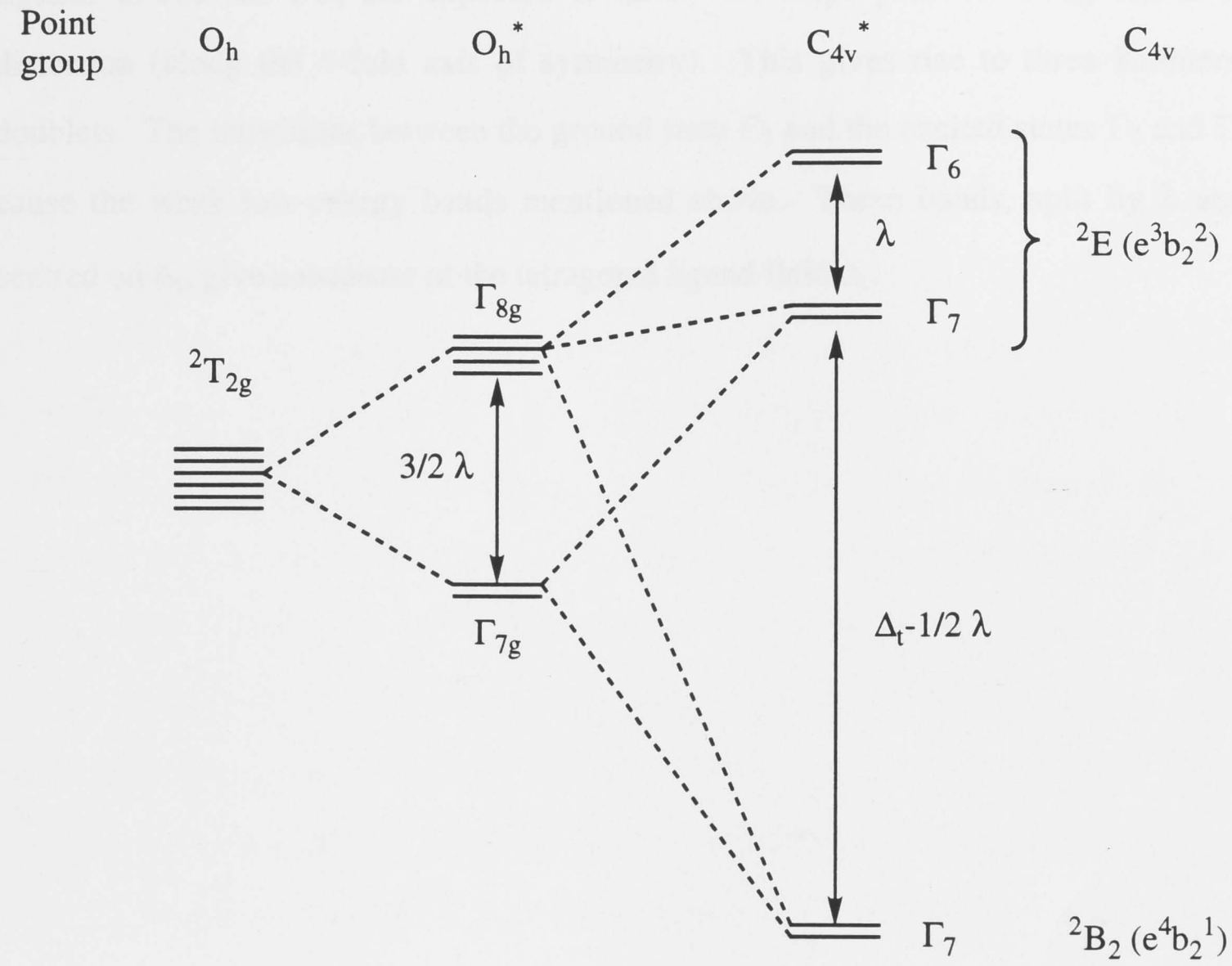

Figure 3.2.6 *Schematic diagram showing successive splitting of the sixfold degenerate $^2T_{2g}$ ground term of a regular octahedral d^5 complex (O_h) by the spin-orbit coupling, 3/2 λ (O_h^*), and then by a* ***very strong*** *tetragonal field Δ_t (in the limiting trans-$[MX_4LL']^{z-}$ case; e.g. L = NO^+) (C_{4v}^*). The absorptions corresponding to the transitions $\Gamma_7 \rightarrow \Gamma_7$ and $\Gamma_7 \rightarrow \Gamma_6$, with energies $\Delta_t \pm \lambda/2$, may be observed in the near-IR region of an electronic spectrum. The picture for the trans-$[MX_4L_2]^{z-}$ complexes (D_{4h}) would be analogous.*

complexes in the near IR (NIR) region.[7,22] In the octahedral t_{2g}^5 complexes $[MX_6]^{z-}$ the sixfold degenerate ground term $^2T_{2g}$ is split by spin-orbit coupling into two states Γ_{7g} (Γ_7^+) and Γ_{8g} (Γ_8^+), as shown in Figure 3.2.6. The spin-orbit coupling constant λ is approximately 3000 cm^{-1} for osmium complexes and 1000 cm^{-1} for ruthenium ones. The *trans*-$[MX_4(L)(L')]^{z-}$ complexes, particularly where at least one of the axial

ligands is NO^+ or CO, are expected to have very large positive tetragonal field distortion (along the 4-fold axis of symmetry). This gives rise to three Kramers' doublets. The transitions between the ground state Γ_7 and the excited states Γ_7 and Γ_6 cause the weak low-energy bands mentioned above. These bands, split by λ and centred on Δ_t, give a measure of the tetragonal ligand field Δ_t.

3.2.2 The Present Work

The optical spectra of the present tetragonal halo-nitrosyl complexes $[MX_4(NO)L]^{z-}$ (L = X or CH_3CN) and their analogues (Table 3.2.1) exhibit similar traits to those of other halide complexes of ruthenium and osmium, examined critically for the first time, as explained above. The main features of the intense charge-transfer manifold are: a principal $e(X_\pi)$ to $b_2(d_{xy})$ band (in some instances accompanied by weak $a_2(X_\pi)$ to $b_2(d_{xy})$ band and a $b_2(X_\pi)$ to $b_2(d_{xy})$ band, almost indistinguishable from the background) with the two bands lying to higher energy corresponding to $e(X_\sigma)$ to $b_2(d_{xy})$ and $e(X_\pi)$ to $b_1(d_{x^2-y^2})^*$ transitions. Weak (particularly for ruthenium) central ion *d-d* bands may be observed in the near-IR region in the tetragonal complexes, which in terms of electron orbitals are the transitions between the $e(d_{xz}$ and $d_{yz})$ and $b_2(d_{xy})$ orbitals, modified by spin-orbit coupling as described in the previous section.

These two types of transitions should allow us to draw a semi-quantitative map reflecting energies of the metal and halide orbitals involved. If surveyed for a series of complexes, such mapping may reveal the influence exerted by a variety of ligands on the energy of the frontier orbitals in tetragonal complexes. The doubly degenerate $e(d_{xz}$ and $d_{yz})$ level of the *trans*-$[MX_4LL']^{z-}$ complexes is particularly sensitive to the π-acceptor strength of the ligands L and L′. The d_{xz} and d_{yz} orbitals interact directly with the vacant π-antibonding orbitals of the axial ligands L and L′, and therefore may be stabilised by π-interactions with π-acidic ligands (*e.g.* CO and NO^+ in particular). At the same time the $b_2(d_{xy})$ orbital is orthogonal to the π-antibonding orbitals of L and L′, hence it cannot be directly stabilised by π-interaction. The $b_1(d_{x^2-y^2})$ and $a_1(d_{z^2})$ orbitals, being effectively σ-antibonding orbitals, may be destabilised by σ-interaction with the halides of the $\{MX_4\}$ plane or the axial ligands respectively. In addition, in a $[MX_4L_2]^z$ complex containing better electron withdrawing (π-acidic) ligands all metal valence orbitals will be indirectly stabilised to some extent, as the effective positive charge on the central ion becomes larger. The latter effect may be relayed to the halide

---

* This high energy band may be obscured, particularly in the chloride complexes, by the solvent or aromatic counter-anion (e.g. $[BzPh_3P]^+$) absorptions.

donor orbitals, however it should be attenuated, because as these orbitals lie further away from the central ion.[4] In this light, an instructive comparison may be drawn between the analogous nitrile, carbonyl and nitrosyl halide complexes. Notably, the halide-to-metal charge-transfer (XMCT) manifold of each $[MX_5L]^{z-}$ complex, while generally retaining the same band shape, is red-shifted by roughly 5000-8000 cm^{-1}, when the CO replaces the nitrile; and by a further 6000-7000 cm^{-1} in the nitrosyl complexes. This reflects the extent of the stabilisation of the *d*-shell acceptor orbitals in relation to the halide donor orbitals in those complexes (Figure 3.2.7).

The energies of the bands assumed as intraconfigurational *d-d* transitions are presented in the Table 3.2.2. The obvious trend is that the $\nu_{d\text{-}d}$ increases as the positive tetragonal field becomes greater, in accord with the increase in the π-acidic properties of the axial ligands L (Figure 3.2.6). In $[RuCl_5(NO)]^{1-}$ the *d-d* band is observed very close to the charge-transfer manifold (on the low energy side of the $a_2(X_\pi)$ to $b_2(d_{xy})$ band) (Figure 3.2.12). In the carbonyl analogue this band is red-shifted by almost 2000 cm^{-1}, while the charge-transfer bands move to the higher energy (*vide supra*). In fact, only the very strong tetragonal field in the carbonyl and nitrosyl complexes of ruthenium (where the spin-orbit coupling constant is *ca.* 3 times smaller than that of osmium) allows us to observe these weak absorptions above 6000 cm^{-1} and they have not been reported before. According to this assignment, the *d-d* bands and the XMCT envelope should converge as L, L′ become more π-acidic in the sequence RCN, CO, NO^+.

We have already stressed that the simplistic linear ligand additivity model for redox potentials does not apply to *trans*-$[MX_4LL']^{z-}$ complexes containing CO and NO^+ ligands. This is rather unfortunate as this model promises predictable E^o values that are simply a linear function of stoichiometry. However, direct correlation of the electrochemical and the spectroscopic data may provide an alternative way to understand and, indeed, predict the redox properties of a complex: according to Jørgensen's concept of a charge-transfer absorption being the result of an intramolecular one-electron redox process it should be possible to correlate (at least

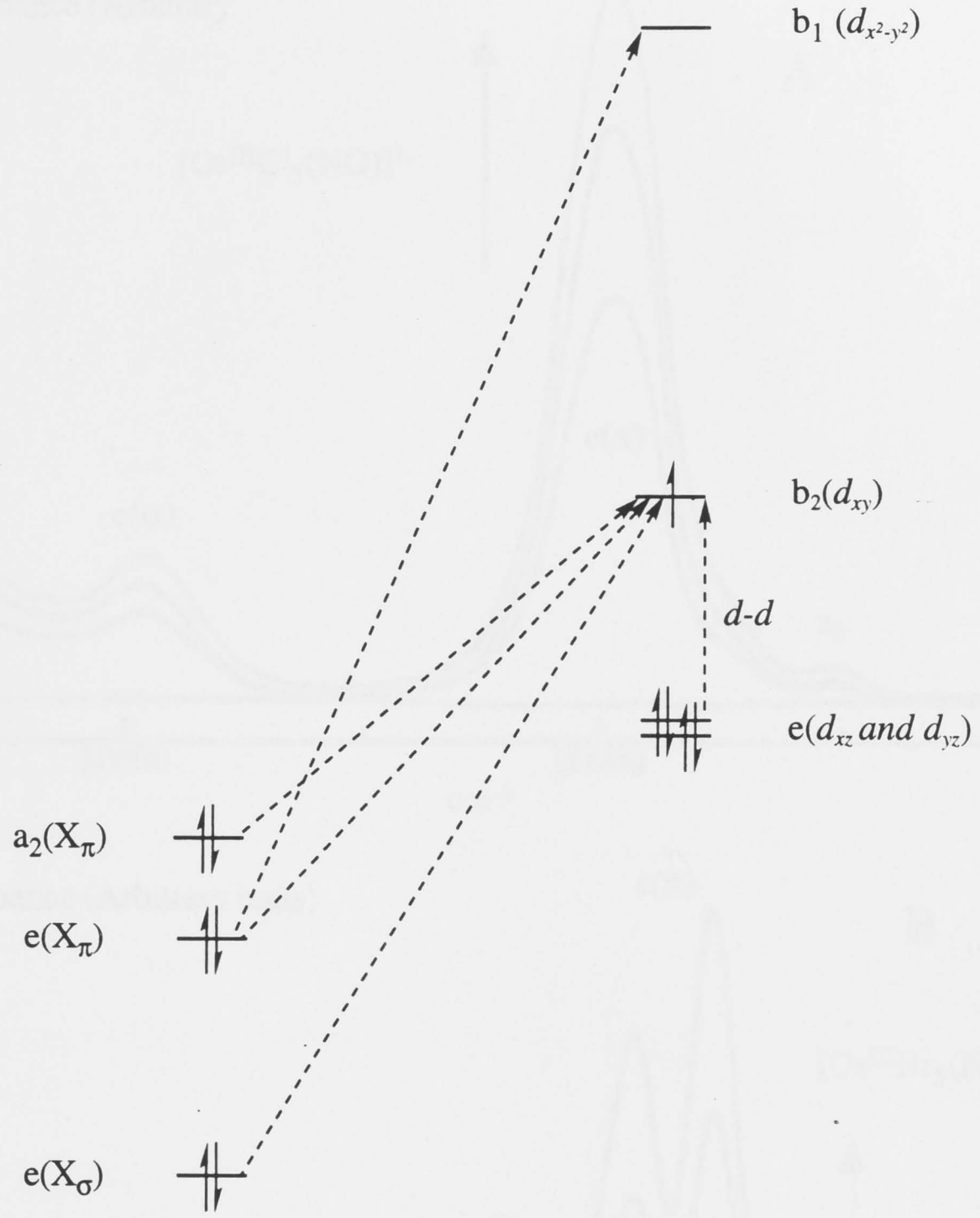

Figure 3.2.7 *Schematic energy diagram* (the map) displaying the main four halide-to-metal charge-transfer bands and d-d transitions in d^5 tetra- and penta-halide complexes (C_{4v} symmetry) of ruthenium and osmium. For simplicity, the halide donor levels are all presented as single orbitals .*

---

* All transitions into the $b_2(d_{xy})$ orbital result in an electron configuration with the three doubly occupied d-orbitals, allowing only one term in the excited state. Thus the position of a corresponding absorption gives us the exact measure of a gap between a donor level and the $b_2(d_{xy})$ orbital. However it is not so in the case of the $e(X_\pi)$ to $b_1(d_{x^2-y^2})$ transition (the latter is only half-occupied in the excited state). Therefore the energy of this absorption is only an approximate indication of the gap between these orbitals.

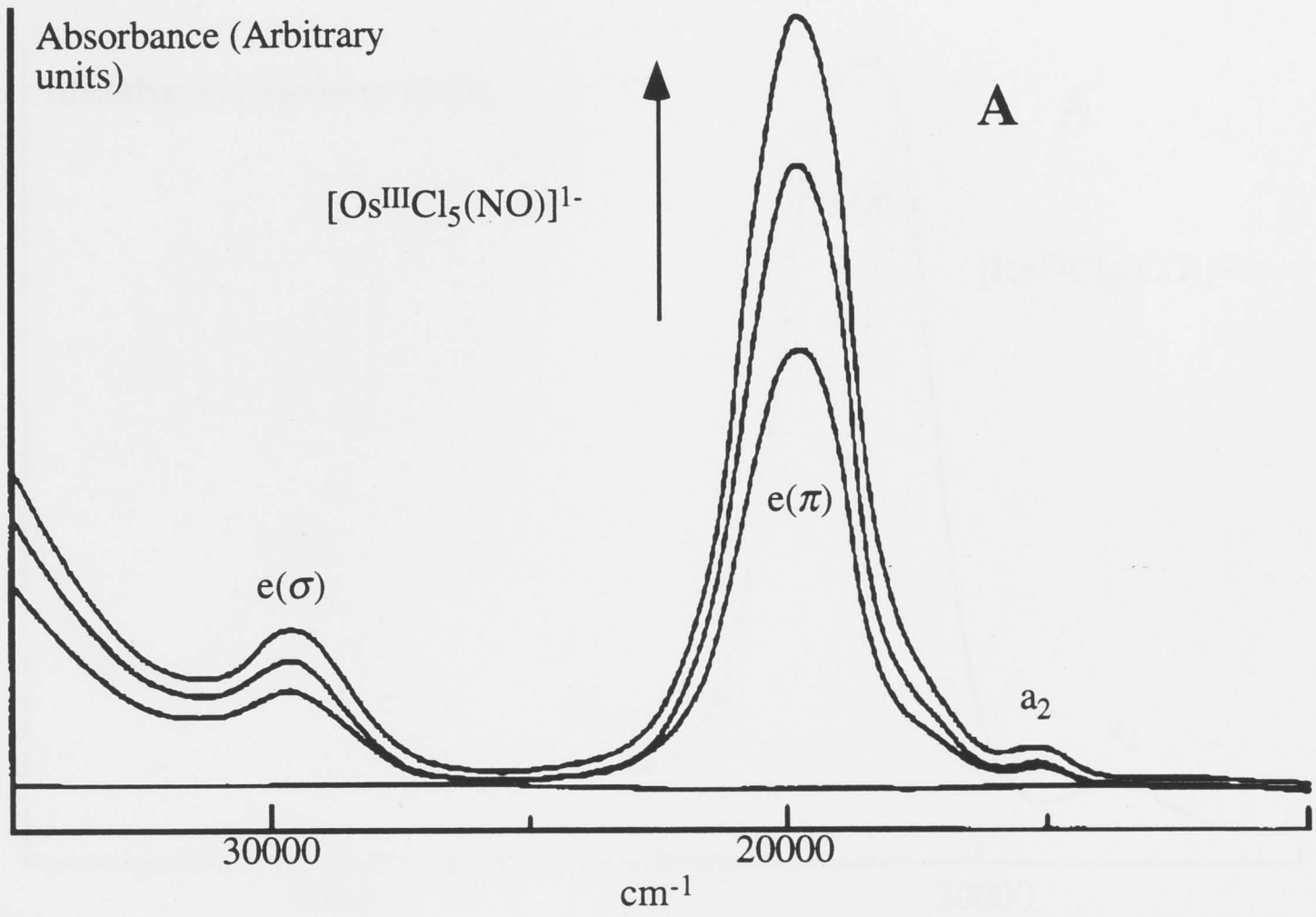

Figure 3.2.8 *Spectral progression accompanying anodic electro-generation of* $[Os^{III}Cl_5(NO)]^{1-}$ (***A***) *and* $[Os^{III}Br_5(NO)]^{1-}$ (***B***) *in a dichloromethane solution at 223 K (-50 °C) and +1.6 V. The featureless spectra of the starting divalent metal complexes were used as the background. The unusual line shape of the bromide complex spectrum (**B**) is due to the combination of both spin-orbit (Br^-) and vibronic coupling.*

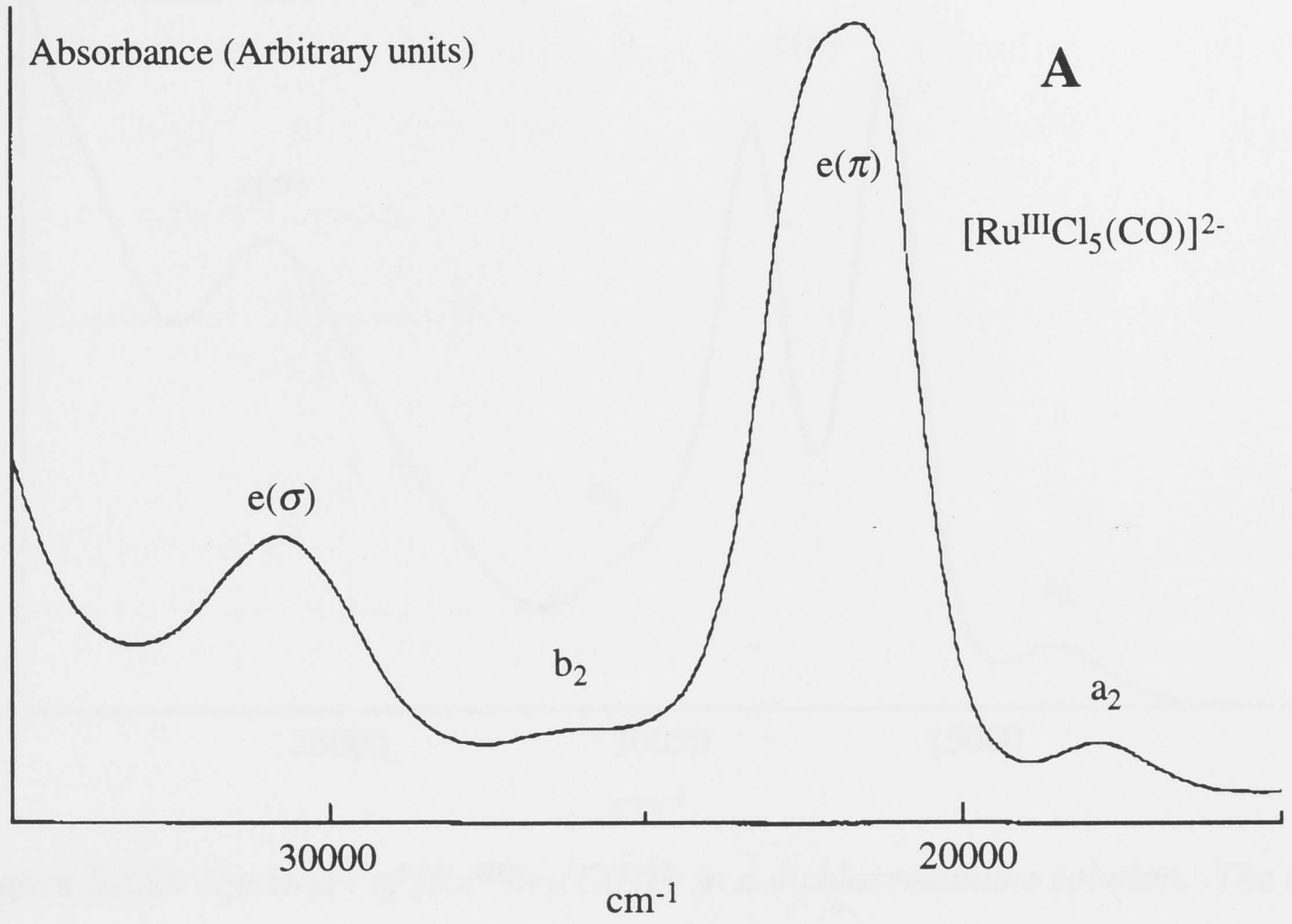

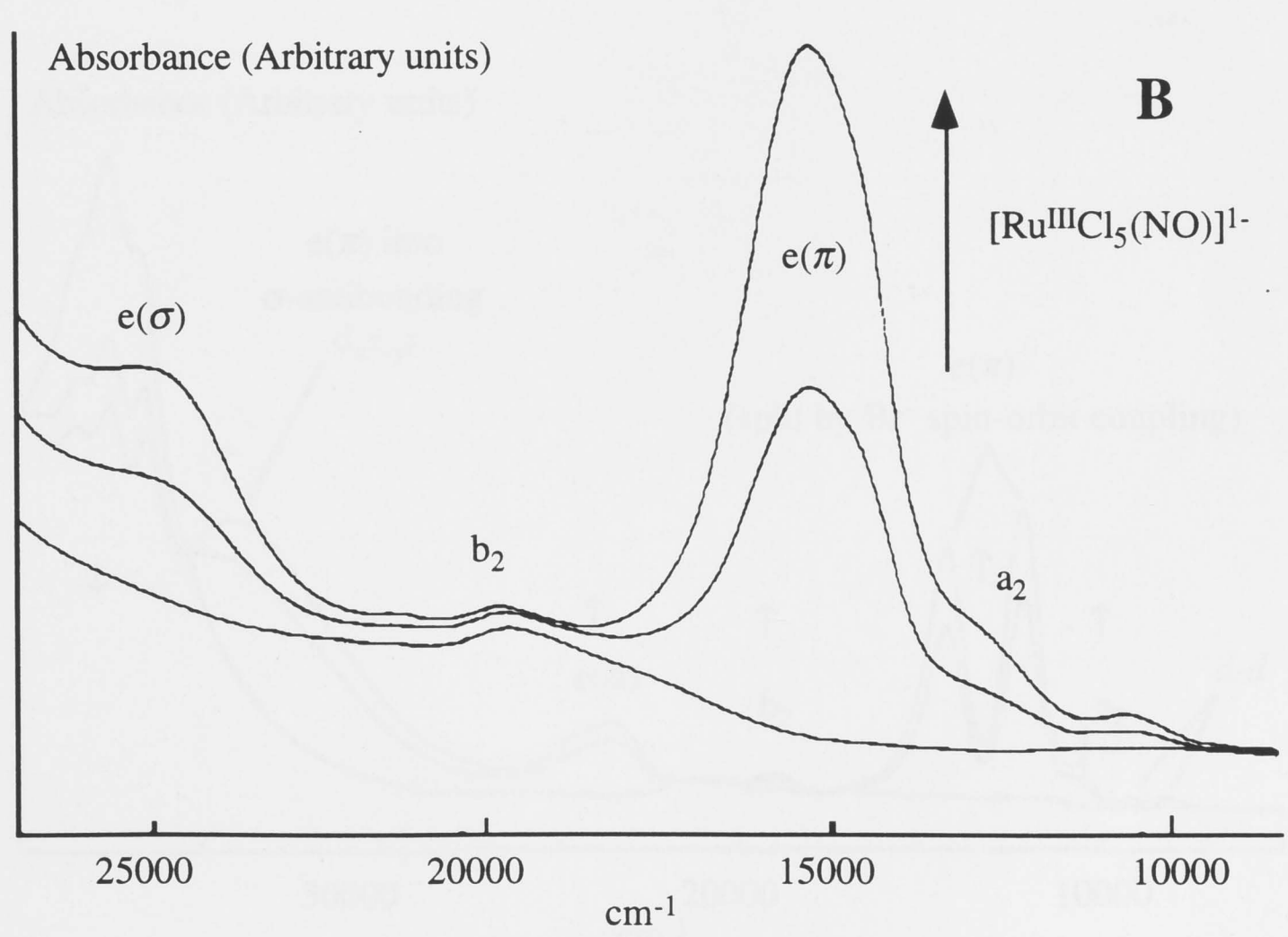

Figure 3.2.9 *Spectrum of $[Ru^{III}Cl_5(CO)]^{2-}$ (**A**) and the spectral progression accompanying anodic electro-generation of $[Ru^{III}Cl_5(NO)]^{1-}$ (**B**) in dichloromethane solution at 223 K (-50 °C) and +2.0 V.*

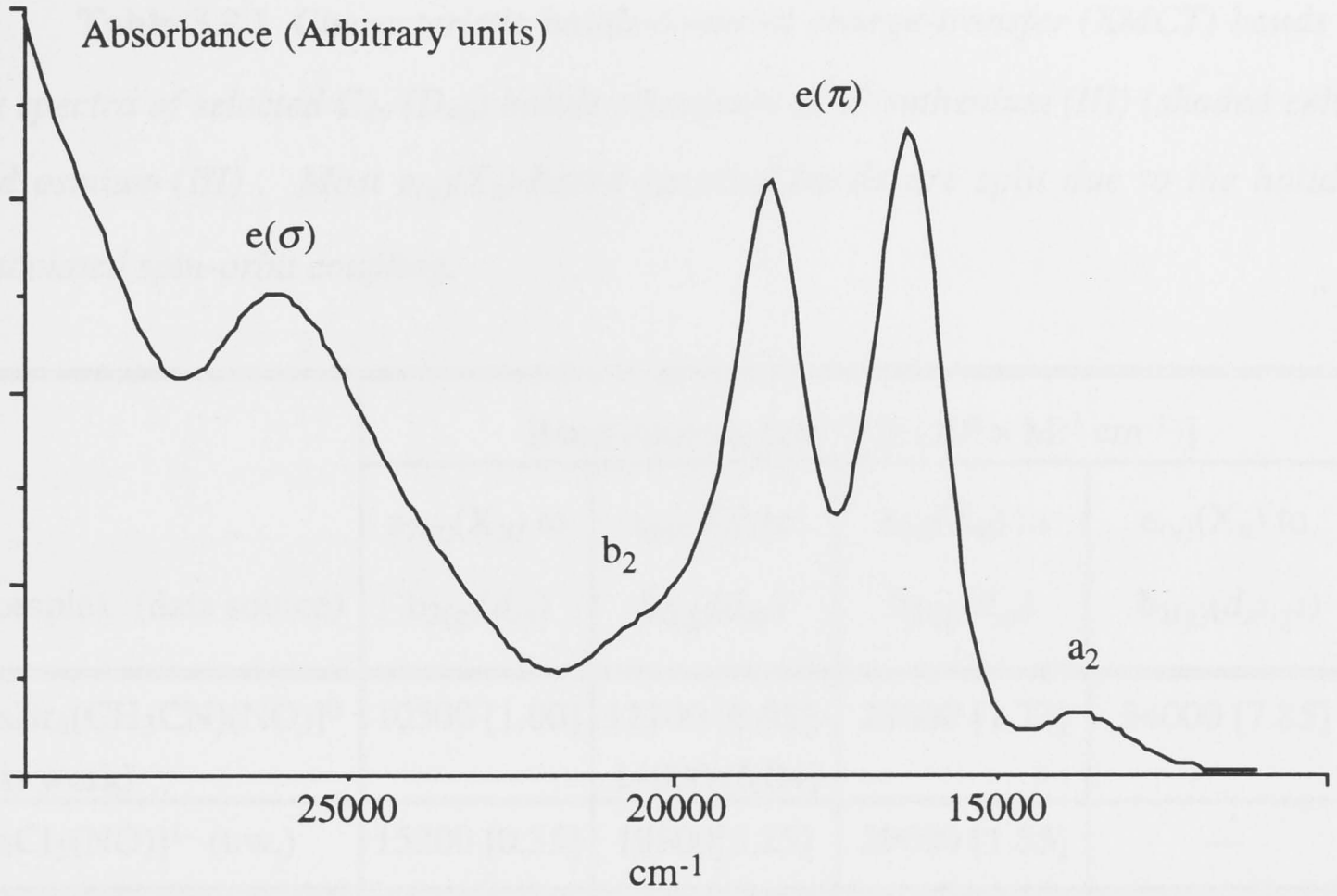

Figure 3.2.10 *Spectrum of $[Ru^{III}Br_5(CO)]^{2-}$ in a dichloromethane solution. The e(π) to d_{xy} CT band is split by spin-orbit coupling associated with the halide.*

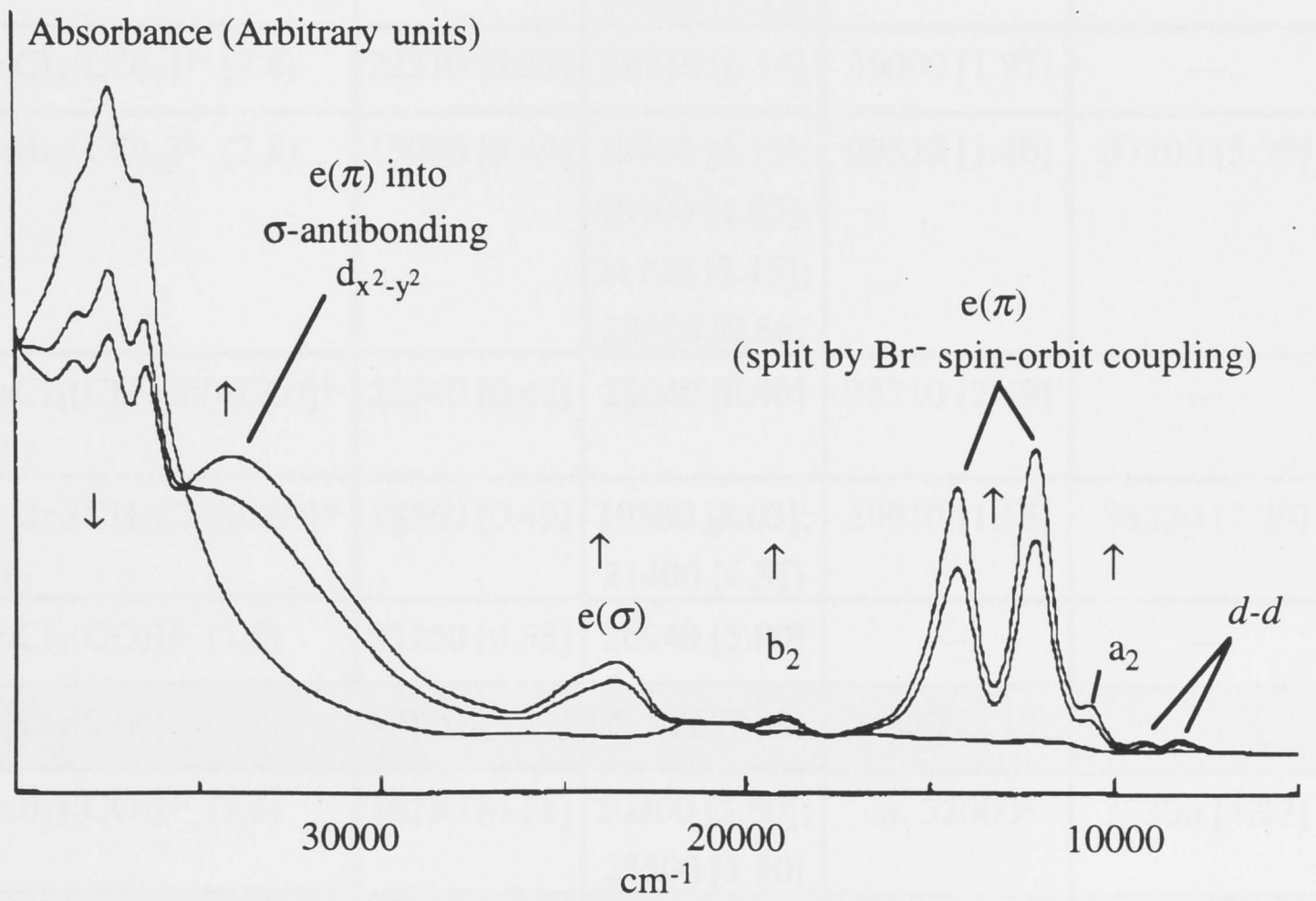

Figure 3.2.11 *Spectral progression accompanying electrochemical oxidation of $[Ph_3BzP]\,[Os^{II}Br_4(CH_3CN)(NO)]$ in an acetonitrile solution at 243 K (-30 °C) and +2.0 V. Arrows indicate the direction of change. The decreasing absorption above 35000 cm^{-1} belongs to the $[Ph_3BzP]^+$ ion migrating from the anode compartment.*

Table 3.2.1 *Characteristic halide-to-metal charge-transfer (XMCT) bands in the spectra of selected C_{4v} (D_{4h}) halide complexes of d^5 ruthenium (III) (shaded cells) and osmium (III) . Most $e_{(u)}(X_\pi)$-based spectral bands are split due to the halide-associated spin-orbit coupling.*

Complex (data source)	Band maxima (cm^{-1}) [ε ($10^3 \times M^{-1} cm^{-1}$)]			
	$a_{2(g)}(X_\pi)$ to $b_{2(g)}(d_{xy})$	$e_{(u)}(X_\pi)$ to $b_{2(g)}(d_{xy})$	$e_{(u)}(X_\sigma)$ to $b_{2(g)}(d_{xy})$	$e_{(u)}(X_\pi)$ to $b_{1(g)}(d_{x^2-y^2})$
$[OsBr_4(CH_3CN)(NO)]^0$ (this work)	10500 [1.00]	12200 [6.65]; 14000 [5.84]	23600 [1.73]	34000 [7.85]
$[OsCl_5(NO)]^{1-}$ (t.w.)	15200 [0.35]	19800[5.25]	29600 [1.55]	---
$[RuCl_5(NO)]^{1-}$ (t.w.)	10600 [0.35]	15200 [6.87]	25000 [3.55]	---
$[OsBr_5(NO)]^{1-}$ (t.w.)	10600 [1.00]	12300 [2.40]; 13600 [5.45]; 15200 [4.50]; 17600 [1.55]	25800 [2.00]	32000[a] [6.10]
$[OsCl_4(CO)_2]^{1-}$ (7,8)	22310 [0.32]	26210 [6.14]	36000 [1.77]	---
$[OsBr_4(CO)_2]^{1-}$ (7,8)	15930 [0.45]	18460 [6.15]; 20100 [4.63]; 21720 [2.15]; 23820 [0.66]	29520 [1.40]	37200 [5.39]
$[OsCl_4(CH_3CN)(CO)]^{1-}$ (7,8)	22540 [0.42]	26040 [8.40]	35710 [2.49]	---
$[OsBr_4(CH_3CN)(CO)]^{1-}$ (7,8)	15560 [0.49]	19380 [8.03]; 21400 [6.31]	29910 [1.55]	38230 [7.29]
$[OsCl_5(CO)]^{2-}$ (7,8)	23150 [0.53]	26940 [5.80]	---	---
$[RuCl_5(CO)]^{2-}$ (t.w.)	17800 [0.39]	21500 [7.40]	30800 [2.14]	---
$[OsBr_5(CO)]^{2-}$ (7,8)	16150 [0.58]	20300 [3.60]; 23500 [1.80]	*ca.* 32000[a]	37300 [4.97]
$[RuBr_5(CO)]^{2-}$ (t.w.)	12680 [0.48]	15330 [5.80]; 17450 [5.30]	25100 [2.65]	32530[a] [10.00]
$[OsCl_4(Bu^tNC)_2]^{1-}$ (7,8)	25320 [1.20]	28570 [5.00]	---	---

[a] shoulder

Table 3.2.1 (cont.)

	Band maxima (cm^{-1}) [ε ($10^3 \times M^{-1} cm^{-1}$)]			
Complex (data source)	$a_{2(g)}(X_\pi)$ to $b_{2(g)}(d_{xy})$	$e_{(u)}(X_\pi)$ to $b_{2(g)}(d_{xy})$	$e_{(u)}(X_\sigma)$ to $b_{2(g)}(d_{xy})$	$e_{(u)}(X_\pi)$ to $b_{1(g)}(d_{x^2-y^2})$
$[RuCl_4(Bu^tNC)_2]^{1-}$ (6)	20610 [0.39]	23870 [5.26]	---	---
$[OsBr_4(Bu^tNC)_2]^{1-}$ (7,8)	19370 [0.47]	21820 [6.22]; 23020 [4.79]; 24880 [1.49]; 26430 [1.13]	31830 [1.21]	---
$[RuBr_4(Bu^tNC)_2]^{1-}$ (6)	15250 [0.30]	17540 [2.85]; 18870 [2.33]	---	---
$[OsCl_5(Bu^tNC)]^{2-}$ (7,8)	22890 [0.16]	29520 [1.05]	---	---
$[OsBr_5(Bu^tNC)]^{2-}$ (7,8)	20230 [0.63]	23000 [5.94]; 26000 [2.08]	31830 [3.47]	---
$[OsCl_4(CH_3CN)_2]^{1-}$ (7,8)	26440 [0.48]	29910 [6.76]; 30860 [6.94]	---	---
$[RuCl_4(CH_3CN)_2]^{1-}$ (5)	21150 [0.51]	24250 [5.90]; 25200 [5.40]	32810 [2.10]	40000 [8.10]
$[OsBr_4(CH_3CN)_2]^{1-}$ (7,8)	20360 [0.45]	23040 [5.82]; 25230 [5.90]	32850 [1.76]	40 590 [13.40]; 43330 [13.14]
$[RuBr_4(PhCN)_2]^{1-}$ (5)	14900 [0.47]	17500 [5.00]; 19600 [4.80]	*ca.* 27000[a]	31600 [16.00]
$[RuCl_4(As(CH_3)_3)_2]^{1-}$ (22)	23210 [0.54]	26530 [5.60]; 27370 [5.40]	---	---
$[OsCl_5(CH_3CN)]^{2-}$ (7,8)	*ca.* 30000[a]	32720 [6.44]	---	42160 [7.80]
$[RuCl_5(CH_3CN)]^{2-}$ (5)	23400 [1.02]	27000 [5.25]	34000 [2.02]	---
$[OsBr_5(CH_3CN)]^{2-}$ (7,8)	*ca.* 22500[a]	25510 [3.39]; 27140 [3.17]	---	39900 [10.39]
$[RuBr_5(PhCN)]^{2-}$ (5)	17900 [1.20]	19750 [3.40]; 21400 [4.10]	---	29350 [10.20]; 31000 [10.80]

[a] shoulder

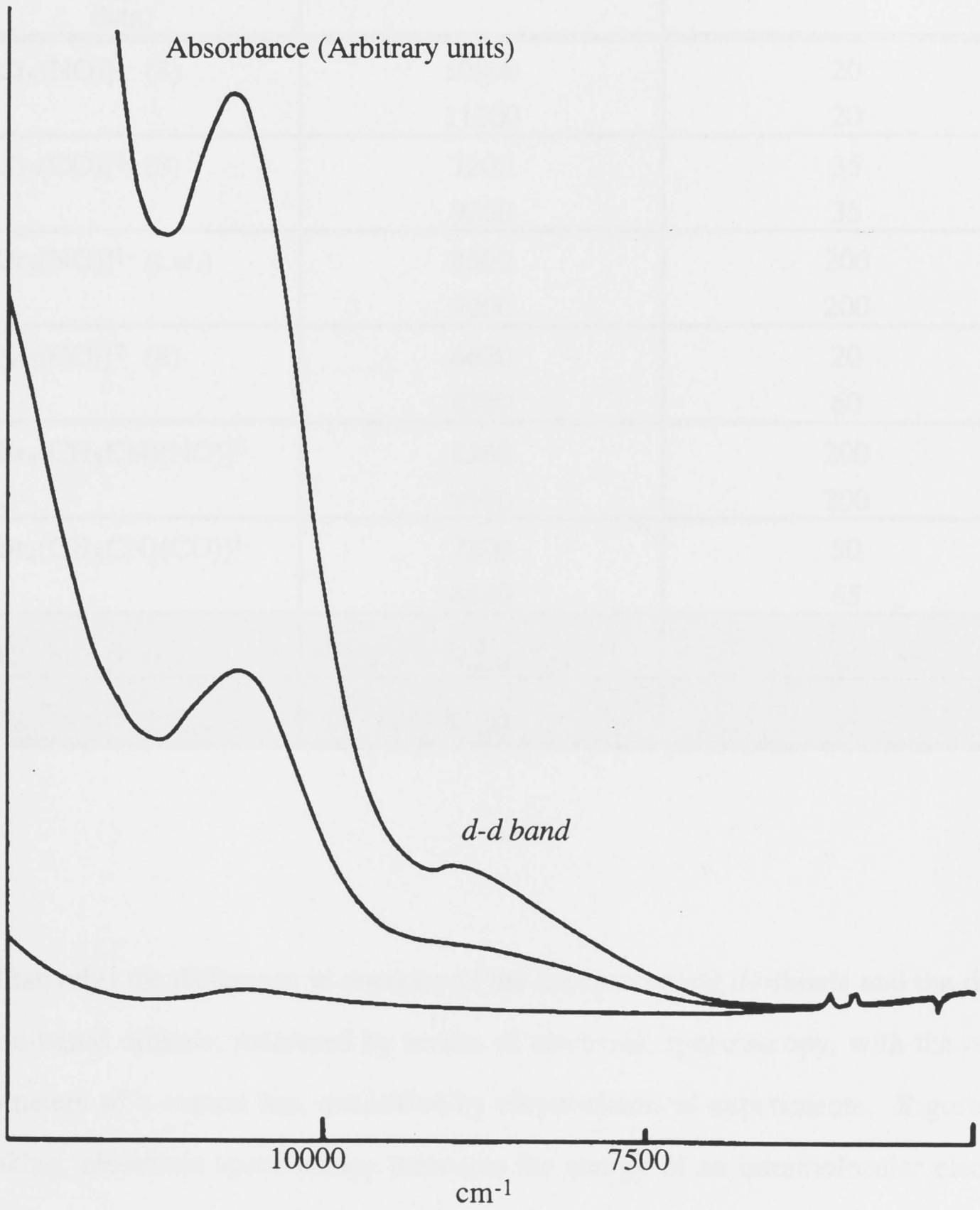

Figure 3.2.12 *Growing spectral progression in the near infra-red region accompanying anodic electro-generation of* $[Ru^{III}Cl_5(NO)]^{1-}$ *in a dichloromethane solution at 223 K (-50 °C) and +2.0 V.*

Table 3.2.2 *Intraconfigurational bands in the Near-IR spectra of tetragonal carbonyl and nitrosyl complexes of ruthenium (III) (shaded cells) and osmium (III) .*

Complex (source of the data)	Band maxima (cm^{-1})	ε ($M^{-1}\ cm^{-1}$)
$[OsCl_5(NO)]^{1-}$ (8)	10800 11500	20 20
$[OsCl_5(CO)]^{2-}$ (8)	7200 9280	35 35
$[OsBr_5(NO)]^{1-}$ (t.w.)	8500 9200	200 200
$[OsBr_5(CO)]^{2-}$ (8)	6620 8390	20 60
$[OsBr_4(CH_3CN)(NO)]^0$ (t.w.)	8200 9100	200 200
$[OsBr_4(CH_3CN)(CO)]^{1-}$ (8)	7200 8840	50 65
$[RuCl_5(NO)]^{1-}$ (t.w.)	9000	45
$[RuCl_5(CO)]^{2-}$ (t.w.)	7260	35

qualitatively) the difference in energies of the acceptor metal *d*-orbitals and the donor halide-based orbitals, measured by means of electronic spectroscopy, with the redox parameters of a central ion, quantified by electrochemical experiments. Rigorously speaking, electronic spectroscopy measures the energy of an intramolecular electron transfer, which is an adiabatic process (the Frank-Condon principle), while the electrochemical methods provide us with thermodynamic data, since the E^o value is directly related to the Gibbs free energy of a redox process. Despite this significant distinction, there have been several successful examples of correlation of charge-transfer energies and electrochemical data.* Metal-to-ligand charge-transfer (MLCT, M^{II} to bipy) were found to be linked with metal-based oxidation potentials and ligand-based reduction potentials in a series of 2,2′-bipyridine and related complexes of

* An early example of such a correlation was described by D.F. Shriver and J. Posner for a series of iron cyanide complexes (*J. Amer. Chem. Soc.* **1966**, *88*, 1672)

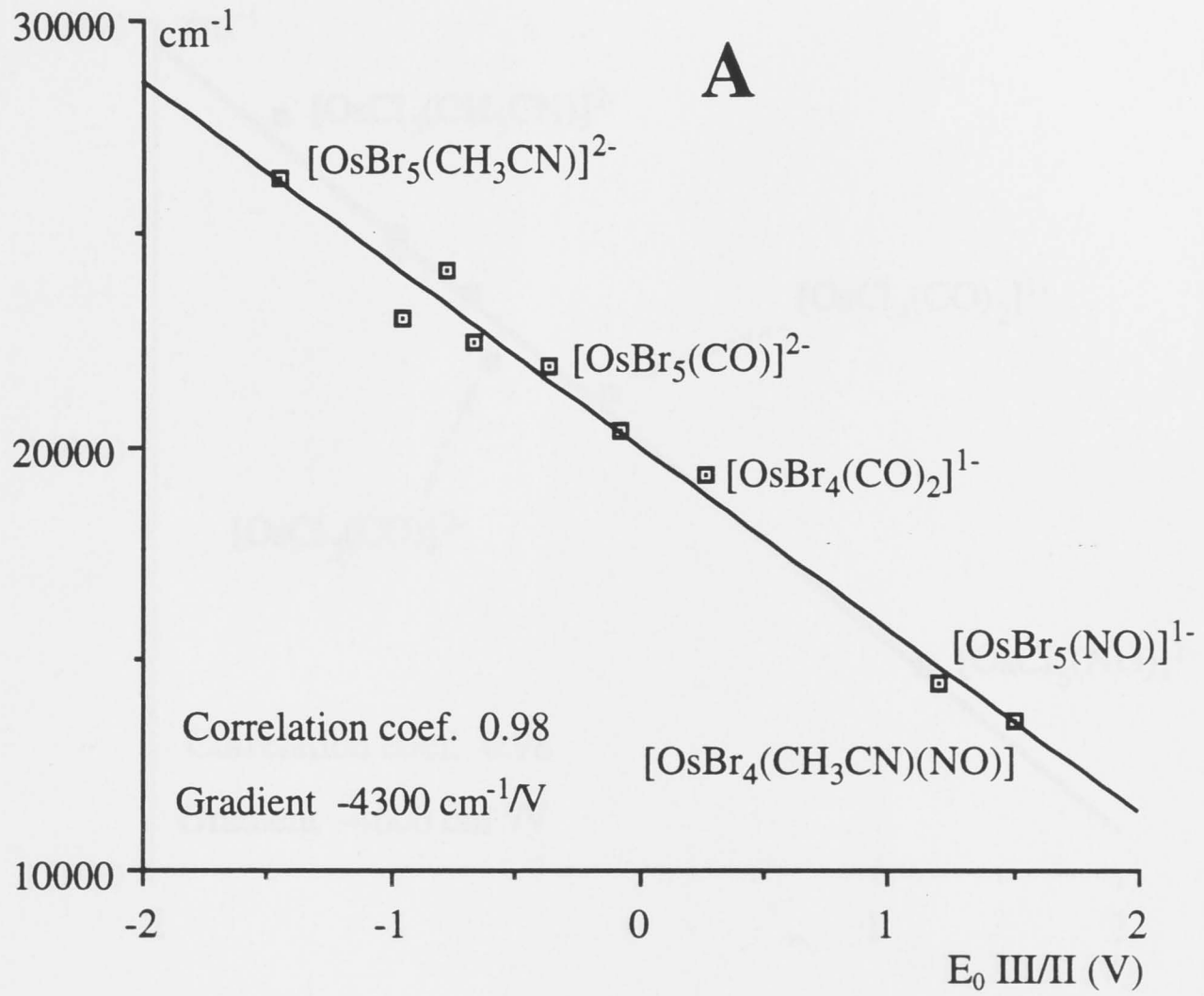

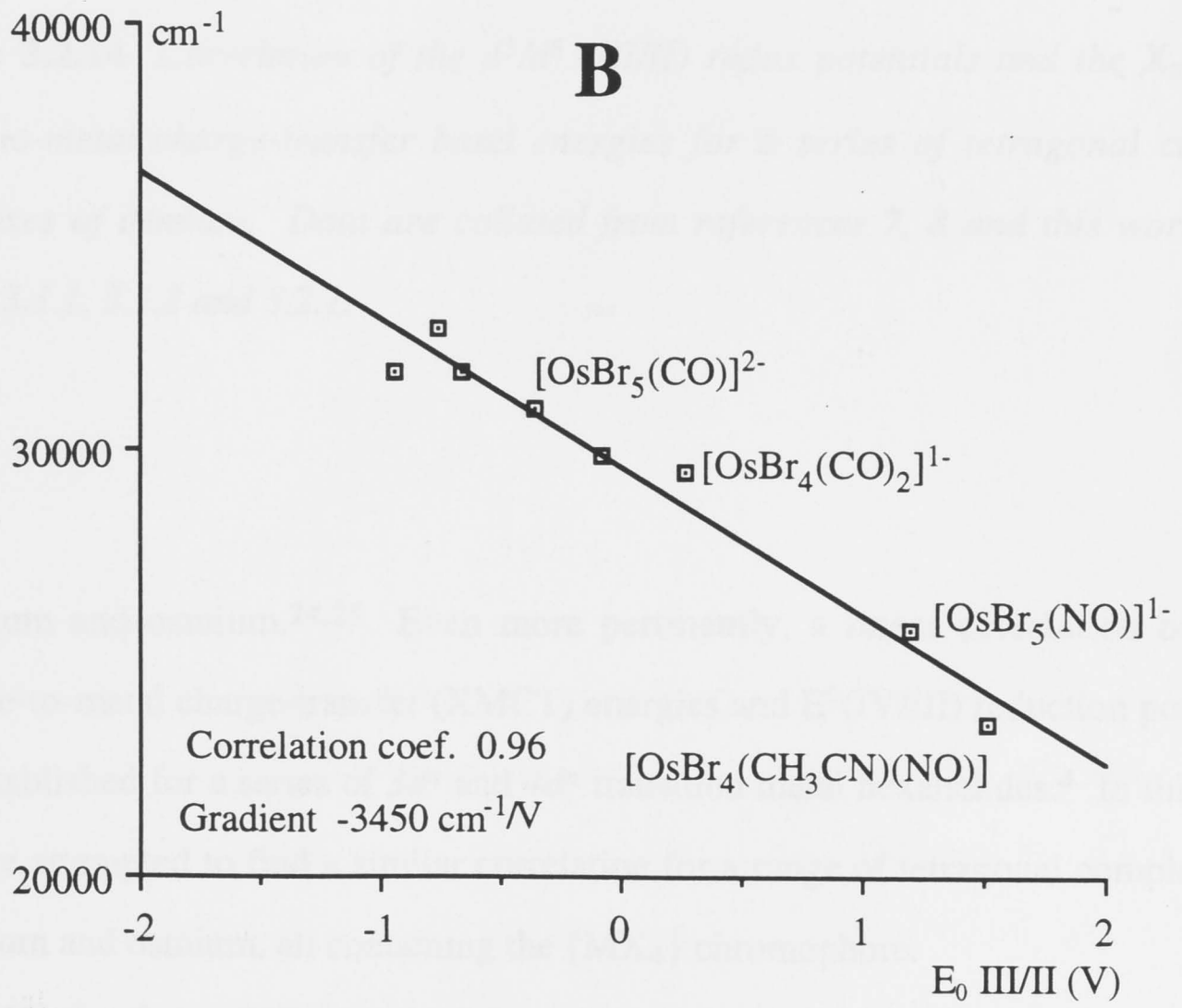

Figure 3.2.13 *Correlation of the d^5/d^6 (III/II) redox potentials and the X_π to d_{xy} (graph* ***A****) or X_σ to d_{xy} (graph* ***B****) halide-to-metal charge-transfer (XMCT) band (centres of gravity) energies for a series of tetragonal bromide complexes of osmium. Data are collated from references 7, 8 and this work. See Tables 3.1.1, 3.1.2 and 3.2.1.*

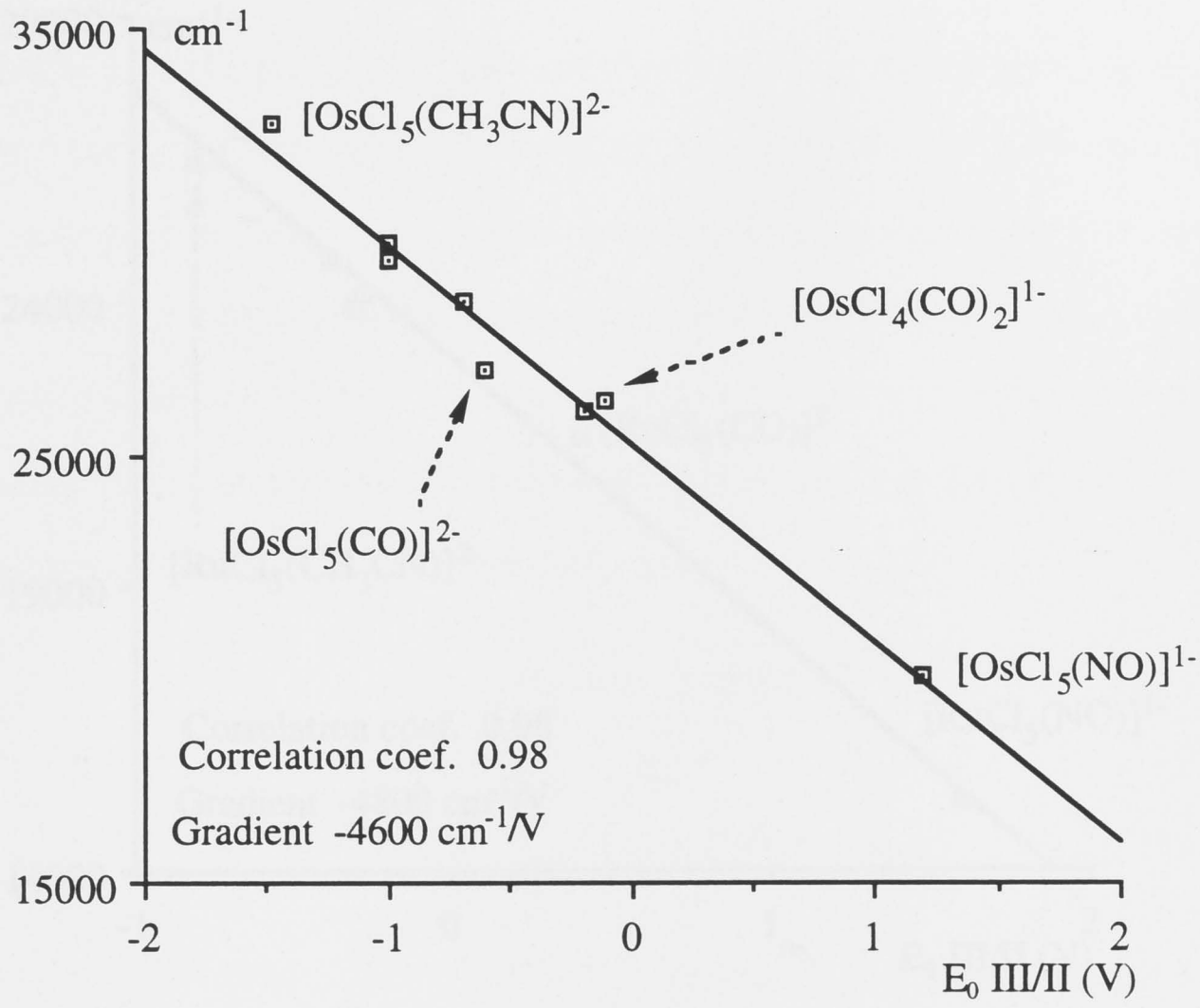

Figure 3.2.14 *Correlation of the d^5/d^6 (III/II) redox potentials and the X_π to d_{xy} halide-to-metal charge-transfer band energies for a series of tetragonal chloride complexes of osmium. Data are collated from references 7, 8 and this work. See Tables 3.1.1, 3.1.2 and 3.2.1.*

ruthenium and osmium.[24,25] Even more pertinently, a linear correlation between chloride-to-metal charge-transfer (XMCT) energies and E^o(IV/III) reduction potentials was established for a series of $3d^n$ and $4d^n$ transition metal hexahalides.[4] In this work we have attempted to find a similar correlation for a range of tetragonal complexes of ruthenium and osmium, all containing the $\{MX_4\}$ chromophore.

None of the III/II couples observed for tetragonal complexes hitherto lies positive of +0.3 V for osmium (Table 3.1.1), making the overall range of determined E^o only 1.6 V. The E^o span is even smaller for ruthenium, at 1.2 V. The newly studied nitrosyl complexes show by far the most positive III/II couple, providing a significant increase of the range of redox potentials (and complementary red-shift in the XMCT

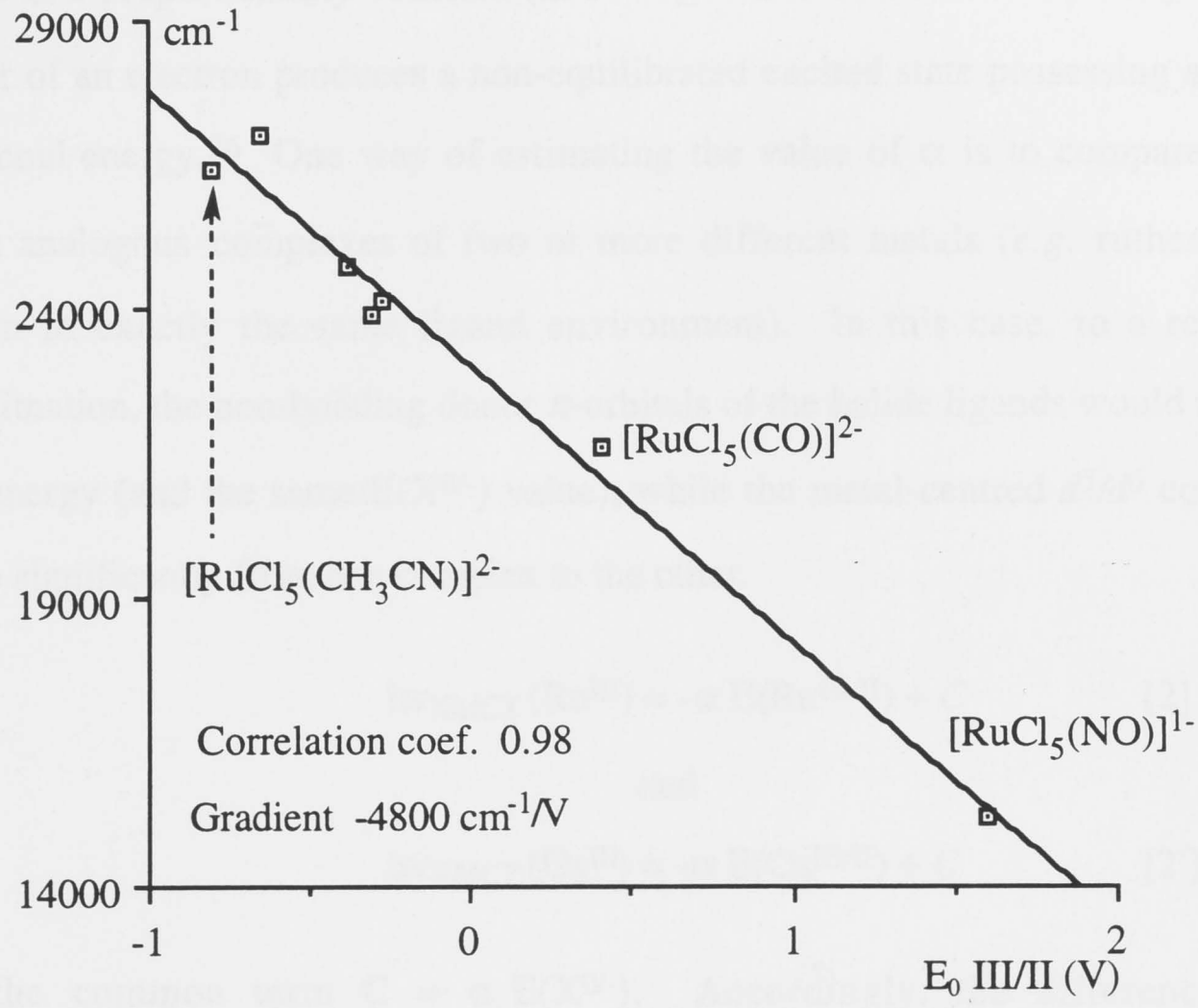

Figure 3.2.15 *Correlation of the d^5/d^6 (III/II) redox potentials and the X_π to d_{xy} halide-to-metal charge-transfer band energies for a series of tetragonal chloride complexes of ruthenium. Data are collated from references 4, 5, 6, 22 and this work. See Tables 3.1.1, 3.1.2 and 3.2.1.*

envelope) recorded for such complexes. Figures 3.2.13 - 15 make this impact quite tangible. It is also important to point out that some of the metal (III) complexes under examination bear a different overall charge: *e.g.* $[OsBr_4(CH_3CN)(NO)]^0$, $[OsBr_5(NO)]^{1-}$, $[OsBr_5(CO)]^{2-}$, and this clearly has not undermined the correlation.

According to Heath and Duff,[4] we can ascribe a notional redox potential, $E(X^{0/-})$, to the halide donor level, such that the energy of the ligand-to-metal charge-transfer can be expressed as follows:

$$h\nu_{XMCT} = \alpha[E(X^{0/-}) - E(M^{III/II})] \qquad [1]$$

Here α is a proportionality constant (in eV/V), which should exceed unity since the transfer of an electron produces a non-equilibrated excited state possessing additional vibrational energy.[26] One way of estimating the value of α is to compare pairs of strictly analogous complexes of two or more different metals (*e.g.* ruthenium and osmium in exactly the same ligand environment). In this case, to a reasonable approximation, the non-bonding donor π-orbitals of the halide ligands would retain the same energy (and the same $E(X^{0/-})$ value), while the metal-centred d^5/d^6 couple will change significantly from one complex to the other.

Then,
$$h\nu_{XMCT}(Ru^{III}) = -\alpha\, E(Ru^{III/II}) + C \qquad [2]$$
and
$$h\nu_{XMCT}(Os^{III}) = -\alpha\, E(Os^{III/II}) + C \qquad [2'],$$

with the common term $C = \alpha\, E(X^{0/-})$. Accordingly, the difference in the charge-transfer energies will be:

$$h\nu_{XMCT}(Os^{III}) - h\nu_{XMCT}(Ru^{III}) = \alpha\,\{E(Ru^{III/II}) - E(Os^{III/II})\} \qquad [3]$$

Using the data from Tables 3.1.2, 3.1.3 and 3.2.1, the α parameter may be calculated according to formula [3]. For example, for *trans*-$[MCl_4LL']^{z-}$ complexes, where M = Ru or Os, on this basis α varies from 1.13 eV/V ($L = L' = CH_3CN$) to 1.46 eV/V ($L = NO^+$, $L' = Cl$). Of course, this is only an estimate, and a wider range of metals is required for more accurate determination of the value of α. However these values are quite close to 1.31 eV/V, which was determined previously from a series of transition metal hexahalides.[4] Yet it should be emphasised that the α parameter is determined by the underlying vibronic coupling and there is no theoretical requirement for it to take the same value in a range of complexes with widely different electronic properties.

To summarise, a plot of ν_{XMCT} *versus* $E^o(M^{III/II})$ yields a linear graph for each set of complexes (chloro- and bromo-complexes of osmium and chloro complexes of ruthenium, Figures 3.2.13 - 15). If the observed shifts in the ν_{XMCT} had reflected merely the degree of stabilisation of the metal *d*-orbitals (in other words, if $E(X^{0/-})$ had remained constant for all complexes), the slope of such a graph, according to formula

[2], would have had a value equal to α (*i.e.* between -8066 and -12100 cm^{-1}/V, due to $1.0 \leq \alpha \leq 1.5$ eV/V). However it is important to bear in mind that, as we mentioned earlier, the build-up of the positive charge on the central ion due to interaction with different π-withdrawing ligands L stabilises all of the frontier electron levels in a molecule. Naturally, the metal orbitals are the most affected, but evidently the halide donor orbitals should also be systematically stabilised to a substantial extent. Therefore, rather than remaining constant, $E(X^{0/-})$ is expected to increase concurrently with $E^{o}(M^{III/II})$, though at a slower rate. Under these circumstances we have to return to formula [1]. The resulting slope of ν_{XMCT} *versus* $E^{o}(M^{III/II})$, which is roughly 0.5 eV/V, confirms that this is the case (Table 3.2.3).

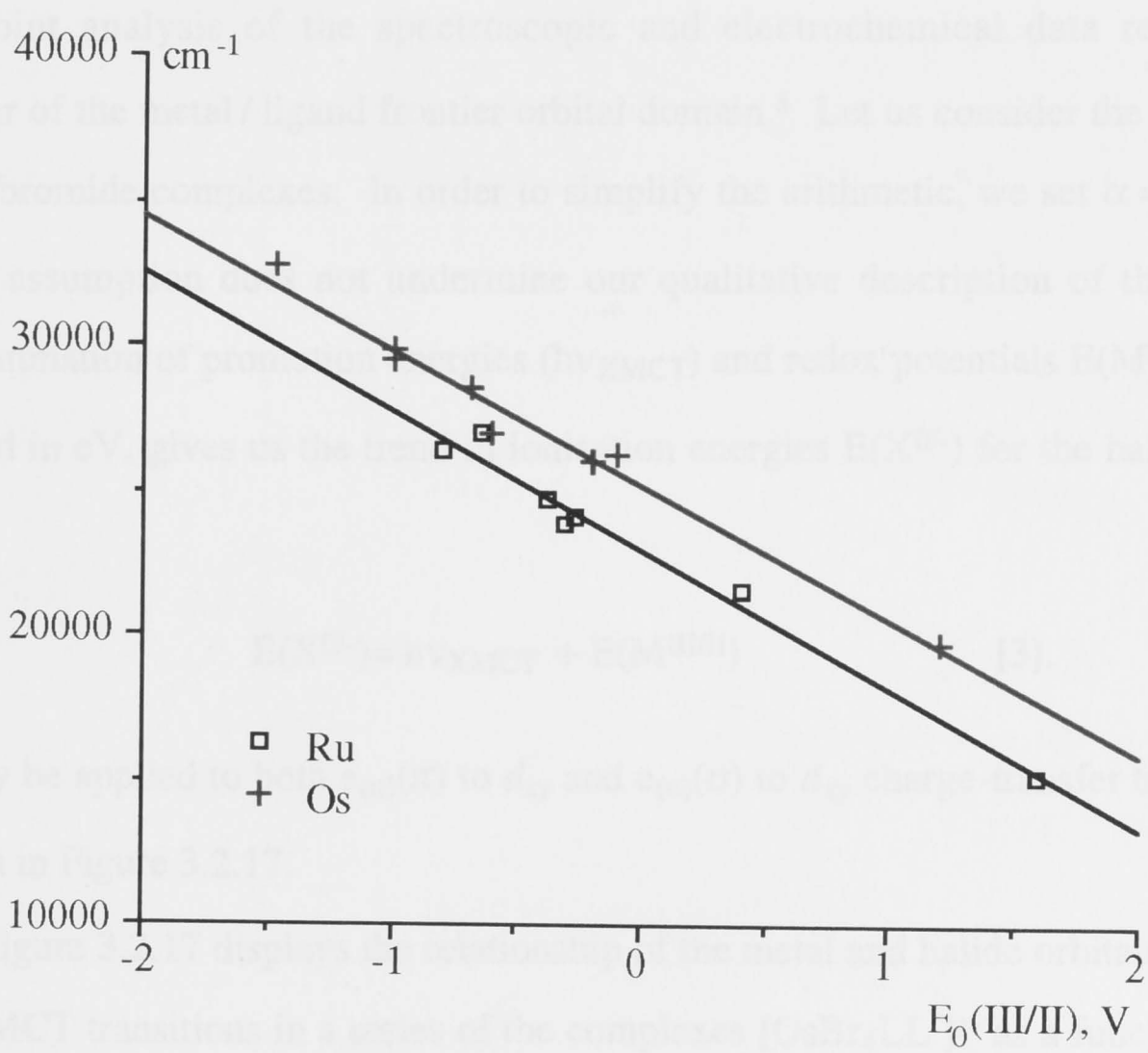

Figure 3.2.16 *XMCT versus redox potential correlation graphs for the tetragonal chloride complexes of ruthenium and osmium (Figures 3.2.14-15). The line for ruthenium is ca. 2500 cm^{-1} lower.*

Table 3.2.3 *Gradients of the plots of the halide-to-metal charge-transfer (XMCT) energies vs. $E(M^{III/II})$ for the different tetragonal $[M^{III}X_4LL']^{z-}$ systems (Figures 3.2.12-14).*

Metal M	Halide X	Type of XMCT	Gradient	
			cm^{-1}/V	eV/V
Os	Br	X_σ to d_{xy}	-3450	-0.43
Os	Br	X_π to d_{xy}	-4300	-0.53
Os	Cl	X_π to d_{xy}	-4600	-0.58
Ru	Cl	X_π to d_{xy}	-4800	-0.59

Joint analysis of the spectroscopic and electrochemical data reveals the behaviour of the metal / ligand frontier orbital domain.[4] Let us consider the tetragonal osmium bromide complexes. In order to simplify the arithmetic, we set $\alpha = 1$ eV/V.* Such an assumption does not undermine our qualitative description of the system. Then, summation of promotion energies ($h\nu_{XMCT}$) and redox potentials $E(M^{III/II})$, both expressed in eV, gives us the trend in ionisation energies $E(X^{0/-})$ for the halide donor levels:

$$E(X^{0/-}) = h\nu_{XMCT} + E(M^{III/II}) \qquad [3].$$

This may be applied to both $e_{(u)}(\pi)$ to d_{xy} and $e_{(u)}(\sigma)$ to d_{xy} charge-transfer transitions, as shown in Figure 3.2.17.

Figure 3.2.17 displays the relationship of the metal and halide orbitals involved in the LMCT transitions in a series of the complexes $[OsBr_4LL']^{z-}$ as a function of the central ion $Os^{III/II}$ redox potential (horizontal axis). The vertical axis represents the $d^{5/6}$, $X_\pi^{0/-}$ and $X_\sigma^{0/-}$ notional oxidation potentials, which means that the top straight line

* In other words, we assume that the energies of the spectral bands are equal to the energy differences between the zero-points of the ground and excited states, so that reorganisation energy is nil.

is simply the graph of $E(Os^{III/II})$ versus itself and depicts the progressive stability of the metal-based HOMO. The other two lines show the dependance of the notional oxidation potentials $E(Br^{0/-})$ of the donor halide σ- (the bottom line) and π-orbitals (the middle line) on the $E(Os^{III/II})$ value. The greater the metal-centred oxidation potential, the lower the energy of each orbital . Overall, the map shows that the halide σ-orbitals lie to lower energies than the π-orbitals, and are affected more sharply by the accumulation of the positive charge on the metal, reflected by the $E^o(Os^{III/II})$ values. This is not unexpected, as the σ-electron pairs are directed towards the metal centre.

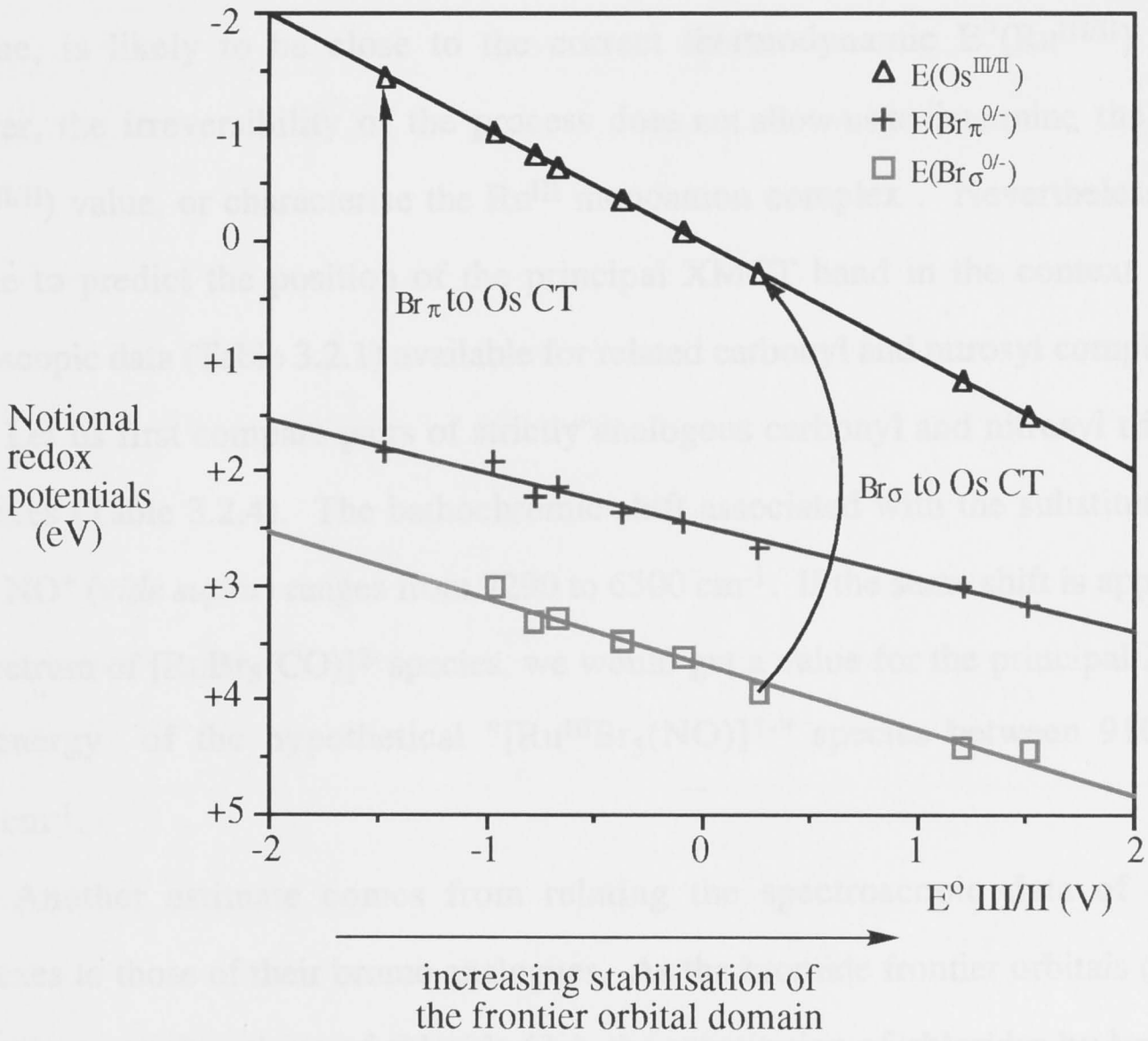

Figure 3.2.17 *Qualitative diagram showing behaviour of the frontier orbital domain in tetragonal osmium bromo-complexes* $[OsBr_4LL']^{z-}$. *The diagram shows the relationship between the metal redox-active orbital and the bromide* σ- *and* π-*orbitals as a function of* $E^o(Os)$ *III/II as described in the text.*

Bursten and Green have commented that: "*the use of electrochemistry as a probe of ligand additivity rests most heavily on the linear relationship between HOMO energy and oxidation potential.*"[27] The observed linear correlations between XMCT and E^o III/II values show that a linear HOMO - oxidation potential relationship holds throughout the family of halide complexes discussed in this chapter. Notably, this applies even to the carbonyl and nitrosyl complexes, even though their redox properties could not be predicted by the simplistic ligand additivity model (section 3.1; Figure 3.1.2).[9,10]

Finally, let us revisit the issue of the missing optical data for the $[Ru^{III}Br_5(NO)]^{1-}$ species. As mentioned earlier, the divalent $[Ru^{II}Br_5(NO)]^{2-}$ species cannot be reversibly oxidised. Its chemically irreversible oxidation occurs at +1.52 V (the position of the anodic peak). This value, being similar to that of the chloro analogue, is likely to be close to the correct thermodynamic $E^o(Ru^{III/II})$ value. However, the irreversibility of the process does not allow us to determine the exact $E^o(Ru^{III/II})$ value, or characterise the Ru^{III} monoanion complex . Nevertheless, it is possible to predict the position of the principal XMCT band in the context of the spectroscopic data (Table 3.2.1) available for related carbonyl and nitrosyl complexes.

Let us first compare pairs of strictly analogous carbonyl and nitrosyl trivalent complexes (Table 3.2.4). The bathochromic shift associated with the substitution of CO by NO^+ (*vide supra*) ranges from 7290 to 6300 cm^{-1}. If the same shift is applied to the spectrum of $[RuBr_5(CO)]^{2-}$ species, we would get a value for the principal XMCT band energy of the hypothetical "$[Ru^{III}Br_5(NO)]^{1-}$" species between 9100 and 10090 cm^{-1}.

Another estimate comes from relating the spectroscopic data of chloro complexes to those of their bromo analogues. As the bromide frontier orbitals (*4p*) lie to higher energy than those of chloride (*3p*), the substitution of chlorides by bromides causes a bathochromic shift of the XMCT spectra of analogous species. For the principal absorption this red-shift varies from 5040 to 6250 cm^{-1} (Table 3.2.5). This gives us the principal XMCT band energy of the same hypothetical "$[Ru^{III}Br_5(NO)]^{1-}$" species between 8950 and 10160 cm^{-1}.

Table 3.2.4 *Comparison of the principal XMCT band energies in pairs of analogous carbonyl and nitrosyl d^5 complexes. Data from Table 3.2.1.*

Complex	Centre of gravity of the principal ($e(X_\pi)$ to $b_2(d_{xy})$) band (cm^{-1})	Δ (cm^{-1})
$[OsBr_4(CH_3CN)(NO)]^0$	13100	7290
$[OsBr_4(CH_3CN)(CO)]^{1-}$	20390	
$[OsCl_5(NO)]^{1-}$	19800	7140
$[OsCl_5(CO)]^{2-}$	26940	
$[OsBr_5(NO)]^{1-}$	14670	7230
$[OsBr_5(CO)]^{2-}$	21900	
$[RuCl_5(NO)]^{1-}$	15200	6300
$[RuCl_5(CO)]^{2-}$	21500	
"$[RuBr_5(NO)]^{1-}$"	unknown	unknown
$[RuBr_5(CO)]^{2-}$	16390	

Table 3.2.5 *Comparison of the principal XMCT band energies in pairs of analogous chloro and bromo d^5 complexes. Data from Table 3.2.1.*

Complex	Centre of gravity of the principal ($e(X_\pi)$ to $b_2(d_{xy})$) band (cm^{-1})	Δ (cm^{-1})
$[OsCl_5(NO)]^{1-}$	19800	5130
$[OsBr_5(NO)]^{1-}$	14670	
$[RuCl_5(NO)]^{1-}$	15200	unknown
"$[RuBr_5(NO)]^{1-}$"	unknown	
$[OsCl_5(CO)]^{2-}$	26940	5040
$[OsBr_5(CO)]^{2-}$	21900	
$[RuCl_5(CO)]^{2-}$	21500	5110
$[RuBr_5(CO)]^{2-}$	16390	
$[OsCl_4(CH_3CN)_2]^{1-}$	30380	6250
$[OsBr_4(CH_3CN)_2]^{1-}$	24130	
$[RuCl_4(PhCN)_2]^{1-}$ (ref. 5)	24110	5560
$[RuBr_4(PhCN)_2]^{1-}$	18550	

Table 3.2.6 *Comparison of the principal XMCT band energies in pairs of analogous d^5 osmium and ruthenium complexes. Data from Table 3.2.1.*

Complex	Centre of gravity of the principal ($e(X_\pi)$ to $b_2(d_{xy})$) band (cm^{-1})	Δ (cm^{-1})
$[OsCl_5(NO)]^{1-}$	19800	4600
$[RuCl_5(NO)]^{1-}$	15200	
$[OsBr_5(NO)]^{1-}$	14670	unknown
"$[RuBr_5(NO)]^{1-}$"	unknown	
$[OsCl_5(CO)]^{2-}$	26940	5440
$[RuCl_5(CO)]^{2-}$	21500	
$[OsBr_5(CO)]^{2-}$	21900	5510
$[RuBr_5(CO)]^{2-}$	16390	
$[OsCl_4(CH_3CN)_2]^{1-}$	30380	5660
$[RuCl_4(CH_3CN)_2]^{1-}$	24720	

Thirdly, we can examine the effects from comparison with the isostructural osmium complexes. The halide-to-metal charge-transfer spectra of the osmium complexes are always blue-shifted. These hypsochromic shifts are between 4600 and 5660 cm^{-1} (Table 3.2.6). This gives us principal XMCT band energy for "$[Ru^{III}Br_5(NO)]^{1-}$" between 9010 and 10070 cm^{-1}.

All three independent tests gave us quite similar results, thus we may conclude that the principal bromide-to-metal charge-transfer transition in the hypothetical "$[Ru^{III}Br_5(NO)]^{1-}$" species would be around 10000 cm^{-1} or even less. This is *ca.* 5000 cm^{-1} (around 30 %) lower than the lowest XMCT band so far found in this class of complexes (*vide supra*). The small gap between the halide $e(X_\pi)$ and the metal $b_2(d_{xy})$ orbital appears consistent with the low stability of the ruthenium halide complexes: for example, the $[Ru^{III}Cl_5(NO)]^{1-}$ complex, which has the corresponding transition at 15200 cm^{-1}, is very unstable at temperatures above 233 K. This proximity

of the halide and metal electron levels apparently makes the thermal (or photochemical) decomposition of the complex more thermodynamically favourable, particularly bearing in mind that such decomposition might involve a transfer of an electron from metal (III) to the halide array with subsequent formation of a free halogen:

$$2\,[M^{III}X_5(NO)]^{1-} \longrightarrow 2\,\{[M^{II}X_4(NO)]^{1-}\} + X_2$$

The non-existent $[Ru^{III}Br_4(CH_3CN)(NO)]^0$ and $[Ru^{III}Br_4(Py)(NO)]^0$ complexes would have had even smaller bromide-to-metal charge-transfer energy. Hence, they would have been even less stable than their penta-bromo analogue.

3.3 Experimental

3.3.1 Electrochemical measurements

Electrochemical measurements and electrosyntheses were carried out in 0.5 M $[Bu^n_4N]BF_4$ solution in CH_2Cl_2 or 0.2 M $[Bu^n_4N]BF_4$ solution in CH_3CN. The electrolyte, $[Bu^n_4N]BF_4$, was prepared as described in section 2.4.2. Dichloromethane was pre-dried over KOH pellets before distilling from CaH_2 immediately prior to an electrochemical experiment. Acetonitrile was purified by the method described by Walter and Ramaley:[28] in succession, analytical grade acetonitrile was heated at reflux over, then distilled from (a) anhydrous $AlCl_3$, (b) alkaline $KMnO_4$, (c) $KHSO_4$ and (d) finally distilled from CaH_2 immediately prior to use.

Cyclic voltammetry (CV) and alternating current voltammetry (acV) measurements were carried out using a PAR-170 Electrochemical system, linked to an XY-recorder or, where appropriate, to a Macintosh LC630 computer *via* an AD Instruments MacLab interface system. A standard three-electrode configuration was used. The working electrode was a platinum disc or a bead, and a platinum rod was used as the auxiliary electrode. The reference electrode was a Ag/AgCl electrode (Metrohm), separated from the solution by two porous glass frits. The internal compartment of the reference electrode was filled with 0.05 M $[Bu^n_4N]Cl$ / 0.45 M $[Bu^n_4N]BF_4$ in CH_2Cl_2 (0.05 M $[Bu^n_4N]BF_4$ for CH_3CN). The external compartment was filled with the standard electrolyte solution, 0.50 M $[Bu^n_4N]BF_4$ in CH_2Cl_2 (or 0.10 M in CH_3CN). Under these conditions ferrocene was oxidised at +0.55 V. Typical scan rates were 200 mV/s for CV and 10 mV/s for acV. The latter were recorded with positive feedback resistance compensation and phase-sensitive detection. The sinusoidal modulation was set at 10 mV and the frequency w = 205 Hz.

The electrochemical cell was a jacketted glass cell (*ca.* 5 mL). The electrolyte solutions were purged with either N_2 or Ar and the cell maintained under an inert atmosphere. Low-temperature measurements were performed with the jacketted glass cell connected to a Lauda RL6 cooling bath with circulating methanol. The

temperature was monitored to within 0.2 °C by a digital thermometer with the probe located directly in the electrochemical solution.

Bulk electrolysis was performed using a jacketted three-compartment cell, with a platinum mesh basket working electrode, double-fritted non-aqueous Ag/AgCl reference electrode and platinum wire counter electrode separated from the bulk solution by two glass frits.

3.3.2 Spectro-electrochemistry

The electrolyte ($[Bu^n_4N][BF_4]$) and solvents (CH_2Cl_2 or CH_3CN) used in the spectro-electrochemical experiments were prepared as described previously. Solutions for spectro-electrochemical experiments were made up as for other electrochemical experiments, *i.e.* 0.5 M $[Bu^n_4N][BF_4]$ in CH_2Cl_2.

Electronic spectra in the range 50000 - 3125 cm^{-1} were recorded using a Perkin-Elmer λ9 double-beam UV/Vis/near-IR spectrophotometer with digital background subtraction capability. The spectra of electro-generated species were collected *in situ*, by the use of an *optically transparent thin layer-electrochemical* (OTTLE) cell,[29] with a platinum minigrid as working electrode (*ca.* 70% transmittance), mounted within the sample compartment of the spectrophotometer. The cell placed in the reference beam was of similar profile, and contained a matching section of platinum minigrid. The OTTLE cell had been calibrated to determine its optical pathlength (0.0279 cm) by recording the spectrum of a solution of known concentration of $K_3Fe(CN)_6$. The sample solution was prepared, purged with either N_2 or Ar and transferred *via* syringe into the sample cell. The working, auxiliary and reference electrodes were added to the sample cell and connected to a Thompson E-series Ministat potentiostat. During a typical experiment the cells (sample and reference) were cryostatted in gas-tight, double-glazed PTFE cell blocks, enabling both the cells and their contents to be cooled by cold N_2 gas. The N_2 gas was chilled by passing it through a copper coil immersed in liquid nitrogen. The temperature of the N_2 gas was controlled automatically by a resistive heater, driven by a Bruker variable tamperature unit VT-1000. The electrolysis was typically carried out at a potential

200 - 300 mV past the relevant E^o value, and continued until the spectrum ceased to change and the current decayed to a constant minimum. After completion, the potential was usually reset and the spectrum of the starting complex regenerated. The observation of sharply defined isosbestic points and the full regeneration of starting spectra, without substantial loss or gain of any features, were taken as evidence for chemical reversibility for the observed process.

3.4 References

1. Bard, A.J., Faulkner, L.R. *Electrochemical methods: Fundamentals and Applications*, John Wiley & Sons, Inc., New York, **1980**, a) 22-26; b) 44-46; c) 228-231
2. Moock, K.H., *Ph.D. Thesis* University of Glasgow, Glasgow, **1985**
3. Heath, G.A., Moock, K.H., Sharp, D.W.A., Yellowlees, L.J. *J. Chem. Soc., Chem. Commun.* **1985**, 1503
4. Duff, C.M., Heath, G.A. *Inorg. Chem.* **1991**, *30*, 2528
5. Duff, C.M., Heath, G.A. *J. Chem. Soc., Dalton Trans.* **1991**, 2401
6. Duff, C.M., Schmid, R.A. *Inorg. Chem.* **1991**, *30*, 2938
7. Heath, G.A., Humphrey, D.G. *J. Chem. Soc., Chem. Commun.* **1991**, 1668
8. Humphrey, D.G. *Ph.D. Thesis* A.N.U.,Canberra, **1992**, Ch. 5
9. Lever, A.B.P. *Inorg. Chem.* **1990**, *29*, 1271
10. Lever, A.B.P. *Inorg. Chem.* **1991**, *30*, 1980
11. Coombe,V.T., Heath, G.A., Stephenson, T.A., Tocher, D.A. *J. Chem. Soc., Chem. Commun.* **1983**, 303
12. Heath, G.A., Humphrey, D.G. *J. Chem. Soc., Chem. Commun.* **1990**, 672
13. Chatt, J., Kan, C.T., Leigh, G.J., Pickett, C.J., Stanley, D.R. *J. Chem. Soc., Dalton Trans.* **1980**, 2032
14. Halpern, J., James, B.R., Kemp, A.L.W. *J. Am. Chem. Soc.* **1966**, *88*, 5142
15. Batista, A.A., Olmo, L.R.V., Oliva, G., Castellano, E.E., Nascimento, O.R. *Inorg. Chim. Acta* **1992**, *202*, 37
16. Jørgensen, C.K. *Mol. Phys.* **1959**, *2*, 309
17. Jørgensen, C.K. *Orbitals in Atoms and Molecules, 2nd printing*, Academic Press, London, **1966**, Ch. 7
18. Jørgensen, C.K. *Prog. Inorg. Chem.* **1970**, *12*, 101
19. Schäffer, C.E., Jørgensen, C.K. *J. Inorg. Nucl. Chem.* **1958,** *8,* 143
20. Lever, A.B.P. *Inorganic Electronic Spectroscopy, 2nd edn.*, Elsevier, Amsterdam, **1984**, Ch. 5, and references therein

21. von Johannsen, F.H., Preetz, W. *Z. Anorg. Allg. Chem.* **1977**, *436*, 143

22. Cipriano, R.A., Levason, W., Mould, R.A.S., Pletcher, D., Webster, M. *J. Chem. Soc., Dalton Trans.* **1990**, 339

23. Yeomans, B.D. *Ph.D. Thesis* A.N.U.,Canberra, **1995,** 164-167

24. Dodsworth, E.S., Lever, A.B.P. *Chem. Phys. Lett.* **1986,** *124,* 152

25. Johnson, S.R., Westmoreland, T.D., Caspar, J.V., Barqawi, K.R., Meyer, T.J. *Inorg. Chem.* **1988**, *27*, 3195

26. Hush, N.S. *Electrochim. Acta* **1968,** *13,* 1005

27. Bursten, B.E., Green, M.R. *Prog. Inorg. Chem.* **1988**, *36*, 393

28. Walter, M., Ramaley, L. *Anal. Chem.* **1973**, *45*, 165

29. Murray, R.W., Heineman, W.R., O'Dom, G.W. *Anal. Chem.* **1967**, *39*, 1666

Six-Coordinate Acetylacetonates of Ruthenium and Osmium: Spectro-Electrochemical Investigations

The preceding chapter explored how the electronic properties of the trans-$[MX_4LL']^{z-}$ complexes of ruthenium and osmium vary when different ligands L/L′ are introduced. The bis-acetylacetonates discussed here have an important similarity with the tetra-halide complexes: they contain a fixed array of four π-donor atoms (oxygens) and two ligands L and L′, which may be either π-acceptors (e.g. PR_3 or CO) or π-donors (e.g. Cl). In this chapter we examine the role that various ligands L play in defining electronic properties of these complexes in contrasting cis and trans geometries.

4.1 Preliminary Remarks

The *tris*-β-diketonato complexes of ruthenium Ru(β-diketonate)$_3$ have been the subject of quite extensive synthetic and electrochemical study.[1,2] R.H. Holm and G.S. Patterson,[3] and subsequently G.P. Satô and co-workers[4,5] have established that the E^o(III/II) values of such compounds form a linear relationship with the sum of Hammett constants[6] (σ_m and σ_p) of the substituents in the β-diketonato moiety. It was demonstrated that there is a linear relationship between ligand composition and E^o(III/II) values in complexes containing different β-diketones[7,8] or a combination of 2,2′-bipyridine ligands and β-diketones.[9] K.R. Seddon and co-workers discovered a linear correlation of the solution E^o(III/II) values with vertical first ionisation energies in the gas phase for a number of volatile Ru(β-diketonate)$_3$ complexes.[10]

Until the most recent years, the general chemistry of ruthenium *bis*-β-acetylacetonates [Ru(acac)$_2$LL′] (Figure 4.1.1) remained surprisingly little studied,

and only a few of them were known: for example, cis-$Ru(acac)_2(CO)_2$ and cis-$Ru(acac)_2(PPh_3)_2$, where Hacac = $HC_3C(O)CH_2C(O)CH_3$. These complexes were prepared by interaction of a ruthenium carbonyl cluster[11] ($Ru_3(CO)_{12}$) or a phosphine complex[12] ($RuCl_2(PPh_3)_3$) respectively with acetylacetone. The two starting materials used in the syntheses are, of course, very different compounds, therefore these preparations could not provide a paradigm of developing a general method leading to a greater variety of six-coordinate *bis*-β-acetylacetonates. This opportunity emerged in 1988-1990, when novel routes to lower symmetry *bis*-β-diketonato complexes of ruthenium were developed: a) by reduction of the corresponding *tris*-β-diketonato-ruthenium(III) by zinc amalgam in presence of incipient ligand[13]; b) by direct reaction between a *tris*-β-diketonato-complex and incoming ligands in presence of strong acids.[14] The first route leads to complexes of divalent ruthenium, while the second yields ruthenium(III) complexes (*cis*-$[Ru^{III/II}(\beta\text{-diketonate})_2L_2]^{1+/0}$). Originally only the complexes with L = CH_3CN were prepared; however, subsequently the "zinc amalgam" method was successfully utilised for preparation of a considerable number of the *cis*-$Ru^{II}(acac)_2L_2$-type complexes.[15,16] One of these species (L = cyclooctene) proved to be a convenient starting material for the ligand L/L′ exchange reactions, which provided a route to a number of novel *trans*-isomers.[15] It is noteworthy that the only other known route to the *trans*-isomers is via reductive substitution of chloride ligands in the $[AsPh_4]$ *trans*-$[Ru^{III}(acac)_2Cl_2]$ complex,[17] which, in our experience, is not an easily prepared compound. These recent developments in synthesis enabled us to carry out an electrochemical and spectroscopic study of a wide family of ruthenium *bis*-β-diketonates, in collaboration with Professor M.A. Bennett and his research group.

Osmium acetylacetonates, unlike ruthenium ones, have not been systematically studied hitherto. The complex $Os^{III}(acac)_3$ was first synthesised[18] by F.P. Dwyer and A.M. Sargeson in 1955:

$$[Os^{IV}Br_6]^{2-} \xrightarrow[\text{room temp.}]{\text{HBr, Ag (wool)}} \xrightarrow[\Delta]{KHCO_3,\ \text{Hacac}} Os^{III}(acac)_3$$

The complex *cis*-$Os(acac)_2(PPh_3)_2$ was prepared by refluxing $OsH_4(PPh_3)_3$ with acetylacetone in toluene.[19] Synthesis of both *cis*- and *trans*-isomers of the $Os^{IV}(acac)_2X_2$ complex (X = Cl or Br) was reported[20] by W. Preetz and H. Petersen in 1979:

$$[Os^{IV}X_6]^{2-} \xrightarrow[\Delta]{H_2O,\ Hacac\ (1:1,\ v:v)} \textit{cis} \text{ and } \textit{trans}\ Os^{IV}X_2(acac)_2$$

The isomers were separated chromatographically and characterised by electronic and vibrational spectroscopy .

The tetravalent osmium *trans*-isomer was also prepared by an alternative way (from $Os_2(\mu\text{-}O_2CCH_3)_4Cl_2$) and characterised by room temperature CV in 1983.[21]

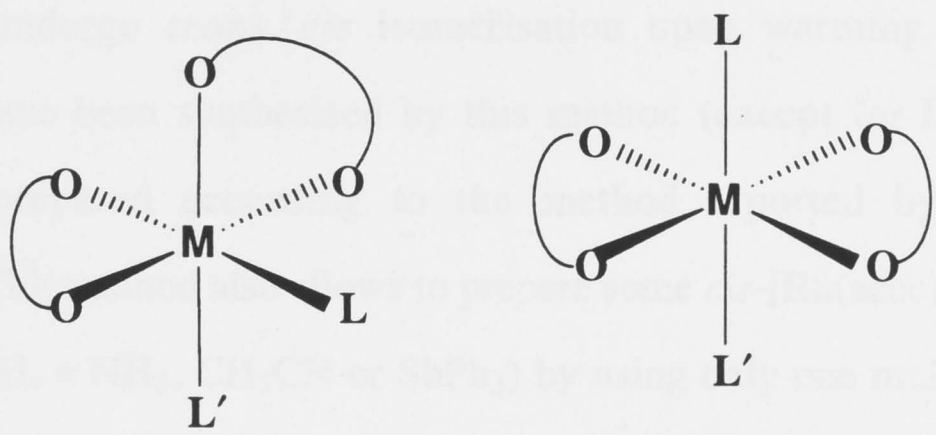

Figure 4.1.1 *Structural formulae of the cis and trans $M(acac)_2LL'$ species.*

4.2 Synthetic Procedures

The majority of the syntheses of the *bis*-acetylacetonato complexes of ruthenium* were carried out by Mr H. Neumann (the group of Professor M.A. Bennett, R.S.C.). Two methods have been normally used:

1) Reductive substitution of $Ru(acac)_3$ with an excess of incoming ligand L

$$Ru^{III}(acac)_3 \xrightarrow{Zn/Hg} [Ru^{II}(acac)_3]^{1-} \xrightarrow{L} \textit{cis}\text{-}Ru^{II}(acac)_2L_2$$

The complexes prepared by this method are always of *cis* configuration (except when L = $N(CH_3)_3$). The complex with L = cyclooctene provides a starting material for the second method.

2) Substitution reaction of cis-$Ru(acac)_2(cyclooctene)_2$ with the equivalent amount of incoming ligand L

$$\textit{cis}\text{-}Ru(acac)_2(cyclooctene)_2 \xrightarrow{L} \textit{trans}\text{-}Ru(acac)_2L_2$$

The reaction should be carried out at room temperature or with cooling, as most *trans*-isomers undergo *trans/cis* isomerisation upon warming. A number of *trans*-isomers have been synthesised by this method (except for L = CH_3CN; this complex was prepared according to the method reported by H. Taube and co-workers[17]). This method also allows to prepare some *cis*-[Ru(acac)(cyclooctene)L]-type complexes (L = NH_3, CH_3CN or $SbPh_3$) by using only one mole of the entering ligand per mole of starting compound.

All complexes prepared by Mr H. Neumann were characterised by elemental analysis and IR and NMR spectroscopy.

A sample of $Os^{III}(acac)_3$ was provided by Dr Grainne Moran (University of N.S.W.). The preparation[21] of *trans*-$[Os^{IV}(acac)_2Cl_2]$ was carried out by Dr Stephen Gheller (R.S.C.).

---

* The author has carried out syntheses (or electro-generation) of the complexes of the *trans*-$[Ru(acac)_2(CH_3CN)_nCl_{2-n}]^z$ series (see section 4.5), where n = 0-2; a representative synthesis of *cis*-$[Ru(acac)_2(CH_3CN)_2]$.

Proton NMR spectroscopy provides an effective tool for discrimination between the *cis* and *trans*-[$Ru^{II}(acac)_2LL'$]-type complexes. The more symmetric *trans*-isomers (for both L_2 and L, L′) display only one acac methyl resonance, while the *cis*-isomers show two in case of [$Ru(acac)_2L_2$] stoichiometry (Figure 4.2.1) and four in case of [$Ru(acac)_2LL'$].

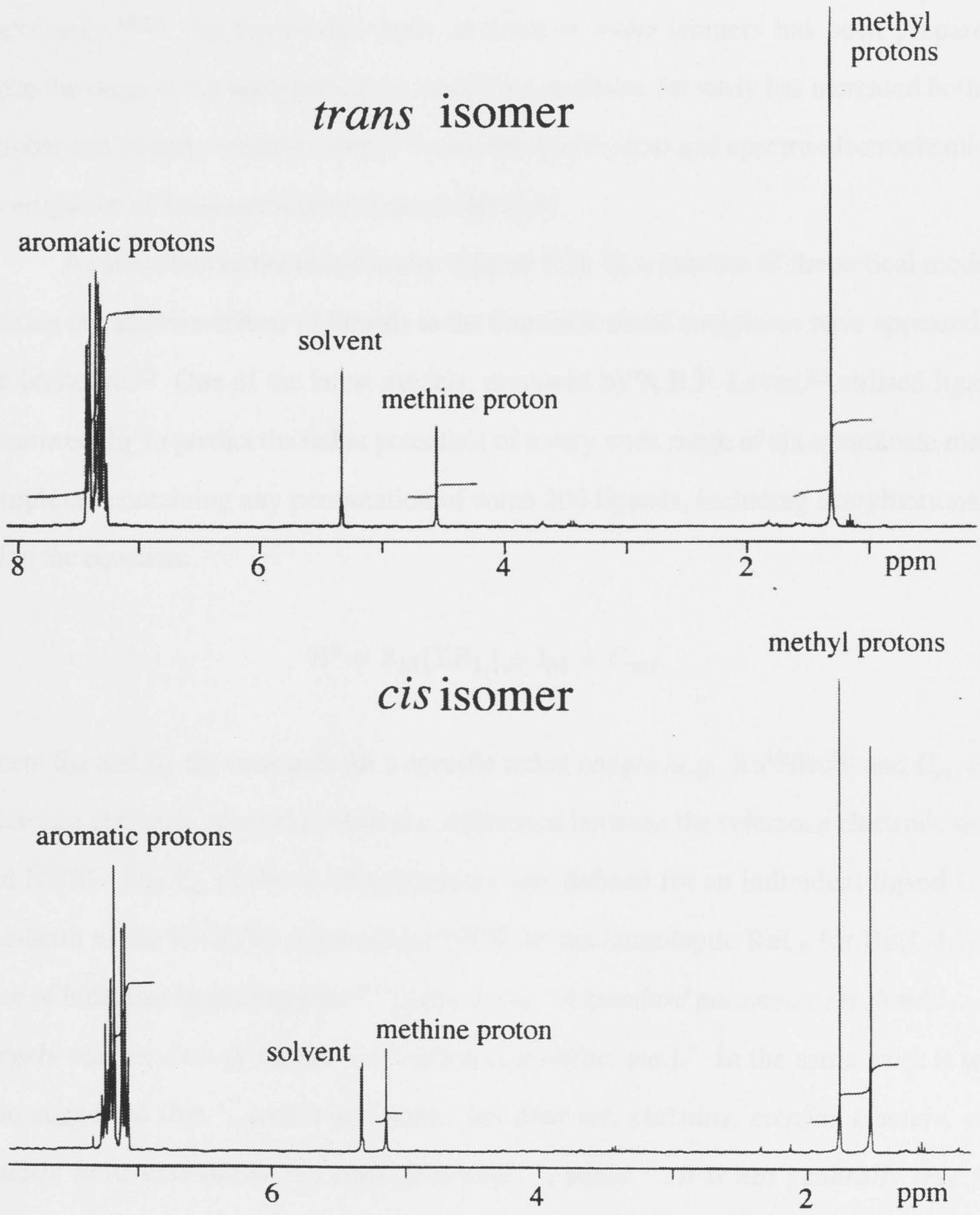

Figure 4.2.1 *Proton NMR spectra of cis and trans isomers of [$Ru^{II}(acac)_2(AsPh_3)_2$] in CD_2Cl_2.*

4.3 Electrochemical Study of Ruthenium *bis*-Acetylacetonato Complexes: Comparative Electrochemistry of the *cis*- and *trans*-Isomers* and Ligand Additivity

As we have already mentioned, a few complexes of the *cis*-$Ru^{II}(acac)_2L_2$ or *cis*-$Ru^{II}(acac)_2(L\text{-}L)$ (L-L is a bidentate ligand, *e.g.* bipyridine) type have been studied previously.[15,16] As part of this work, an array of *trans* isomers has been prepared. Since the range of *bis*-acetylacetonato complexes available for study has increased both in number and variety, we have carried out an electrochemical and spectro-electrochemical investigation of these novel ruthenium compounds.

As described in the introductory chapter (Ch. 1), a number of theoretical models treating the additive effects of ligands in the transition metal complexes have appeared in the literature.[22] One of the latest models, proposed by A.B.P. Lever,[23] utilised ligand parameters E_L to predict the redox potentials of a very wide range of six-coordinate metal complexes containing any permutation of some 200 ligands, including acetylacetonate, using the equation:

$$E^o = S_M[\Sigma E_L] + I_M + C_{ref},$$

where S_M and I_M are constants for a specific redox couple (*e.g.* Ru^{III}/Ru^{II}) and C_{ref} is a reference electrode correction term (*i.e.* difference between the reference electrode used and NHE). The E_L (Table 4.3.1) parameter was defined for an individual ligand L as one-sixth of the E^o(III/II) value *versus* NHE for the homoleptic RuL_6 (or $Ru(L\text{-}L)_3$ in case of bidentate ligand) species.** Lever wrote: "*A standard parameter set should ... be largely independent of isomerism (cis/trans, mer/fac, etc.).*" In the same work it was also suggested that "*...within the ruthenium data set, cis/trans, mer/fac isomers, etc. usually have essentially the same potential...*", while "*...it is not generally true for organometallic species, where such differences may be 0.1- 0.2V.*" The extent of the present family of *cis*- and *trans*- ruthenium *bis*-β-acetylacetonates gives us an opportunity

---

* Also see Appendix 1.

** As homoleptic RuL_6 complexes are not available for many ligands L, the majority of the E_L values were derived from a series of 2,2′-bipyridine complexes ($[Ru(bipy)_nL_{6-2n}]^{m+}$).

Table 4.3.1 *Lever's parameters E_L (in Volts)[23] for the ligands used in the present study. Bidentate ligands contribute twice the listed E_L value to ΣE_L.*

Ligands	E_L (V)
chloride (Cl^-)	-0.24
2,4-pentanedionate (acetylacetonate)	-0.08
1,2-diaminoethane (ethylenediamine)	0.06[a]
ammonia (NH_3)	0.07[b]
pyridine (C_5H_5N)	0.25
trimethylphosphine ($P(CH_3)_3$)	0.33
triethylphosphine ($P(C_2H_5)_3$)	0.34
acetonitrile (CH_3CN)	0.34
tert-butylisocyanide (Bu^tNC)	0.36
1,2-*bis*(diphenylphosphino)ethane (dppe)	0.36
methyldiphenylphosphine (PCH_3Ph_2)	0.37
triphenylstibine ($SbPh_3$)	0.38
triphenylarsine ($AsPh_3$)	0.38
triphenylphosphine (PPh_3)	0.39
trimethyl phosphite ($P(OCH_3)_3$)	0.42
carbon monoxide (CO)	0.99

to check these suggestions and to determine how successfully Lever's Linear ligand additivity model can be applied to such complexes.

All the studied $[Ru(acac)_2LL']^{z\pm}$ complexes display a one-electron fully reversible III/II couple (for example, see Figure 4.3.1).* These results are presented in Tables 4.3.2 - 4.3.3. It is evident that the III/II couple is strongly dependent on the

---

[a] This E_L parameter substitutes for the missing E_L of the analogous $(CH_3)_2NCH_2CH_2N(CH_3)_2$ ligand (TMEDA).

[b] This E_L parameter substitutes for the missing E_L of the analogous $N(CH_3)_3$ ligand.

* Voltammograms were routinely recorded under the conditions described in the previous chapter.

donor/acceptor properties of the ligands L/L′ and also on the ligand arrangement in the complex (where both *cis* and *trans* isomers are available). The E^{o}(III/II) values range from +1.10 V (*cis*-isomer L = CO, L′ = PPh_3) to -0.95 V (*trans*-isomer L = L′ = Cl). As one would expect, the π-acceptor ligands (*e.g.* CO and phosphines) render the oxidation potentials more positive. At the same time, complexes containing amines (neither π-donor, nor π-acceptor ligands) or chlorides (π-donor ligands) display a far less positive III/II couple. In addition, some of the complexes show a voltammetrically accessible, though not always reversible IV/III oxidation (Table 4.3.4). The observed IV/III couples are far more positive than unity, with the single exception of the *trans*-$[Ru^{III}(acac)_2Cl_2]^{1-}$ species.

In 1980 J. Chatt, C.J. Pickett and co-workers[24] showed that *polarisability* and *electron richness* of a particular binding site are crucial in determining ligand effects in a complex. The polarisability of a binding site depends on a number of factors including its geometry. Therefore, the same ligands in *cis* and *trans* isomers may exert a different influence on the properties of the central ion. Indeed, comparing III/II couples of the *bis*-acetylacetonato complexes, one notices the *cis* isomers are always harder to oxidise than the *trans*, although this difference can be as little as 0.05 V or as large as 0.49 V. As early as 1957 Chatt and Ahrland measured redox potentials of some systems of the type $L_2Pt^{IV}Cl_4 / L_2Pt^{II}Cl_2$ (L = a phosphine) and observed that the *cis*-isomers have slightly more positive oxidation potentials.[25] In a series of transition metal complexes $[M(CO)_2(dppe)_2]^{z+}$ *cis* and *trans* isomers (M = Mn, Cr, Mo, W; z = 0, 1, 2) were found to have unequal oxidation potentials.[26]

Likewise B.E. Bursten and co-workers observed a difference of 0.16 V in redox potentials of the *cis/trans*-$[Mn(CO)_2(CNCH_3)_4]^{1+}$ isomeric pair.[27] The rationalisation of this observation was provided by direct application of Angular Overlap model (AOM) as follows: in the *cis* isomer the HOMO (redox $d\pi$ orbital) is stabilised by a π-interaction with one strong π-acid (CO), while in the *trans* isomer no such direct interaction occurs. This idea was later generalised by B.E. Bursten, who proposed a "ligand additivity" model.[22,28] This model assumed that for a binary system $[ML_nL'_{6-n}]$ the energy of each $d\pi$ orbital is linearly dependent on: *a)* the number of ligands of each

Table 4.3.2 *ΣE_L (Table 4.3.1) and observed E^o III/II redox potentials of these $Ru(acac)_2LL'$ complexes for which both cis and trans isomers have been isolated. See also Table 4.3.3 overleaf.*

L	L′	ΣE_L *vs* NHE (V)	Geometric isomer	E^o III/II *vs* Ag/AgCl (V)	ΔE^o (V)
C_5H_5N	C_5H_5N	+0.18	*cis*	+0.01	0.05
			trans	-0.04	
CH_3CN	CH_3CN	+0.36	*cis*	+0.24[a]	0.12
			trans	+0.12	
$P(CH_3)_3$	$P(CH_3)_3$	+0.34	*cis*	+0.26	0.26
			trans	0.00	
$AsPh_3$	$AsPh_3$	+0.44	*cis*	+0.34	0.19
			trans	+0.15	
PPh_3	PPh_3	+0.46	*cis*	+0.37[a]	0.30
			trans	+0.07[a]	
PCH_3Ph_2	PCH_3Ph_2	+0.42	*cis*	+0.37	0.33
			trans	+0.04	
$P(OCH_3)_3$	$P(OCH_3)_3$	+0.52	*cis*	+0.70	0.48
			trans	+0.22	
Bu^tNC	Bu^tNC	+0.40	*cis*	+0.74[a]	0.49
			trans	+0.25[a]	
CO	$P(cyclohexyl)_3$	-	*cis*	+0.92	0.28
			trans	+0.64	
CO	PPh_3	+1.06	*cis*	+1.10	0.34
			trans	+0.76[a]	

[a] This electrochemical measurement was originally carried out by Lynne Wallace (ref. 16) and repeated in the present work.

Table 4.3.3 *ΣE_L (Table 4.3.1) and observed E^o III/II redox potentials of $Ru(acac)_2LL'$ complexes, for which either a cis or trans isomer has been isolated . See also Table 4.3.2 on the previous page.*

L	L′	ΣE_L *vs* NHE (V)	Geometric isomer	E^o III/II *vs* Ag/AgCl (V)
CO	$AsPh_3$	+1.05	*cis*	+1.05
Cyclooctene	Cyclooctene	-	*cis*	+0.77[a]
Cyclooctene	$SbPh_3$	-	*cis*	+0.44
Cyclooctene	CH_3CN	-	*cis*	+0.44
$SbPh_3$	$SbPh_3$	+0.46	*cis*	+0.39
$Ph_2PCH_2CH_2PPh_2$ (dppe)		+0.40	*cis*	+0.32[a]
Cyclooctene	NH_3	-	*cis*	+0.23
$P(C_2H_5)_3$	$P(C_2H_5)_3$	+0.36	*trans*	-0.13
$N(CH_3)_3$	$N(CH_3)_3$	-0.18	*trans*	-0.20
$(CH_3)_2NCH_2CH_2N(CH_3)_2$ (TMEDA)		-0.20	*cis*	-0.35
Cl	CH_3CN	-0.22	*trans*	-0.42
Cl	Cl	-0.80	*trans*	-0.95

[a] data from ref. 16

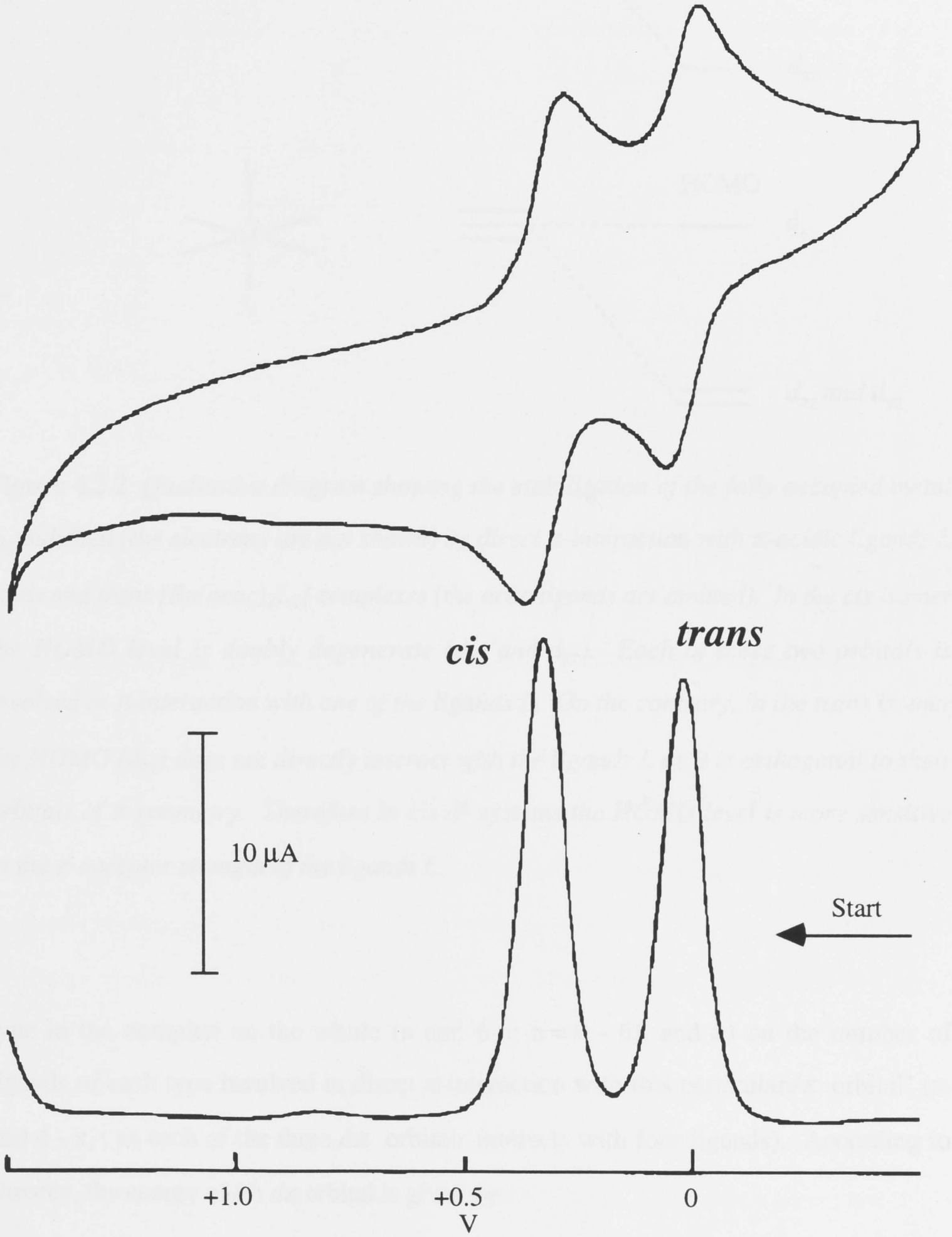

Figure 4.3.1. *CV (top) and acV (bottom) of cis and trans-Ru(acac)$_2$(PCH$_3$Ph$_2$)$_2$] in similar concentrations in dichloromethane at 235 K.*

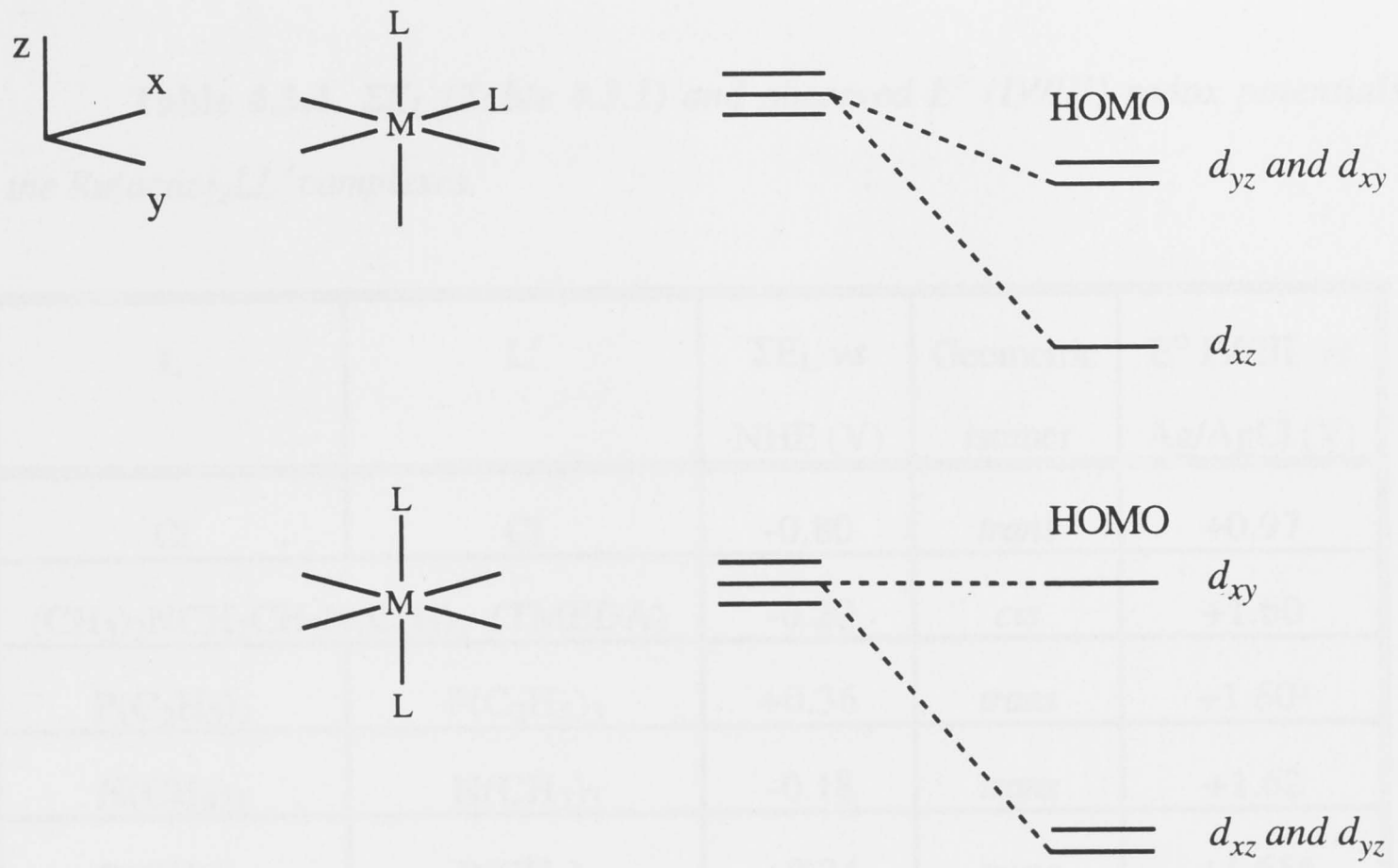

Figure 4.3.2 *Qualitative diagram showing the stabilisation of the fully occupied metal t_{2g}-subshell (the electrons are not shown) by direct π-interaction with π-acidic ligands L in cis and trans [Ru(acac)$_2$L$_2$] complexes (the acac ligands are omitted). In the cis isomer the HOMO level is doubly degenerate (d_{xy} and d_{yz}). Each of these two orbitals is involved in π-interaction with one of the ligands L. On the contrary, in the trans isomer the HOMO (d_{xy}) does not directly interact with the ligands L as it is orthogonal to their orbitals of π symmetry. Therefore in cis d^6 systems the HOMO level is more sensitive to the π-acceptor strength of the ligands L.*

type in the complex on the whole (n and 6-n; n = 0 - 6), and *b)* on the number of ligands of each type involved in direct π-interaction with this particular$d\pi$ orbital* (x_i and 4 - x_i , as each of the three $d\pi$ orbitals interacts with four ligands). According to Bursten, the energy of *i*th $d\pi$ orbital is given by:

$$\varepsilon_i = a^o + nb^L + (6 - n)b^{L'} + x_i c^L + (4 - x_i)c^{L'},$$

where a^o is a characteristic constant of the metal ion in a particular oxidation state; b^L and $b^{L'}$ are constants describing the overall isotropic energetic effect upon the central ion of

* Lever's model (ref. 23) ignores the latter contribution.

Table 4.3.4 *ΣE_L (Table 4.3.1) and observed E^o (IV/III) redox potentials of the $Ru(acac)_2LL'$ complexes.*

L	L′	ΣE_L *vs* NHE (V)	Geometric isomer	E^o IV/III *vs* Ag/AgCl (V)
Cl	Cl	-0.80	*trans*	+0.97
$(CH_3)_2NCH_2CH_2N(CH_3)_2$ (TMEDA)		-0.20	*cis*	+1.60
$P(C_2H_5)_3$	$P(C_2H_5)_3$	+0.36	*trans*	+1.60[a]
$N(CH_3)_3$	$N(CH_3)_3$	-0.18	*trans*	+1.62
$P(CH_3)_3$	$P(CH_3)_3$	+0.34	*trans*	+1.65[a]
C_5H_5N	C_5H_5N	+0.18	*cis*	+1.65
			trans	+1.68
$AsPh_3$	$AsPh_3$	+0.44	*trans*	+1.74
CH_3CN	CH_3CN	+0.18	*trans*	+1.88

binding to ligands L and L′; c^L and $c^{L'}$ are constants describing the effect of direct π-covalent interaction of the *i*th $d\pi$ orbital with ligands L and L′ respectively. Constants c^L and $c^{L'}$ are therefore measures of the relative π-donor / acceptor properties of the ligand L and L′.

Let us apply this model to the present family of *bis*-acetylacetonato d^6 complexes of ruthenium. The qualitative energy diagram for the $d\pi$ orbitals in these complexes is shown in Figure 4.3.2. The energy of the Ru^{II} HOMO, which determines the d^5/d^6 (III/II) oxidation potential, is given by:

$$\varepsilon_{HOMO}(cis) = a^{Ru} + 2\times b^L + 4\times b^{acac} + 1\times c^L + 3\times c^{acac} \qquad \text{for } cis \text{ isomers}$$

and

[a] Irreversible, *i.e.* CV lacks a return wave even at 235 K. This potential corresponds to the observed anodic peak potential.

$$\varepsilon_{HOMO}(trans) = a^{Ru} + 2\times b^{L} + 4\times b^{acac} + 4\times c^{acac} \qquad \text{for } trans \text{ isomers}$$

The difference between the HOMO energies is then given by:

$$\Delta\varepsilon_{HOMO}(trans - cis) = c^{acac} - c^{L}$$

This means that in d^6 *bis*-acetylacetonato complexes, $Ru(acac)_2L_2$, $\Delta\varepsilon_{HOMO}(trans - cis)$ and ΔE^o depend on the difference in π-donor / acceptor properties of the ligands.* As the π-donor / acceptor properties of acetylacetonato moieties, on the one hand, and ligands such as phosphines and Bu^tNC, on the other, differ greatly, the difference in E^o III/II (ΔE^o) between *cis* and *trans* isomers containing those ligands reaches almost 0.5 V. It is noteworthy that ΔE^o grows in line with the π-acceptor strength of ligand L stabilising the HOMO (Table 4.3.2). In *cis* complexes containing three kinds of ligands ($[Ru(acac)_2(P(cyclohexyl)_3)(CO)]$ and $[Ru(acac)_2(PPh_3)(CO)]$), as shown in Figure 4.3.3, the *d*-orbital interacting with the weaker π-acceptor only (*i.e.* the phosphine) will be the HOMO, and therefore ΔE^o is similar to that observed for their *bis*-phosphine analogues.

Figure 4.3.3 *Qualitative diagram showing the stabilisation of the metal t_{2g}-subshell in cis $Ru(acac)_2(CO)(PR_3)$ d^6 complexes.*

* The c^{acac} parameter refers to the π-covalent interaction of *one* acac-derived O-donor.

While it is now clear that Lever's ligand additivity model does not work for the unified family of *cis* and *trans* $[Ru(acac)_2LL']^{z\pm}$ complexes, linear correlation may be found between experimentally determined $E^o(III/II)$ values and ΣE_L for sets of *cis* and *trans* isomers considered separately. Let us plot the observed III/II oxidation potentials *versus* ΣE_L. Figure 4.3.4 shows a linear correlation for the family of *trans* isomers. The slope of the graph (0.85) gives us the effective S_M polarisability parameter of Lever's equation for the family of *trans* isomers.

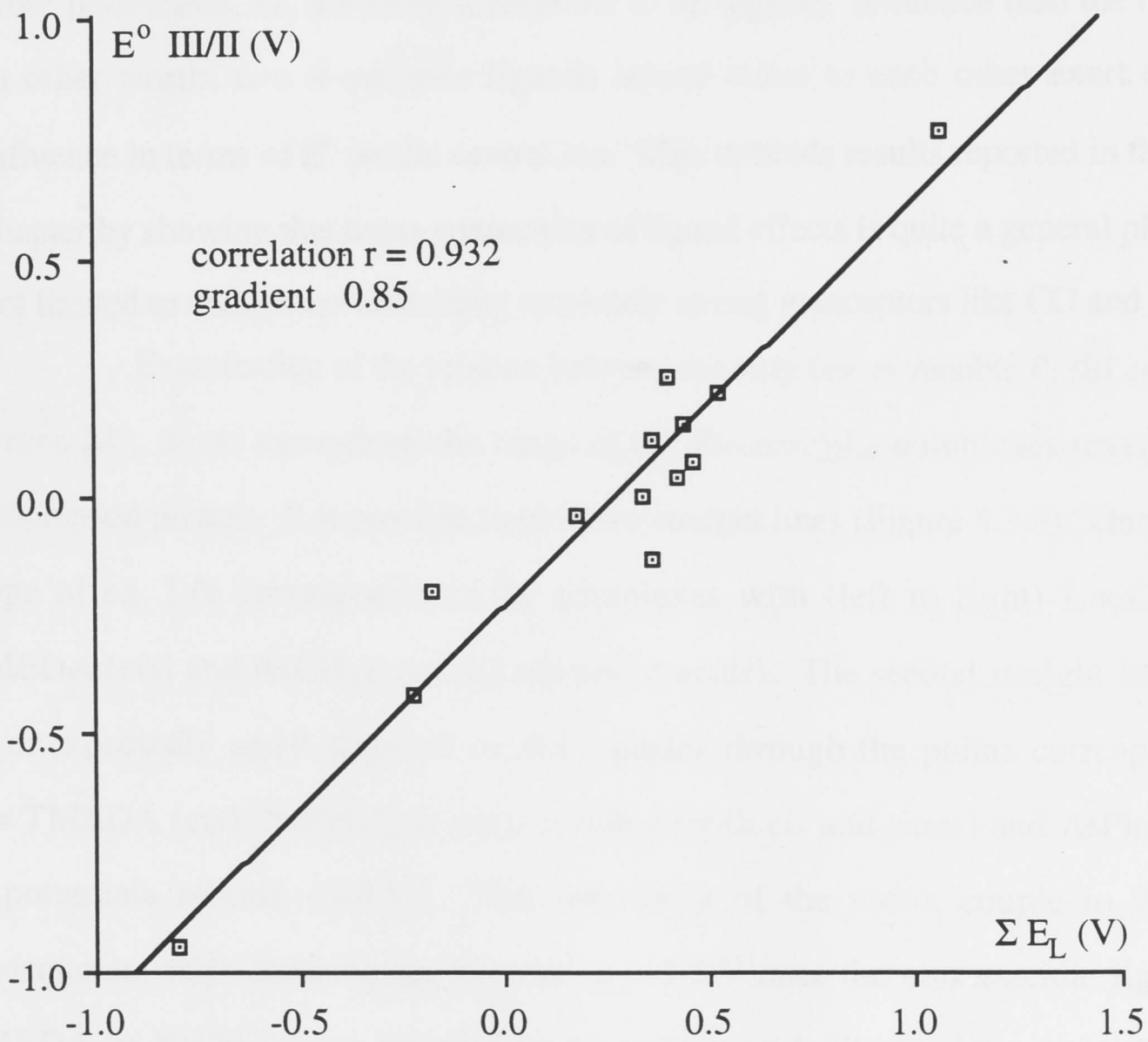

Figure 4.3.4 *Correlation of the observed $Ru^{III/II}$ couples with ΣE_L for a series of trans $Ru(acac)_2LL'$ complexes. Data from Tables 4.3.2 and 4.3.3.*

In the family of *cis* isomers the two data points for $(Ru(acac)_2(Bu^tNC)_2$ and $Ru(acac)_2(P(OCH_3)_3)_2$ apparently fall far above the straight line* (Figure 4.3.5). However if these two complexes are excluded the linear correlation is almost perfect.

The slope (S_M parameter) is equal to 1.15.

The S_M parameter is an important indicator of metal-ligand interaction. A greater value of S_M indicates a greater sensitivity of the central ion toward the ligands in a series of complexes. The S_M parameter was conceived to be constant and characteristic of a given metal ion in a given couple regardless of ligand set.[23] Especially, it would be expected to converge on unity for the Ru (III/II) couple, because this particular couple was used by Lever as a Standard Electrochemical Data Set for derivation of the E_L parameters.[23] A comparison of the slopes (1.15 and 0.85 respectively) obtained for the series of *cis* and *trans* $[Ru(acac)_2L_2]$ isomers reveals that the studied *cis* systems are more polarisable, *i.e.* are more susceptible to the ligands' influence than the *trans* ones. In other words, two π-acceptor ligands bound *trans* to each other exert diminished influence in terms of E^o on the central ion. This upholds results reported in the previous chapter by showing that *trans*-attenuation of ligand effects is quite a general phenomenon not limited to complexes containing extremely strong π-acceptors like CO and NO^+.

Examination of the relation between the very few reversible IV/III couples and Lever's ΣE_L terms throughout the range of the $Ru(acac)_2L_2$ complexes reveals a more complicated picture. It is possible to plot two straight lines (Figure 4.3.6). One, having a slope of *ca.* 1.0, corresponds to the complexes with (left to right) L = Cl (*trans*), TMEDA (*cis*) and $N(CH_3)_3$ (*trans*) (all non π-acids). The second straight line, having an unexpectedly small slope of *ca.* 0.2, passes through the points corresponding to L = TMEDA (*cis*), $N(CH_3)_3$ (*trans*), pyridine (both *cis* and *trans*) and $AsPh_3$ (*cis*) (all at potentials around +1.6 V). The sensitivity of the redox couple to the ligand environment falls dramatically beyond *ca.* +1.5 V once the non π-acidic ligands (Cl, TMEDA or $N(CH_3)_3$) are replaced by the mild π-acids like pyridine or $AsPh_3$. Such insensitivity of the observed E^o to the changing ligand environment in pyridine and arsine complexes, reflected by the small value of the slope, may indicate that the oxidation

---

* This observation indicates stronger than predicted stabilisation of the HOMO by pronounced π-acceptor ligands (Bu^tNC and $P(OCH_3)_3$) in these complexes.

process may now be (acac) ligand-based (*i.e.* $(acac)^{0/1+}$ oxidation). Indeed, as the *d*-orbitals contract with the increasing central charge of the central ion,[24] the metal orbitals are now more stabilised than in the case of the previously examined Ru (III/II) oxidation (*vide supra*), so that it may become easier to remove an electron from the (acac) levels rather than from the *d*-orbitals of the metal. The (acac) ligand levels are in turn a lot less sensitive to changing the other ligands L than those of the central ion.

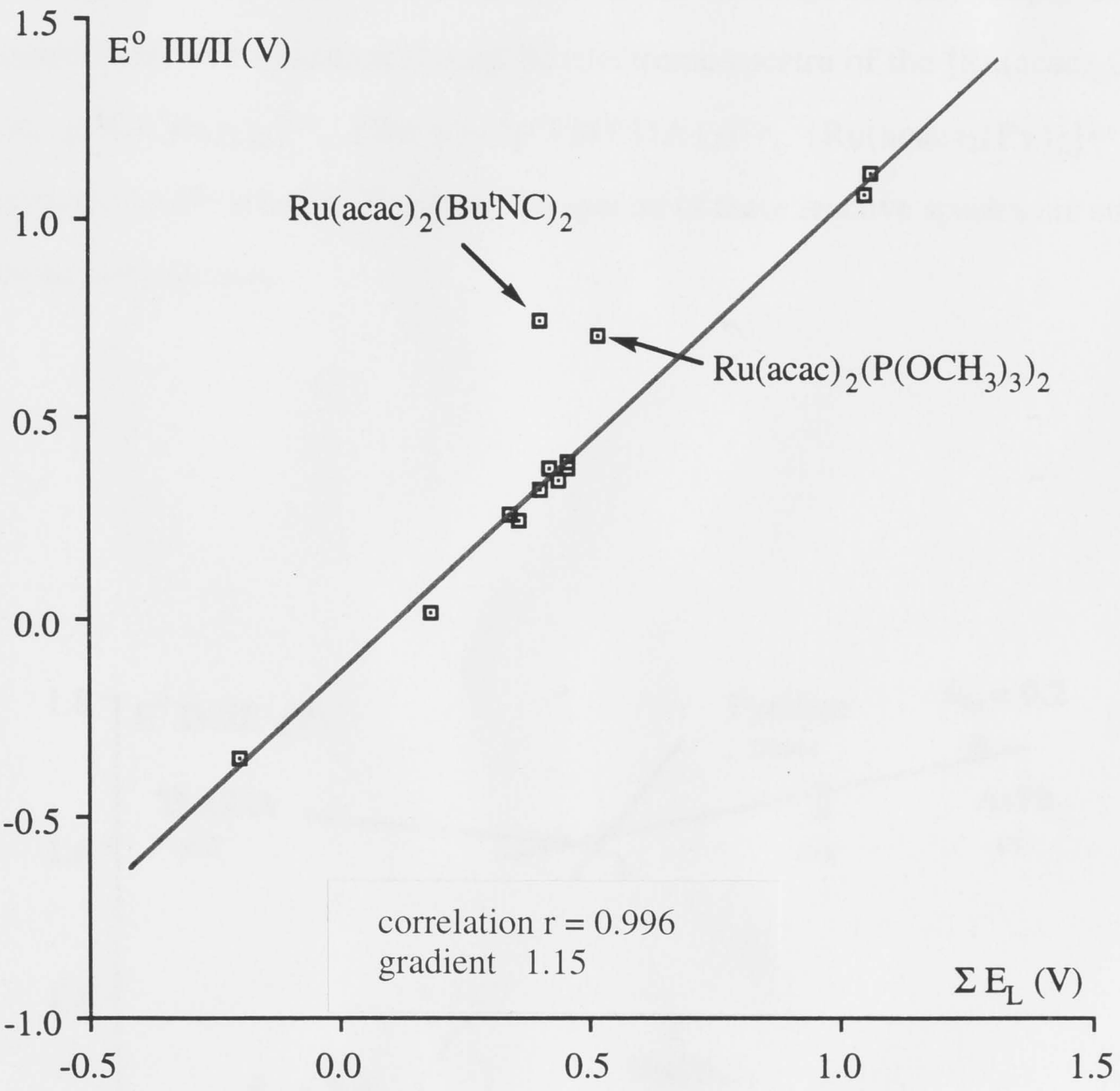

Figure 4.3.5 *Plot of the observed $Ru^{III/II}$ couples versus ΣE_L for a series of cis $Ru(acac)_2LL'$ complexes. The graph also illustrates that the E_L paramerers for Bu^tNC and $P(OCH_3)_3$ ligands are underestimated by approximately 0.15 V and 0.10 V respectively. Data from Tables 4.3.2 and 4.3.3.*

The reduction potential for the coordinated (acac) ligand in an Ir(III) complex is estimated at -3.0 V.[29] The difference between $(acac)^{0/-1}$ reduction and $(acac)^{0/1+}$ oxidation potentials may be estimated from the energy of the (acac) π to π^* electron promotion in a coordinated (acac) ligand, which is usually close to 36000 cm^{-1} (or *ca.* 4.5 eV) (see section 4.4). This estimate gives us the redox potential for the $(acac)^{0/1+}$ oxidation of *ca.* +1.5 V, which closely matches the second redox potentials of the pyridine and arsine complexes.

The crucial distinction between the metal-based Ru (IV/III) couple and the ligand-based $(acac)^{0/1+}$ oxidation should the electronic spectra of the $[Ru(acac)_2Cl_2]^o$, $[Ru(acac)_2(N(CH_3)_3)_2]^{2+}$, $[Ru(acac)_2(TMEDA)_2]^{2+}$, $[Ru(acac)_2(Py)_2]^{2+}$ and $[Ru(acac)_2(AsPh_3)_2]^{2+}$ species. However, the spectra of these reactive species are subject of a separate investigation.

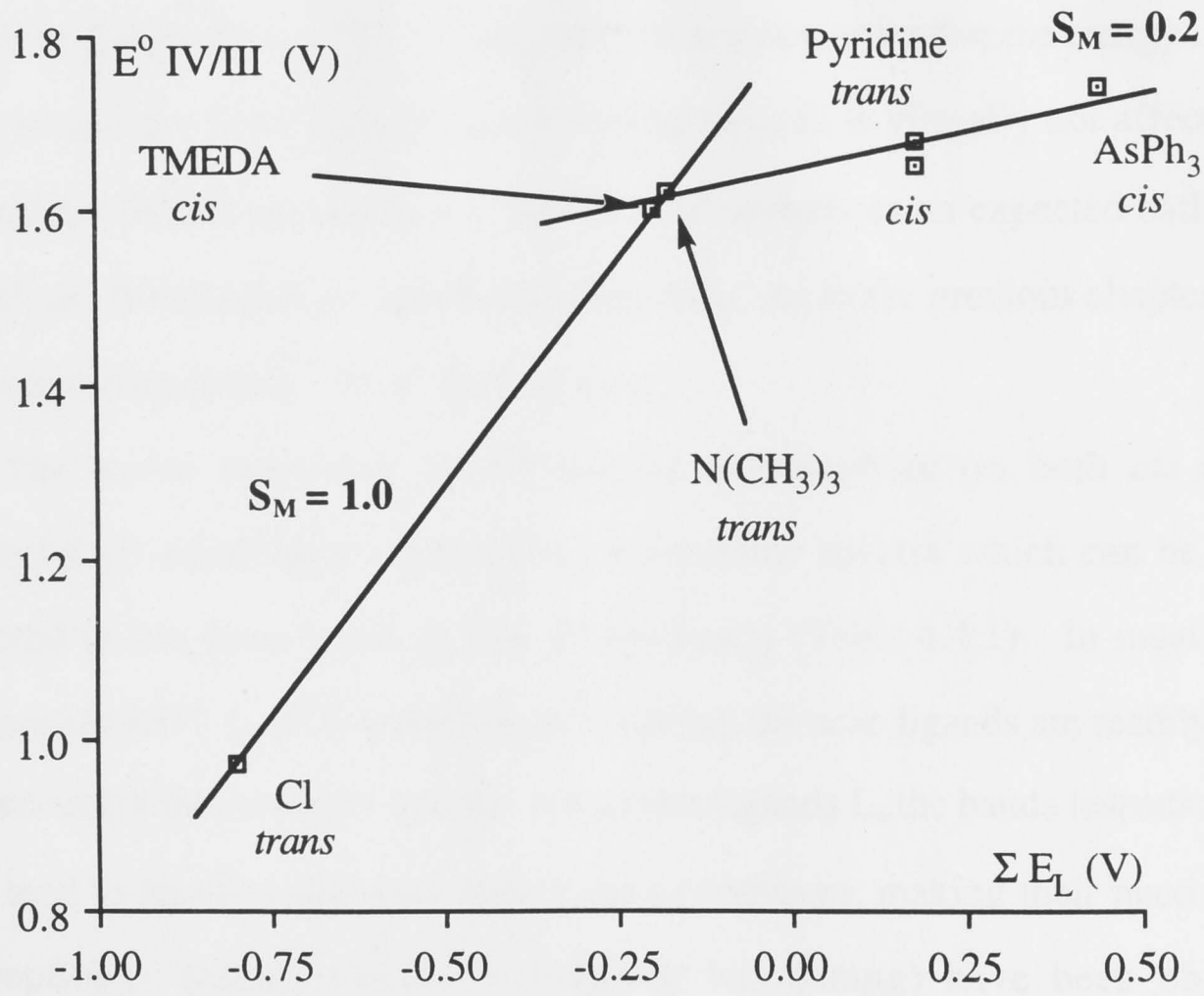

Figure 4.3.6 *Plot of the observed reversible $Ru^{IV/III}$ couples versus ΣE_L for a series of $Ru(acac)_2L_2$ complexes. Data from Tables 4.3.4.*

4.4 Spectro-electrochemical Study of Ruthenium *bis*-Acetylacetonato Complexes

Most of the described acetylacetonato complexes of divalent and particularly trivalent ruthenium are deeply coloured compounds. The intense colours are due to electron promotion from the acetylacetonato ligands to the central ion or *vice versa*. The charge-transfer spectra of both d^6 and d^5 $Ru(acac)_3$ and $Ru(acac)_2L_2$-type complexes have been investigated in our laboratory by Graham Heath and co-workers, and are well understood.[16,29] Figure 4.4.1 shows the spectral progression accompanying electrochemical reduction of $Ru(acac)_3$ in an OTTLE cell. The spectrum of the d^5 $Ru^{III}(acac)_3$ comprises three well-defined absorption bands at 37400, 28800 and 20000 cm^{-1}. These bands are assigned as follows: the ligand-based (acac-based) π to π^* electron promotion (37400 cm^{-1}); the metal-to-ligand $d\pi$ to π^* CT (28800 cm^{-1}); the ligand-to-metal π to $d\pi$ CT (20000 cm^{-1}). In the electro-generated d^6 $[Ru^{II}(acac)_3]^{1-}$ the metal t_{2g}-subshell is fully filled, and no low energy ligand-to-metal charge-transfer absorptions are observed. The charge-transfer spectrum of this species consists of two bands at 36600 and 19800 cm^{-1} that are assigned as the π to π^* electron promotion and the metal-to-ligand $d\pi$ to π^* CT respectively. It is noteworthy that the energy of the acac π to π^* band close to its position in the free ligand and is virtually not affected by the charge of the central ion, while the MLCT band undergoes an expected bathochromic shift with the lowering of the metal oxidation state. As in the previous chapter, we shall limit further discussion to the d^5 Ru^{III} species.

The lower symmetry $\{Ru^{III}(acac)_2\}$ chromophore (in both *cis* and *trans* $[Ru(acac)_2L_2]^z$ complexes) contributes to electronic spectra which can be generally interpreted in the same terms as that of $Ru(acac)_3$ (Table 4.4.1). In most cases the bands, acac to Ru^{III} LMCT in particular, involving the acac ligands are readily assigned. However, under the influence of some π-acceptor ligands L, the bands (especially the CT bands) tend to broaden and sometimes even to converge, making their maxima almost imperceptible. Similar effects (vibrational broadening) have been observed in

bis-bipyridine complexes of ruthenium containing π-acceptor ligands (*e.g.* phosphines or isocyanides).[30]

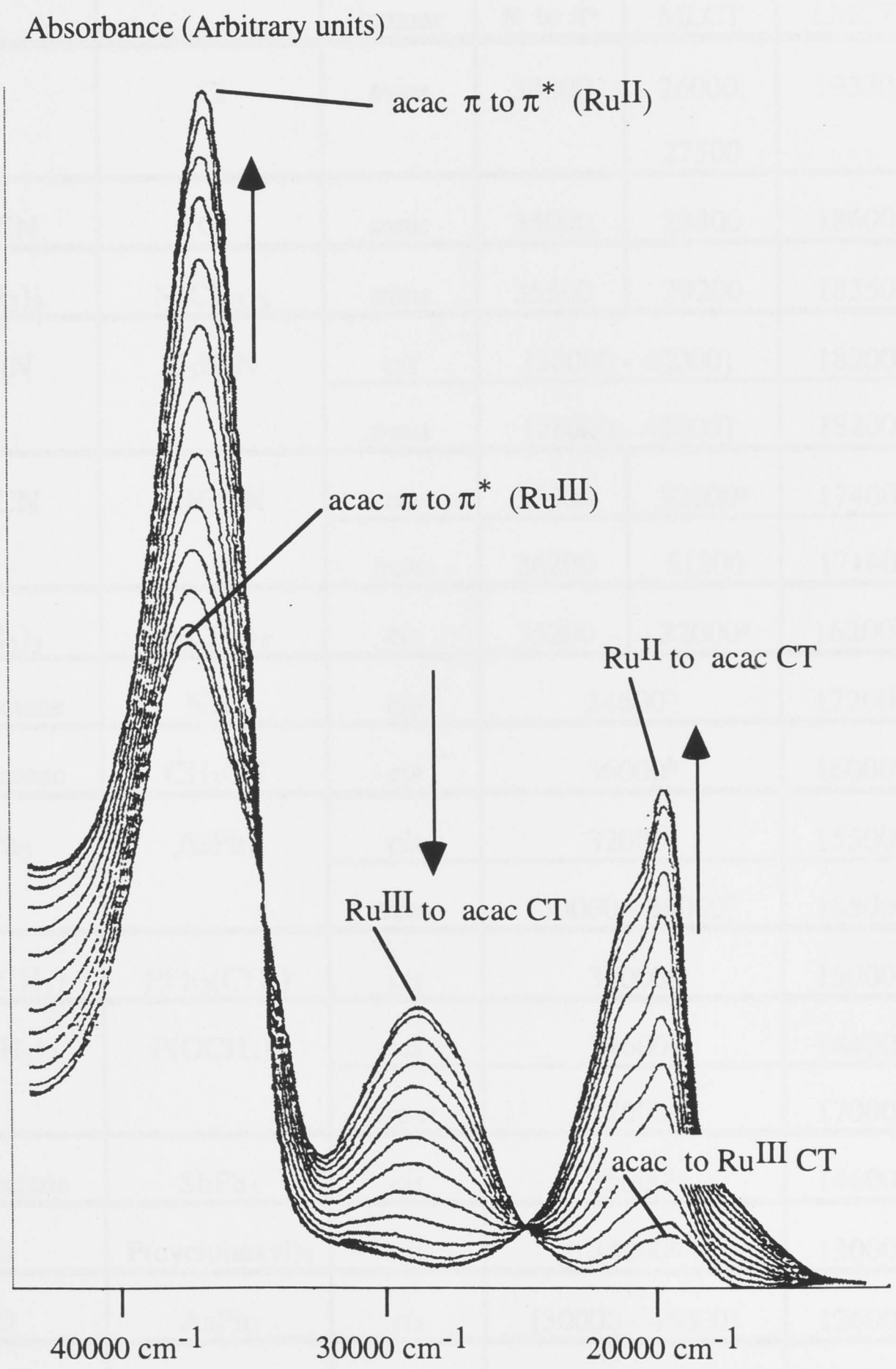

Figure 4.4.1 *Spectral progression accompanying electrochemical reduction of $Ru(acac)_3$ in an OTTLE cell.*

Table 4.4.1 *Principal band maxima observed for $[Ru^{III}(acac)_2LL']^z$ species. In a number of complexes π to π^* and MLCT absorptions coalesce producing one broad band. Tentative assignments are listed in square brackets.*

L	L′	Geometric isomer	Band maxima (cm^{-1})		
			π to π^*	MLCT	LMCT
Cl	Cl	*trans*	34000	26000; 27500	19370
CH_3CN	Cl	*trans*	35000	28800	18600
$N(CH_3)_3$	$N(CH_3)_3$	*trans*	35500	29200	18350
C_5H_5N	C_5H_5N	*cis*	[30000 - 42000]		18200
		trans	[28000 - 42000]		18200
CH_3CN	CH_3CN	*cis*	35200	32000[a]	17400
		trans	36200	31200	17160
$P(CH_3)_3$	$P(CH_3)_3$	*cis*	35200	32000[a]	16200[b]
Cyclooctene	NH_3	*cis*	34600[b]		17200[b]
Cyclooctene	CH_3CN	*cis*	36000[b]		16000[b]
$AsPh_3$	$AsPh_3$	*cis*	32000[b]		15500[b]
		trans	[30000 - 34000]		16500[b]
$PPh_2(CH_3)$	$PPh_2(CH_3)$	*cis*	34000[b]		15000[b]
$P(OCH_3)_3$	$P(OCH_3)_3$	*cis*	34600[b]		14400[b]
		trans	37000[b]		17000[b]
Cyclooctene	$SbPh_3$	*cis*	35000[b]		14600[b]
CO	P(cyclohexyl)$_3$	*cis*	34800[b]		13000[b]
CO	$AsPh_3$	*cis*	[30000 - 45000]		12600[b]
CO	PPh_3	*cis*	[30000 - 45000]		12400[b]
		trans	[30000 - 45000]		16800[b]

[a] shoulder
[b] very broad band

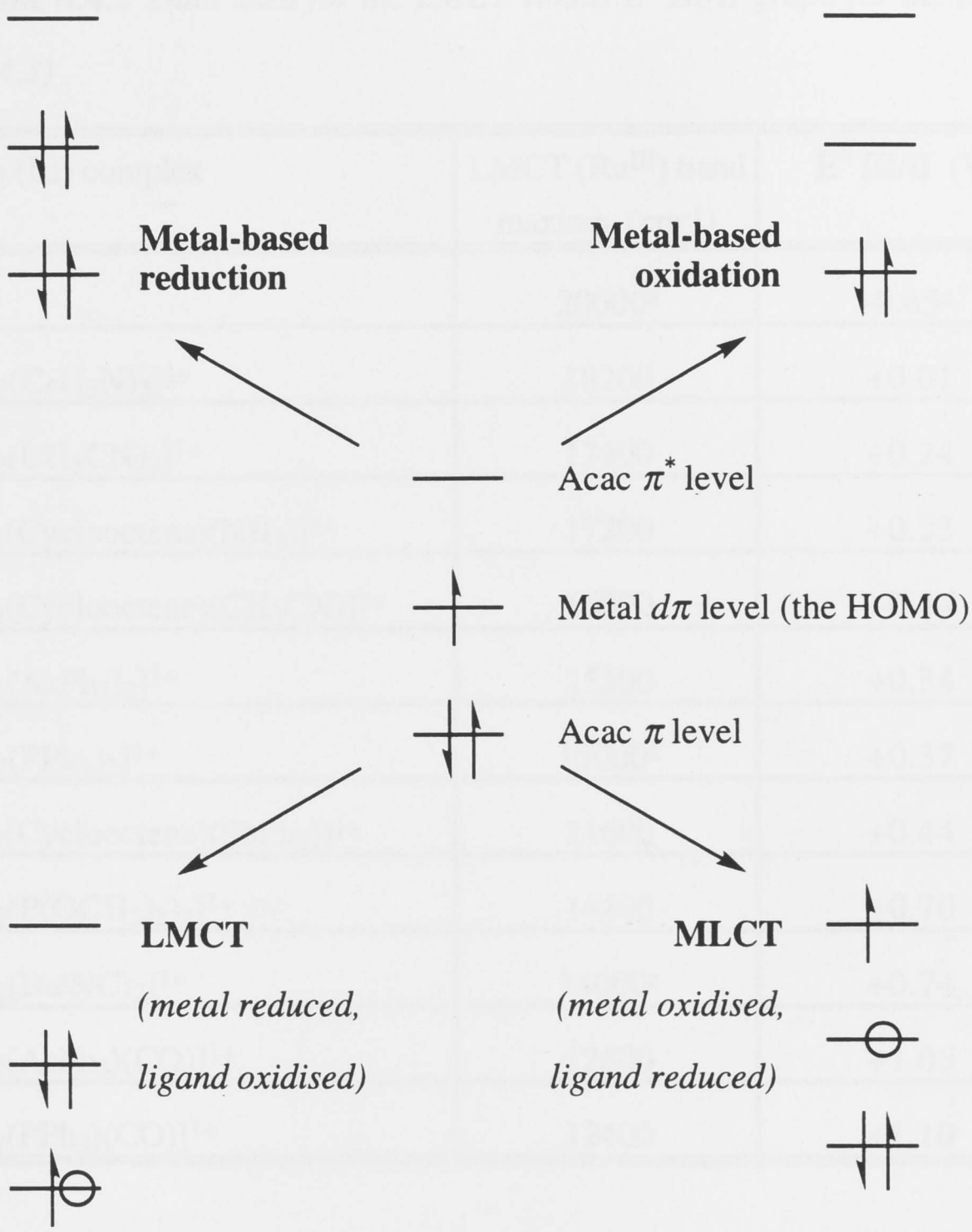

Figure 4.4.2 *Schematic diagram showing transformations of the frontier orbital domain of the d^5 $[Ru^{III}(acac)_2L_2]^z$-type complexes upon various electron transfer processes.*

As we have seen in Chapter 3, electrochemical and spectroscopic techniques can complement each other. Spectro-electrochemical methods allow us to obtain electronic spectra of the $[Ru^{III}(acac)_2L_2]^z$ type complexes electro-generated *in situ*, as most of these compounds are isolated in divalent state.

Table 4.4.2 *Data used for the LMCT versus E^o III/II graph for the* ***cis*** *isomers (Figure 4.4.3)*

Ruthenium (III) complex	LMCT (Ru^{III}) band maxima (cm^{-1})	E^o III/II (V)
$Ru(acac)_3$	20000[a]	-0.65[a]
$[Ru(acac)_2(C_5H_5N)_2]^{1+}$	18200	+0.01
$[Ru(acac)_2(CH_3CN)_2]^{1+}$	17400	+0.24
$[Ru(acac)_2(Cyclooctene)(NH_3)]^{1+}$	17200	+0.23
$[Ru(acac)_2(Cyclooctene)(CH_3CN)]^{1+}$	16000	+0.44
$[Ru(acac)_2(AsPh_3)_2]^{1+}$	15500	+0.34
$[Ru(acac)_2(PPh_3)_2]^{1+}$	15000[a]	+0.37
$[Ru(acac)_2(Cyclooctene)(SbPh_3)]^{1+}$	14600	+0.44
$[Ru(acac)_2(P(OCH_3)_3)_2]^{1+}$	14400	+0.70
$[Ru(acac)_2(Bu^tNC)_2]^{1+}$	14000[a]	+0.74
$[Ru(acac)_2(AsPh_3)(CO)]^{1+}$	12600	+1.05
$[Ru(acac)_2(PPh_3)(CO)]^{1+}$	12400	+1.10

Table 4.4.3 *Data used for the LMCT versus E^o III/II graph for the* ***trans*** *isomers (Figure 4.4.3)*

Ruthenium (III) complex	LMCT (Ru^{III}) band maxima (cm^{-1})	E^o III/II (V)
$[Ru(acac)_2Cl_2]^{1-}$	19370	-0.95
$[Ru(acac)_2Cl(CH_3CN)]^0$	18600	-0.42
$[Ru(acac)_2(N(CH_3)_3)_2]^{1+}$	18350	-0.20
$[Ru(acac)_2(C_5H_5N)_2]^{1+}$	18200	-0.04
$[Ru(acac)_2(CH_3CN)_2]^{1+}$	17160	+0.12
$[Ru(acac)_2(P(OCH_3)_3)_2]^{1+}$	17000	+0.22
$[Ru(acac)_2(PPh_3)(CO)]^{1+}$	16800	+0.76

[a] data from ref 16

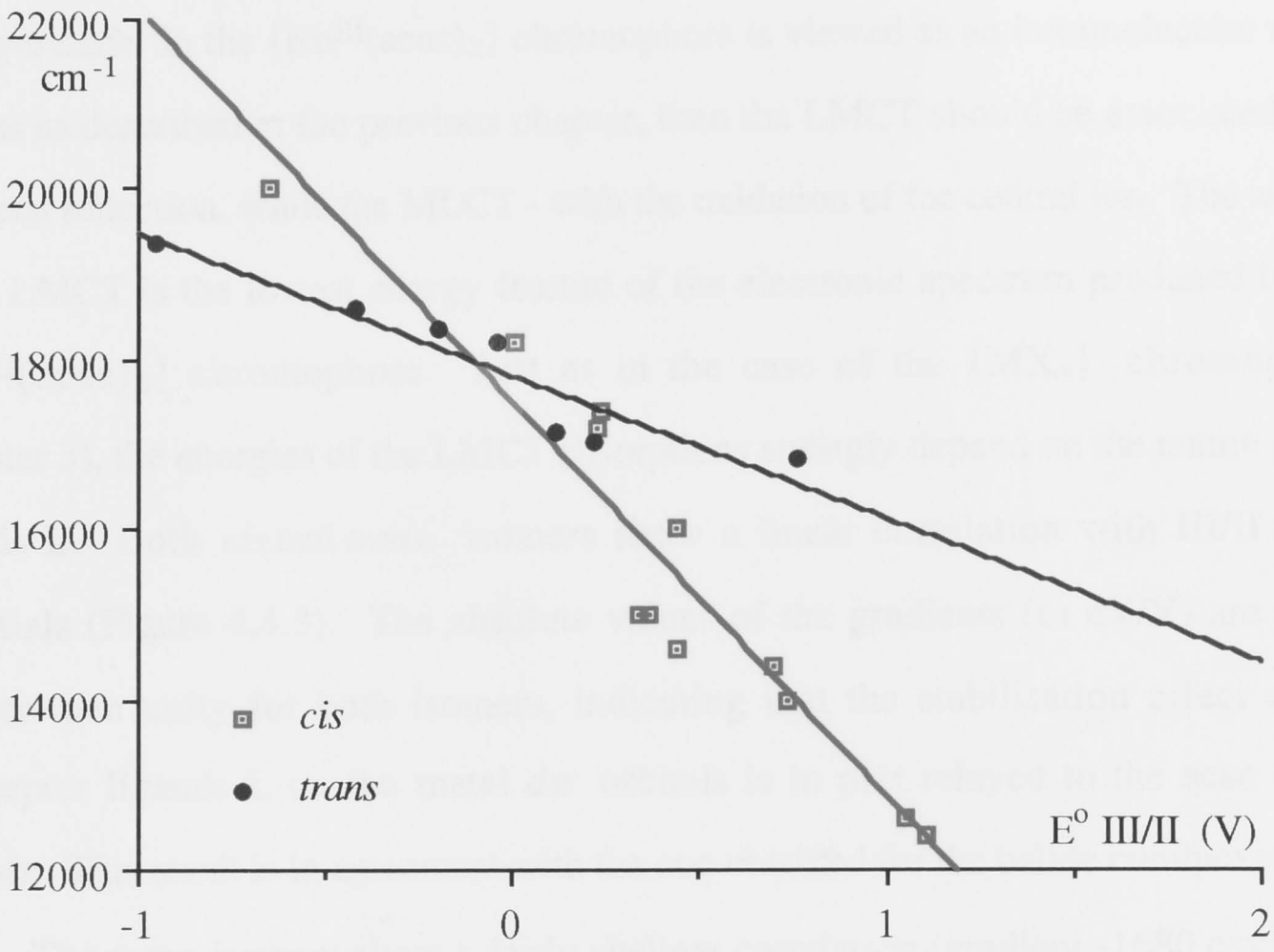

Figure 4.4.3 *Correlation of the d^5/d^6 (III/II) redox potentials and the acac-to-metal charge-transfer (LMCT) energies for the series of* ***cis*** *(shown in red) and* ***trans*** *(shown in blue) $Ru^{III}(acac)_2LL'$ complexes and $Ru(acac)_3$. The slopes are -4630 cm^{-1}/V or -0.57 eV/V(**cis**) and -1680 cm^{-1}/V or -0.21 eV/V(**trans**). Correlation coefficients are 0.91and 0.89 respectively. Data from Tables 4.4.2 and 4.4.3.*

Table 4.4.3 *Data used for the MLCT versus E^o IV/III graph (Figure 4.4.4).*

Ruthenium (III) complex	MLCT (Ru^{III}) band maxima (cm^{-1})	E^o IV/III (V)
trans-$[Ru(acac)_2Cl_2]^{1-}$	27500	+0.97
$Ru(acac)_3$	28800[a]	+1.10[a]
trans-$[Ru(acac)_2(N(CH_3)_3)_2]^{1+}$	29200	+1.62
trans-$[Ru(acac)_2(CH_3CN)_2]^{1+}$	31200	+1.88

[a] data from ref 16

Figure 4.4.2 shows transformations of the frontier orbital domain of the d^5 $Ru(acac)_2L_2$-type complexes upon various electron transfer processes. If a charge-transfer in the $\{Ru^{III}(acac)_2\}$ chromophore is viewed as an intramolecular redox process as described in the previous chapter, then the LMCT should be associated with the metal reduction, while the MLCT - with the oxidation of the central ion. The acac to Ru^{III} LMCT is the lowest energy feature of the electronic spectrum produced by the $\{Ru^{III}(acac)_2\}$ chromophore. Just as in the case of the $\{MX_4\}$ chromophore (Chapter 3), the energies of the LMCT absorptions strongly depend on the nature of the ligands L. Both *cis* and *trans* isomers show a linear correlation with III/II redox potentials (Figure 4.4.3). The absolute values of the gradients (in eV/V) are much smaller than unity for both isomers, indicating that the stabilisation effect of the π-acceptor ligands L on the metal $d\pi$ orbitals is in part relayed to the acac donor π levels. This result is in agreement with the one obtained for the halide comlpexes.

The *trans* isomers show a fairly shallow correlation (gradient -1680 cm^{-1}/V or -0.21 eV/V). The gradient of the LMCT - E^o III/II relationship is almost three times greater for a series of *cis* complexes (-4630 cm^{-1}/V or -0.57 eV/V). Such a contrast between the *cis* and the *trans* isomers suggests a different sensitivity of the acac donor π levels to the degree of the stabilisation of the central ion $d\pi$ acceptor levels (concurrent with the accumulation of the positive charge on the metal), given by the E^o III/II values (see Chapter 3).

While LMCT bands experience a red shift with the growing π-acceptor strength of the ligands L, the MLCT absorptions, on the contrary, are blue-shifted. As a consequence of this, the MLCT bands are not easy to discern in many ruthenium (III) *bis*-acetylacetonates containing π-acceptor ligands: in some cases the MLCT band appears as a shoulder on the more intense acac π to π^* peak, and frequently the two bands coalesce completely (for example, see Figure 4.4.5). This is not merely "guesswork" as we can project the likely location of the MLCT (Ru^{III}) band from the electrochemical data. Figure 4.4.4 displays a plot of a few well-defined MLCT band energies versus available E^o IV/III values. The estimated slope of 0.41 eV/V is again much smaller than unity, indicating that not only the donor (metal $d\pi$), but also the

acceptor (acac π^*) levels become more stabilised when π-donor ligands (*e.g.* acac and Cl) are substituted by a π-innocuous ($N(CH_3)_3$) or a mild π-acceptor ligands (CH_3CN).

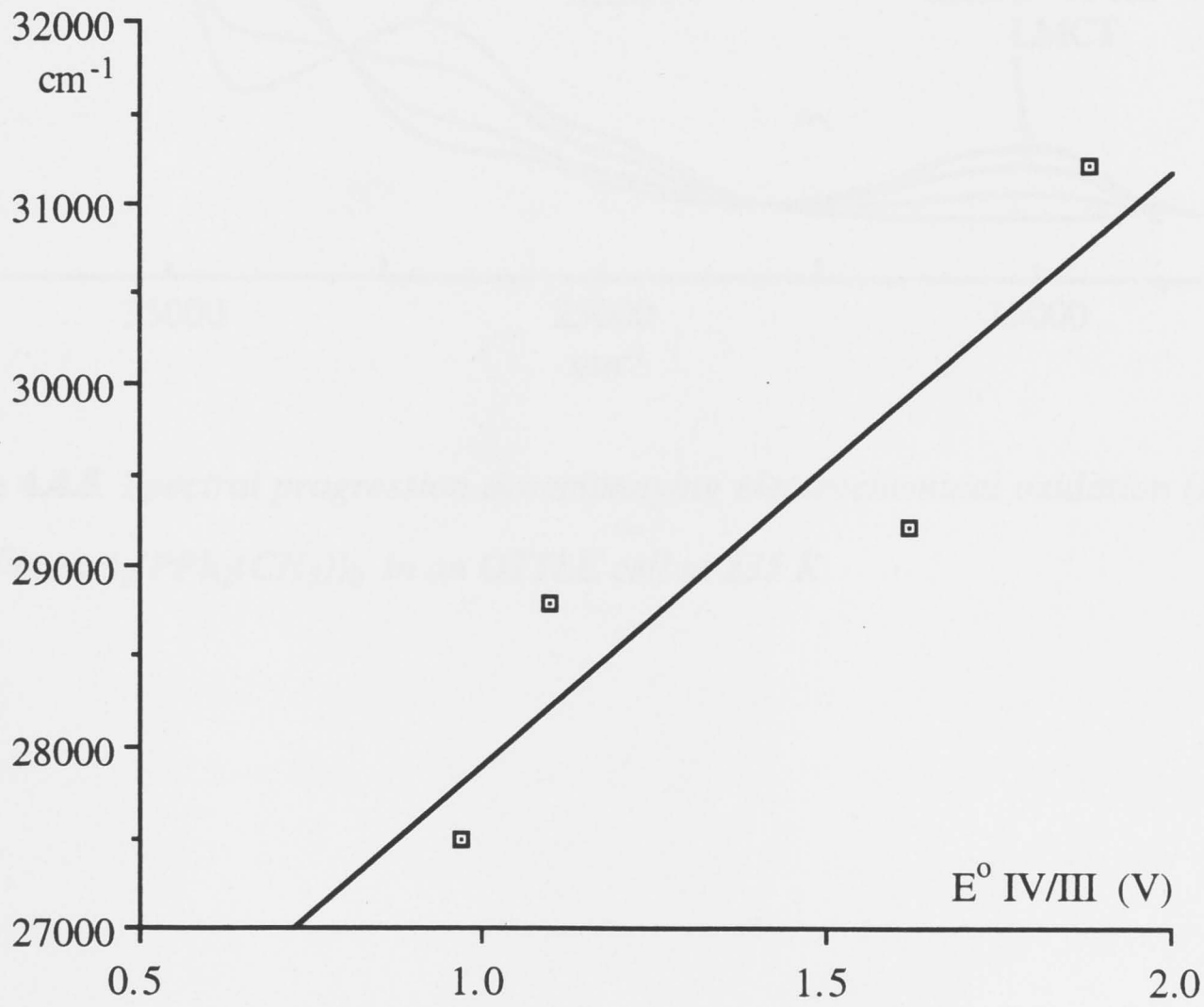

Figure 4.4.4 *Plot of the d^4/d^5 (IV/III) redox potentials and the metal-to-acac charge-transfer (MLCT) energies for four of $Ru^{III}(acac)_2L_2$-type complexes and $Ru(acac)_3$. Data from Table 4.4.3. The slope of the graph is ca. 3270 cm^{-1}/V or 0.41 eV/V.*

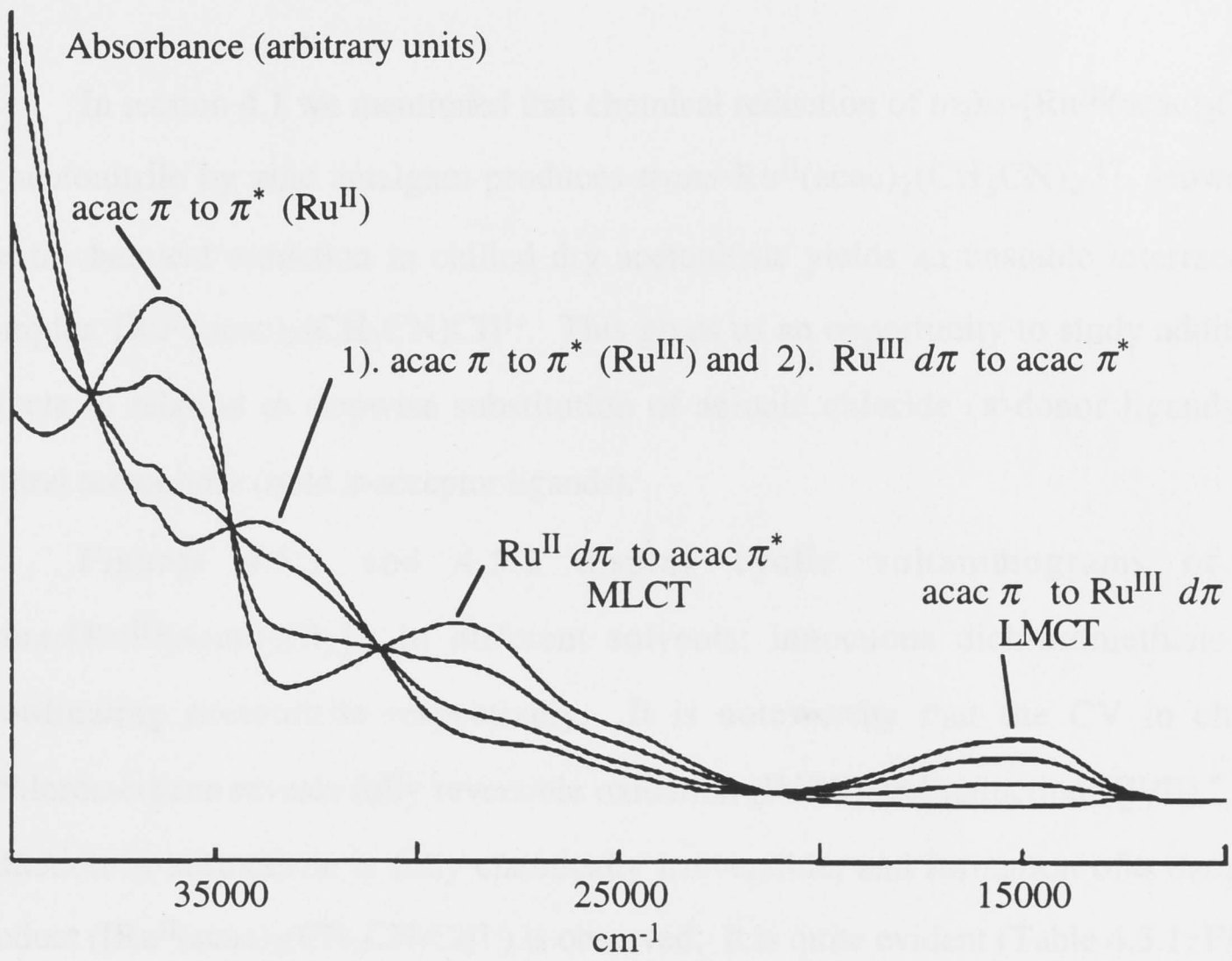

Figure 4.4.5 *Spectral progression accompanying electrochemical oxidation (III/II) of cis-$Ru^{II}(acac)_2(PPh_2(CH_3))_2$ in an OTTLE cell at 235 K.*

4.5 Spectro-electrochemistry of the series of chloro / nitrile complexes, *trans*-$Ru(acac)_2(CH_3CN)_n(Cl)_{2-n}$

In section 4.1 we mentioned that chemical reduction of *trans*-$[Ru^{III}(acac)_2Cl_2]^{1-}$ in acetonitrile by zinc amalgam produces *trans*-$Ru^{II}(acac)_2(CH_3CN)_2$.[17] However, electrochemical reduction in chilled dry acetonitrile yields an unstable intermediate complex $[Ru^{II}(acac)_2(CH_3CN)Cl]^{1-}$. This gives us an opportunity to study additivity effects in relation to stepwise substitution of anionic chloride (π-donor ligands) by neutral acetonitrile (mild π-acceptor ligands).

Figures 4.5.1 and 4.5.2 display cyclic voltammograms of the *trans*-$[Ru^{III}(acac)_2Cl_2]^{1-}$ in different solvents: innocuous dichloromethane and coordinating acetonitrile respectively. It is noteworthy that the CV in chilled dichloromethane reveals fully reversible oxidation (IV/III) and reduction (III/II).* The reduction in acetonitrile is fully chemically irreversible, and formation of a daughter product ($[Ru^{II}(acac)_2(CH_3CN)Cl]^{1-}$) is observed. It is quite evident (Table 4.5.1; Figure 4.5.3) that the E_{obs} of the daughter product lies halfway between the the E^o III/II values of the *trans*-$[Ru^{III}(acac)_2Cl_2]^{1-}$ and *trans*-$Ru^{II}(acac)_2(CH_3CN)_2$ complexes. The optical spectra** of the dichloro (Figure 4.5.4), *bis*-acetonitrile (Figure 4.5.5), and the mixed complex (Figure 4.5.6) have been recorded. The intermediate complex was prepared and characterised *in situ* in an OTTLE cell. This entailed reduction of the dichloro complex ($[Ph_4As]$ *trans*-$[Ru^{III}(acac)_2Cl_2]$) in acetonitrile solution, followed by the II/III oxidation of the daughter product. The optical data of the trivalent complexes are consistent with the trend in the E^o III/II values (table 4.5.1; Figure 4.5.7).

Thus the set of *trans*-$[Ru(acac)_2(CH_3CN)_n(Cl)_{2-n}]^z$ (n = 0, 1, 2) complexes presents another good example of a linear additive system, similar to the halide / nitrile family described by G.A. Heath and C.M. Duff (Chapter 3; refs. 4,5).

---

* The reduction is only reversible at temperatures below 260 K.

** Assignment of the optical spectra was given in the preceding section. See Table 4.4.1.

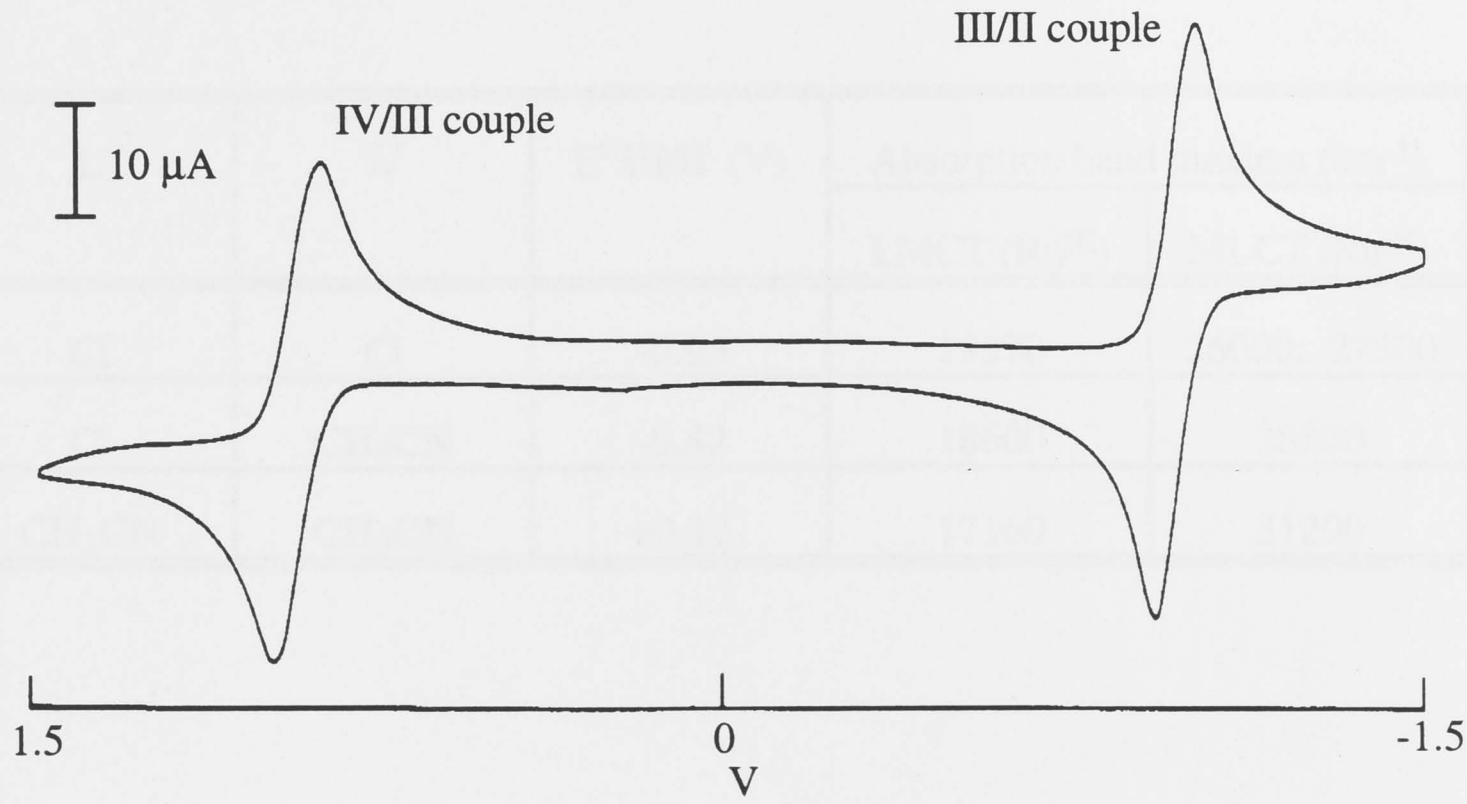

Figure 4.5.1 *Cyclic voltammetry of* $[Ph_4As]$ *trans-*$[Ru^{III}(acac)_2Cl_2]$ *in dichloromethane at 233 K*

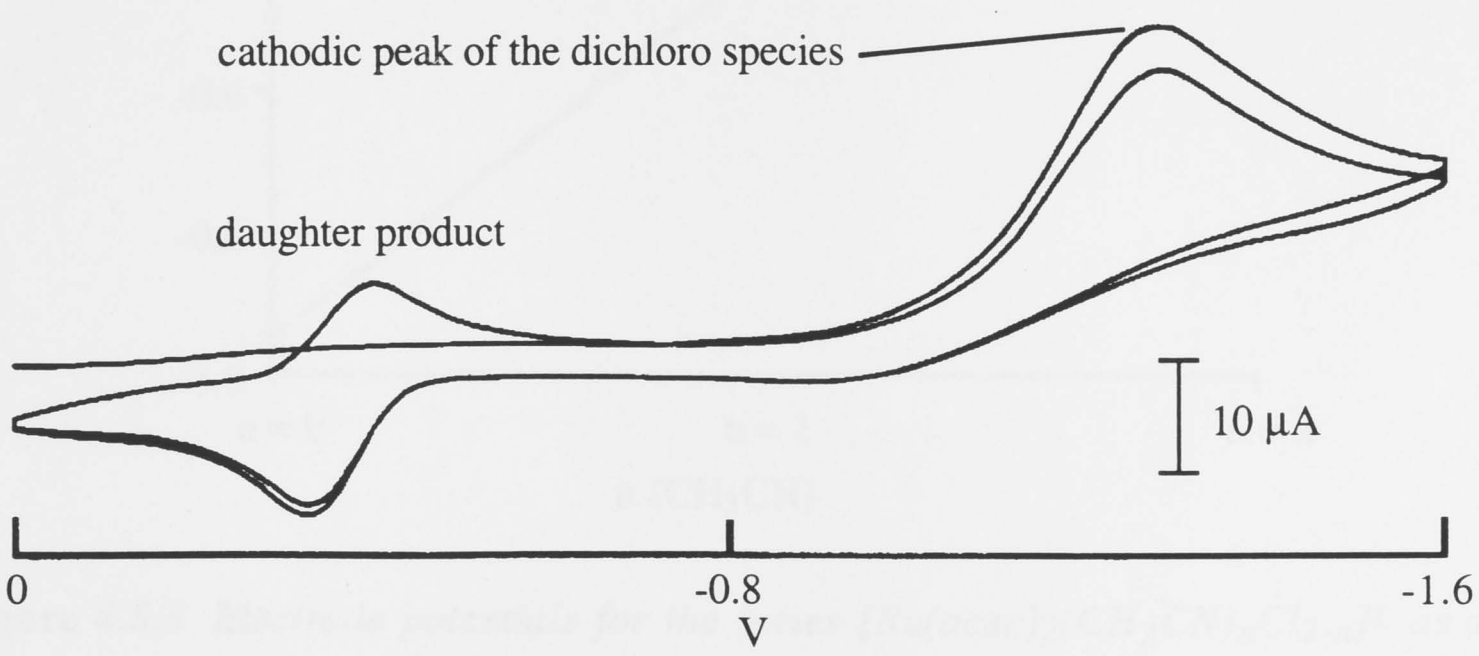

Figure 4.5.2 *Cyclic voltammetry of* $[Ph_4As]$ *trans-*$[Ru^{III}(acac)_2Cl_2]$ *in acetonitrile at 253 K: formation of a daughter product* ($[Ru^{II}(acac)_2(CH_3CN)Cl]^{1-}$) *is observed.*

Table 4.5.1 *Comparative electronic properties of the series of chloro/nitrile complexes, trans-[Ru(acac)2(L)(L′)]z*

L	L′	E^o III/II (V)	Absorption band maxima (cm^{-1})	
			LMCT (Ru^{III})	MLCT (Ru^{III})
Cl	Cl	-0.95	19370	26000; 27500
Cl	CH_3CN	-0.42	18600	28800
CH_3CN	CH_3CN	+0.12	17160	31200

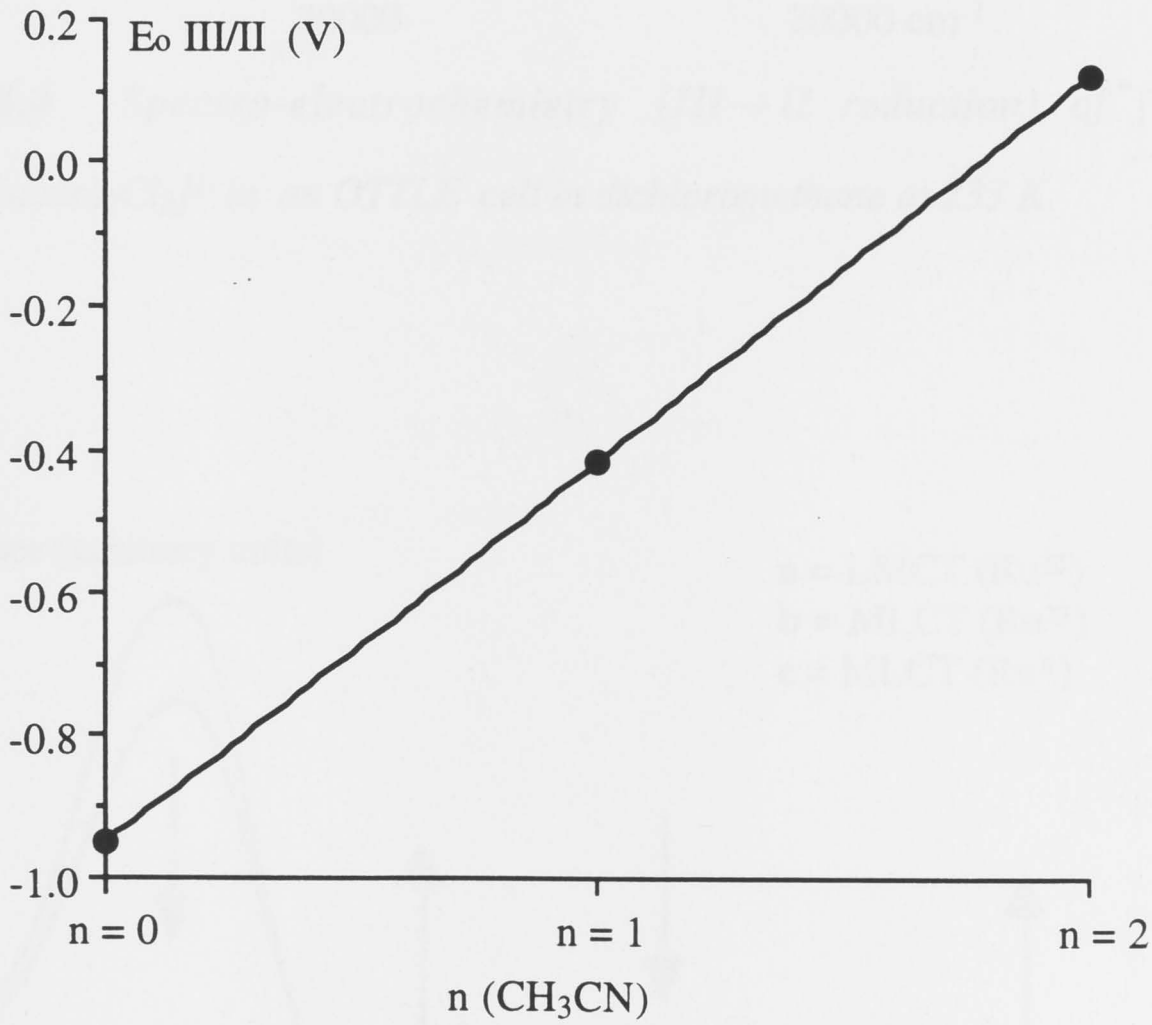

Figure 4.5.3 *Electrode potentials for the series $[Ru(acac)_2(CH_3CN)_nCl_{2-n}]^z$ as a function of stoichiometry. E^o III/II values (Table 4.5.1) are plotted versus* n. *The slope is +0.54 V per substitution, which is similar the "expected" slope of +0.6 V observed for the E^o III/II in the $[RuX_{6-n}(CH_3CN)_n]^z$ (X = Cl, Br) series (see Chapter 3).*

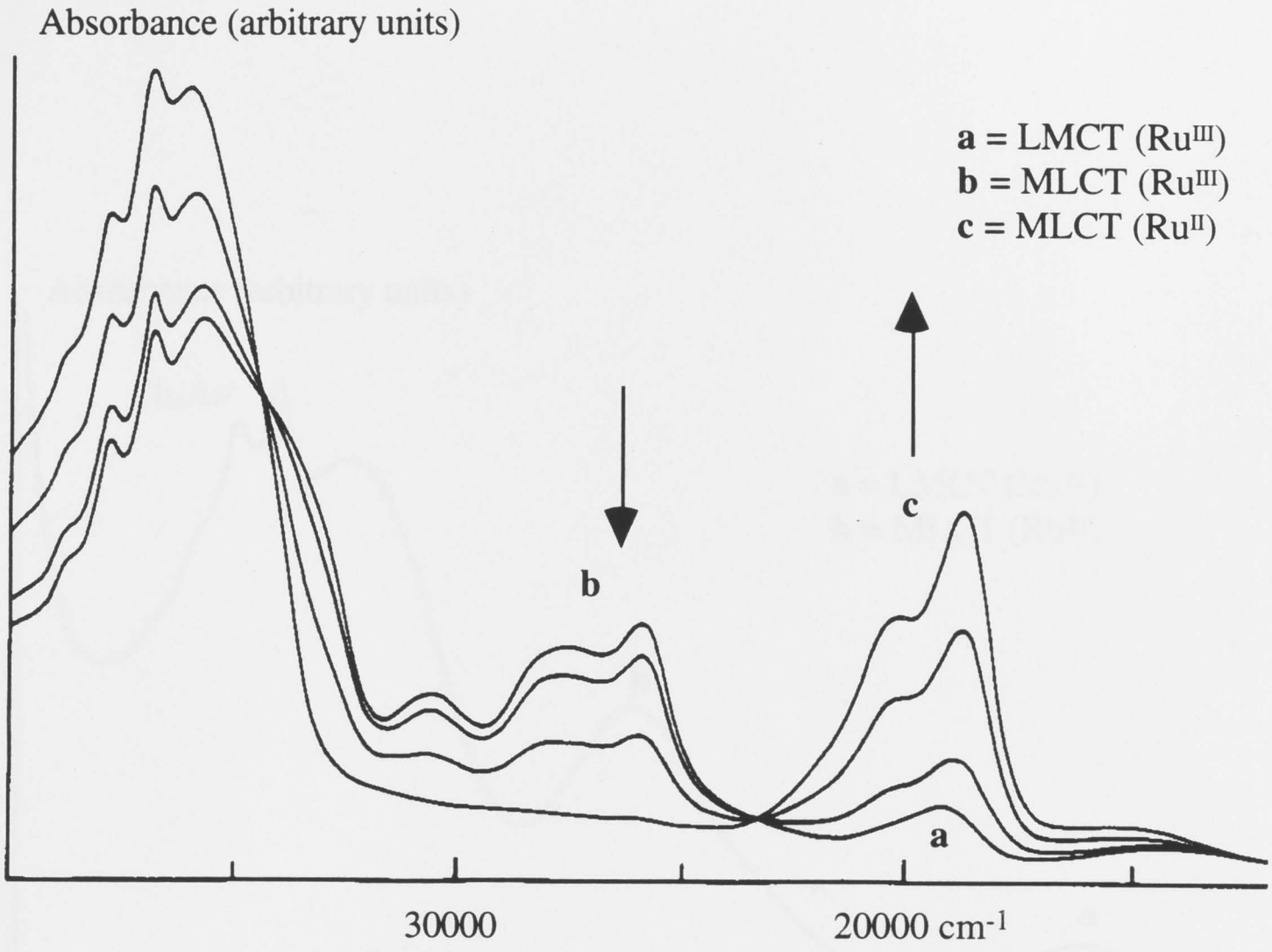

Figure 4.5.4 *Spectro-electrochemistry (III→II reduction) of $[Ph_4As]^+$ trans-$[Ru^{III}(acac)_2Cl_2]^{1-}$ in an OTTLE cell in dichloromethane at 233 K.*

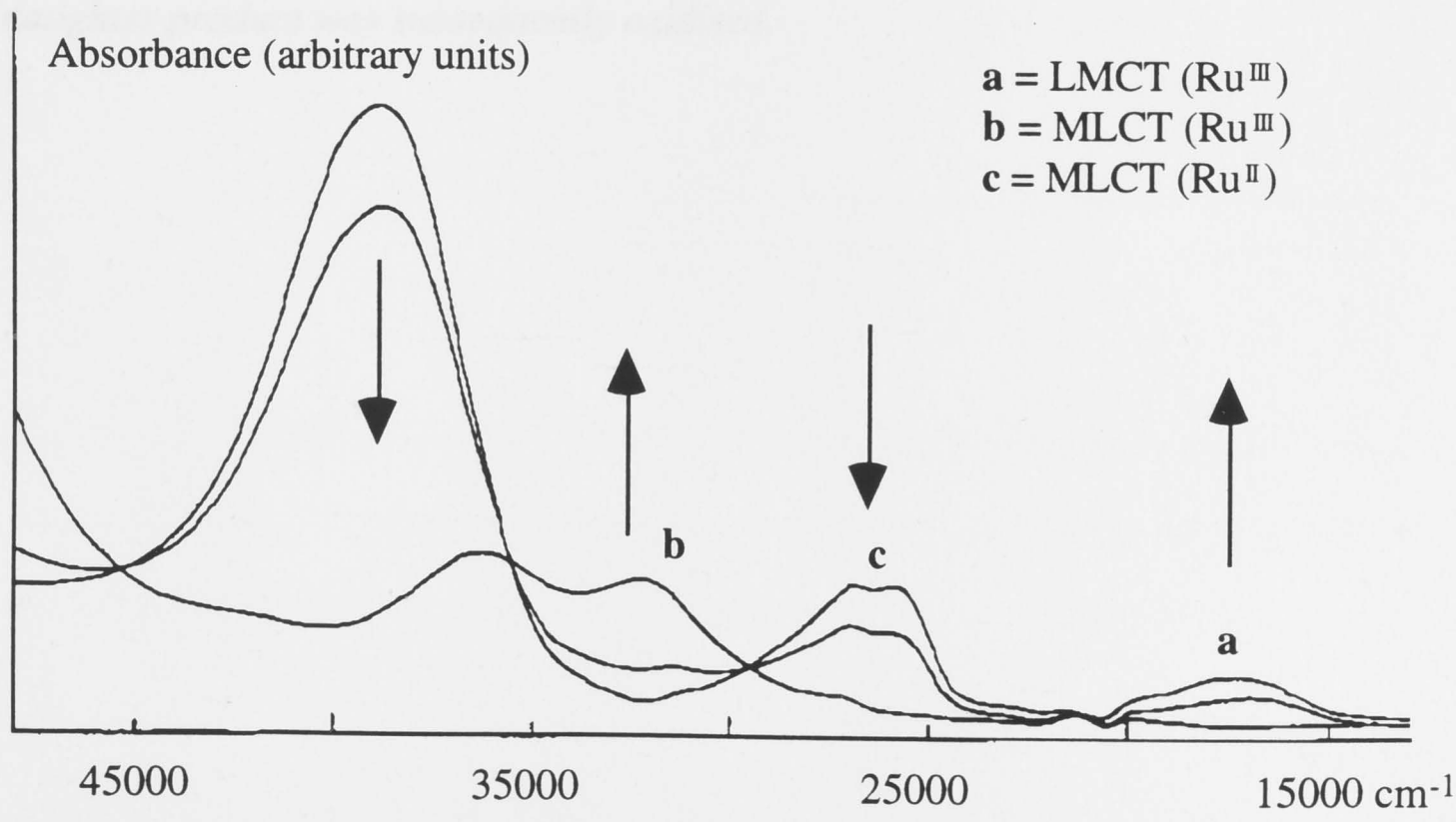

Figure 4.5.5 *Spectro-electrochemistry (II→III oxidation) of trans-$[Ru^{II}(acac)_2(CH_3CN)_2]$ in an OTTLE cell in acetonitrile at 240 K.*

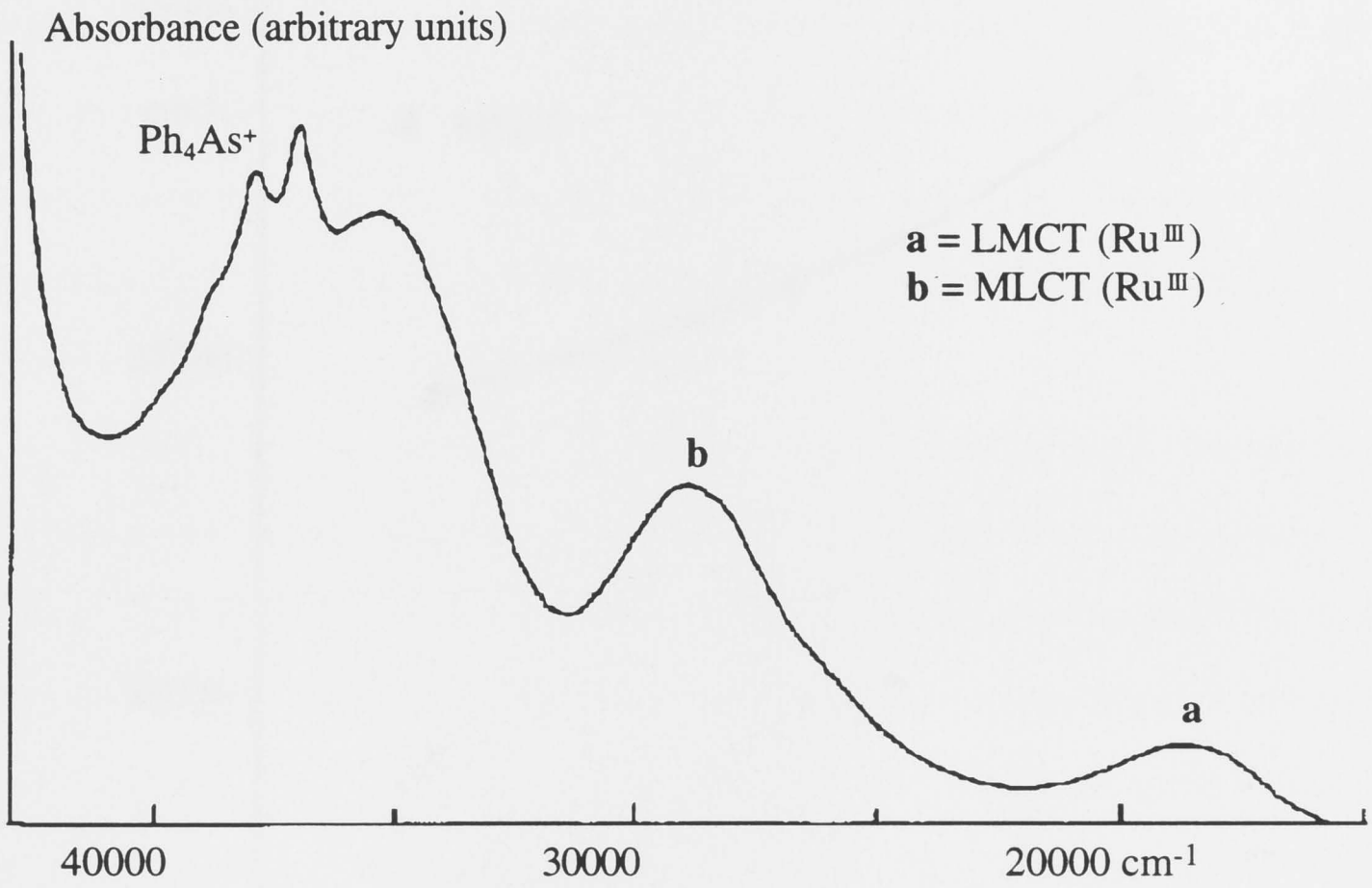

Figure 4.5.6 *Spectrum of an intermediate complex $[Ru^{III}(acac)_2(CH_3CN)Cl]$ prepared in situ in an OTTLE cell . The starting dichloro complex $[Ph_4As]^+$ trans-$[Ru^{III}(acac)_2Cl_2]^{1-}$ was initially reduced in acetonitrile solution at 253 K, and the daughter product was subsequently oxidised.*

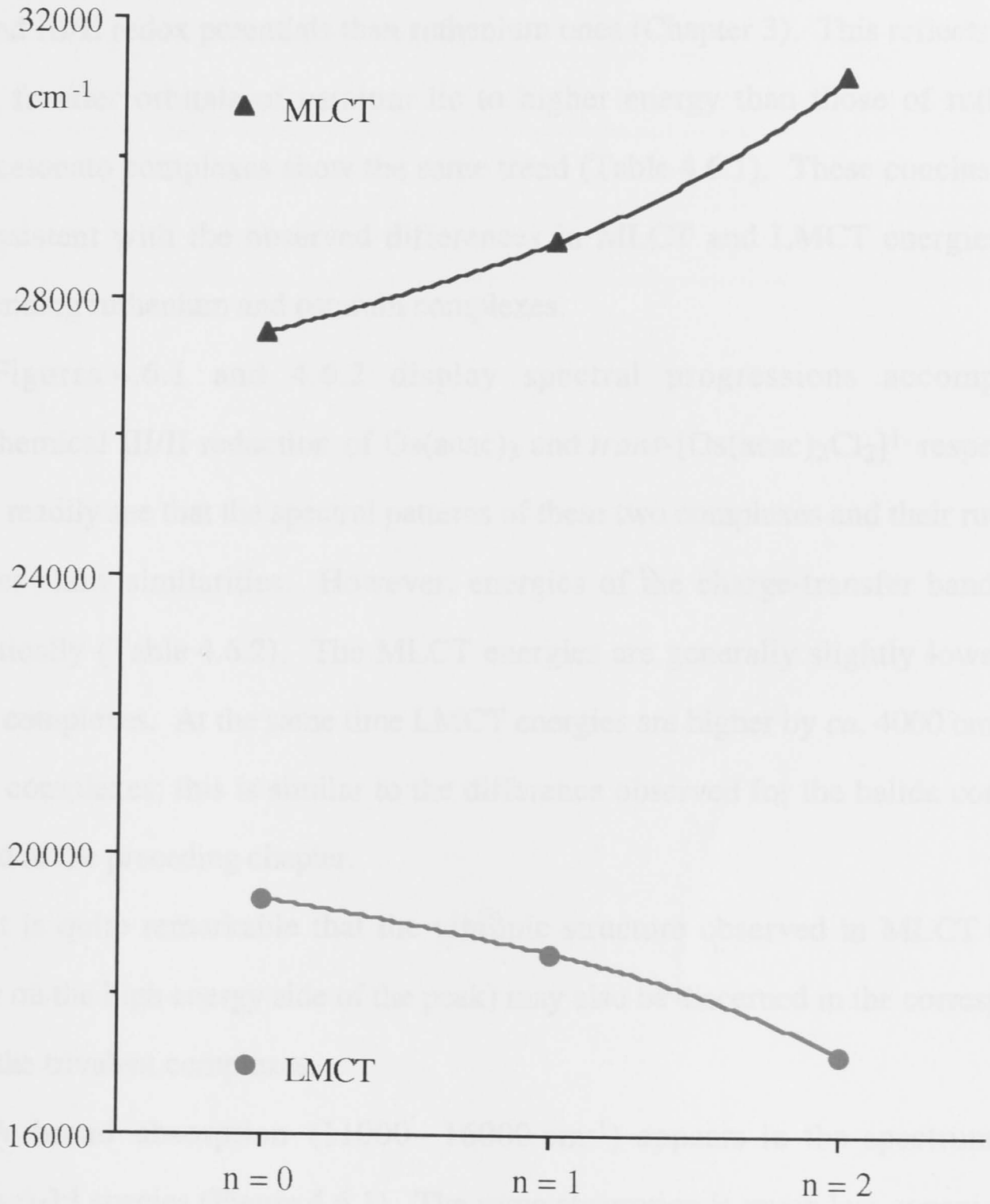

Figure 4.5.7 *Ruthenium (III) MLCT (red) and LMCT (blue) absorption band energy as a function of stoichiometry. Band maxima (Table 4.5.1) are plotted versus n for the* $[Ru(acac)_2(CH_3CN)_nCl_{2-n}]^z$ *series. The points are connected by arbitrary interpolation.*

4.6 Comparative Spectro-electrochemistry of the $M(acac)_3$ and *trans*-$M(acac)_2Cl_2$ complexes, where M = Ru or Os

We have already seen that the osmium halide complexes have more negative IV/III and III/II redox potentials than ruthenium ones (Chapter 3). This reflects the fact that the frontier orbitals of osmium lie to higher energy than those of ruthenium. Acetylacetonato complexes show the same trend (Table 4.6.1). These conclusions are also consistent with the observed differences in MLCT and LMCT energies of the corresponding ruthenium and osmium complexes.

Figures 4.6.1 and 4.6.2 display spectral progressions accompanying electrochemical III/II reduction of $Os(acac)_3$ and *trans*-$[Os(acac)_2Cl_2]^{1-}$ respectively. One can readily see that the spectral patterns of these two complexes and their ruthenium analogues show similarities. However, energies of the charge-transfer bands differ systematically (Table 4.6.2). The MLCT energies are generally slightly lower in the osmium complexes. At the same time LMCT energies are higher by *ca.* 4000 cm^{-1} in the osmium complexes; this is similar to the difference observed for the halide complexes described in the preceding chapter.

It is quite remarkable that the vibronic structure observed in MLCT (M^{II}) (a shoulder on the high energy side of the peak) may also be discerned in the corresponding band of the trivalent complexes.

A broad absorption (11000 - 16000 cm^{-1}) appears in the spectrum of the $[Os^{II}(acac)_3]^{-1}$ species (Figure 4.6.1). The same absorption is much less conspicuous in the spectrum of the ruthenium analogue (Figure 4.4.1). This must be a spin-forbidden component. Such low energy absorptions were observed and assigned as spin-forbidden bands in a series of $[M^{II}(bipy)_3]^{2+}$ complexes (M = Fe, Ru and Os).[31] Similarly, these bands were also found to be much more intense in the osmium complexes than in the iron and ruthenium ones.

Table 4.6.1 *Comparative redox properties of the trans-$[M(acac)_2Cl_2]^z$ and $M(acac)_3$ complexes (M = Ru, Os)*

Metal	*trans*-$[M(acac)_2Cl_2]$		$M(acac)_3$	
	E^o IV/III (V)	E^o III/II (V)	E^o IV/III (V)	E^o III/II (V)
Ru	+0.97	-0.95	+1.14	-0.57
Os	+0.20	-1.58	+0.51	-1.07

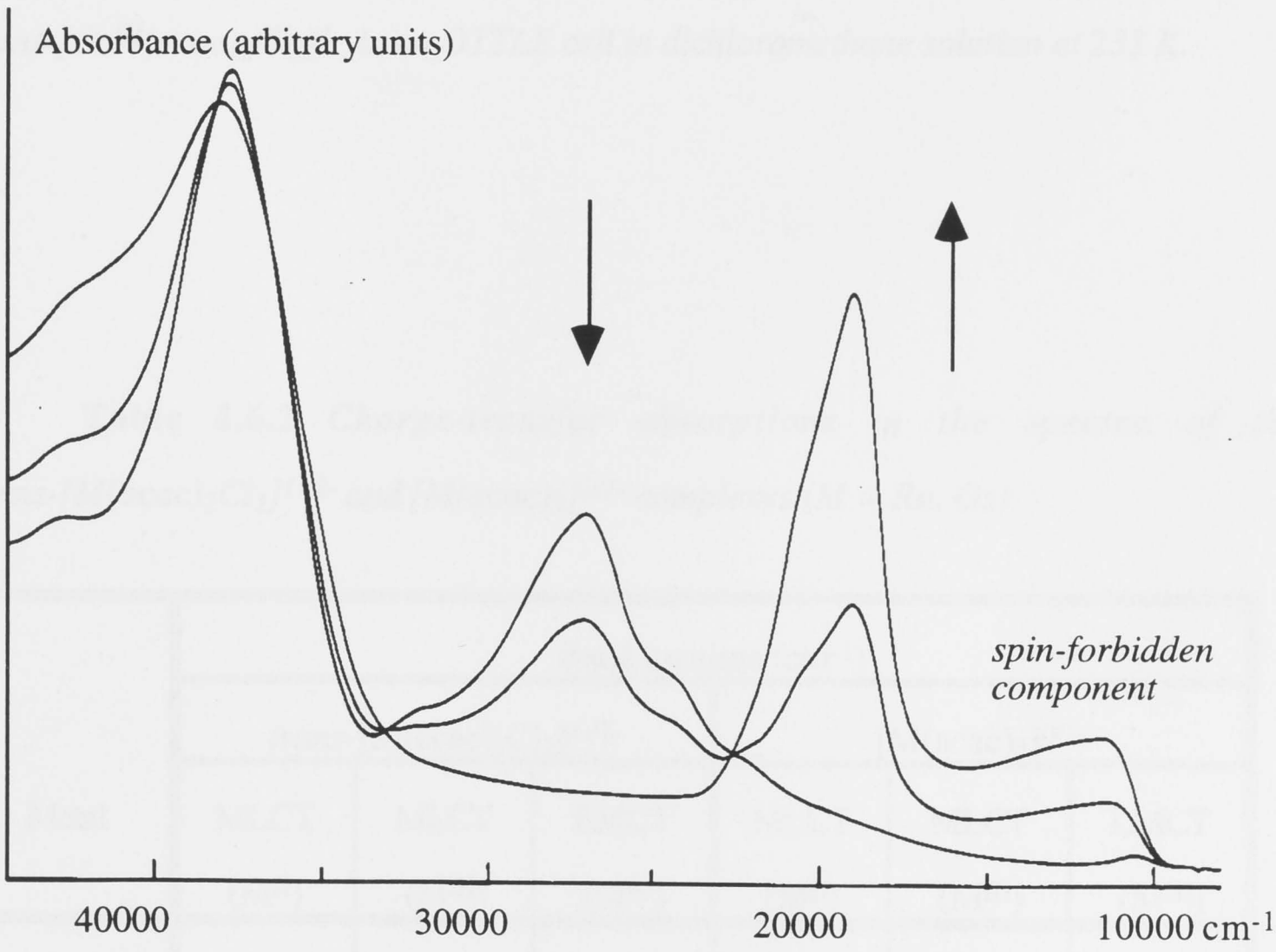

Figure 4.6.1 *Spectral progression accompaniyng electrochemical III/II reduction of $Os(acac)_3$ in an OTTLE cell in dichloromethane solution at 233 K.*

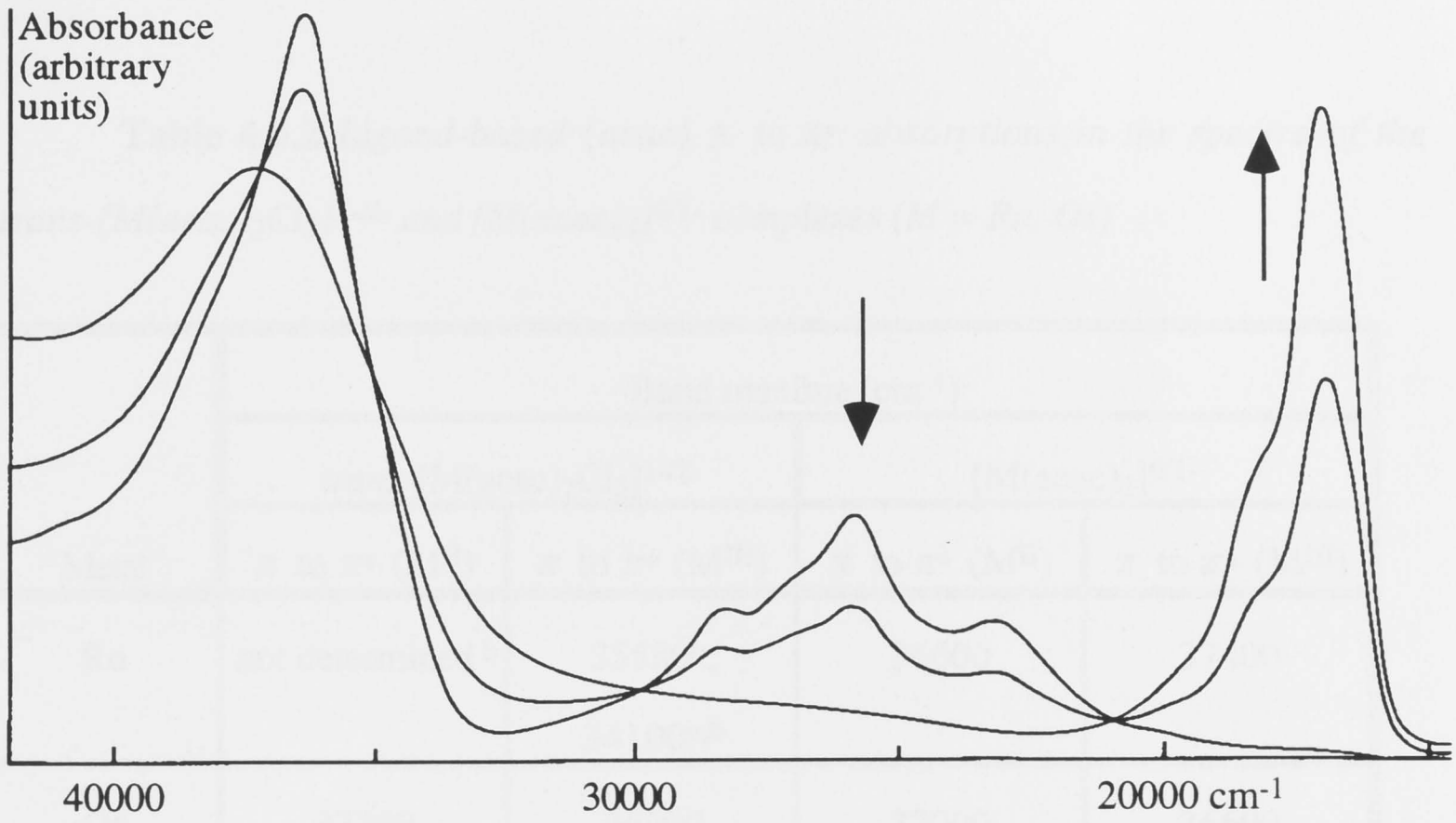

Figure 4.6.2 *Spectral progression accompaniyng electrochemical III/II reduction of trans-$[Os^{III}(acac)_2Cl_2]^{1-}$ in an OTTLE cell in dichloromethane solution at 233 K.*

Table 4.6.2 *Charge-transfer absorptions in the spectra of the trans-$[M(acac)_2Cl_2]^{1-/2-}$ and $[M(acac)_3]^{0/1-}$ complexes (M = Ru, Os)*

Metal	Band maxima (cm^{-1})					
	trans-$[M(acac)_2Cl_2]^{1-/2-}$			$[M(acac)_3]^{0/1-}$		
	MLCT (M^{II})	MLCT (M^{III})	LMCT (M^{III})	MLCT (M^{II})	MLCT (M^{III})	LMCT (M^{III})
Ru	18800; 20200	26000; 27500	19370	19800; 21000[a]	28800	20000
Os	17000; 18000[a]	25800; 28300[a]	23200	19000; 20500[a]	27000	*ca.* 24000[a]

[a] shoulder

Table 4.6.2 *Ligand-based (acac) π to π^* absorptions in the spectra of the trans-$[M(acac)_2Cl_2]^{1-/2-}$ and $[M(acac)_3]^{0/1-}$ complexes (M = Ru, Os)*

Metal	Band maxima (cm^{-1})			
	trans-$[M(acac)_2Cl_2]^{1-/2-}$		$[M(acac)_3]^{0/1-}$	
	π to π^* (M^{II})	π to π^* (M^{III})	π to π^* (M^{II})	π to π^* (M^{III})
Ru	not determined [b]	35580[b]; 34100[a,b]	36600	37400
Os	37200	36200	37000	36600

[a] shoulder

[b] The π to π^* bands are partially obscured by aromatic absorptions in the spectra of $[Ph_4As]$ *trans*-$[Ru^{III}(acac)_2Cl_2]$. A solution of tetra-n-butylammonium salt of the Ru^{III} complex has been prepared to determine the energy of π to π^* (Ru^{III}) transition. See the next section.

4.7 Experimental

The electrochemical and spectro-electrochemical experiments were performed as described in the previous chapter. Likewise, the redox potentials are quoted *versus* . the Ag/AgCl reference electrode, against which ferrocene ([$FeCp_2$]) is oxidised at +0.55 V.

[$AsPh_4$] *trans*-[$Ru^{III}(acac)_2Cl_2$], Cs *trans*-[$Ru^{III}(acac)_2Cl_2$] and *trans*-[$Ru(acac)_2(CH_3CN)_2$] were prepared according to the methods described in the literature.[17] The dichloromethane solution of [Bu^n_4N] *trans*-[$Ru^{III}(acac)_2Cl_2$] was prepared by extraction of the corresponding caesium salt into 0.5 M [Bu^n_4N] Cl solution in freshly distilled dichloromethane. A sample of *cis*-[$Ru(acac)_2(CH_3CN)_2$] was prepared according to Kobayashi's method.[13]

4.8 References

1. Schröder, M., Stephenson, T.A. in *Comprehensive Coordination Chemistry*, Pergamon Press, Oxford, **1987**, *4*, 423 and references therein
2. Seddon, E.A., Seddon, K.R. *The Chemistry of Ruthenium*, Elsevier, Amsterdam, **1984**, 136-137 and 200-105, and references therein
3. Patterson, G.S., Holm, R.H. *Inorg. Chem.* **1972**, *11*, 2285
4. Takeuchi, Y., Endo, A., Shimizu, K., Satô, G.P. *J. Electroanal. Chem.* **1985**, *185*, 185
5. Endo, A., Shimizu, K., Satô, G.P. *Chem. Lett.* **1985**, 581
6. Hammett, L.P. *Physical Organic Chemistry*, McGraw-Hill Book Company, New York, **1970**
7. Hoshino, Y., Endo, A., Shimizu, K., Satô, G.P. *J. Electroanal. Chem.* **1988**, *246*, 225
8. Hoshino, Y., Yukawa, Y., Maruyama, T., Endo, A., Shimizu, K., Satô, G.P. *Inorg. Chim. Acta* **1990**, *174*, 41
9. Haga, M., Matsumura-Inoue, T., Shimizu, K., Satô, G.P. *J. Chem. Soc., Dalton Trans.* **1989**, *371*
10. Aynetchi, S., Hitchcock, P.B., Seddon, E.A., Seddon, K.R., Yousif, Y.Z., Zora, J.A., Stuckey, K. *Inorg. Chim. Acta* **1986**, *113*, L7
11. Calderazzo, F., Floriani, C., L'Eplattenier, F. *J. Chem. Soc. (A)* **1969**, 1378
12. Gilbert, J.D., Wilkinson, G. *J. Chem. Soc. (A)* **1969**, 1749
13. Kobayashi, T., Nishina, Y., Shimizu, K., Satô, G.P. *Chem. Lett.* **1988**, 1137
14. Kashahara, Y., Hoshino, Y., Shimizu, K., Satô, G.P. *Chem. Lett.* **1990**, 381
15. Bennett, M.A., Neumann, H. unpublished results
16. Wallace, L. *Ph.D. Thesis* A.N.U.,Canberra, **1991**, Ch. 5
17. Hasegawa, T., Lau, T.C., Taube, H., Schaefer, W.P. *Inorg. Chem.* **1991**, *30*, 2921
18. Dwyer, F.P., Sargeson, A.M. *J. Amer. Chem. Soc.* **1955**, *77*, 1285
19. Queiros, M.A.M., Robinson, S.D. *Inorg. Chem.* **1978**, *17*, 310

20. Preetz, W., Petersen, H. *Z. Naturforsch.* **1979**, *34b*, 595

21. Behling, T., Wilkinson, G., Stephenson, T.A., Tocher, D.A., Walkingshaw, M.D. *J. Chem. Soc., Dalton Trans.* **1983**, 2109

22. Bursten, B.E., Green, M.R. *Prog. Inorg. Chem.* **1988**, *36*, 393

23. Lever,A.B.P. *Inorg. Chem.* **1990**, *29*, 1271

24. Chatt, J., Kan, C.T., Leigh, G.J., Pickett, C.J., Stanley, D.R. *J. Chem. Soc., Dalton Trans.* **1980**, 2032

25. Ahrland, S., Chatt, J. *J. Chem. Soc.* **1957**, 1379

26. Wimmer, F.L., Snow, M.R., Bond, A.M. *Inorg. Chem.* **1974**, *13*, 1617

27. Treichel, P.M., Mueh, H.J., Bursten, B.E. *Israel J. Chem.* **1976/77**, *15*, 253

28. Bursten, B.E. *J. Amer. Chem. Soc.* **1982**, *104*, 1299

29. Heath, G.A, Smeulders, J.B.A.F. *XXVII International Conference on Coordination Chemistry, Broadbeach, QLD* **1989**, Abstract W 39

30. Dodsworth, E.S., Lever, A.B.P. *Chem. Phys. Lett.* **1988**, *124*, 152

31. Thomson, A.J., Skarda, V., Cook, M.J., Robbins, D.J. *J. Chem. Soc., Dalton Trans.* **1985**, 1781

Appendix 1

Comparative Electrochemistry of the *cis* and *trans*-$[OsBr_4(L)_2]^{z-}$ Complexes, where L = CH_3CN and CO

A1.1 Results and Discussion

The relationship of the electrochemical properties of geometric isomers of the transition metal complexes is important for better understanding of the Ligand Additivity concept. Chapter 3 explored redox properties of *cis* and *trans* isomers of ruthenium *bis*-acetylacetonato complexes. In this Appendix the results of an electrochemical study of the *cis*- and *trans*- $[OsBr_4(L)_2]^{z-}$ complexes are presented.

The *bis*-nitrile studied here complexes show similar III/II and, especially, IV/III redox couples (Table A1.1 and Figures A1.1 - 2). This is not unexpected as acetonitrile is deemed to be a moderate π-acceptor. Therefore, in the light of Bursten's additivity model,[1] which itself rests on the Angular Overlap model (AOM), we may expect only small difference in E^o values between the geometric isomers of mixed bromide nitrile complexes, particularly in higher oxidation states.

The *cis* and *trans bis*-carbonyl tetrabromide complexes make a striking contrast to their *bis*-nitrile analogues. The comparison of the III/II redox couples of these species shows an enormous difference of 0.82 V (Table A1.1 and Figure A1.3). To our knowledge, such a big difference in redox properties between the isomeric complexes has not been reported in the literature hitherto. It is clearly largely due to a vast difference in π-donor / acceptor properties between the halide and the carbonyl ligands (see Chapter 3).

This example allows us to emphasise yet again that the redox potentials of isomeric complexes containing the same ligand set may be quite different. Therefore,

caution must be exercised in application of simplistic Ligand Additivity models,[2] especially for complexes containing two kinds of ligands which vary greatly in their π-backbonding characteristics (*e.g.* CO and Br^-).

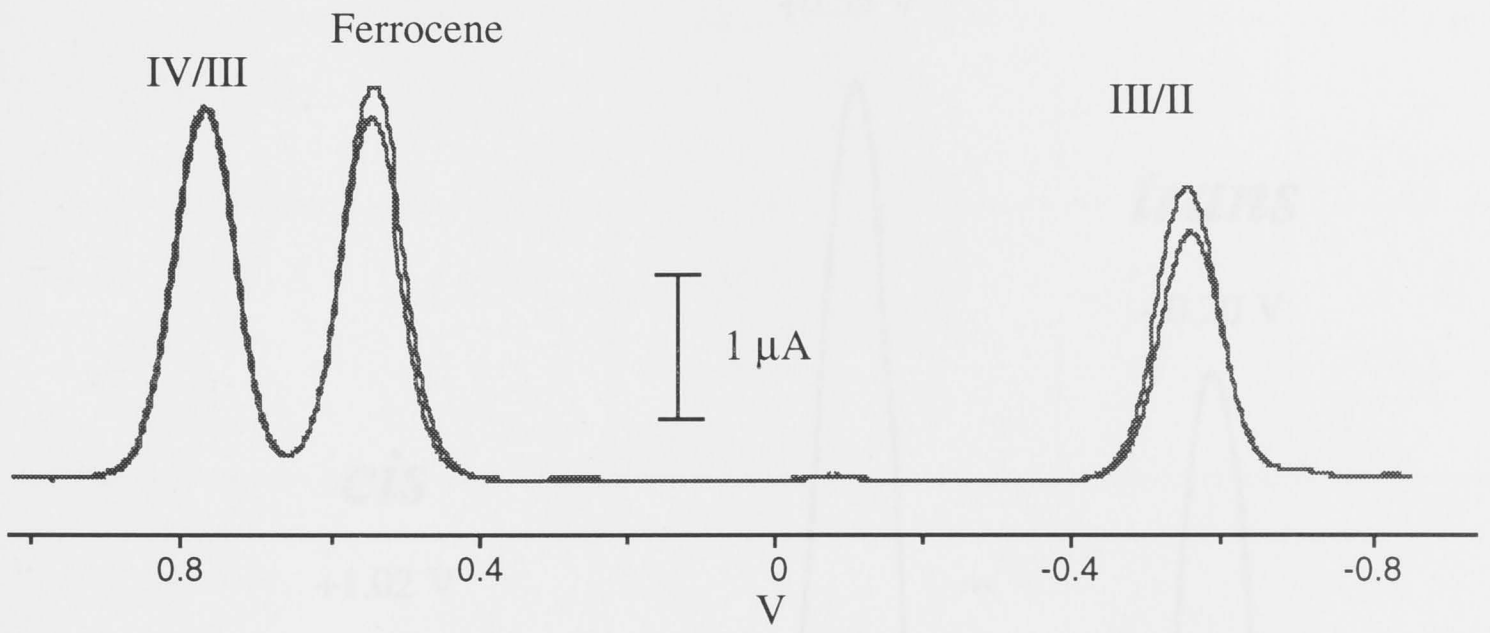

Figure A1.1 *Alternating current cyclic (acV) voltammetry of the cis-$[OsBr_4(CH_3CN)_2]^{z-}$ species in dichloromethane at 233 K. Ferrocene added for reference (+0.55 V).*

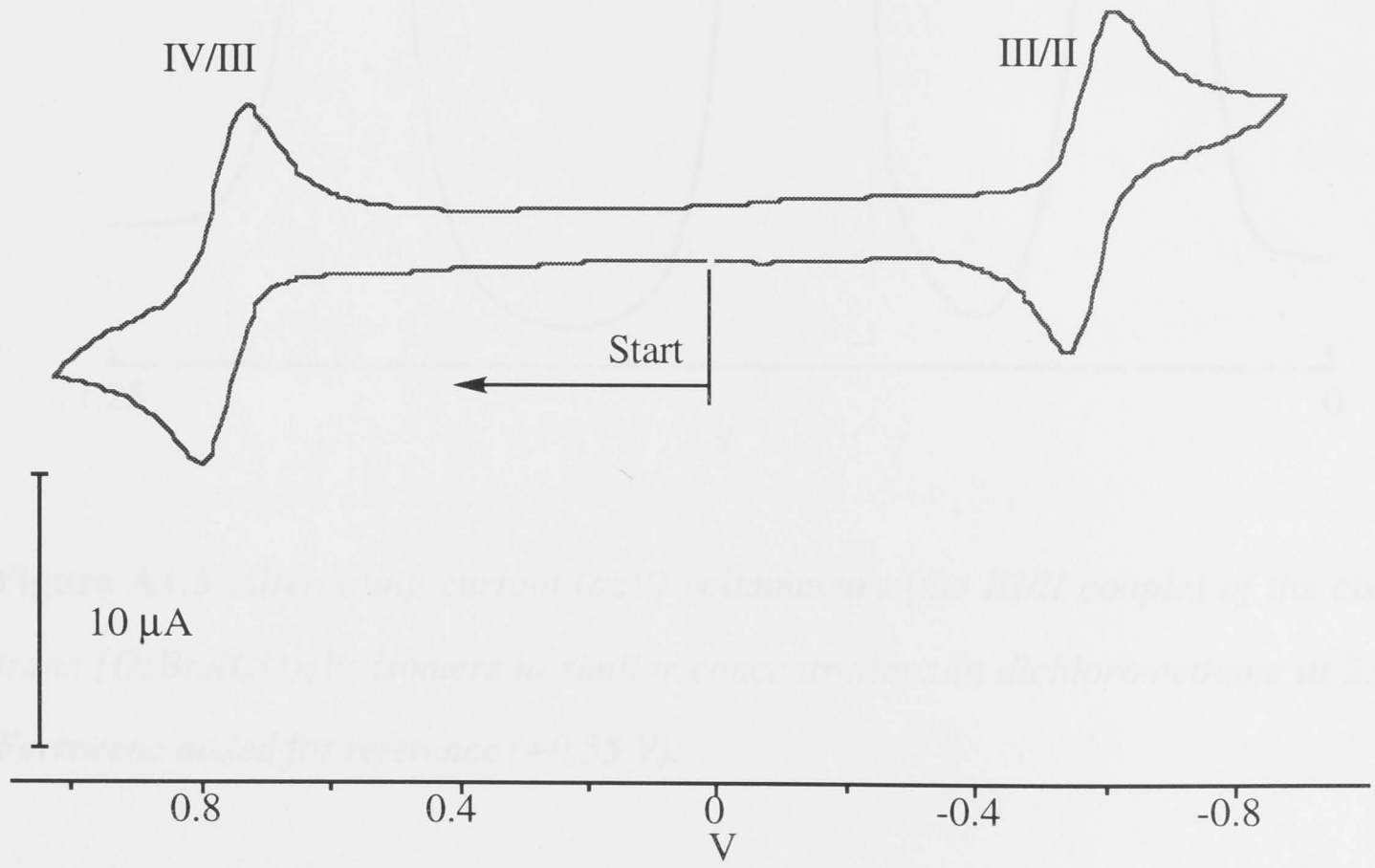

Figure A1.2 *Cyclic voltammetry (CV) of the cis-$[OsBr_4(CH_3CN)_2]^{z-}$ species in dichloromethane at 233 K.*

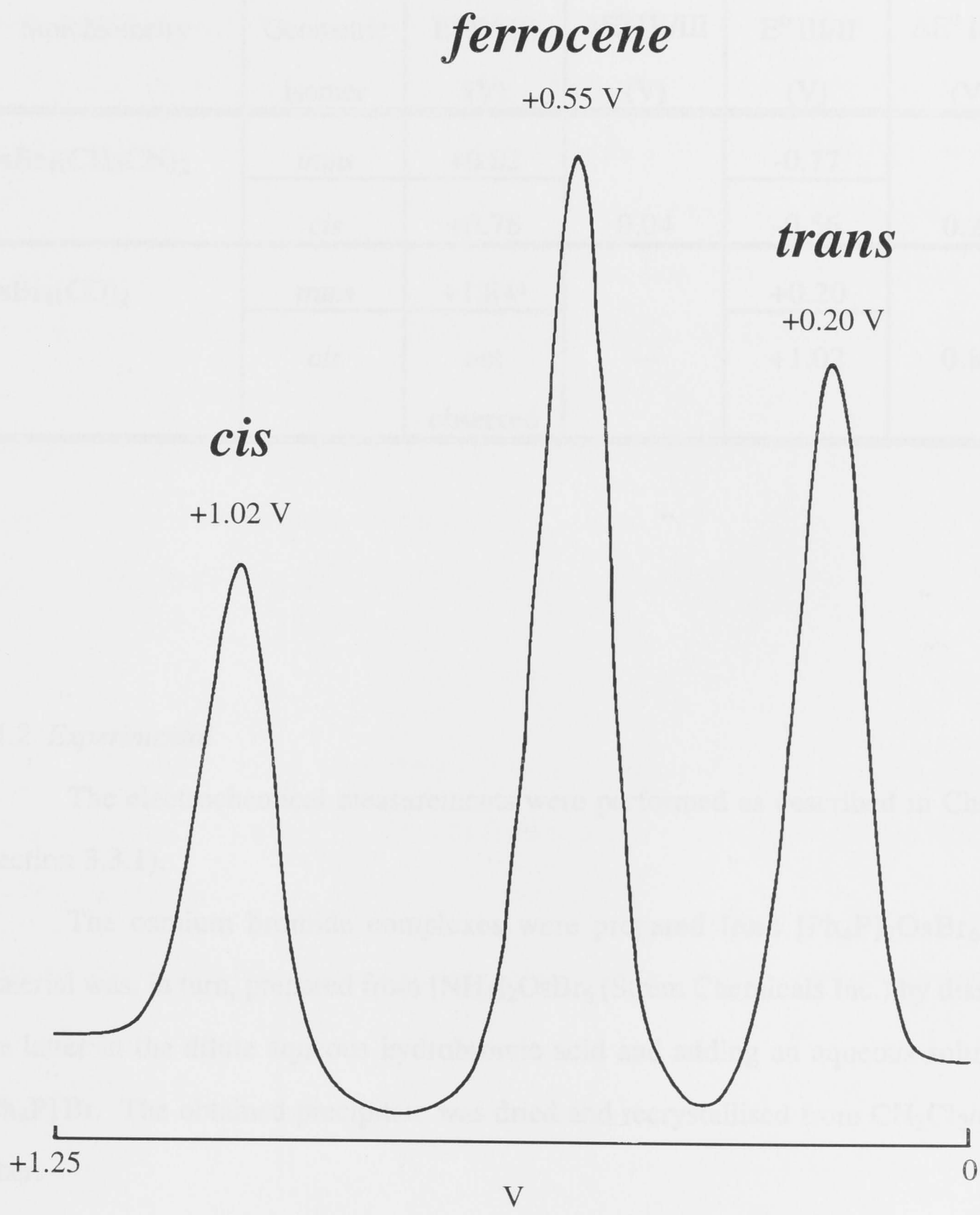

Figure A1.3 *Alternating current (acV) voltammetry (the III/II couple) of the cis and trans* $[OsBr_4(CO)_2]^{z-}$ *isomers in similar concentrations in dichloromethane at 233 K. Ferrocene added for reference (+0.55 V).*

Table A1.1 *Redox properties of the $[OsBr_4(L)_2]^{z-}$ complexes. The E^o values shown correspond to reversible electrode processes in dichloromethane at 233 K.*

Stoichiometry	Geometric isomer	E^o IV/III (V)	ΔE^o IV/III (V)	E^o III/II (V)	ΔE^o III/II (V)
$OsBr_4(CH_3CN)_2$	*trans*	+0.82		-0.77	
	cis	+0.78	0.04	-0.56	0.21
$OsBr_4(CO)_2$	*trans*	+1.84[a]		+0.20	
	cis	not observed	---	+1.02	0.82

A1.2 Experimental

The electrochemical measurements were performed as described in Chapter 3 (section 3.3.1).

The osmium bromide complexes were prepared from $[Ph_4P]_2OsBr_6$. This material was, in turn, prepared from $[NH_4]_2OsBr_6$ (Strem Chemicals Inc.) by dissolving the latter in the dilute aqueous hydrobromic acid and adding an aqueous solution of $[Ph_4P]$ Br. The obtained precipitate was dried and recrystallised from CH_2Cl_2/diethyl ether.

The *trans* isomers ($[Bu^n_4N]$ $[Os^{III}Br_4(CO)_2]$ and $[Bu^n_4N]$ $[Os^{III}Br_4(CH_3CN)_2]$) have been prepared according to the methods devised in our laboratory.[3]

The salts of *cis*-$[Os^{II}Br_4(CO)_2]^{2-}$ have been prepared as described in the literature.[4] The previously unreported $[Ph_4P]$ *cis*-$[Os^{III}Br_4(CH_3CN)_2]$ compound was prepared as follows:

---

[a] This couple is not fully reversible.

Tetraphenylphosphonium cis tetrabromo bis (acetonitrile) osmate (III)

$[Ph_4P]_2OsBr_6$ (0.10 g, 0.07 mmol) was dissolved in acetinitrile (20mL) and zinc amalgam (*ca.* 0.5 mL) was added. After stirring the mixture for not more than 20 min the solution turned pale yellow. It was separated from the amalgam and evaporated to dryness. The residue was redissolved in the mixture of CH_2Cl_2 and absolute ethanol (15mL; 1:1, v:v). The solution was passed through a bed of celite in order to remove undissolved matter. The solution was slowly evaporated in a crystallising dish at ambient temperature to induce the formation of the dark brown crystals. The crystals were then separated, washed by diethyl ether and dried in the air for 24 hours.

IR: weak C-N stretch at 2250 cm^{-1}.

UV-VIS: 21400 cm^{-1} (2440 M^{-1} cm^{-1}) , 24700 cm^{-1} (4920 M^{-1} cm^{-1}), 29500 cm^{-1} (1820 M^{-1} cm^{-1}) **in dichloromethane**

Yield: 0.06g (0.06 mmol; 85 %) $[Ph_4P]$ $[OsBr_4(CH_3CN)_2]$

Table A1.2 *The results of the elemental analysis of the cis isomers. Elemental analyses were performed by the Microanalytical Services Unit at the Research School of Chemistry, A.N.U.*

Compounds	Empirical formulae	Mass %, Found (Calculated)			
		C	H	N	P
$[Ph_4P]$ *cis*-$[Os^{III}Br_4(CH_3CN)_2]$	$C_{28}H_{26}N_2POsBr_4$	35.93 (36.11)	2.80 (2.81)	2.76 (3.01)	3.11 (3.33)
$[Ph_4P]_2$ *cis*-$[Os^{II}Br_4(CO)_2]$	$C_{50}H_{40}P_2OsBr_4O_2$	48.60 (48.25)	3.22 (3.24)	0.00 (0.00)	4.99 (4.98)
$[Bu^n{}_4N]_2$ *cis*-$[Os^{II}Br_4(CO)_2]$	$C_{34}H_{72}P_2N_2OsBr_4O_2$	38.72 (38.86)	6.76 (6.91)	2.42 (2.67)	-

A1.3 References

1. Bursten, B.E. *J. Amer. Chem. Soc.* **1982**, *104*, 1299
2. Lever,A.B.P. *Inorg. Chem.* **1990**, *29*, 1271
3. Humphrey, D.G. *Ph.D. Thesis* A.N.U.,Canberra, **1992**
4. Johannsen, F.H., Preetz, W., Scheffler, A. *J. Organomet. Chem.* **1975**, *102*, 527

X-Ray Crystal Structures

A2.1 Crystal structure of [$BzPh_3P$] [$OsBr_4(CH_3CN)(NO)$] • 0.5 (C_6H_6)

Table A2.1.1 *Crystallographic Data for ($BzPPh_3$) [$OsBr_4(NO)(CH_3CN)$] • 0.5(C_6H_6) at 173K.*

chem formula	$C_{30}H_{28}Br_4N_2OOsP$
fw	973.36
cryst system	monoclinic
spacegroup	$P2_1/n$
a, Å	10.372(1)
b, Å	19.520(2)
c, Å	16.188(2)
β,°	96.13(1)
V, Å^3	3258.8(6)
Z	4
d_{calcd}, g cm^{-3}	1.984
μ[Mo Kα], cm^{-1}	88.9
cryst dimens, mm	0.22 × 0.24 × 0.26
X-radiation	Mo Kα
λ, Å	0.7107
data range, ° in 2θ	4 - 60
no. unique data	9521
no. data refined	6391 [$I > 3\sigma(I)$]
no. variables	356
R	0.046
R_w	0.053
GOF	1.65
F(000)	1843.5

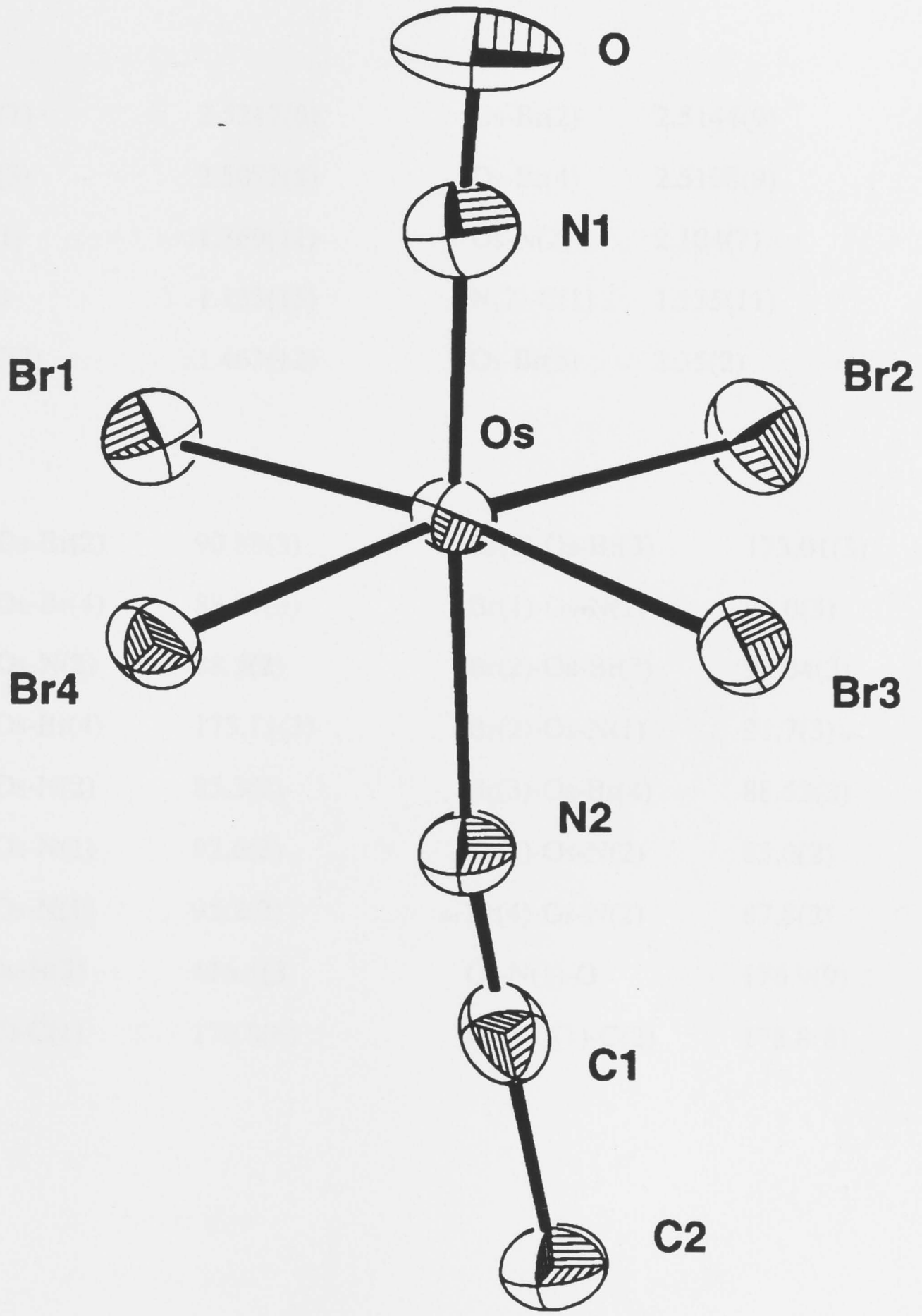

Figure A2.1.1 *Thermal ellipsoid diagram of the* $[OsBr_4(NO)(CH_3CN)]^-$ *anion with labelling of the non-H atoms at 173 K. Ellipsoids show 50% probability levels.*

Table A2.1.2 *Interatomic distances (Å) and angles (°) for non-hydrogen atoms of the complex anion in* $(BzPPh_3)[OsBr_4(NO)(CH_3CN)]\bullet 0.5(C_6H_6)$ *at 173K.*[*]

Os-Br(1)	2.5217(8)	Os-Br(2)	2.5144(9)
Os-Br(3)	2.5072(8)	Os-Br(4)	2.5108(9)
Os-N(1)	1.769(11)	Os-N(2)	2.104(7)
N(1)-O	1.133(15)	N(2)-C(1)	1.135(11)
C(1)-C(2)	1.463(12)	Os-Br(5)	2.35(2)

Br(1)-Os-Br(2)	90.88(3)	Br(1)-Os-Br(3)	173.01(3)
Br(1)-Os-Br(4)	88.77(3)	Br(1)-Os-N(1)	94.0(3)
Br(1)-Os-N(2)	88.5(2)	Br(2)-Os-Br(3)	91.04(3)
Br(2)-Os-Br(4)	173.11(3)	Br(2)-Os-N(1)	91.7(3)
Br(2)-Os-N(2)	85.3(2)	Br(3)-Os-Br(4)	88.52(3)
Br(3)-Os-N(1)	92.6(3)	Br(3)-Os-N(2)	85.0(2)
Br(4)-Os-N(1)	95.2(3)	Br(4)-Os-N(2)	87.8(2)
N(1)-Os-N(2)	176.1(3)	Os-N(1)-O	176.9(9)
Os-N(2)-C(1)	170.8(6)	N(2)-C(1)-C(2)	178.8(8)

[*] For this compound, at the early stage of refinement, it was noticed that the thermal ellipsoid for the nitrogen of the NO moiety was elongated in the direction of the N–O vector and that the N-O bond was unreasonably short (0.95(1)Å). A similar phenomenon had previously been observed for the structure of $[Os(NO)Br_5]^{2-}$ where there was disordering of the NO and Br groups (Chapter 2; ref. 20). A model was set up with a Br atom of occupancy 0.05 at 2.51Å from the Os on the Os–O vector and with N and O having occupancy 0.95. Agreement factors were slightly improved, the N-O distance was now sensible and the thermal ellipsoids on N and O were more as expected, so this model has been retained and is presented here.

A2.2 Crystal structure of [$BzPh_3P$] [$RuBr_4(CH_3CN)(NO)$] • 0.5 (C_6H_6)

Table A2.2.1 *Crystallographic Data for ($BzPPh_3$)[$RuBr_4(NO)(CH_3CN)$] • 0.5(C_6H_6) at 293 K.*

chem formula	$C_{30}H_{28}Br_4N_2OPRu$
fw	884.23
cryst system	monoclinic
spacegroup	$P2_1/n$
a, Å	10.388(1)
b, Å	19.830(3)
c, Å	16.259(2)
β,°	94.17(1)
V, $Å^3$	3340.6(6)
Z	4
d_{calcd}, g cm^{-3}	1.758
μ[Cu Kα], cm^{-1}	102.3
cryst dimens, mm	0.17 × 0.10 × 0.10
X-radiation	Cu Kα
λ, Å	1.5418
data range, ° in 2θ	3 - 120
no. unique data	4963
no. data refined	3476 [$I > 3\sigma(I)$]
no. variables	352
R	0.038
R_w	0.058
GOF	1.41
F(000)	1715.72

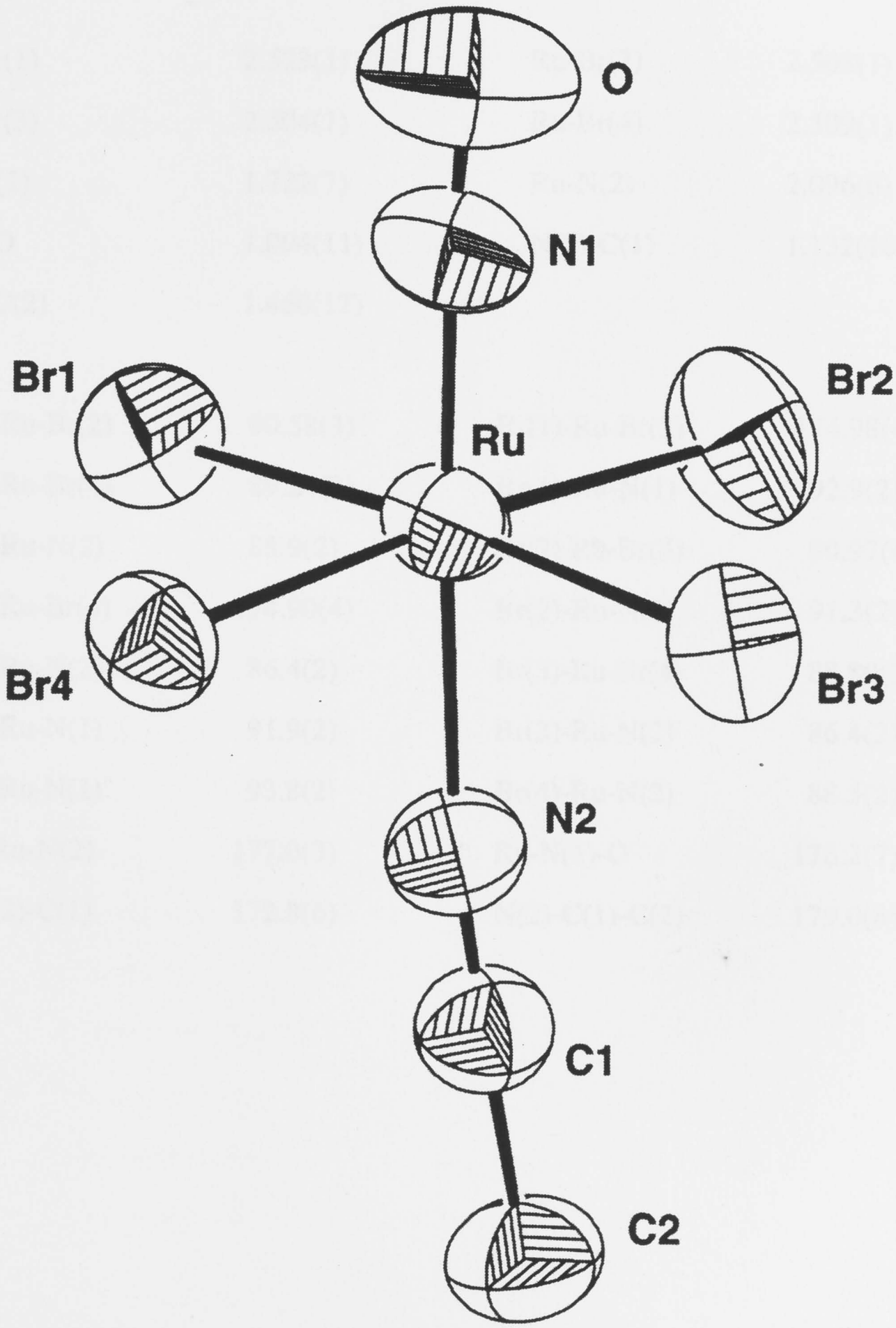

Figure A2.2.1 *Thermal ellipsoid diagram of the $[RuBr_4(NO)(CH_3CN)]^{1-}$ anion with labelling of the non-H atoms. Ellipsoids show 50% probability levels.*

Table A2.2.2 *Interatomic distances (Å) and angles (°) for non-hydrogen atoms of the complex anion in* $(BzPPh_3)[RuBr_4(NO)(CH_3CN)]\bullet 0.5(C_6H_6)$.

Ru-Br(1)	2.523(1)	Ru-Br(2)	2.508(1)
Ru-Br(3)	2.504(1)	Ru-Br(4)	2.509(1)
Ru-N(1)	1.722(7)	Ru-N(2)	2.096(6)
N(1)-O	1.094(11)	N(2)-C(1)	1.132(10)
C(1)-C(2)	1.460(12)		

Br(1)-Ru-Br(2)	90.58(3)	Br(1)-Ru-Br(3)	174.98(4)
Br(1)-Ru-Br(4)	89.24(3)	Br(1)-Ru-N(1)	92.9(2)
Br(1)-Ru-N(2)	88.9(2)	Br(2)-Ru-Br(3)	90.97(4)
Br(2)-Ru-Br(4)	174.90(4)	Br(2)-Ru-N(1)	91.3(2)
Br(2)-Ru-N(2)	86.4(2)	Br(3)-Ru-Br(4)	88.80(3)
Br(3)-Ru-N(1)	91.9(2)	Br(3)-Ru-N(2)	86.4(2)
Br(4)-Ru-N(1)	93.8(2)	Br(4)-Ru-N(2)	88.5(2)
N(1)-Ru-N(2)	177.0(3)	Ru-N(1)-O	176.2(7)
Ru-N(2)-C(1)	172.8(6)	N(2)-C(1)-C(2)	179.0(8)

A2.3 Crystal Structure of $(BzPPh_3)[RuBr_4(NO)(C_5H_5N)]$

Table A2.3.1 *Crystallographic Data for $(BzPPh_3)[RuBr_4(NO)(C_5H_5N)]$ at 293 K.*

chem formula	$C_{30}H_{27}Br_4N_2OPRu$
fw	883.22
cryst system	monoclinic
spacegroup	$P2_1/c$
a, Å	12.918(1)
b, Å	13.525(1)
c, Å	18.532(2)
β,°	93.60(1)
V, Å^3	3231.5(5)
Z	4
d_{calcd}, g cm^{-3}	1.815
μ[Cu Kα], cm^{-1}	112.3
cryst dimens, mm	0.04 × 0.09 × 0.23
X-radiation	Cu Kα
λ, Å	1.5418
data range, ° in 2θ	4 - 120
no. unique data	4650
no. data refined	3500 [$I > 3\sigma(I)$]
no. variables	352
R	0.041
R_w	0.059
GOF	1.42
F(000)	1711.7

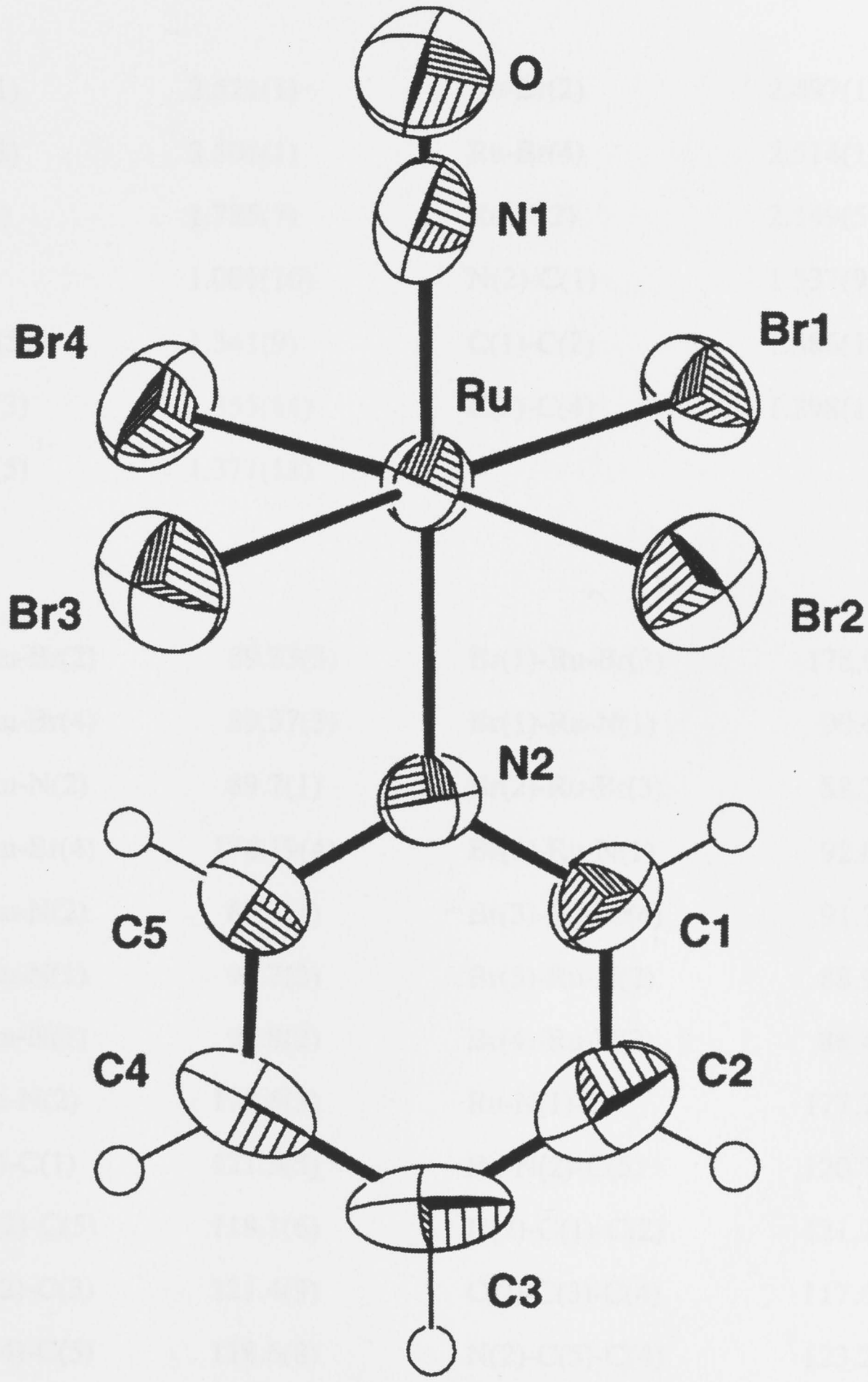

Figure A2.3.1 *Thermal ellipsoid diagram of the* $[RuBr_4(NO)(C_5H_5N)]^{1-}$ *anion with labelling of the non-H atoms. Ellipsoids show 50% probability levels; H atoms are drawn as circles of arbitrary small radius.*

Table A2.3.2 *Interatomic distances (Å) and angles (°) for non-hydrogen atoms of the complex anion in* $(BzPPh_3)[RuBr_4(NO)(C_5H_5N)]$.

Ru-Br(1)	2.521(1)	Ru-Br(2)	2.497(1)
Ru-Br(3)	2.508(1)	Ru-Br(4)	2.514(1)
Ru-N(1)	1.785(7)	Ru-N(2)	2.149(5)
N(1)-O	1.001(10)	N(2)-C(1)	1.337(9)
N(2)-C(5)	1.341(9)	C(1)-C(2)	1.386(12)
C(2)-C(3)	1.355(14)	C(3)-C(4)	1.398(15)
C(4)-C(5)	1.377(11)		

Br(1)-Ru-Br(2)	89.83(3)	Br(1)-Ru-Br(3)	178.05(5)
Br(1)-Ru-Br(4)	89.57(3)	Br(1)-Ru-N(1)	90.7(2)
Br(1)-Ru-N(2)	89.7(1)	Br(2)-Ru-Br(3)	88.72(4)
Br(2)-Ru-Br(4)	176.19(4)	Br(2)-Ru-N(1)	92.0(2)
Br(2)-Ru-N(2)	87.8(1)	Br(3)-Ru-Br(4)	91.79(4)
Br(3)-Ru-N(1)	90.7(2)	Br(3)-Ru-N(2)	88.9(1)
Br(4)-Ru-N(1)	91.8(2)	Br(4)-Ru-N(2)	88.4(1)
N(1)-Ru-N(2)	179.6(3)	Ru-N(1)-O	177.7(7)
Ru-N(2)-C(1)	121.3(5)	Ru-N(2)-C(5)	120.7(5)
C(1)-N(2)-C(5)	118.1(6)	N(2)-C(1)-C(2)	121.2(7)
C(1)-C(2)-C(3)	121.4(9)	C(2)-C(3)-C(4)	117.6(8)
C(3)-C(4)-C(5)	118.6(8)	N(2)-C(5)-C(4)	123.2(7)

A2.4 Crystal Structure of $[Bu^n_4N]_2[Ru(NO)Cl_4]_2$

Table A2.4.1 *Crystallographic Data for $[Bu^n_4N]_2[Ru(NO)Cl_4]_2$.at 213 K.*

Empirical Formula	$C_{16}H_{36}N_2ORuCl_4$
Formula Weight	515.36
Crystal Colour, Habit	orange, prism
crystal system	monoclinic
lattice type	Primitive
spacegroup	$P2_1/n$
a, Å	9.611(2)
b, Å	21.033(2)
c, Å	12.029(1)
β,°	93.66(1)
V, $Å^3$	2426.8(4)
Z	4
d_{calcd}, g cm^{-3}	1.410
μ[Cu Kα], cm^{-1}	93.31
crystal dimensions	0.12 x 0.06 x 0.04 mm
X-radiation	Cu Kα
λ, Å	1.54178
data range, ° in 2θ	3.0 - 120.0
no. unique data	3969
no. variables	217
R	0.028
R_w	0.029
GOF	1.34
F(000)	1064.0

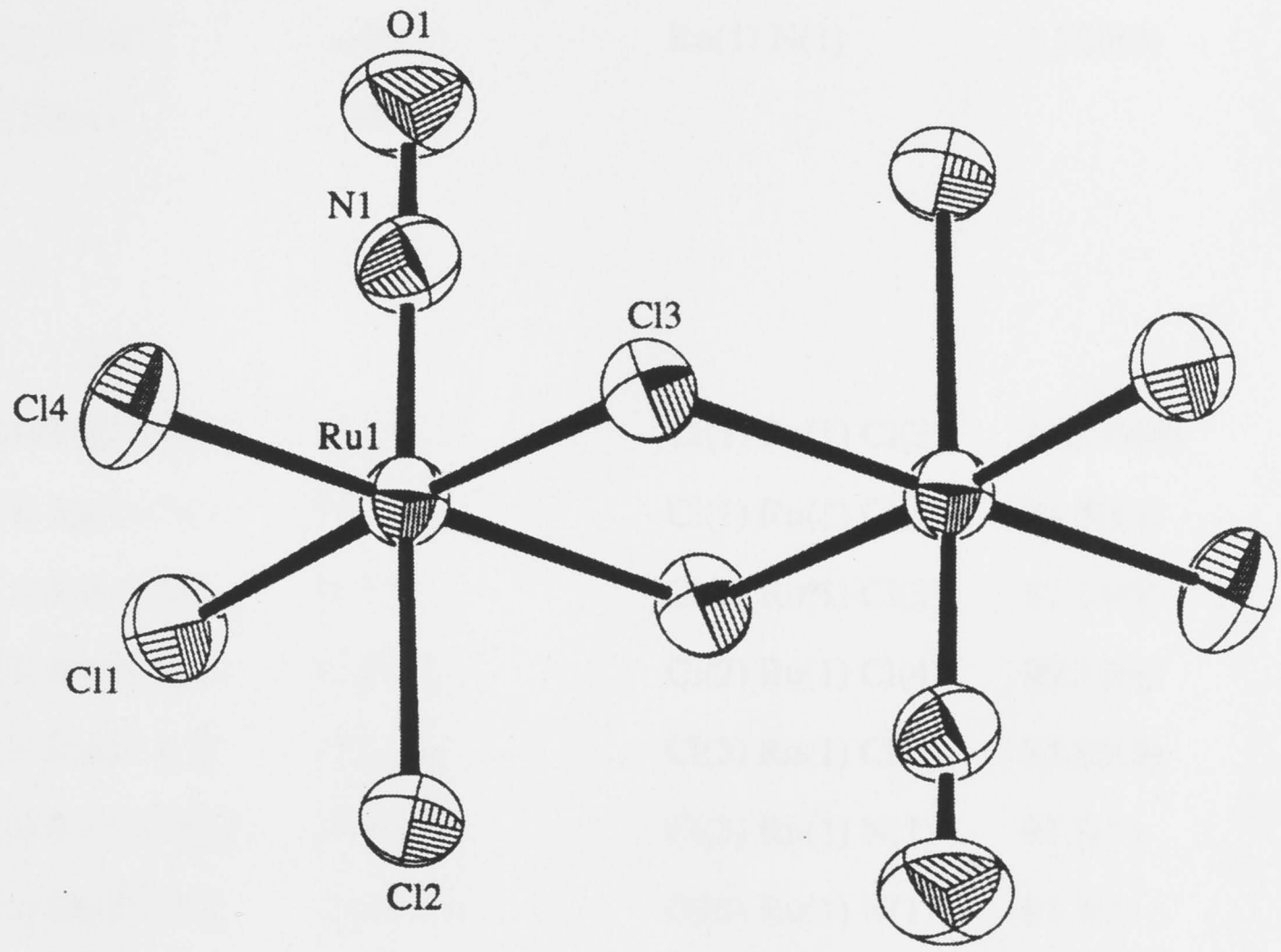

Figure A2.4.1 *Thermal ellipsoid diagram of the $[Ru(NO)Cl_4]_2^{2-}$ anion. Ellipsoids show 50% probability levels.*

Table A2.4.2 *Interatomic distances (Å) and angles (°) in the* $[Ru(NO)Cl_4]_2^{2-}$ *complex anion.*

Ru(1) Cl(1)	2.354(1)	Ru(1) Cl(2)	2.331(1)
Ru(1) Cl(3)	2.412(1)	Ru(1) Cl(3)	2.410(1)
Ru(1) Cl(4)	2.338(1)	Ru(1) N(1)	1.728(3)
O(1) N(1)	1.147(4)		

Cl(1) Ru(1) Cl(2)	89.85(4)	Cl(1) Ru(1) Cl(3)	176.49(4)
Cl(1) Ru(1) Cl(3)	92.25(4)	Cl(1) Ru(1) Cl(4)	91.50(4)
Cl(1) Ru(1) N(1)	91.5(1)	Cl(2) Ru(1) Cl(3)	87.14(4)
Cl(2) Ru(1) Cl(3)	87.64(3)	Cl(2) Ru(1) Cl(4)	89.77(4)
Cl(2) Ru(1) N(1)	178.4(1)	Cl(3) Ru(1) Cl(3)	85.85(3)
Cl(3) Ru(1) Cl(4)	90.28(4)	Cl(3) Ru(1) N(1)	91.5(1)
Cl(3) Ru(1) Cl(4)	175.44(4)	Cl(3) Ru(1) N(1)	91.3(1)
Cl(4) Ru(1) N(1)	91.2(1)	Ru(1) Cl(3) Ru(1)	94.15(3)
Ru(1) N(1) O(1)	179.3(3)		